NEWCASTLE UNIVERSITY

SCHOOL OF MECHANICAL AND SYSTEMS ENGINEERING

An Energy, Exergy and Economic Modeling Study based on Utilizing waste Heat Energy of a C200 Microturbine to Power ORC, Absorption Chiller and Desalination Units

By

Basim M.A Makhdoum

B.Sc, M.Sc.

A thesis submitted to the School of Mechanical and Systems Engineering
for the degree of

Doctor of Philosophy

In Mechanical Engineering

Supervised by

Professor Brian Agnew

21st March 2012

Abstract

The motivation for this investigation into microturbine and desalination processes is the desire to combat problems caused by frequent high temperature conditions related to the spread of global warming. The small-scale power microturbine C200, designed by the Capstone Co., was chosen. Also, a single effect absorption chiller was employed in this study. The method of thermal vapor compression multi-effect distillation desalination was chosen as a potable water producer. Also, the organic Rankine cycle was powered by low-grade heat energy. Each model was simulated and investigated on a stand-alone basis under ISO conditions using off-design simulations. The ORC, absorption chiller and TVC-MED desalination process were separately driven with the same amount of fuel consumption into microturbine. All the base and proposed models were simulated by using a software package called IPSEpro. The economic accessibility and profitability of all the proposed models was examined.

Integrating the microturbine with the ORC unit led to the generation of an extra 4.10% of electric power compared to that produced by the absorption chiller, and 7.80% for TVC-MED desalination. However, the lowest carbon emission rate for all models was achieved by using a microturbine with TVC-MED desalination with a reduction of 46.80%. Accordingly, the EUF of the TVC-MED desalination was 9.20% higher than when an absorption chiller was used, and 42.40% higher than when ORC was used. ORC gained the lowest EUF. The higher rate of exergetic efficiency was found when utilising the microturbine with the single effect absorption chiller with a value of 31.00%, as compared to ORC and TVC-MED, which registered rates of 23.11%, and 22.42% respectively.

The results of economic study showed that, if the selling price was £0.023/kWh, then the profitability evaluation results would not be attractive for investment. However, if investment was made into a microturbine, then the electricity price could be set at £0.040/kWh or £0.060/kWh, resulting in a desirable economic feasibility for all combined models.

Acknowledgments

Firstly, I thank Almighty God for giving me the courage, determination and guidance in conducting this research work.

I would like to express my sincere appreciation to my supervisor, Professor. Brian Agnew for his intelligence, generosity and guiding me through my research work. Your time, and supporting are really appreciated.

I would like to thank my colleagues who have generously provided their time and valuable suggestions to this research study.

Finally, I would like to thank my parents and my wife Abrar for their prayers, encouragement, support and unlimited patience during the period of study.

IN THE NAME OF ALLAH

THE MOST GRACIOUS AND THE MOST MERCIFUL

Table of contents

Lists of Figures

Chapter 2

Chapter 3

Chapter 4

Chapter 5

Chapter 6

Lists of Tables

Chapter 2

Chapter 3

Chapter 4

Chapter 5

Chapter 6

Chapter 7

Abbreviations

CHP	Combined cycle heat power
CF	Concentration factor
CFCs	Chlorofluorocarbons
CH_4	Methane
CO_2	Carbon Dioxide
ESDU	Engineering Sciences Data Unit
G	Generator
HFCs	Hydroflurocarbons
HRSG	Heat Recovery Steam Generator
ISO	International Standards Organization
LiBr	Lithium Bromide
MDK	The IPSEpro model development kit
MED	Multi effect distillation desalination process
MSF	Multi stage flash
MT	Microturbine
MVC	Mechanical vapour compression
N_2O	Nitrous Oxide
NaREC	New and Renewable Energy Centre
O&M	Operational and maintenance
ORC	Organic Rankine cycle
PFCs	Per fluorocarbons
PSE	Process simulation environment
PSEconomy	Process simulation economy
PSExcel	Process simulation MS Excel
RO	Reveres Osmosis
SF_6	Sulphur hexafluoride
SimTech	Simulation Technology
SWCC	Saline water conversion corporation
TVC	Thermal vapour compression

Nomenclature

ΔT	Temperature difference	K
ARR	Average rate of return	%
C	Heat capacity rate	W/K
CF	Capacity factor	%
CFN	Cash flow net	
COP	Coefficient of performance	-
Cp	Specific heat	kJ/kg K
C-Value	Cost per unit Q/ΔT	£/(W/K)
E	Exergy	kW
e	Specific exergy	kJ/kg
EUF	Energy utilization factor	%
g	Gravity	N
GOR	Gain output ratio	-
h	Enthalpy	kJ/kg
L	Load	-
LHV	Low heating value	kJ/kg
w, $\dot{m}$	Mass and mass flow rate	kg/s
M	Molar mass	kg/kmol
NBCR	Net benefit cost ratio	-
NP	Average annual net profit	
NPV	Net present value	£
NTU	Number of transfer unit	-
O&M	Operation and Maintenance cost	£
P	Pressure	bar
PBP	Payback period	year
PR	Performance ratio	-
$\dot{Q}$	Heat transfer rate	kW
$\bar{R}$	Universal gas constant	kJ/kmol.K
r	Pressure ratio	-
s	Entropy	kJ/K
ShC	Specific heat consumption	kJ/kg
T	Temperature	˚C
TCI	Total capital investment	
UA	Heat transfer area × overall heat transfer coefficient	kW/K
v	Velocity	m/s
W	Power	kW
x	Molar fraction	-
Z	Altitude	m

Subscripts and superscripts

c	refer to cold stream
c,w	Cooling water
CH	Chemical
C.C	Combustion chamber
Eva	Evaporator
F	Fuel
gas	Exhaust gas stream
h	refer to hot stream
hw	Hot water
j	Surface conditions
KN	Kinetic
lm	Log mean
min	Minimum
o	Reference condition
PH	Physical
PT	Potential
sol	Solution
T	Turbine
t	Project lifetime
w	Water
z	Number of year

Greek Symbols

α A mount of CO_2/ton of fuel
γ Specific heat ratio
ε Effectiveness
η Efficiency
η_I Exergetic efficiency
Θ Molar Gibbs function of formation
Ψ Exergy destruction ratio

Chapter 1

Introduction

1. Introduction:

The idea of establishing a microturbine for generating electricity originated in 1988 with the Capstone Company [1]. By 1994, the vast majority of industries had achieved rapid changes in the power generation market. New opportunities had opened up for the heat and power users to reduce costs, increase power quality and reliability, and attain a reasonably low emission rate. One of these valuable opportunities was the possibility of investing in small-scale energy resources that could be integrated into a manufacturing plant or an institute's overall operation. These technologies can be managed locally in order to ensure that they reach both the optimised performance target and the specific requirements for both electricity and thermal energy. Energy managers and building operators can thus plan to use heat and power services at less cost, with lower levels of emissions, better reliability and greater control, compared to what had previously been available from the utility grid. Such requirements led to the emergence of microturbines as leading candidates for meeting these requirements to provide reliably generated electric and thermal energy. Furthermore, there is a need for small power generation that provides reliable electricity to remote areas where grid power is limited. Although diesel engines were commonly used in the past for the purposes of power generation, they were expensive to use. The alternative option is to operate a gas turbine in a simple Brayton cycle. However, gas turbines generate power on a large scale in terms of megawatts, and those that generate less than 1 MW are very costly. This again points to the need for microturbines that can generate power in the range of 5-200 kW [2]. The microturbine is basically a small-scale unit of the gas turbine that has been recently established in order to limit the consumption of electric power in kW. It contains the same major components as the gas turbine - a compressor, a combustion chamber, and a power turbine.

Due to the spread of global warming, the need to find a reliable solution for controlling the amount of the CO_2 emission rate is essential. Secondly, there is an urgent need to help people living in arid or semi-arid zones meet their needs for electricity and fresh water. Thirdly, it is necessary to minimise the effect of ambient conditions on the microturbine performance operating under the collected ambient condition data found in Jeddah city in Saudi Arabia.

Such developments have played a significant role in encouraging more research into microturbines and thermal energy so as to facilitate the development of a new

generation of reliable power systems. The growth in the potential market has led to an increased demand for thermal and mechanical energy as well as electricity, and microturbines have been considered one of the most advanced forms of energy generation [3]. Microturbines thus represent very effective ways of generating clean power for distributed energy applications when installed for the purposes of cooling, heating and generating electricity (CHP) [3].

No microturbine has so far been used in the Saudi market. Therefore, the idea of introducing this small-scale unit will certainly have some advantages for the community and is very likely to be of great use in providing a reliable solution for the shortages of electricity and potable water. Also, Jeddah is one of the most attractive cities in Saudi Arabia due to its costal and commercial location. Furthermore, Jeddah city has a high number of resort villages located in the coastal area, which many people use for vacations. Each village contains 20 to 30 accommodation units, all of which require electricity and fresh water. However, these villages may soon face disconnection of electricity as there is often no power station nearby which can provide a reliable electric supply. A microturbine (CHP) can easily fulfil such demands for power and water while maintain a low emission rate. At the same time, it can facilitate the operation of a single effect absorption chiller or organic Rankine cycle in order to stabilize variations in ambient temperature, or can provide extra electric power without increasing the fuel consumption rate. In this study the potential effect of the temperatures and humidity in Jeddah city on microturbine performance has been considered in detail. Another important factor here is that thermal desalination technologies are not common in small-scale water production, and can be powered by waste heat energy from high-grade heat. Therefore, the opportunity to model and simulate small-scale multi-effect distilled desalination has been a considerable challenge. This study was devised to investigate the possibility of integrating the different systems with a microturbine in order to improve performance and minimise the impact on the environment. Using the real data collected directly from manufacturers and the products' sites, thermal and economic investigations will be performed for each proposed system. Then a final comparison between all proposed models will be made, based on the first and second thermodynamic laws and results of economic feasibility assessments.

As the microturbine is considered one of the most advanced forms of distributed energy generation, it is necessary to demonstrate the modelling of a stand-alone

microturbine system and to provide a number of parametric studies. Also, a number of applications of microturbine CHPs will be modelled and investigated according to first and second law thermodynamic analysis. This will strongly help in expanding future energy options, and in raising the value of energy production for health and environmental purposes. Furthermore, as a result of limited studies of microturbines, combined with other thermal applications such as ambient performance and exergy analysis, a number of gas turbine studies have been considered for comparative analysis in order improve this study's validation.

This research study has been based on the microturbine C200, designed by the Capstone Company in 2008, which generates 200 kW. It is considered to provide the maximum number kWs that can be generated by one unit [4]. However, more research needs to be carried out on the C200 microturbine to achieve a better view of its capabilities, and to overcome the challenge of involving it in a CHP system such as an organic Rankine cycle (ORC) and single effect absorption chiller, as no recent studies have reported the use of these applications with a C200 microturbine (CHP).

Computational modelling and simulation has become a foundation for all studies, training and certificating applications. It saves time and money, offers flexibility, enables reliability and offers control with high quality findings. Hence, bearing in mind the limitations in funding for such experimental work, this can be considered as an excellent method of investigating the performance of all the proposed models in a range of different conditions. All the models were simulated by the software package IPSEpro and were created using SimTech Simulation Technology. A section of IPSEpro is called PSEconomy, which was used to perform the economic mathematical calculations for each proposed model.

1.2 Layout of the Thesis:

This thesis consists of seven chapters and supporting appendices. The present chapter outlines the aims, motivation and inspiration of this study while the other chapters are arranged as follows:

- Chapter 2 introduces the literature review, which covers the related topics regarding to this study, including the microturbine, organic Rankine cycle, the absorption chiller, the desalination process, the waste heat energy recovery system and water sources in Saudi Arabia.
- Chapter 3 presents a description of the simulation software package employed in this study, and performs mathematical modelling of the energy and exergy analysis. Also, the real modelling data and the weather data for the intended location are introduced here.
- Chapter 4 describes the process of base plant modelling, which explains each model individually and includes the results of modelling and parametric studies.
- Chapter 5 presents all the proposed models and parametric studies of each. There are also comparisons between all the models with regard to their energy and exergy analysis results.
- Chapter 6 presents an economic study of the models, in order to investigate their economic profitability and feasibility. A sensitivity study is also included for the purposes of comparison, through which some analysis and discussion of each model is presented.
- Chapter 7 concludes the presentation of both the thermodynamic and economic results for all the proposed models and provides recommendations for future work.

Chapter 2

Literature Review

2.1 Microturbine:

Microturbines are small components of modern electricity generators that burn gaseous and liquid fuels, creating high-speed rotation, which in turn operates the generators. Work on small stationary and automotive gas turbines has very much benefited from recent developments in the microturbine process [5]. The vast majority of gas turbines today are jet engines, turboprops or turbo shaft engines. A separate class of industrial gas turbine is used in power generation and other heavy-duty applications [1].

Many applications and advantages of microturbines have helped create a rapidly increasing power generation market. A handful of these advantages are highlighted as follows, which describes the beauty of the microturbine. First, the environmental performance of the microturbine is very impressive, thanks to decades of intensive research. In fact, microturbines can now operate with fuels which produce much lower NOx emissions than previously possible. Therefore, microturbines can be considered as an environmentally friendly alternative. The environmental dimension is especially important when it comes to the current environmental situation. Secondly, another very important factor is the availability of gas as a fuel of choice for smaller scale industrial and cogeneration applications. Other reasons in favour of employing microturbines are that they are quick to install, easy to maintain, and also have a short payback period [6].

Generally speaking, a microturbine consists of the same major components as a normal gas turbine (though on a considerably smaller scale): the air compressor, the combustor and the turbine Fig [2-1], [7]. From a technical point of view, a microturbine can be used with a single shaft, and all the components can be found on the same shaft that drives the generator [8].

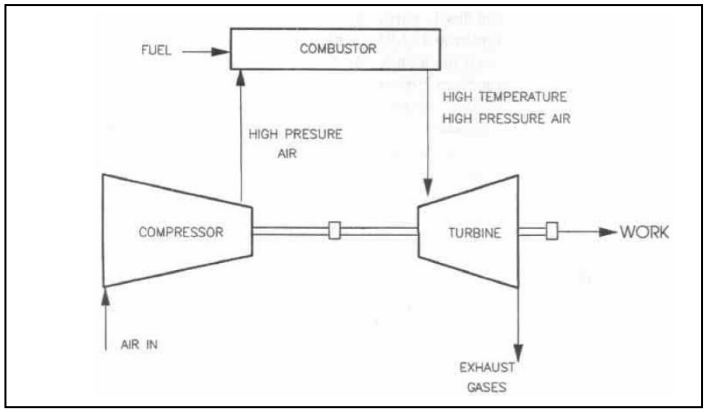

Fig [2-1], simple Brighton cycle

2.2 History and Background:

According to Kolanowski [1], Capstone was founded in 1988 and has been marketing successful units since 1998. The Capstone Turbine Corporation is the world's leading producer of low-emission microturbine systems, and was the first to market a commercially viable air bearing turbine technology. The company has shipped thousands of Capstone turbines to customers worldwide. These award-winning systems have logged millions of documented runtime operating hours. They provide minimal maintenance requirements, digital power control, quiet operation free of vibration, a factory installed modem for remote monitoring and operation and multiple gases fuel capability. The record shows that 3,000 units of microturbines have operated around the world and this number is increasing as more successful research work is conducted to meet more customers' requirements.

Moreover, the microturbine engine consists of a combustion chamber, a recuperator and a rotor (single shaft where the compressor, turbine and generator are placed) as shown in Fig [2-2]. The latter contains a compressor wheel where the intake air is compressed, a power turbine wheel and a generator. Using a single rotor to operate the microturbine means that the speed of the compressor is equal to the speed of the generator. The Ingersoll-Rand Company (IR), who use two separate shafts to run microturbine, have manufactured another microturbine design. One shaft is connected with the compressor and microturbine, and a free power turbine and generator link the second shaft, see Fig [2-3].

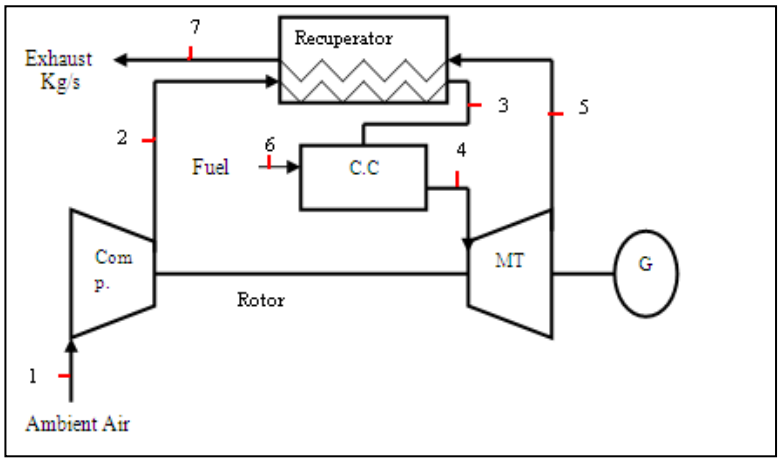

Fig [2-2] single-shaft Microturbine.

Both designs supply the microturbine industry. However, in the case of the first design by Capstone, connecting all the components on a single shaft means the speed of the compressor and generator are equal. This could lead to changes in all the parts connecting with this shaft in case of less oil lubrication. Capstone has solved this problem by inventing the air bearing, which will be discussed in the next section. The second design by the IR Company is reliable and provides a separate control for intake air speed and generator speed. On the other hand, it requires relatively high costs in maintenance, and requires an oil lubricant system [1].

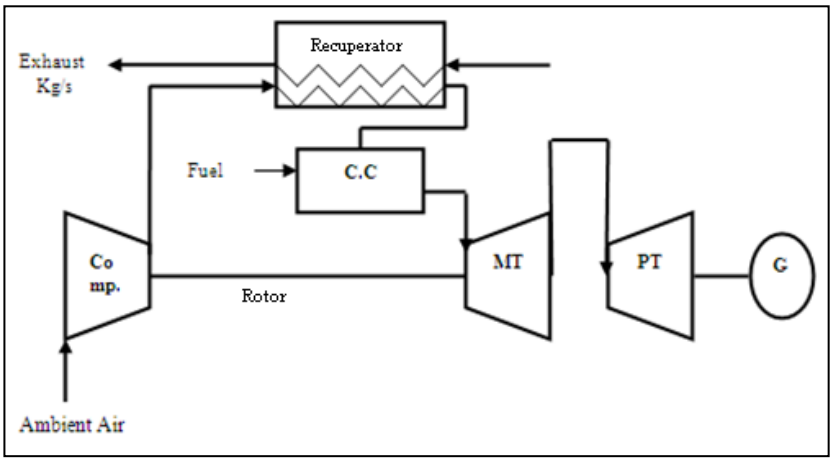

Fig [2-3] double-shaft microturbine.

2.3 Microturbine Components:

The basic components of a microturbine are the compressor, turbine, generator, and recuperator. The compressor and turbine represent the heart of a microturbine, mounted on a single shaft along with the electric generator. The benefit of having one moving shaft (single –shaft) is that it contributes to less maintenance and higher reliability than turbines with two or more shafts [3].

In order to meet the aim of this study, research work must be examined and carried out on the performance of all microturbine system components.

2.3.1 Recuperator:

The simple cycle of a gas turbine has been covered in the fields of power generation for over half a century. Most major contributors are working continuously in order to improve compressor and turbine efficiencies, and increase the inlet temperature of the turbine. The common option for improving the cycle efficiency has always been associated with the use of exhaust heat recovery exchangers. Recuperators have experienced limited acceptance due to their large size, unreliability and high installation and maintenance cost [9]. Currently, recuperators are essential to many users options, and with the microturbine the recuperator is necessary to achieve engine efficiency of 30% and higher [10].

Recuperators have been described across a wide range of literature. They are placed in the microturbine cycle as a heat exchanger that increases the temperature of the compressor outlet air before it goes to the combustion chamber by cooling the low pressure exhaust flow provided from the turbine. This contributes to a reduction in fuel needed to heat the compressed air to the required turbine inlet temperature. A recuperator becomes essential in microturbines to achieve the efficiency levels needed to be competitive in continuous duty services [1]. The recuperator has to be effective to a high percentage (approximately 90%) to achieve the desired ratio between the actual heat transferred to the maximum achievable heat transferred.

The durability of the recuperator is considered a design and economic issue for microturbine developers. Previously in the industry of gas turbines the developers experienced leaks in their recuperators due to differential thermal expansion accompanying thermal transients. However, a quite durable version of microturbine has been proven recently in testing and commercial applications. This improvement in durability has occurred due to the use of higher strength alloys and higher quality

welding, along with improved engineering design to avoid internal differential expansion that causes stress, followed by cracks and leakage [3].

On the basis of selecting a better choice for the manufacturing of microturbines, a study was conducted by Kaikko and Backman [11] to investigate the effect of different configurations and control methods on the technical and economic performance by including a recuperator and a non-recuperator in a microturbine. The study shows that, despite the high cost of the recuperator, it has a remarkable effect on the performance of the design points of the microturbine by increasing the electrical efficiency by 30%. However, the heat output was decreased compared to non-recuperated cycles of the same power output. Moreover, on the economic side the non-recuperated cycle has a higher maximum profit flow for the given microturbine size. In conclusion, the non-recuperated cycle has higher potential for feasibility at design point operation. Gomes et al. [12] supported this result in a different study by stating that non-recuperator cycle is cheaper and more appropriate. However, Kaikko and Backman [11] describe the economic feasibility of a specific design point. Hence, different situations and conditions can change this conclusion. Also, the study was carried out on microturbine stand alone, while microturbines can be used as high energy grade that supply low heat energy grade. In this case, the exhaust's high temperature is needed, which can be gained by including the recuperator in the microturbine design. This can also affect the economic study feasibility. Also, McDonald [13] summarises important parameters for a low cost recuperator design, which use a minimum number of parts, and almost reach the high ratio of utilisation of material, well-welded construction, compact lightweight heat exchanger and ease of installation.

2.3.2 Fuel and Combustion Chamber System:

Microturbines can deal with different types of fuel: liquid such as diesel and kerosene or gas fuel, for instance natural gas. However, a number of considerations must be taken into account in the burning process in the combustion chamber. As microturbines designers realized that the fuel quality was not likely to be very pure, the mass of gas entering the combustion chamber had to vary. This meant the fuel system had to be designed to handle different masses of fuel flow.

The fuel type could affect the stability of the combustion system. Since the microturbine is considered as an environmentally friendly alternative engine, the use of gas and natural gas has been discussed according to their impact on the combustion

system and the amount of NOx emission. Burning fuel with a significant amount of carbon monoxide and acetylene causes a reduction in combustor life. Hence, high combustor temperatures are obtained. Liquid fuel generally has higher NOx levels than natural gas. Since the temperature of combustion and NOx production are very close, fuel containing high levels of carbon monoxide and acetylene will create more NOx production. Also, liquid fuel with a poor atomisation quality will result in reduced combustion chamber life [1].

A case study has been performed by Gomes et al [12] using natural gas in a microturbine to reach low emission levels at the full power setting. Mixing the air and fuel before entering the combustion allows clean combustion at relatively low temperatures. Also, there is an injector to balance the ratio of air and fuel mixture in order to obtain the optimal temperature for minimum NOx production. Thus, the higher air to fuel ratio results in lower flame temperature. Bullin [14] stated that natural gas is a common fuel of choice in microturbines. The natural gas is usually supplied at a low pressure, less than 1 PSI. To obtain efficient combustion and clean emission a gas boost compressor is needed. To gain a high fuel pressure (natural gas) Capstone incorporates a rotary flow compressor to boost the inlet gas pressure to the required combustion chamber pressure. Furthermore, to control the quantity of the inlet mass fuel, a fuel valve has been installed in the system to pass the needed flow rate of gas to the combustion [1].

2.3.3 Bearing System:

The microturbine shaft is supported by either oil-lubricated or air bearings. The former are mechanical bearings which come in three types: high speed metal ball or roller, floating sleeve ceramic surface, which shows benefits in terms of life and operating temperature. Oil bearings require an oil pump, oil-filtering system, and oil cooling. These needs obviously add an extra cost and maintenance needs. As microturbine contains a small-scale shaft, there is a greater likelihood of contamination due to lubrication oil. Therefore, frequent replacement and maintenance process are required to obtain an efficient engine [3]. This has encouraged more research studies to pursue the optimal solution for bearings of small-scale units with low cost and maintenance. This has led to an outstanding invention by Capstone to provide an air bearing. This technology provides a lubrication solution to previously existing technologies. The use of air bearings in Capstone turbines

contributes to providing simplicity in operation, reliable longer engine life. No scheduled maintenance is required and the unit's ecological footprint is reduced [14],[15]. Air bearings have been in service on airplane cooling system for many years. They allow the high-speed shaft of the turbine to spin on a thin layer of air. This results in low friction. No oil, oil pump or cooling system is required. Soares [3] adds that the repeated starting-up and shutting down in microturbines becomes a concern to air bearings, due to metal-on-metal friction. However, Kolanowski [1] reported that air-bearings come into contact with the unit shaft only when the unit is at rest. To prevent undesirable friction, upon shutdown the rotor is grabbed electrically to prevent coast down of the rotor, thus preventing any rubbing of the shaft on the air bearing.

The principle of air bearing operation is similar to an air hockey table. The turbine shaft rides on the cushion of the air bearing. Also, the space between the rotating parts has a near frictionless cushion. This is because the unique aerodynamic shape of the Capstone invention pulls a very thin layer of air into this space. As a result the parts are no longer in contact. Moreover, the little heat generated that occurs within the bearing is reduced and dissipated as air flows through the bearing [15].

2.4 Microturbine Electric Power Generation:

A battery supplied uninterruptable power supply [UPS] is used to power the generator for start up. This case is engaged when the system is operating independently of the grid. A different starting system is used in the case of a two-shaft design [3].

A digital power controller is used in a single-shaft design to convert the high frequency AC power produced by the generator into commercially useable electricity. Power electronics is considered a critical component in single-shaft microturbine design, and has led to significant design challenges, particularly in matching the required load to turbine output. Most microturbine power electronics are designed to produce three-phase electricity. The electronic components of the microturbine control all of the engine, generator operating and start-up function. They also allow for remote monitoring and operation [3].

2.5 Microturbine Applications and Performance:

Microturbines have proved their suitability to the market for a variety of distributed applications due to their flexibility in connection method, ability to be arraigned in

parallel to provide electricity to a larger load, and their provision of reliable power and low emissions profile.

Customers in light industrial facilities and in financial service, such as health care, schools, and other commercial institutional buildings, are targeting microturbine system applications [3].

Ho et al. [6] pointed out that there are three primary reasons behind the growth of the microturbine market. Firstly, they are less polluting than other forms of power generating devices. Secondly, the availability of gas as a fuel of choice for smaller-scale industrial and cogeneration applications. Thirdly, the microturbine is quick to install, easy to maintain, and has a small payback period compared to other power generating facilities. However, he provides these points and the use and the cost of recuperator in microturbine unit was not mentioned, as many authors have stated - [1],[3],[16] - that the recuperator has a significant influence on the microturbine's system, either raising the unit cost or the efficiency.

Microturbines can be a competitive option, especially in a location where power from the local grid is hard to get or extremely expensive to install. Also, electric service availability is limited and service points tend to be far apart in remote locations. Therefore, it is expensive to install an electrical distribution system to connect it to local grid for small users. However, remote power applications can also include oil and gas production fields, such as coal mines and landfills where gas products are available. These areas are likely to be far from the grid, and even when served by grid, they become expensive due to their exposure to environmental destruction such as unstable weather conditions and fire, which result in loss of electricity. Thus, the fuel flexibility of microturbines becomes a significant asset in these facilities, and this may be considered evidence for the early market success of microturbines. Furthermore, the mutable unit of a microturbine can be installed together to meet the required capacity and site reliability [3].

2.6 Waste Energy Recovery and CHP:

The recovery of waste heat energy has been one of the main concerns over the last two decades, not only for engineers but also for most economists and environmentalists. Waste energy, and in particular waste heat energy, is the main focus of this study.

A number of energy sources are available, but most of them need to be converted into more usable forms, such as electrical energy, mechanical energy or thermal energy. Due to the limitations of the second law of thermodynamics, almost any energy conversion process is inefficient, involving loss of the energy being converted. Therefore, developing new technologies that benefit from that waste energy is essential, not just economically, but also environmentally.

A number of theories have explained the increase in global average temperatures and the rise in the sea water levels as a natural cycle or phenomenon, such as the Milankovitch theory, which considers climate change to be an expected result of the changes in the Earth's orbit around the Sun [17]. However, the majority prefer the man-made global warming theory, which is based on an old theory introduced by Svante Arrenius in 1896, and states that the continual emission of carbon dioxide caused by combustion of coal will intensify the greenhouse effect, which will cause global warming [18]. Hence, it is believed that the industrial revolution, which started around 1800, has caused the most dramatic increase in carbon dioxide levels [17],[18]. Furthermore, as stated in the Kyoto Protocol, by September 2006 a total of 169 countries had signed the agreement calling for reduction in the emissions of certain greenhouse gases such as carbon dioxide (CO_2), methane (CH_2), nitrous oxide (NO_2), sulphur hexafluoride (SF_6), perfluorocarbons (PFCs) and hydrofluorocarbon (HFCs) [19]. Chae et al. [20], and Peacock [21] suggested that utilising industrial waste heat energy would contribute to the reduction in the emission of greenhouse gases.

The microturbine system is considered a high-grade heat energy (source) by producing a high exhaust gas temperature. Thus, this can be recovered to produce low heat grade energy. CHP (combined heat power) systems combine on-site power generation with the use of by-product heat. Continuous base load operation and the effective utilising of the thermal energy contained in exhaust gas have enhanced the economics of microturbine generation. The high temperature of the exhaust gas from a microturbine can be used directly for applications such as process heating or drying. It can also be used to operate thermally activated equipment, for example absorption chillers for cooling purposes that can be used on-site or off-site, or ORC (Organic Rankine Cycle) to provide extra electricity to cover the required needs. Commercial institutional buildings and light industrial facilities whose demand for electrical power, heating and cooling or other thermal needs occur at the same time, are usually

best suited for microturbine CHP application. Microturbines can provide electricity to replace a part of the facility demand; in order to reduce the cost of long term consumed electricity, which can be expensive when reliant on the main supplier. Also, a study has been carried out by Peacock [21] indicating that CHP systems have the potential to significantly reduce the carbon footprint.

Improvements in the cycle of the microturbine have been gained through many engineering designs. Air bearings eliminate the contamination that occurs from oil-bearing and reduces the scheduled microturbine maintenance. Although recuperators are considered heat exchangers that add extra costs to the economic visibility of microturbines, they have proved their reliability by achieving 30% of the cycle of electric efficiency. This will raise the turbine inlet temperature to 950°C. It will also provide a clean emission by reducing the combustion temperature, which decreases the amount of carbon dioxide [16]. Since the microturbine delivers a greater amount of waste heat energy compared to other engine technology, CHP becomes a natural market for it. This is also considered a valuable credit when it comes to the economic aspect, which is the driving force behind any project [3].

Following on the microturbine cycle improvements, Delattin et al. [22] demonstrated that water or steam injection into the compressed air coming from a compressor boosts cycle performance. Their study investigated the possible benefits of steam injection on the electric efficiency compared to dry cycle (without steam injection). The results showed that a 5.1% increase in efficiency was gained. However, to obtain the desired increase of efficiency, CHP mode had to disabled. Delattin et al. [22] offered no explanation for the partial load mode in steam injection. Since the compressed air contained 40% of injected water and 3.3% was superheated, internal pipe scale and contaminations were more likely to occur. Hence, more scheduled maintenance would have to be carried out.

This study has focused on the CHP of microturbines, which used the waste heat energy from the exhaust of a microturbine and utilised it in another thermal system to raise the efficiency of the system, and reduce the carbon footprint.

2.7 The Effect of Ambient Temperature:

A microturbine is small-scale gas turbine. It operates according to the Brighton cycle, as shown in Fig [2-1]. Thus, it follows the laws of physics where its performance is concerned. In other words, the changes in thermodynamic properties occurring in the

gas turbine are also employed in microturbines in the same situation. The gas turbine industry has set the design condition at ISO or ambient conditions, which is 15°C and pressure 1 Bar. The same rules in microturbines are applied to identify the output power at ISO conditions, which is normally considered a design point. Variation from ambient temperature will cause changes in the power output of the turbine [1]. The power output decreases due to the decreased air density with increasing temperature, and the decrease in efficiency is obtained because the compressor requires more power to compress air at high temperatures. Also, the air density changes with altitude. Density decreases at increasing altitudes, and therefore power output decreases [3]. Depending on the type and specification of the microturbine, its electric power output and efficiency are sensitive to changes in the ambient temperature [1]. As mentioned previously, the increase in the ambient temperature causes a reduction in the air density. Then the mass flow rate entering the compressor reduces and causes a decrease in the compressor pressure ratio and specific work, which in turns causes a reduction in the turbine pressure ratio, but without changing in its specific work [3],[23]. The reduction in the gas turbine pressure ratio is more than the increase in the compressor pressure ratio, which leads to a reduction in the gas turbine power output and efficiency.

The gas turbine is a standardised machine and it can work in different ambient conditions, which means that the compressor of the gas turbine is designed for a constant air volume [24]. Hosseini et al. [25] also indicated that the gas turbine compressor is designed for constant air volume flow, which makes the electric power output reliant on the ambient temperature through the specific mass flow rate. Furthermore, the compressor output pressure is decreased if the ambient temperature increases, which reduces the gas turbine cycle's efficiency, while an increase in air density reduces the gas turbine’s heat rate and increases its specific fuel consumption. Also, it has been found that for each 1°C increase in ambient air temperature, the electric power output of the gas turbine decreases by 0.5% to 0.9% and by 0.27% for the combined cycle. According to Yunho Hwang [26], one of the important characteristics that affects microturbine performance is the dependence of microturbine efficiency on the ambient temperature and the dependence of the power factor on ambient temperature, which is defined as the ratio of the microturbine power output to its rated power output. Yunho [26] also found that when the ambient

temperature increases more than 26.7°C, the power factor decreases, although the turbine speed is maintained at the maximum.

2.8 Partial load:

At non-peak hours, the microturbine can be operated at less than full power. The output power is reduced by decreasing rotational speed, which reduces the temperature rise and pressure ratio through the compressor and temperature drop through the turbine. Then the recuperator inlet temperature does not rise because of the reduction in turbine inlet temperature. Besides the decrease in power output, this change in operating conditions also reduces efficiency. These decreases in power output and efficiency are a result of the reduction in fuel mass flow, which leads to a decrease in the turbine inlet temperature [3].

These parametric studies are discussed and observed in the following chapters concerning the effect of temperatures, pressure variations and operating on part-load conditions.

2.9 Organic Rankine Cycle (ORC):

Over the last century, economic growth has dramatically increased in the world. This can be exemplified by the increasing number of vehicles and the multiplication of energy-consuming domestic equipments which has caused a growth in energy demand. This demand has mostly resulted in a massive consumption of fossil fuels, which causes many serious environmental problems, for instance global warming or atmospheric pollution that in turn affect the ozone layer and climate conditions [27].

The use of an Organic Rankine power cycle to recover low-grade thermal energy is becoming widely recognised as a major technology in power engineering [28]. Integrating the ORC to the energy system, such as a power plant, could achieve using low-grade energy (waste heat) to generate high-grade energy (work) [30]. The simple Rankine Cycle contains four components: a heat supplier (evaporator), power turbine, condenser and pump. The cycle begins when the refrigerant is heated in the boiler (heat exchanger) to a high temperature (A), and then transferred to the turbine where it is expanded to produce electrical energy (B). The refrigerant then passes to the condenser where it is turned into liquid (C) before being returned to the boiler to complete the cycle (D) Fig [2-4]. Despite the fact that they are linked with low

efficiencies, typical ORCs are reliably flexible, have a good safety record and only require low maintenance [31]. Additionally, the reduction in fuel cost allows ORCs to be more attractive than other low-grade heat applications [31]. The use of an ORC can result in a decrease in the specific emission of environment pollutants such as carbon dioxide due to the fact that no additional fuel is consumed [29]. Many studies have been carried out to operate ORCs as part of the power system; for example, with solar heat energy and geothermal energy [28,30].

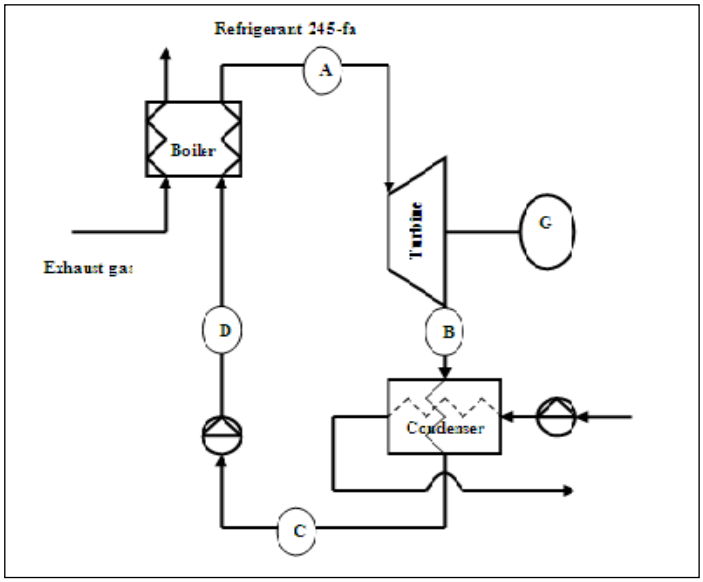

Fig [2-4], ORC process.

An ORC can not only be operated by the waste heat energy derived from a power plant but also in a solar system. Another application for ORCs is geothermal plants, where the geothermic heat sources vary in temperature from 50°C to 350°C. In cases of low-temperature geothermal sources that are less than 100°C, the ambient temperature has a significant effect on power plant efficiency [28,30].

The thermodynamic improvement has taken place in the organic Rankine cycle by adding a recuperator heat exchanger, so the vapour in the turbine is used to heat up the working fluid at the exhaust of the pump in order to spend less energy in the boiler. This enhancement adds an extra feasible cost to the system, since the temperature of the waste heat energy is enough to heat the working fluid to the desired temperature. However, it is considered a useful improvement in some applications when the source temperature is low and the boiling temperature of water (steam) cannot be reached, such as with geothermal and solar energy [27] [28].

Donghong et al. [29] used waste heat energy of 377°C produced from a gas turbine to power an ORC generating about 100kW. Furthermore, a type of refrigerant working

fluid R-245fa was selected for the ORC. They concluded that using the full load of the exhaust heat contributes to a higher grade of heat source, and this will improve the system output net power.

2.9.1 Working Fluid selection:

The usual working fluid for the Rankine cycle is water under pressure. The ORC process uses an organic working fluid instead of water. In contrast to water, the expansion in the turbine ends for most organic fluid not in a wet steam regime, however, but in a gas phase above condenser temperature. Hence, a recuperator is used to improve efficiency. Organic working fluid is preferred compared to water when the maximum source temperature is low and/or the power plant is small. Furthermore, at low source temperature, using the organic fluid as a working fluid through the cycle will lead to a higher efficiency in the turbine, and in partial load, than employing water as a working fluid [31]. Also, Saleh et al. [32] state that for low temperature heat sources the advantage of organic fluids can be noticed, because of the volume ratio of the working fluid at the turbine inlet and outlet. This ratio can be smaller for organic fluid than for water, and hence a simpler and cheaper turbine can be used.

This leads to the use of refrigerants or hydrocarbons as a working fluid. The behaviour of the ORC cycle is strictly dependent on the physical properties of the working fluid, which are considered as an important key influence on the cycle [27]. Also, Saleh et al. [32] mention an important aspect of the choice of working fluid, which is the temperature of the heat source, which can range from 100°C at low heat to medium temperature at 350°C. Moreover, the influence of the working fluid on the system's efficiency has been demonstrated in the literature by examining various types of working fluids, for instance isentropic, dry and wet ones [33]. Hung [34] reported that the irreversibility of the system depends on the type of working fluid and of heat source. So, better performance can be reached with lower irreversibility. Also, Larjola [35] pointed out that a higher power output could be obtained if the temperature difference between the heat source and the temperature of the working fluid in the evaporator was reduced due to its lower irreversibility.

Accordingly, many factors have to be examined for better selection of organic working fluid. First of all, the critical temperature of the working fluid. As Schuster et

al. [30] pointed out, fluid with a higher critical temperature allows a higher boiling temperature. However, it has lower pressure and thereby lower pressure differences are obtained. Also, the low critical temperature results in low thermal efficiency in the working fluid [33]. Secondly, the molecular weight of working fluid also plays an important role in fluid selection. A fluid with high molecular weight has a lower reduction in the enthalpy, and also has a higher critical point, which allows higher temperature sources to be used without superheat and according to that, a greater efficiency obtained [36]. Next, at higher temperatures the organic fluids usually suffer chemical deterioration and decomposition. Therefore, the maximum source temperature is limited and has to suit the chemical stability of the organic fluid. Moreover, a fluid with a high latent heat and density will absorb more energy from the source temperature in the evaporator, so both the required flow rate and the size of the facility are reduced, and also the pump consumption. Furthermore, the main parameters are the Ozone Depleting Potential (ODB) and Greenhouse Warming Potential (GWP) [27]. The protection of the ozone layer and the reduction of greenhouse gas emissions has resulted in various regulations on the international, European and national level. On the international level, the Montreal Protocol on substance stated that the ozone layer is the most important agreement. It controls the production and utilization of ozone depleting substances. The effect on the ozone layer has also been considered in the Kyoto meeting [19]. At the European level, regulation 2037/2000 bans the marketing of Ozone Depletion Potential (ODB) directly or after a transitional period [30].

The most important parameter to take into account in ORC is the efficiency of the cycle. Several simulations have been performed with different working fluids in the literature targeting their potential efficiencies. Table [2-1] shows the thermodynamic properties and the environmental data for the some working fluids [27]. Liu et al. [33] performed a simulation on an ORC with various working fluids for a hot temperature of 150°C and a cold temperature of 30°C. The result showed that R-123 had a slightly better efficiency than isopentane R-601a. Lemort [37] compared three working fluids on an ORC application hot side temperature 130°C, cold side 30°C. R-123, R-245fa and R-134a were taken as a working fluid in this experiment. The circulated efficiencies were respectively: 9.71, 9.3, and 9.74%.

Working Fluid	Slop of saturation vapour line	Critical point	Vaporization heat at 1 atm. [Kj/kg]	Boiling temperature at 1 atm.	Safety	Atmospheric lifetime	O DP	Net GWP 100 year (2012)	Phase Out year
R-123	Isentropic	184°C-36.7 bar	171.5	27.7°C	Non-flammable	1.3	0.012	53	2030
R-134a	Wet	101°C-40.6 bar	217.2	-26.4°C	Non-flammable	14	~0	1320	-
R-245fa	Isentropic	145°C-36° bar	197.5	14.6°C	Non-flammable	7.6	~0	1020	-
R-601a	Dry	187°C-33.7 bar	342.8	27.5°C	Flammable	-	~0	~20	-

Table [2-1], Thermodynamic properties of selected working fluid [27]

From the table [2-1] and from all the considered factors in terms of organic fluid selection, R-245fa has a high molecular weight than R-134a; and it is an isentropic, which allows better superheating than the wet vapour line at the exhaust of the evaporator. The critical temperature and the atmospheric lifetime of R-245fa are higher than R-134a. Although R-123 has the highest critical temperature and lowest atmospheric lifetime, it is considered as a non-null ODP and will be forbidden after 2030. Using R-245fa has been recommended to use as working fluid by Fluorocarbons and sulphur hexafluoride organisations [38], whereas R-134fa was recommended by Lemort [37]. Therefore, a comparison between R-134fa and R-245fa will take place on the proposed organic rankine cycle model, and the working fluid with better outcome results will be chosen.

As was mentioned previously, Donghong Wei et al. [29] used an ORC heated by a high-grade heat energy source where R-245fa was in use as a working fluid. The airflow was used in the cooling process at the condenser to cool the expanded outlet working fluid from the turbine. The condensing condition of the working fluid is relative to its evaporating condition. The pressure and temperature increase in the condenser by a small airflow, as well as the vaporizing temperature and pressure in the evaporator. As a result, the temperature difference was reduced between the working fluid and the exhaust. As a consequence of that, the system output net power and efficiency were decreased. Furthermore, with the increase of air mass flow rate, the vaporizing temperature and pressure decreases, and the system output performance was increased. However, a high rate of the cooling air flow will make

the working fluid have too much sub-cooling when it goes out of the condenser, so heating it again to the saturated state in the evaporator will consume a lot of heat, which in turn decreases the system's output performance. The ambient variation has a significant impact on the system's performance. Under high ambient temperature, the system's output performance was decreased, and the output power was also decreased more than 30%. In this case, maximizing the operating of the system at full load can improve its performance, since system efficiency and net power increase as the exhaust flow rate or temperature increases.

2.10 Absorption Chillers:

The use of absorption chiller as an energy conversion system in a microturbine becomes a challenging point, since the absorption chiller can provide a capacity from 10 to 40 tons [26]. It can therefore be utilised as a low-grade heat energy source by the waste heat of a microturbine in order to generate a cooling effect that can be used for air conditioning or refrigeration purposes.

Historically, according to Abrahamsson et al., in 1992 [39] Baltzar von Platen and Carl Munters from the Royal institute of Technology in Stockholm, introduced their degree project in which they invented absorption refrigeration. Then they established two companies one year later, AB Arctic and Platen-Munters Refrigeration System, and started the commercial production of the absorption refrigerator. By the 1960s, US manufactures had 100% of the worldwide market for lithium bromide/water absorption chillers, and in the late 1960s the Japanese entered the marketplace, introducing direct-fired and multi-stage absorption chillers. However, during this time, the oil price was in the range of $3 per barrel, and so electricity was affordable, which had a positive effect on the operation of electrical refrigerators [40].

The oil crisis that occurred in 1973 drove the real development in absorption chillers, motivating researchers and manufactures to consider a system that used energy in a more efficient way, and was capable of better utilisation of waste heat energy. From then on, worldwide sales of absorption refrigerators started growing, as can be seen in Fig [2-5], which is reproduced from an Oak Ridge National Laboratory publication.

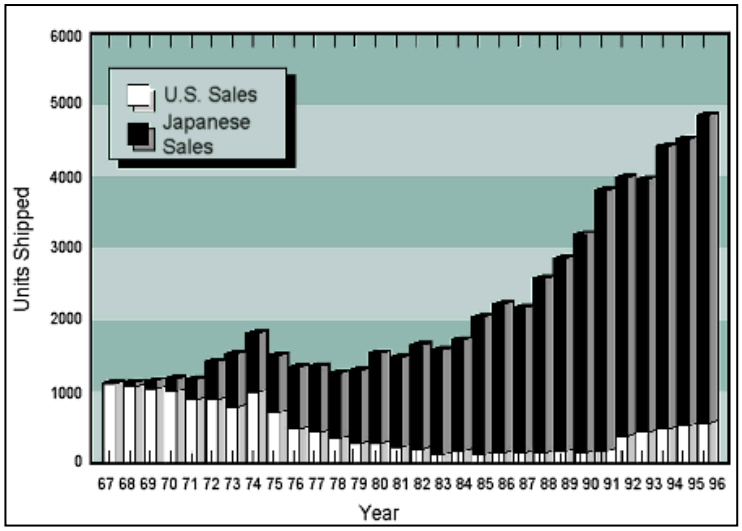

Fig [2-5], worldwide sales of the absorption refrigerator [41]

Another factor that encouraged the development and marketing of the absorption refrigerator was the categorisation of chlorofluorocarbons (CFCs) in the early 1990s as one of the alkyl halides chemical group, which are believed to be responsible for some environmental issues such as ozone depletion. This encouraged more research to find better alternatives. The Kyoto protocol [19], which calls for a reduction in greenhouse gas emissions, also encourages the use of waste heat energy utilisation systems such as absorption chillers.

2.10.1 System Fundamentals:

The working principle of the absorption chiller that generates a low capacity refregrent effects is the same as the large unit that produces a high capacity, along with the thermodynamic properties throughout the system. Absorption chillers and refrigerator cycles work according to similar techniques. Both cycles evaporate the refrigerant at a relatively low pressure to create the cooling effect, and then condense it at high pressure to reject its heat. The main difference between the two cycles is the mechanism by which the refrigerant reaches the high-pressure level. In the normal vapour compression refrigerator a compressor generates a high pressure in the working fluid, while in the absorption chiller cycle the compressor is replaced by an absorber, pump and generator, and a secondary fluid, which transports the refrigerant from the absorber to the generator [42].

According to many authors [26, 43, 44], the main operating factor of an absorption chiller is the waste heat that is obtained from a microturbine or gas turbine. It has been

stated that driving lithium bromide by the waste heat of the gas engine leads to many benefits. For instance, increasing the efficiency of the plant, reducing both operating costs and energy requirements, and producing environmental pollution at lower levels [26, 45, 46].

A single-effect water/lithium bromide chiller has been integrated in this study and it is powered by the microturbine's waste heat energy. Fig [2-6] shows the complete cycle of a single-effect absorption chiller, in which the low-pressure mixture of vapour and liquid refrigerant (A) enters the evaporator, where it boils as a result of absorbing the heat from the warm water used to transfer the cooling effect to the cooling load. The low-pressure vapour (B) is then drawn into the relatively lower pressure absorber, where it will be absorbed by the absorbent that rejects some heat to the coolant fluid. A small pump is then used to push the new mixture to the high-pressure side of the cycle, which is the generator. A recuperator heat exchanger is used between the absorber and the generator to transfer the heat between the mixture going to the generator and the absorbent going back to the absorber in order to reduce the heat energy required to boil the refrigerant in the generator, as well as pre-cooling the concentrated absorbent solution, which in turns reduces the required flow rate of cooling fluid through the absorber. The external heat energy is supplied to the generator in order to increase the mixture's temperature to the degree at which only the refrigerant evaporates and is separated from the absorbent, which needs a higher temperature to boil. The absorbent is then drawn back into the low-pressure side of the cycle, the absorber, to complete its cycle, while the high-pressure vapour refrigerant (C) enters the condenser where it condenses while rejecting its heat to a coolant fluid. The high-pressure liquid refrigerant (D) now passes through an expansion device that reduces its pressure to evaporate again using the heat of the relatively warm incoming chilled water.

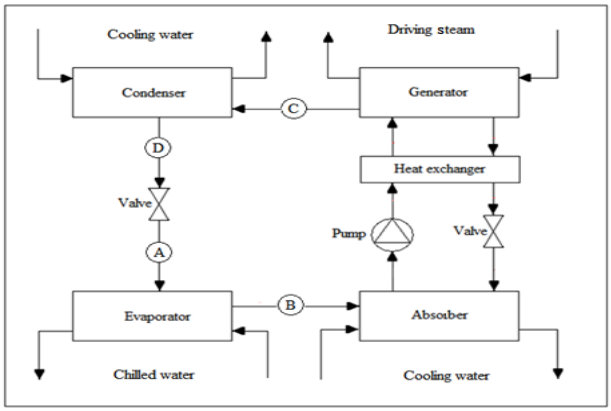

Fig [2-6], single effect absorption chiller.

The system has no moving parts except the pump, which is quieter and more economic than the compressor in the normal refrigerator. Moreover, the system can be used as low grade heat energy at a temperature in the range of 90°C to 130°C in the generator [42, 45].

A single effect absorption chiller can achieve a coefficient of performance (COP) in the range of 0.6 to 0.8, where the COP is defined as the ratio of evaporator cooling capacity to the heat energy required by the generator. There are many types of chillers, such as ammonia/water chillers and ammonia/water/hydrogen refrigerators. However, using lithium bromide as a working fluid in these types is considered one of the best choices among hundreds of working fluids [46]. Considering an average absorption chiller model, the absorption cycle refrigerant/absorbent mixture circuit can be analysed using the aqueous lithium bromide solution equilibrium chart that is shown in Fig [2-7].

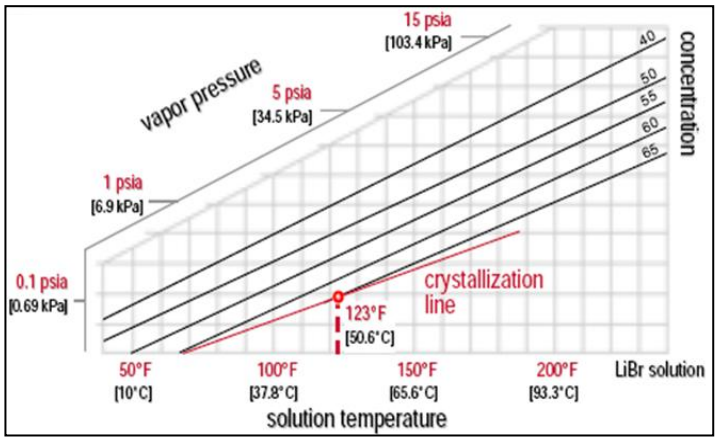

Fig [2-7], Crystallization line of the LiBr solution [42]

Furthermore, one of the most important factors that limit the operation of the absorption chiller is the phenomenon of crystallization. The crystallization line of LiBr solution is shown in Fig [2-7] with respect to temperature, pressure and concentration. It can be observed that if one or more of these variables changes, the salt leaves the solution in a solid crystalline form, making it inoperative. This could be due to electricity failure or a leak of air into absorption chiller, and if the chiller cools the water a highly fluctuating temperature may occur. The result is a crystallized salt inside the heat exchanger interrupting the chiller's operation. However, safety controllers are used in modern absorption chillers to monitor and control the solution concentrations and temperatures to avoid crystallization. Accumulation of air inside the chiller may also affect the absorption chiller's efficiency. This happens if the air leaks into the chiller changing its operating pressure and temperature, and this is encouraged by low pressure. To resolve

this issue, a control system called a purge system is used, which maintains the chiller operating temperature and pressure, and detects any leak through the cycle [42, 45].
Moreover, different designs of absorption chiller are commercially available, and can be classified by the heat source, operating fluid type, effect number and coolant fluid.
The most common classification of absorption chillers with a short comment for each type is illustrated in table [2-2]. The direct-fired chiller is not applicable for use with the waste heat energy recovery applications as it includes its own powering mechanism. The water-ammonia absorption chiller is similar to the LiBr-water chillers, and each fluid operates different absorption chillers. The air-cooled absorption chillers are similar to the water-cooled chillers, except that the chillers need cooling towers, which adds extra costs.

Classification	Type	Comments
Heat Source	Direct-Fired	Includes a burner that operates on natural gas or fuel oil
	Indirect-Fired	Utilizes any eternal low-grade heat i.e. solar or waste
Fluid Type	Water-Ammonia	The water is used as an absorbent, while the ammonia is the refrigerant. Can achieve less than 0°C, but ammonia is a toxic gas
	LiBr-Water	The water is a refrigerant, while the LiBr is the absorbent
Effect Number	Single-Effect	Includes single generator, condenser, evaporator, absorber, heat exchanger and pump.
	Double-Effect	Includes additional generator, heat exchanger and pump.
Coolant Fluid	Water-Cooled	Both condenser and absorber are air-cooled; there is no need for a cooling tower
	Air-Cooled	Both condenser and absorber are water-cooled; there is a need for a cooling tower

Table [2-2], Absorption chiller classification [42, 45]

Single effect and double-effect absorption chillers have the same operational principle, except that face that double-effect has two generators, which are powered by an external heat source, and the water vapour generated in this generator is used as a heat source for the second generator. The required temperature of the heat source in this case needs to be in the range of 155°C to 205°C, which is higher than that required for the singe-effect absorption chiller [42]. Thus, this type of absorption chiller has not been

considered in this study, because it is not suitable for waste heat utilisation application, as the exhaust mass of the microturbine's waste heat energy is limited.

2.10.2 Microturbine efficiency enhancement and absorption chiller cooling effect:

One of the factors that affect microturbine performance is the ambient condition, which includes temperature, pressure and humidity. The microturbine is first a gas turbine and therefore follows the laws of physics where its performance is concerned [2]. The chilled water provided from an absorption chiller can be employed to pre-cool the intake air entering the microturbine. It has been found that if the absorption chiller is used for an in-site purpose by utilising the chilled water to per-cool the intake air entering the microturbine, that microturbine's efficiency can be improved [26]. A study has been carried out by Ameri and Hejazi [47] on 170 gas turbine units in Iran to observe the effect of the variation in ambient temperature, and it has been found that the variation of ambient temperature caused a loss of 20% of the rated capacity of all gas turbine units. They also conducted another study on only five gas turbines, and the difference between the ambient temperature and the ISO conditions was on average 11.8°C. As a result of this research it has been concluded that, for each 1°C increase in ambient temperature, the power output decreased by 0.74%, and cooling the compressor's intake-air temperature was suggested to improve the gas turbine cycle efficiency, which can be applied on the microturbine cycle to gain a desired improvement in cycle efficiency. Therefore, one of the most valuable applications of the absorption chiller is in cooling the intake air entering the compressor of the microturbine or gas turbine to the ISO temperature of below 15°C. Integrating the absorption chiller into the microturbine not only improves the cycle performance, but also helps the microturbine to work as a prime mover by utilising its waste heat energy, which increases its energy utilisation factor (EUF) and simultaneously reduces the CO_2 emission rate.

In the Arabian Gulf areas, where the average ambient temperature varies by more than 30°C from summer to winter, a study has been done by Adel et al. [48] which shows that using an absorption chiller powered from the waste heat of the exhaust gases to cool the compressor intake air is recommended in these areas. Also it was found that the compressor air temperature was cooled down from 40°C to 30°C by using the exhaust

gas with a mass flow rate of 300kg/s at 450°C of gas turbine, which increased the power output by 10%. Although a 10% increase in the power output had been achieved, it could have been even more than that if they had used a larger size of absorption chiller producing a higher capacity in order to cool the inlet-air to the ISO condition (15°C) or lower than that, as reported by Boyce [49], who proved that the absorption chiller is capable of cooling the inlet-air to 10°C.

Another study shows that using the LiBr/water absorption system to cool intake air into microturbine compressor to the ISO level increased the output power by up to 13% if the cooling capacity was used at 40°C. Also, other factors benefit from this pre-cooling, Lower costs, investment and maintenance are required than for the normal air-cooling system [26]. However, in this study, the microturbine was used to provide the power to operate the single effect absorption chiller system, and the generated cooling capacity from the absorption chiller was used for condenser sub-cooling and air pre-cooling in both systems, and also to pre-cool the inlet air to the microturbine compressor. Thus, higher output power could be achieved, as well as lower intake air temperature if all the chilled water with higher mass flow rate from the absorption chiller was just used to pre-cool the intake air to the microturbine compressor.

As is pointed out by Kakaras et al. [50], the variation in the ambient temperature could lead to power loss. This could be more than 20%, and coupled with an increase in the specific fuel consumption. This effect of ambient temperature was demonstrated on a simple cycle of stand-alone gas turbine and on a combined cycle gas turbine using a computer simulation (IPSEpro) for the integration of an evaporative cooler and an absorption chiller to reduce the temperature of the compressor intake air. The results indicated that for the combined gas turbine cycle both the power output and the efficiency improved by 6.8% and 0.44% respectively.

Another study conducted by M. Medrano et al. [51] showed that the effect of using the waste heat energy of the microturbine to power the absorption chiller had a significant effect on the performance of the chiller when the temperature of the inlet chilled water increased with a constant intermediate level temperature, or if the inlet cooling water temperature decreased with a constant low temperature level. Both cases resulted in high COPs and higher cooling capacities, which in turn contributed to a better cooling to the microturbine intake-air compressor. However, the microturbine used in Medrano's study generated 30 kW, and this study can be improved if the microturbine

generates higher output power, due to generating higher mass flow rate and exhaust gas temperature. Also, the absorption chiller unit used in this study was generating a cooling capacity in the range of 60 kW. However, a high cooling capacity can lead to a significant improvement to the gas or microturbine cycle.

Carles et al. [52] discuss the effect of ambient temperature on microturbine performance. The power and efficiency of the microturbines decrease at high levels of inlet air temperature. The main reason for this degradation is the lower mass of fluid circulating through the system that is obtained from an inlet volume of air with a lower density. For part of this study, they used the exhaust temperature of four units of microturbines which were powered by biogas fuel, each unit generating 30kW to drive a single effect absorption chiller. Moreover, the obtained chilled water will be used to condense water in the biogas pre-treatment process and cool the inlet air to the microturbine's compressor. It was found that, the inlet air temperature was reduced to 10°C, and the carbon footprint decreased.

Alhazmy and Najjar [53] pointed out that the performance of gas turbine power can be improved by a cooling effect on the inlet ambient air. This study used two different air coolers to cool compressor intake-air. First, a water spraying system was used, which improved the power output by 1.95% and the efficiency by 0.18% at an ambient temperature of 50°C. In the second method, a cooling coil cooler system was employed, which also improved the gas turbine power output by 18%. However, both methods demand electricity to be operated which consumes some of the generated power. If no external source of power is provided other than gas turbine, then the electric power and the efficiency of the plant are reduced. These results clearly showed that neither the spray cooling method nor coil cooler was as efficient as in-site cooling by the absorption chiller, which raised the efficiency of microturbine in Carles et study [52].

These studies and many others [54, 55] tend towards the same conclusion, which is that using an absorption chiller to cool the intake-air of any microturbine or gas turbine is economically viable, and can both enhance the microturbine performance and reduce its environmental impact. However, these studies only used the first law analysis to examine their performance on the power plant after retrofitting the cooling system. Moreover, this study aimed to use both first and second law analysis in the assessment of the power plant after the improvement and to investigate the environmental benefit.

2.11 Desalination:

Over the past two decades, an extensive amount of research into desalination processes has been undertaken either to improve product quality or to reduce the fresh water cost through minimizing fuel consumption, using alternative energy sources or improving process efficiency.

Desalination can be defined as the process that removes the excess salt and other minerals from seawater or brackish water in order to obtain fresh water suitable for animal consumption or irrigation. If almost all of the salt is removed it can be consumed by humans. The concept of desalination was processed a long time ago, and humans have known about it for more than two thousand years [56].

The first distillation process was reported by St. Basil in the late 400s AD, and is believed to have been performed by seamen using a fire to boil the seawater inside a vessel and then using a natural sponge as a condenser over the mouth of the vessel [56].

The need for desalination became more pressing with European colonialism, in order to serve remote areas of the world. This encouraged the development of the desalination process, and a number of studies were published on the topic. Perhaps the most important contribution was that of Degrand in France in 1833, with his recovery of the heat of the evaporation in the feed water, which improved the economy of his single-effect evaporation machine. This can be thought of as the first attempt at utilizing waste heat [56]. On the other hand, in 1855, Fick dialyzed solutions through an artificial membrane formed from collodion. The work of both Fick, and Graham who followed him and who has been credited with the first use of the term dialysis to explain the discriminating diffusion process across semi-permeable membranes, can be considered as the first application of the pressure-driven membrane process, which is known today as the RO desalination process [57].

2.11.1 Water resources in Saudi Arabia:

Saudi Arabia is an arid zone country with limited water resources. The geographic location plays a role in increasing the demand for desalination. Al-Sahlawi reported that, by 2010, the desalination domestic demand for water will satisfy more than 70% in Saudi Arabia [58]. According to a United Nations report, Saudi Arabia is the world's leading producer of desalinated water. In 2000, 21% of the world's

desalinated water was produced in Saudi Arabia [59]. Furthermore, Saline Water Conversion Corporation (SWCC) is responsible for water development and it is authorised by the government. SWCC has never stopped planning for and installing new desalination plants everywhere in the kingdom, in order to meet the 3% annual increase in potable water demand [58].

In addition, more studies and research are needed to improve the current plant, and finding new development ideas for desalination becomes very important for meeting all need for potable water, be it industrial, domestic, and agricultural needs, or people who are living in remote arid or semi-arid zones.

2.11.2 Desalination Methods:

The desalination process is classified according to two main categories: the thermal process and the membrane process. The former is the oldest and most commonly used. The thermal process is also divided into two main types according to the separation method used, which are evaporation and freezing. The freezing process is not commonly used as the evaporation process for a number of reasons, for instance difficulties in handling. Only the most common technique of desalination process will be briefly covered in the following section. Generally, the main desalination processes are summarised in Fig [2-8].

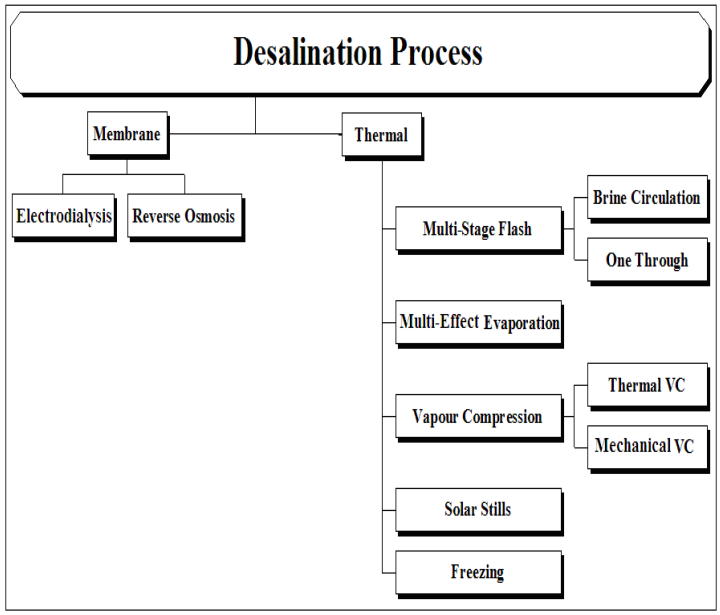

Fig [2-8], Desalination process categories

The main mechanical technique of desalination is to use a form of energy to separate the excess salt and other unwanted minerals from seawater or brackish water. The desalination process may be characterised according to the form of energy used in the separation process, which can be mechanical, electrical or thermal energy. The heating and cooling processes are included in the thermal energy separation method.

2.11.3 Thermal desalination process:

Thermal desalination is also known as a phase-change separation process since it contains a change in the water from liquid state to vapour state, which occurs in evaporation, or in the solid state which can be found in the freezing process.

2.11.4 Multi-stage flash:

A company in Scotland called Weirs of Cathcart gained a patent of the inventing the multi-stage flash process (MSF). This was about fifty years ago. As reported by James Birkett, Waterhouse had outlined the idea of this process in 1900 [56]. Using both temperature and pressure explains the main function of this thermal process, in order to flash a portion of seawater into steam in multiple stages. This process uses high-grade heat energy to boil the feed water, as well as electric power to raise the pressure of the feed water. Fig [2-9] shows a single-stage of the multi-stage flash process. The working cycle of this process begins with the seawater being fed into a container called a brine heater in order to be heated under high pressure to a temperature ranging between 90°C and 120°C. Then, this high-pressure stream of hot water is suddenly led to another container stage, which has a lower pressure than that in the brine heater. This sudden change in pressure at high temperature causes the water to boil rapidly and a portion of it to flash into stream. The remaining water proceeds to another stage at lower pressure than the previous stage to repeat the same cycle of flashing. The generated steam condenses in the tubes of a heat exchanger carrying the feed seawater at an ambient temperature to the brine heater, passing through each flashing stage. This will raise the temperature of the feed water, which will reduce the thermal energy needed in the brine heater to increase its temperature [59, 60].

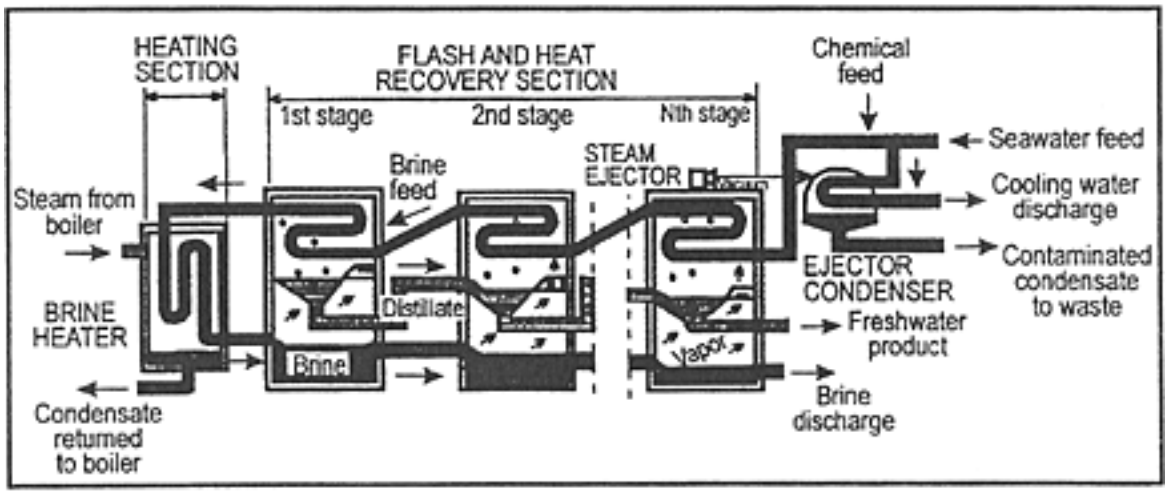

Fig [2-9], Multi-stage flash process (MSF)

After the final stage the condensed steam is collected as potable water, which is then chemically treated to adjust its hardness before storage or usage. The distillate can be exposed to contamination by brine mist produced from the sudden evaporation into water vapour, so a separator called a demister separates it from the condensing vapour. This process is called 'once through MSF', which means that the remaining water gained from the last stage drains to the sea, while the feed water is pumped directly into the plant coming from the sea.

Multi-stage flash technology is considered a mature technology, due to its simplicity in construction, operation and maintenance. It has no moving machinery except for normal pumps. However, the difficulty of this process can be found in a part where an increase in the top brine temperature takes place (TBT). In order to improve the performance ratio of this process, which is limited to 120°C to avoid corrosion and control scale, despite that anti-scale treatment is already in use [59, 61, 62]. In general, this process consumes 4kWh of electric power with $8m^3$ of steam at a temperature between 90-120°C, at lower than atmospheric pressure, to produce $1m^3$ of potable water [59]. Therefore, the multi-stage flash process is not included in this study and cannot be operated with microturbine waste heat energy, due to its high consumption of both electricity and high-grade heat energy.

2.11.5 Multi-effect distillation

Multi-effect distillation (MED) simply uses distillation processes, which are evaporation and condensation, to produce potable water. The fundamentals of this process are just like any other thermal desalination process. However, the MED desalination process uses boiling in order to evaporate seawater, leaving the salt on the heating surfaces as a result of water evaporation. This diminishes the efficiency if the top boiling temperature is limited to 70°C.

From the historical overview, in 1560 the first large land-based plant was built in Tunisia [56], which makes this method the oldest distillation process used for seawater desalination. A high water quality, reliable design and good operating history have played a role in distinguishing MED from other desalination process. Also, on a mass production basis, it provides a relatively high unit capacity and high performance ratio by adding an extra number of effects, which in turn reduce the cost of desalinated water [59].

The MED process shares the same concept with the MSF process. The concept of MED is to reduce the pressure through a number of effects, and each effect has lower pressure than the previous one. This allows the seawater to boil and evaporate multiple times but without providing any extra thermal or electric energy after the first effect. The following Fig [2-10] shows the MED process where steam, typically at a temperature of 70°C and with low pressure (0.2 to 0.4 bar), is fed into a series of tubes where it releases its heat and condenses, heating the surface of the tube [59].

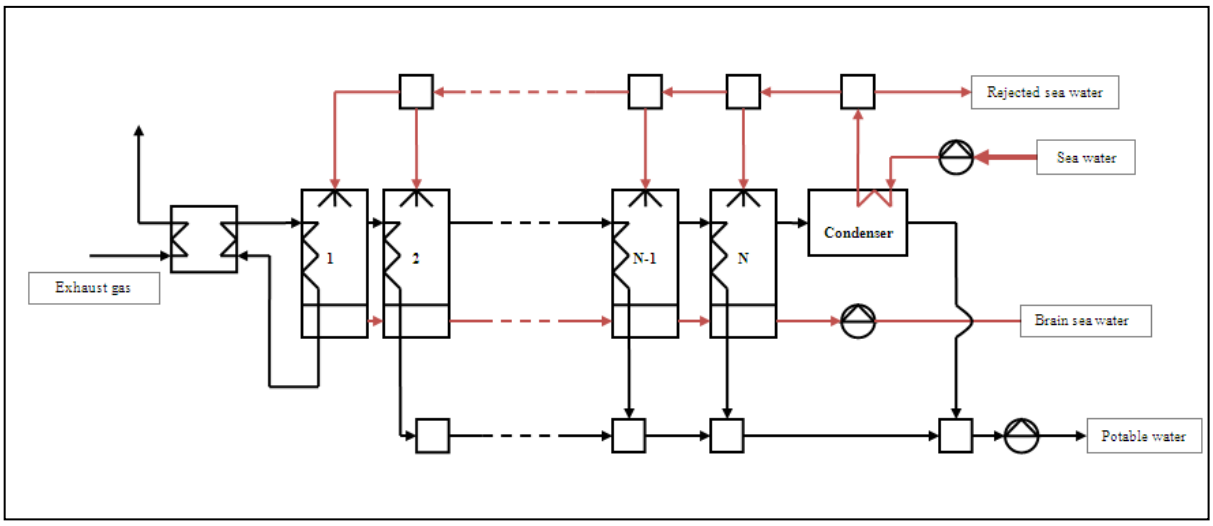

Fig [2-10], MED desalination process.

The seawater is sprayed onto the surface of the evaporation tubes to obtain fast boiling and evaporation. On the other side of this tube the steam condenses and goes back to be used in the boiler again, while the water left from the first effect transfers to the next effect with a lower pressure than the previous one. Then the same cycle is repeated in the subsequent effect. The steam generated from the last effect leads to a condenser to condense and preheat the feed seawater before entering the process [61, 62].

Two types of MED are in operation to produce potable water. The first type is low temperature multi-effect distillation (LT-MED), where the incoming steam temperature is 70°C, while the last effect has a temperature in the range of 40°C. These temperatures reach the standard of eliminating scale formation through the cycle, and make it possible for efficient recovering of any type of waste heat energy, as well as enhancing the plant availability and reducing the cost of maintenance by allowing the use of cheaper material. The second type doubles the capacity that can be produced and more effects can be built within the unit. In this type it is necessary to add a chemical pre-treatment to control scale formation [59, 60, 61].

The improvement of the MED desalination process was obtained by installing a steam ejector that uses a high-pressure steam, which is called motive steam, that expands through the steam ejector's nozzle at high velocity. The high velocity steam entrains a suction steam that is extracted from a low-pressure steam stream, located between the last effect and the condenser of the MED plant. Both motive steam and suction steam are then forced into a mixing chamber and combined to power the MED brine heater. So, the amount of steam needed to power the MED is reduced and this also increases the thermal efficiency of the plant [61, 62]. This process is known as thermal vapour compression multi-effect distillation (TVC-MED), as illustrated in Fig [2-11]. Installing the steam ejector in the TVC-MED desalination process is the only difference that cannot be found in the MED desalination process. Other than that, both processes are similar.

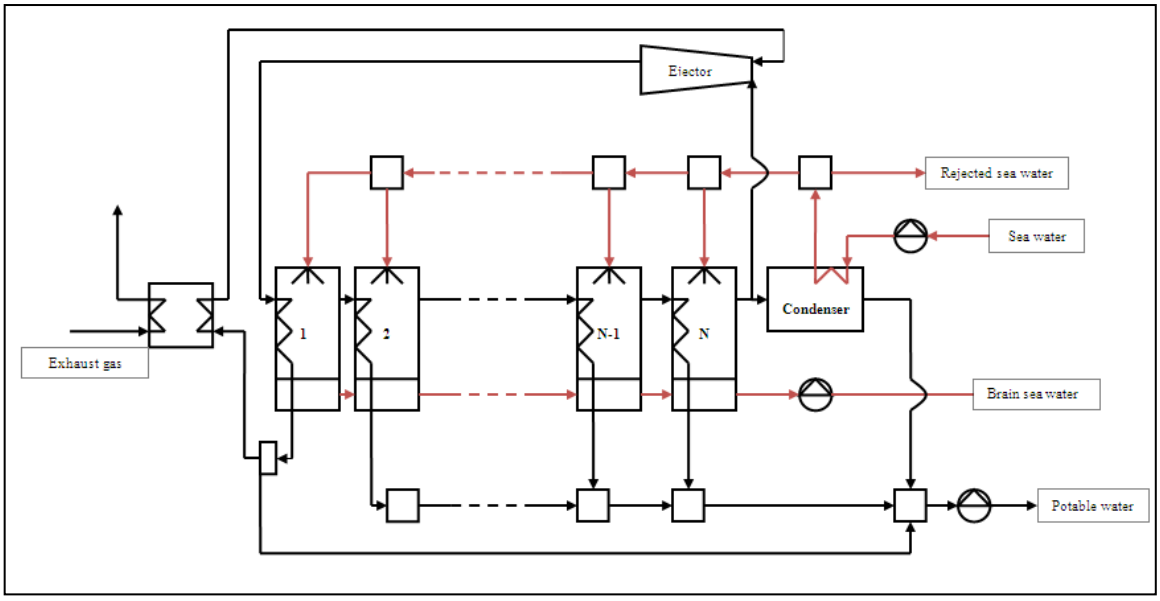

Fig [2-11], TVC-MED desalination process.

The flow of non-condensable gases inside the MED desalination's condenser and evaporators becomes an issue that affects its performance. These gases are caused by a leakage of ambient air into the evaporators that are operating at vacuum pressure, or from the gases dissolved in the feed seawater, such as N_2, O_2 or CO_2 [63]. These gases reduce the heat transfer between surfaces and prevent the vapour from reaching them by building a layer on the surfaces, which also causes a reduction in the condensation rate. The effect of non-condensable gases can be treated by better designing, manufacturing and close inspection of the outer surface to prevent any leaks [63]. However, in the MED process the effect of these gases is minimal compared to other thermal desalination processes, due to the low evaporating temperature, which is in a range of 40-70°C [62].

Among all types of desalinations systems, MED is considered the most efficient thermodynamic method. Therefore, this type of thermal desalination has been included in this study. Since the thermal desalination technologies are not common for small scale water production, and it can be powered by the waste heat energy from high-grade heat, the opportunity of modelling and simulating small scale multi-effect distilled desalination (MED) is becoming a great challenge. The choice of MED in this study was based on a number of factors, as summarised by Kronenberg and Lokiec [64]. Firstly, a long plant life that exceeds about 25 years due to low corrosion

rates, is due to the low operating temperature of 70°C. Secondly, a low product cost as a result of consuming low-grade heat energy and less operating and maintenance costs. In addition, due to the low level of corrosion and scaling rates, there is high reliability and availability (typically 95%), and also minimal maintenance is required.

2.11.6 Membrane Desalination process:

Membrane desalination is another type of separation mechanism in desalination technology, and it can be defined as a semi-permeable barrier that just allows water to pass through with no salts. This process is considered the main concept of the membrane desalination process. A number of separation techniques are available as mentioned in Fig [2-8]. However this study will only concentrate on reverse osmosis due to its ability to be driven by a small-scale power plant.

2.11.7 Reverse osmosis:

The phenomenon of osmosis was observed in 1748 by the French cleric, Abbe Nollet. Up until 1867, only membranes of animal or plant origin were used in water production. The first synthetic membrane was made of copper ferro cyanide by Traub [65].

Reverse osmosis (RO) is a pressure driven separation technique based on a property of certain polymers called semi-permeability. These polymers are very permeable to water, but their permeability for dissolved substances is low. This is a pressure driven membrane process in which the natural flow of osmosis is reversed by applying pressure in excess of the osmotic pressure. The process starts when the feed sea water passes through the pre-treatment unit in order to prevent salt precipitation or micro-organism growth, and then proceeds to a pressure vessel where it is forced to high pressure, and at this time its salt concentration is maintained, discharging a portion of it at this point before it passes through a membrane as shown in Fig [2-12]. The pressure applied in reverse osmosis applications varies from 15 to 25 bars for brackish water and 60 to 70 bar for seawater. This variation in pressure depends on a number of factors, such as water temperature and salinity. After this the potable water passes through the membrane assembly with a small amount of salt and then proceeds to the post-treatment unit where it is stabilised for storage or usage [66]. A high salt rejection as well as high permeability should be considered in the used membrane,

with regards to the potable water. Moreover, in cases of fouling and deformation, the membrane should have an efficient resistance against these factors [65, 67].

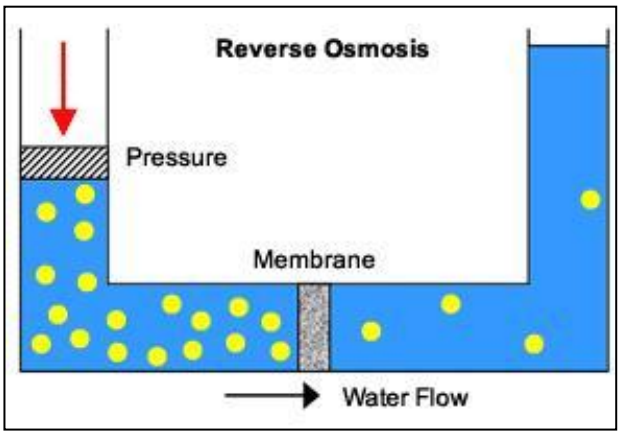

Fig [2-12], Reverse Osmosis.

Currently, two types of membrane are commonly in use, which are the hollow fibre and the spiral-wound models. The former is made of a large number of fibres folded to form bundles, with a plastic tube inserted in the centre, and the assemblies inside it are wrapped and sealed, so this leads to a compact overall design by allowing the largest possible surface area per unit of volume, which makes the membrane easier to maintain or replace. The latter type, which is the spiral-wound model, is made of a flat sheet membrane enclosed between layers of permeate carrier materials and cast into a support fabric, forming a leaf. Two or more leaves are usually rolled into a cylinder, and attached to a permeate tube. The advantage of this model is its ability to be operated at high pressure, up to 80 bar, and also it has a good resistance to fouling [60, 61, 62].

As concerns this study, the membrane separation technique is not involved due its high electricity consumption rate.

2.11.8 Utilization in Desalination Plants:

The demand for potable water is gradually increasing and the available source of potable water is facing shortages, particularly in arid or semi arid zones. The desalination plant has become one of the most efficient thermal applications that can recover waste thermal heat energy. Moreover, the operational costs in desalination

plants could be significantly reduced by waste heat energy, which will ensure a low-cost product and enhance desalination plant reliability.
A brief review of integrating the high-grade energy to operate the desalination process will be provided through a number of published studies.

In 1981, Tidball [68] described the use of an RO desalination plant by using a turbine to provide the electrical energy to the high-pressure RO pumps. The design of the turbine was to utilise the energy from the high pressure discharged waste brine from the RO plant itself to provide 30% of the electricity required by the plant's pump. The study was aimed at using the high-pressure discharged waste brine from the RO plant to provide 30% of the electricity required by the plant's pump. The used turbine was designed to support this idea. This design succeeded and 750m^3/day of potable water was produced with an approximate consumption of 2.5 kWh/m^3. It was concluded that the system's economic feasibility is controlled by the temperature and availability of the waste heat source and the salinity of the feed water.

A paper was published by Aypar [69] suggesting how an MED desalination plant might be built that utilized the waste heat of two 60MW gas turbines, recovering 300 tons of saturated and pressurised waste water coming out of the boiler. This study was performed as a solution for the shortage of potable water in Cyprus. It was found that the production rate of the MED desalination plant could be affected by its temperature difference. At a temperature difference of 10°C, the production of 80m^3/h could be achieved by the MED desalination plant.

Henry and Teresa [70] have conducted a comparison between two or more processes in order to address the ideal desalination process for a source of energy. They have investigated the best desalination process for the utilisation of waste heat energy in a 1000t/day sulphuric acid plant. A comparison was made between the MSF, MED and TVC desalination processes based on the first low thermodynamic analysis. It was concluded that, on an economic basis, the MED process was the best with a unit cost of 0.9\$/m^3, followed by the TVC-MED process with 1.74\$/m^3. On the production basis the result shows that the TVC-MED produced 5680m^3/day, while the MED produced 3400m^3/day and the MSF 1150m^3/day.

Another study included a comparison between the MSF and MED desalination processes was performed by Shih [71]. A sulphuric acid plant's heat exchanger was used to recover the heat from circulating acid and preheat the feed seawater. Satisfying the sulphuric acid plant's demand for cooling water was the purpose of integrating the desalination process into the system. The study concluded that the MED process was able to produce 54720m^3/day of potable water. However, it was found that operating the MSF process by the provided source was impossible if the amount of seawater was limited for the benefit of the waste heat source plant. Even if this was not the case for such a source, the MSF process only produced 18288m^3/day at a very low gain output ratio of 1.78 in comparison with 4.48 for the MED process.

A comparison between the RO and MED processes was carried out by Methnani [72]. This study was performed by operating two different power plants, a 600MW combined cycle (C.C) power plant and a 660MW gas-cooled reactor. The MED process in the gas-cooled plant was coupled with the pre-cooler and the inter-cooler, while in the C.C power plant the heat recovery steam generation (HRSG) unit powered it. Both power plants are directly powered by the OR process. The findings showed that the MED process in both power plants performed similarly, by producing 100,000m^3/day of potable water, and the gain output ratio (GOR) was 8, with a specific heat consumption of 80.67kWh/m^3. However, the thermal energy utilisation in the (C.C) power plant was better by 12.7%. Also, a same amount of 100,000m^3/day of potable water was produced by OR, with an electrical consumption of 285MWh, which means 23% of the total generated power. The conclusion of this study indicated that the potable water cost was lower in the RO than the MED process. However, a study performed by Nisan and Benzarti [73] also discussed the comparison between RO and MED, which concluded that the most profitable and economical results are obtained in the MED desalination.

A computer simulation tool was developed by Kamali and Mohebinia [74] in order to investigate the difference between the MED and TVC-MED processes. The study showed that the GOR in TVC-MED improved to 8.8 in comparison with MED, where GOR was 8. The potable water in TVC-MED was 1800m^3/day, while it was 1536m^3 /day in the MED process. It has also been reported that if the heat transfer area of the

used condenser is increased, the performance of TVC-MED can be improved by showing a better GOR. Moreover, according to Kronenberg and Lokiec [64], the TVC-MED process is considered an improvement on the traditional MED process.

Most of the studies showed the effect of using the waste heat energy for recovery in the desalinations process from the economic and thermodynamic points of view. However, the effect of this integration on the environment has not been commonly reported. Thus, one of this study's aims is to calculate and investigate the environmental impact before and after improvement. In addition to evaluating the thermal utilization of the consumed fuel, it is necessary to calculate the amount of carbon dioxide emitted from the plant in kjCO_2/kW, as well as providing the energy analysis to evaluate the plant's performance. The exergy analysis is employed as part of this study, which provides more accurate and specific results.
The most efficient and economical desalination process reported in the literature was the TVC-MED followed by the MED process. Therefore, these two types of desalination were involved in this study to determine the most efficient process based on the environmental impact of each process, as well as the first and second thermodynamic law analysis.

2.12 Exergy Analysis:

Exergy analysis was involved in this study to evaluate the performance of all the proposed plants. This investigation was employed on all plants before and after integration. The exergy is defined by introducing its fundamentals and reviewing a number of studies that involved exergy analysis as a part of their findings.

The first law of thermodynamics states that energy cannot be destroyed and is concerned only with the amount of energy, paying less attention to its quality. The second law of thermodynamics states that the entropy of an isolated system that is not in equilibrium would tend to increase over time. Therefore, according to the second law the energy is not totally useful work. As a result of increasing in entropy, a portion of the energy can be degraded. The exergy is defined as the maximum theoretical useful work obtainable that brings the system to equilibrium with the environment. The use of exergetic analysis can exactly clarify the inefficiencies among the plant's components and figure out the case and location of any degradation

of energy, as well as finding the true magnitude. Neglecting the nuclear, electrical, surface tension, and magnetic effects, the total exergy of a system consists of four components: kinetic exergy E^{KN}, potential exergy E^{PT}, chemical exergy E^{CH} and physical exergy E^{PH} [75, 76, 83].

$$E = E^{KN} + E^{PT} + E^{CH} + E^{PH} \tag{2-1}$$

If the above equation (1) is expressed on the basis of mass, it will denote the total specific exergy (e) and can be written as follows:

$$e = e^{KN} + e^{PT} + e^{CH} + e^{PH} \tag{2-2}$$

The kinetic exergy can be defined as the exergy of the system due to its motion. The potential exergy can be defined as the stored exergy within the system:

$$e^{KN} = \frac{1}{2}V^2 \tag{2-3}$$

$$e^{PT} = gZ \tag{2-4}$$

Both the kinetic and potential exergies are neglected in this study, as it is assumed that there is no variation in the system's speed or elevation [75-77]. The chemical exergy (E^{CH}) is the maximum theoretical work obtainable as it passes to a chemical equilibrium with the reference environment at a constant temperature and pressure [78]. The fuel stream was modelled as an ideal gas, and its chemical exergy is calculated as follows [79]:

$$E_{Fuel} = \Theta \times \eta_{COM} \times \dot{m}_{Fuel} \times LHV \tag{2-5}$$

where (Θ) denotes the molar Gibbs function of formation. The chemical specific exergy for all other streams can be calculated with the following equation:

$$e^{CH} = \overline{R} T_o \ln x_i^e \tag{2-6}$$

where ($\bar{R}$) and (x_i^e) denote the universal gas constant and the mole fraction of gas (i) in the environmental gas phase, and T_o represents the environmental temperature [75]. Most streams have a small chemical value, so they cancel each other out during the analysis as there is no change in value across most of the system components. Therefore, it can be ignored, causing a negligible error in subsequent calculations [75-77], with the exception of the chemical exergy in the fuel stream.

The physical exergy (E^{PH}) is the maximum theoretical work achievable when the system passes from its initial state at pressure P and temperature T to the reference condition at pressure P_o and temperature T_o. The physical exergy can be calculated as follows:

$$e^{PH} = (h - h_o) - T_o \times (s - s_o) \tag{2-7}$$

where h and s denote the enthalpy and entropy respectively and the subscript (o) refers to the reference condition. Assuming that all components are operating in a steady state then the exergy balance can be expressed as follows [80, 81]:

$$\Sigma \dot{m} e_{in} = \Sigma \dot{m}_{out} + \Sigma_j (1 - \frac{T_o}{T_j}) \dot{Q} + \dot{W}_{net} + \dot{E}_D \tag{2-8}$$

where (E^D) denotes the exergy destruction rate as it is commonly referred to the availability destruction, the irreversibility, and the lost work, which is dependent on the boundary selection. The exergy balance equation (2-8) represents the exergy loss associated with heat transfer between the surface of the selected boundary and the reference conditions. Moreover, based on the system boundary selection, this term vanishes if $T_o=T_j$. In this study, it is assumed that the system is well insulated, so this term will be ignored as the boundary chosen satisfies $T_o=T_j$ [77, 78].

The exergetic efficiency (η_{II}) is used as a performance parameter to evaluate the thermodynamic performance of the overall plant. It is defined as the ratio between the exergy of product and the exergy of the input fuel [75].

$$\eta_{II} = \frac{E_p}{E_{Fuel}} \tag{2-9}$$

In addition, the exergy destruction of component (i) in the power plant is used once to compare to the total exergy destruction of all components (Ψ_D). Also, it compares to the rate of fuel supplied to the system (Ψ_{Fuel}), as follows:

$$\Psi_D = \frac{E_{D,i}}{E_{D,total}} \quad \text{and} \quad \Psi_{Fuel} = \frac{E_{D,i}}{E_{fuel}}$$

(10)

The exergy destruction for each component is obtained by calculating the exergy balance, and then finding the other exergy parameters by using the exergy destruction in calculations.

2.12.1 Power Plant

A study has been carried out by Ameri et al. [82] performing an exergy analysis for a 420 MW provided by two gas turbines combined with two HRSG units. The main source of exergy destruction in the gas turbine was caused by the combustion chamber due to the chemical reaction and the large temperature difference between the burner and the working fluid as has been indicated. It also resulted in the gas turbine cycle having the highest exergetic efficiency of 44% in comparison with the other components of the plant.

Another study [79] investigated the exergy analysis of a 320MW gas turbine. It was found that the combustion chamber was the main cause of the plant's exergy destruction.

2.12.2 Organic Rankine Cycle:

A few studies have been carried out to evaluate the exergy analysis of ORC in comparison with the studies published on energy analysis.

An exergy analysis was evaluated by Donghong et al. [29] in an ORC with refrigerant fluid of R245fa that was powered by the waste heat energy of a gas turbine. It was found that the distribution exergy destruction rate in the system varied from component to component. However, the biggest exergy destruction rate was found in the evaporator, due to high rate of heat transfer and the mixing process. Also, it was

noticed that, as the exhaust temperature or its mass flow rate increased, the exergy destruction in the evaporator and condenser increased.

Al Sulaiman et al. [83] integrated the ORC unit in their study for an electrical power production. The ORC was powered by a biomass combustor, and n-octane was selected as a working fluid through the ORC. It was found that the two main sources of exergy destruction are the biomass combustor and the ORC evaporator with 2200kW and 1500kW respectively. They used the pinch point equation, which was given to be the difference between the working fluid temperature and the exhaust temperature from the biomass combustor in the evaporator of ORC. The variation in pinch point value had an impact to the exergy destruction of this study, as it was concluded when the pinch point increased and the exergy destruction decreased. Therefore, the exergy destruction of the biomass combustor decreased from 2200kW at 20 K to 2000kW at 60 K, and in the ORC evaporator it was decreased from 1500kW to 1300kW at 20 K, 60 K respectively. It was finally suggested that an improvement in biomass combustor and ORC evaporator design was important for reducing the exergy destruction.

Tchanche et al. [28] used a micro-organic Rankine cycle powered by a solar system to derive a small-scale reverse osmosis desalination system. The working fluid in this study was R134a. The results showed that the highest exergy loss occurred in the turbine, which represented 65% of the total exergy destroyed in the system. It was stated that the poor performance of the expander was due to the irreversibilities during the expansion process. For example, radial and flank leakage and thermal losses. However, this study was not in agreement with the results of other studies. This could be due to the fact that the mechanical efficiency of the turbine was 60%, or the inlet pressure into the turbine was high, as stated by Al Sulaiman et al. [83], who discussed the effect of the turbine's inlet pressure variations on the exergy efficiency and exergy destruction rate. The pressure limit was from 1000 to 5000 kPa, and it was found that, as the turbine inlet pressure increased, the exergy efficiency increased by about 3%. However, Al Sulaiman et al. [84] powered the ORC by solid oxide fuel with n-octane refrigerant fluid, and produced 500kW of electric power. They concluded that the most significant source of exergy destruction rate is the ORC evaporator, which was in agreement with most studies.

2.12.3 Absorption Chiller:

The exergy analysis for absorption chiller has been investigated by few studies compared with energy analysis study. The performance of 2357kW single effect water-cooled LiBr absorption chiller and COP value of 0.76 was studied by Kaushik and Arora [86]. This unit was designed by a computer programme and the exergy investigations showed that the highest exergy destruction of the cycle was found in the absorber 191.72kW, followed by the condenser 109.76kW, and then the evaporator and generator for 86.28kW and 55.5kW respectively. Moreover, the exergy efficiency of this cycle was 11.75%.

Another study was carried out by Misra et al. [87] in a single-effect absorption chiller with a COP value of 0.71. The results indicated that the highest exergy occurred in the evaporator 12.75kW. This study is not in agreement with the previous findings by Kaushik and Arora [86]. This could be due to the fact that the inlet and outlet streams in the evaporator were below the reference condition, as their exergy values were negative.

A computer programme was developed by Agnew and Talbi [88] to investigate a single-effect absorption chiller. It was reported that the generator represents the main cause of cycle exergy destruction due to the heat transfer process, followed by the absorber and then the evaporator and the heat exchanger, which is in agreement with a study performed on the same absorption chiller by Sencan et al. [89], who found that the maximum exergy destruction was in the generator, followed by the heat exchanger, condenser and then the evaporator.

2.12.4 Desalination Plant:

Exergy analysis has been covered by a limited number of studies compared to energy analysis. A TVC-MED desalination plant has been studied by Sayyaadi and Saffari [80] to investigate the performance of a seven-effect TVC-MED desalination plant. It has been found that the most significant exergy destruction is caused by the steam ejector in the rate of 1069.3kW, while the evaporator only caused 524kW exergy destruction. Moreover, a similar study by Choi et al. [90] stated that the exergy destruction in TVC-MED plant is caused due to the heat transfer process in the steam ejector, evaporator and compressor, or due to a pressure drop in pumps, condenser, valves and evaporator during the flashing process. In this study, four TVC-MED desalination plants have been tested, each with a different number of effects. The

production capacity of potable water was between 4500m^3/day and 2000m^3/day. The results indicated that the steam ejector was the main cause of the all plants exergy destruction, which was mostly represented by 70% of the plant's total exergy followed by the evaporator.

Mabrouk et al. [91] published another study that confirmed these findings, a comparison between TVC-MED and the mechanical vapour compression multi-effect distillation (MVC-MED) processes, in addition to MSF and RO desalination process. The exergy analysis results demonstrated that the main cause of exergy destruction was found in the steam ejector of the TVC-MED plant, followed by the condenser and then the evaporator. It was concluded that the lowest exergy destruction and specific power consumption were obtained in the TVC-MED. However, these results are not in agreement with a similar study carried out by Hamed et al. [92] where it was found that the main cause of the plant's irreversibility is in the evaporator, due to the high temperature of the heat input. Besides the TVC-MED process, MVC and multi effect boiling (MEB) were included in this study, in order to compare their total exergy destructions. As a result, the TVC-MED was found to be the most exergy-efficient with 135kW, compared with 142kW, 227kW for MVC and MEB respectively.

In conclusion, different studies showed various results of exergy analysis for similar plants. This is due to the fact that the definition and the selection of the reference condition, system boundary, exergy destruction and efficiency equation are classified by the researchers. Thus, the exergy analysis is considered as a tool that adds improvements to power plant performance [75].

2.13 Chapter Summary:

Different topics were introduced in this chapter covering the applications and performance of microturbine, organic Rankine cycle, absorption chillers and desalination units. Moreover, the waste heat energy recovery and a brief review of the water resources in Saudi Arabia were also presented. Energy and exergy analysis fundamentals were also discussed with a number of studies that used in power plant, microturbine, organic Rankine cycle, and absorption chiller and desalination process. Therefore, a number of guidelines have been drawn from this chapter to be applied as a part of this study due to number of reasons that mentioned in detail earlier, and this can be pointed as follows:

- The exhaust of microturbine will be used as a waste heat energy source to operate another thermal system.
- A single effect water/LiBr absorption chiller will be employed as a cooling system.
- An ORC will be adopted to provide extra output power with law fuel combustion, and working fluids of R-245fa and R-134fa will be compared to choose the better.
- TVC-MED and MED desalination process will be compared based on energy and exergy results and choose the better.
- Exergy analysis will be performed.
- The effect of proposed models on the environment will be evaluated in details.

Chapter 3

Methodology

3. Methodology:

This chapter explains the tools used in this study for modelling, simulating and examining the proposed thermal models. This includes the simulation software with all its modules and library models. A description of the first law analysis is also included here with explanations of first law efficiency, effectiveness, number of transfer units (NTU), and the other first low performance parameters that were used to evaluate the proposed plant performance. The second law analysis will also be presented in this chapter in order to conduct the exergy analysis, and the methods used for calculating the entropy and enthalpy of certain streams will be outlined. Weather data for Jeddah City are included and the real data collected for the modelling of each plant is described.

3.1 Modelling and Simulation Tools:

Simulation and computational modelling has become a fundamental element of most studies, training, and certification applications. Employing these methods can save money and time. They also offers flexibility, and enable repeatability, control and the pushing of boundaries. This method proved to be very efficient for testing and running the proposed model, and for examining its performance in different conditions. The software used in this study was IPSEpro, published by the SimTech Company, which provides modelling tools and services for the power industries. IPSEpro is a set of software modules that creates, analyses and utilises models for new or existing process plants throughout their life cycles.

IPSEpro is a very flexible modelling system for calculating heat balances and simulating processes. At the first level, it allows any problem to be represented graphically and mathematically as a network of collected and connected components. This can be carried out by using the model development kit (MDK). At the second level, the calculation and obtaining of results is performed in the process simulation environment (PSE).

IPSEpro not only calculates the heat balances of models, but can also predict design and off-design performance, verifiy and validate measurements during an acceptance test, and plan modifications and re-powering of existing plants, as well as providing the ability to monitor and optimise plant performance online. A number of models were employed in the IPSEpro design suit. However, only some of them were used in this study.

IPSEpro software was applied to industrial and research companies such as Rolls-Royce and NaREC, which allowed more credit for the SimTech company. Also, Gigimayr, Nixdorf and Pogoreutz carried out a study of 18 types of simulation software, with the purpose of evaluating the suitability of this simulation software for thermodynamic calculations. The comparison was performed on a two-pressure heat recovery steam generator (HRSG) with a water steam cycle and a heating condenser, and design and off-design cases were also employed. The results showed that the IPSEpro was one of the software that was recommended for simulating a thermodynamic study [93]. It was subjected to validation throughout this study where it was proven to be accurate [93]. The real data of this study was collected and modelled accurately by using this software, and the same output of the real plant was also provided [94].

3.2 Process Simulation Environment (PSE)

PSE is the most important part of IPSEpro. It allows a creation of a process model based on components from a model library, and applies analysis via optimised mathematical methods. This process assures reliable fast and accurate calculations. It can easily model a process consisting of one or more objects in an easy-to-use flow sheet editor, by selecting a component as an icon from a model library, which is shown as a sidebar in the PSE screenshot (Fig 3-1). All the data related to the process model is then entered directly onto a flow sheet.

PSE carries out a mathematical analysis of the system, and then works out a numerical solution. At the analysis stage, PSE determines a method to reach the optimum solution for the equation system. In case of solving several equations simultaneously, PSE combines them into groups, and during the analysis phase, the optimum numerical method for each group is selected by PSE.

During the process of reaching the numerical solution, the variables in the system are iterated until the relative change in each variable is less than a certain threshold εx, or when the difference between the left and the right side of each equation, also called the function residual, is less than a certain threshold εf. In that case, PSE uses the x-tolerance (Ex) as the total error for all variables, and the y-tolerance (Ef) as the total error for all equations.

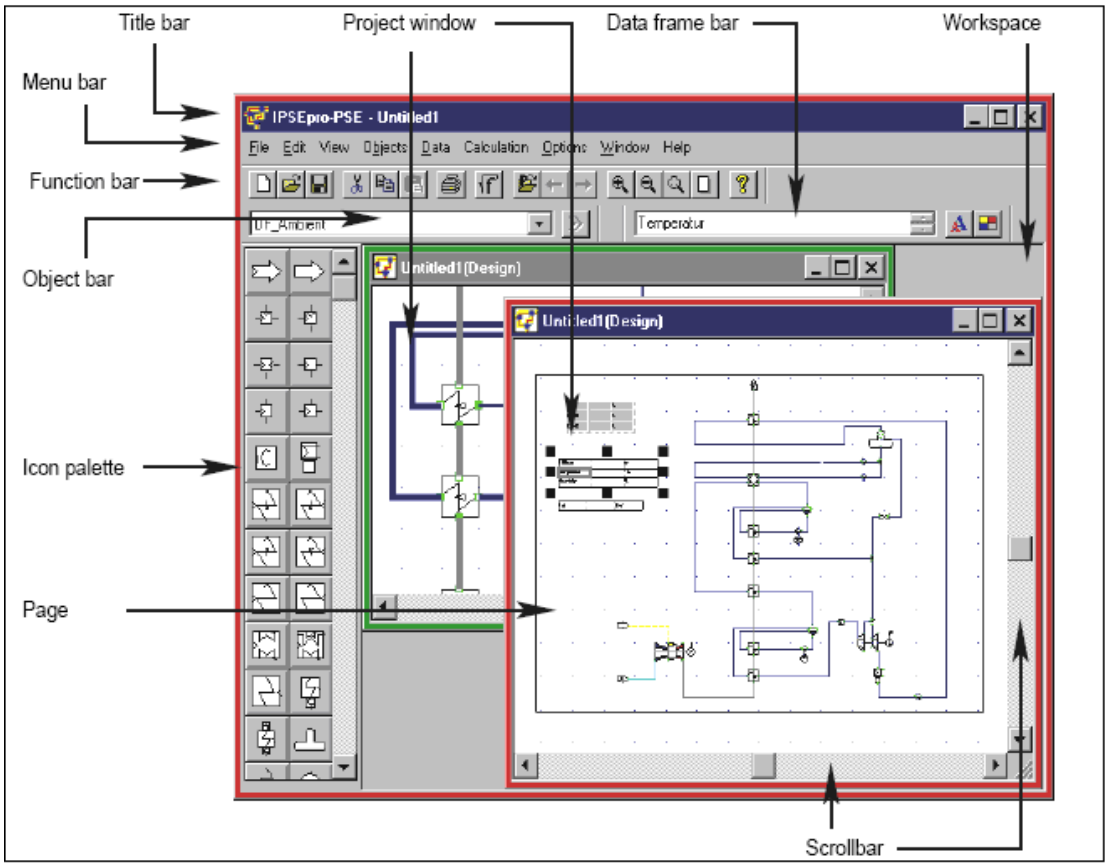

Fig [3-1], IPSEpro screenshot.

Based on the assumption that each variable contributes equally to the system solution, and the total number of variables in the system can be abbreviated as (n), the error permitted for a single variable is:

$$\varepsilon_x = \frac{E_x}{\sqrt{n}} \qquad (3\text{-}1)$$

And the error permitted for a single equation is:

$$\varepsilon_f = \frac{E_f}{\sqrt{n}} \qquad (3\text{-}2)$$

If the error takes place while the system is in the process of solving equations, PSE terminates the solution process and issues an error message showing that the system of equations is either structurally or numerically singular, or does not converge within the given number of solution steps, or that an error has occurred in the built-in or external numerical functions.

PSE offers a wide range of controlling and monitoring functions such as:

- Default value editor
- Solver parameters

- Free equations editor
- Dataset manager
- Calculation protocol
- Data frame
- Data table sheet
- Measurement editor

The default value editor uses default values for all data including variables (both values and limits), parameters, tables and switches, in order to reduce the time required for entering data. These default values are taken from a default value database that can be configured using MDK.

The free equation editor allows the establishment of relationships between different objects within PSE projects. A free equation is very similar to a model equation except that it does not belong to a single object. Instead, free equations are linked to an individual dataset of a PSE project. Free equations have the same syntax as standard model equations, and both use the model description language MDL.

PES provides that a valuable feature such as e-mail can be used to send a project file to another IPSEpro user. It also allows the use of templates and macros to exchange pre-defined information between one project and another in order to create a project in a short time.

3.3 Process Simulation MS Excel (PSExcel)

Data can be exchanged between PSE and MSExcel through the PSE-MS Excel module. PSExcel provides a special MS Excel template (PSExcel.xlt) and an MS Excel add-in (PSExcel.xla), which in turn supports this data exchange. The date can be incorporated from PSE projects into an Excel worksheet, and the project report can be illustrated. PSE-MS Excel can also present a series of different calculations in a PSE project, by varying the values of some items in the component models.

The data variation of a PSE-project can be easily used in PSExcel, and the variation results of the project can be displayed in the form of diagrams or curves in MS Excel. The term variation of a PSE project stands for the fact that the process calculation can be performed (n) times, adopting different input data each time. The variation can be two or three-dimensional, depending on the number of variation parameters. Also, the variation can be updated once it is created in the system. A great deal of information

about the library models used in a project can be generated by a PSE-MS excel integration module, which allows the creation of a diagram that shows the values of a certain item belonging to different library models of a process.

The data that can be exchanged between PSE and PSExcel are the values of items belonging to objects which are available in a PSE-project. These items can be of the following types: variable, parameters, table or switch. Based on the Windows dynamic data exchange (DDE) mechanism, PSE allows data exchange with a second MS Windows application. Only by using the extra pre-defined commands in Excel can this kind of data, which becomes available after the installation of the PSExcel integration module, be used. Therefore, using this module merely requires some basic knowledge of MS Excel. Another way to manage the data exchange between PSE and MS Excel is to use the subroutines, which are also available after installation of the PSExcel integration module, for integration. In order to do this, a basic knowledge of Visual Basic macro programming is required. The pre-defended commands under the PSExcel in MS Excel, which become available after the PSExcel integration module installation, are as follows:

- Insert item
- Create variation
- Delete inserted tables
- Update inserted items
- Add item to send list
- Run simulation
- Restart variation
- Rename woksheet

A PSExcel module is employed in IPSEpro software to carry out off-design studies of projects. This can be done through two commands: ‘create variation’ and ‘restart variation’. Although all the commands are easy to use, these two commands will be explained in more detail.

The ‘create variation’ command allows the automatic creation of a series of calculations in PSE. Each calculation will be performed with the same initial values, except that one or two item values called variation parameters will be updated before the next calculation starts.

A variation can be two or three-dimensional, depending on the number of variation parameters. The initial and final values and the step width must be set for each variation parameter, using the command's windows, as shown in Fig [3-2],[95].

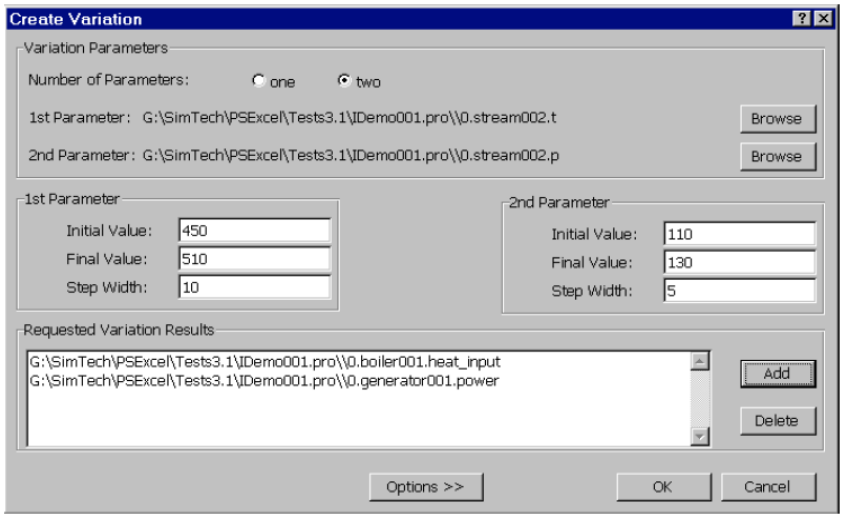

Fig [3-2], Create variation window

3.4 Model Development Kit (MDK)

A new component of IPSEpro software can be created, and a Model Development Kit (MDK) can be used to modify an existing one. This new or modified component can be translated into a form that can be used by the process Simulation Environment module (PES). MDK has two functions: firstly, it builds new component models graphically by designing an icon that represents the model, and mathematically by describing the model's behaviour using the model description language (MDL). Secondly, the model descriptions can be translated into a binary format by MDK's model compiler. This assures high performance when the process model is solved in the PSE [96].

The modelling concept is based on three different process components connected hierarchically: units, connection, and global. Thus, objects can only refer to other objects on a lower hierarchical level, as shown in Fig [3-3]. On the other hand, units represent actual pieces of equipment, and within a network structure they represent the 'nodes'. Therefore, both connections and global cab be referenced, but not other units. They are represented graphically by icons to simplify the interaction with the program.

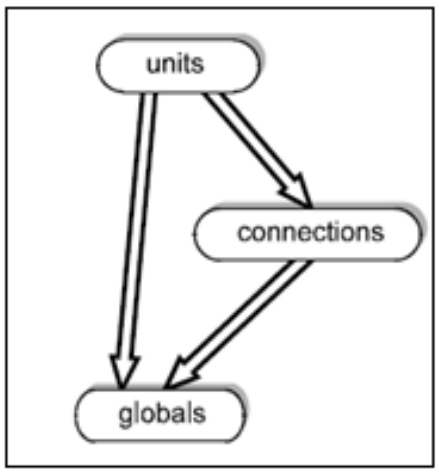

Fig [3-3], MDK modelling concept

As no new component was employed in this study, other than that included in the standard libraries, MDK was used only to combine three libraries: refrigeration, desalination and advance power plants. First of all, the libraries were opened in MDK, and then by using copy/paste, the desalination and refrigeration libraries were added to the advanced power plant library. To resolve the name conflict, a choice was made to overwrite the advanced power plant class with the desalination and refrigeration class, as both libraries share a model class number. Lastly, the new combined library was saved as a new library and compiled.

3.5 Libraries

A number of libraries, which cover a wide range of process plans, were provided by SimTech, and MDK supplied the means of creating a new library. As mentioned, three libraries have been used in this study.

3.5.1 Advanced power plant library

This library design was based on wide experience gained with the power process-modelling package IPSE. It was implemented with the aim of allowing the modelling of a wide range of thermal power plants. including conventional power plants, cogeneration plants, and combined cycle plants.

The advanced power plant library has 49 icons and each one represents a unit of any power plant construction, such as a condenser, boiler, heat exchanger or turbine. Also, a new or modified icon can be added to the library by MDK. Furthermore, each unit of the advanced power plant library has specialised off-design models. While the

design models focus on less data input and on fast convergence, the off-design models emphasise optimum interaction with the design models.

A data base of physical properties, such as water levels and the wide range of chemical components that might be used in a combustion system, was also included in this library Fig [3-4]. The library allows the manually creation and editing of a composition, which can be described in terms of mass friction when the sum of all mass frictions equals 1.0 [97].

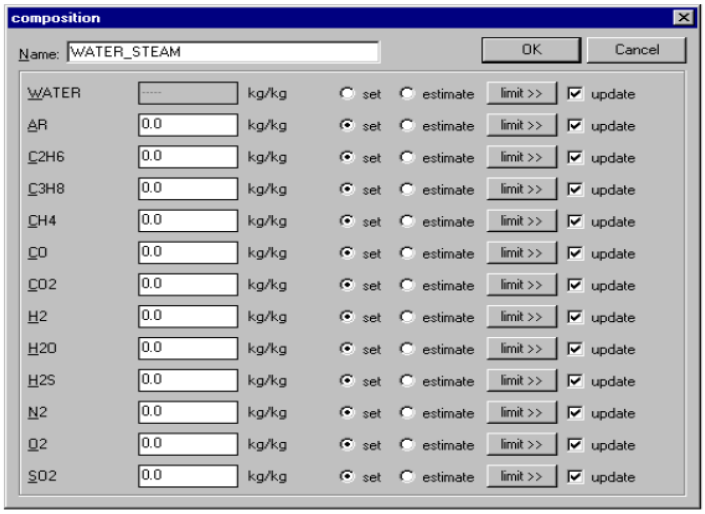

Fig [3-4], chemical components in library database

3.5.2 Refrigeration process library

A number of advanced thermal compression processes can be modelled using the refrigeration process library, which includes 50 refrigerants. This library has been created and modelled according to the agreement obtained by the US National Institute of Standard and Technology for the development of a reference data programme.

This library includes all the necessary component models for designing and analysing all refrigerants employed in this study, which examines an ORC and absorption refrigeration system. Certain components, such as desorbers, evaporators and generators were designed for design and off-design analysis. The library also provides a physical properties database, including a wide range of refrigerants for both absorption and ORC processes.

The library includes many working fluids, such as NH_3/H_2O and $LiBr/H_2O$ working fluid global. The following connections allowed were:

- Stream for an NH_3/H_2O mixture
- Stream for $LiBr/H_2O$ mixture
- Stream using refrigerants
- Shaft and the standard composition

Furthermore, the library includes 33 pure refrigerants such as ammonia, butane, carbon dioxide, ethane, isobutene, propane, propylene, R245, R134. Also, it contains 19 pre-defined mixtures of refrigerants and lists their physical properties [98].

3.5.3 Desalination process library

This library includes the necessary components for modelling and designing desalination process such as multi-stage flash (MSF), multi-effect desalination (MED) and thermal vapour compression (TVC-MED). As well as the individual pieces of equipment, there are heat exchangers and pumps and valves that are compatible with the desalination process. Like all libraries, this library can be edited and modified by using MDK.

A mathematical function was included to show the physical properties of pure water and aqueous salt solution. A database for water and gaseous chemical components concerning desalination also exists in this library [99].

3.5.4 PSEconomic Module:

An extension module of IPSEpro simulating software is PSEconomy software, with which the economy process of a system is analysed and optimised [122]. Basically, the life economic performance is analysed by implementing a dynamic investment cost that is capable of carrying out an economic investigation. PSEconomic can be used as stand-alone software, which obtains its economic data directly from the user in a similar manual way to the MS Excel spreadsheet. In the current study, the economic data, including the cost and the model's performance, were entered directly. An automatic calculation procedure then took place to obtain the results of the models' economic performance.

This programme is capable of defining and estimating the following points:

- The cost structure with regard to investment costs.
- Operating scenarios for the full operating life of a process system.

- Operation and maintenance costs which can be estimated throughout the operating life of a process system.
- The cost of the process system when optimised.

All the required data were entered manually at an annual date. The real economic data concerns the proposed models and includes the capital costs, operation and maintenance and project lifetime. A screen shot of the PSEconomic window includes two parts, as shown in Fig [3-5]. The first part is the project navigator, which presents an overview of the project data in a tree structure shape. It is also used to browse the project data. Secondly, the content view explains and shows the entered data of the selected project navigator

Furthermore, more details of the PSEconomic calculation methods and the economic process are clearly discussed and explained in the chapter devoted to economic study.

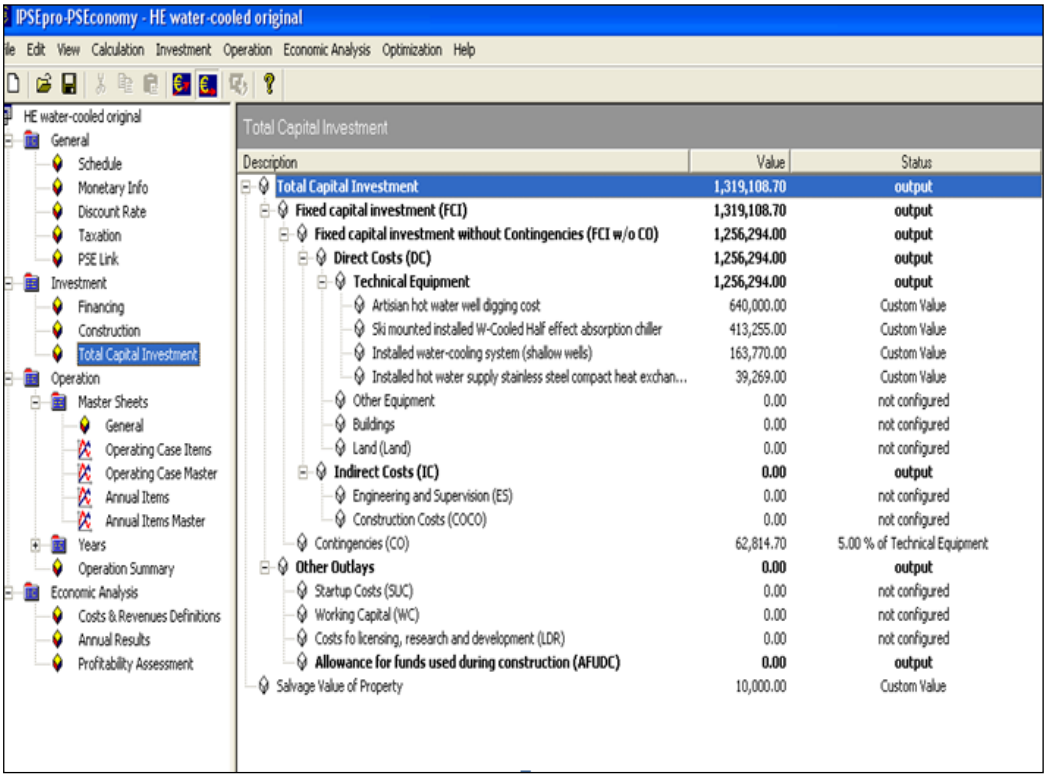

Fig [3-5], Screenshot of PSEconomic window

3.6 Weather data

This study could be valid in many areas around the world. Nevertheless, the ambient conditions are one of the challenges here, due to their effect on the performance of power output and the efficiency of the plant as was mentioned in the literature review. Jeddah City in Saudi Arabia has been selected as a location for this study and its weather condition data are required.

Jeddah is the second largest city in Saudi Arabia after the capital Riyadh, and is located at 21° 29′ 31″ N, 39° 11′ 24″ E as shown in Fig [3-6], [100]. Also, it is considered to be the commercial capital of Saudi Arabia. In addition, the city's geographical location places it at the heart of the region covered by the Middle East and North Africa; other countries' capitals can be reached within two hours by flying. Jeddah can thus be defined as the commercial centre of the Middle East [16]. Also, Jeddah's industrial district is the third largest industrial city in Saudi Arabia after Jubail and Yanbu.

Fig [3-6], Jeddah city location

The weather data was gained from the Presidency of Metrology and Environment, Saudi Arabia [101], which represents the Ministry of Defence and Aviation.

The weather data obtained showed the mean and extreme readings for each month over a 23-year period from 1985 to 2008. The obtained reading of the mean value

consists of the maximum and the minimum values. Also, the highest recorded temperature and the lowest temperature during this period are provided. The obtained weather data is presented on monthly basis, as shown in Table [3-1], while Fig [3-7] simplifies the data in a linear chart form.

	Mean temperature			Extremes temperature reading			
Month	Max	Min	Mean	Max	Year	Min	Year
Jan	27.5	15.1	19.8	35.4	1985	5.7	2000
Feb	28.3	16.2	22.2	38.3	2004	6.5	1992
Mar	31.1	16.9	24	39.4	2001	8.7	1992
Apr	34.7	20.7	27.7	43.6	1991	11.5	1997
May	38.2	23.8	31	49	2003	16.6	2008
Jun	40	25	32.5	50	2006	18	1993
July	41.1	26.3	33.7	50	1989	21.3	2005
Aug	41.3	27.1	34.2	49	2006	20.4	1997
Sep	39.9	26.1	33	49	2006	19	2006
Oct	36.9	23.6	30.2	48.4	2004	14.3	2000
Nov	33.3	19.9	26.6	45.7	1991	13.5	1994
Dec	29.4	16.1	22.7	42	2004	7.8	2004
Max	41.3			50			
Min		15.1				5.7	
Mean			28.1				

Table [3-1], Jeddah city weather data

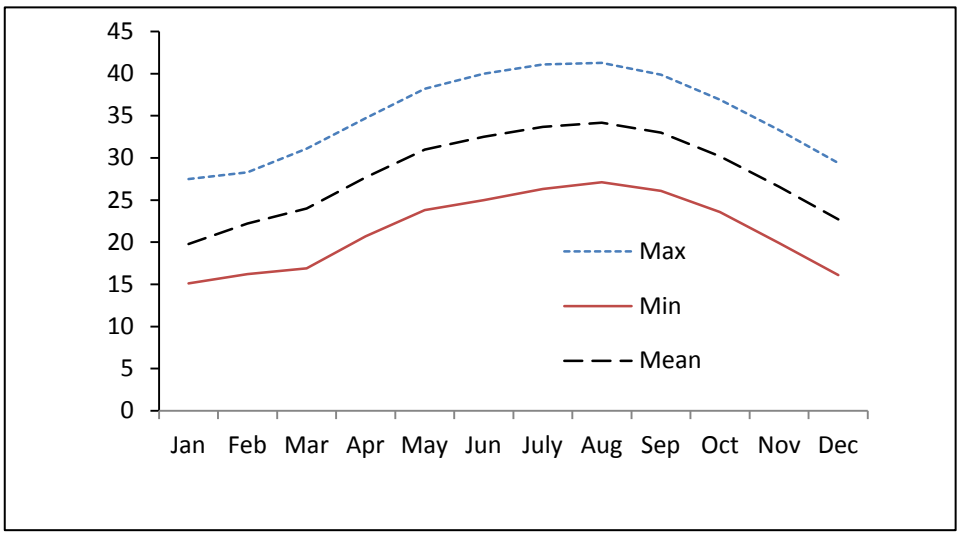

Fig [3-7], maximum, minimum and mean temperatures of Jeddah city

From Table [3-1], and Fig [3-7], it can be seen that the mean temperature in Jeddah City during this period varies from the minimum value of 15.1°C to the maximum value of 41.3°C. Statistical weather data of Jeddah city from 1985 to 2008 was illustrated in Fig [3-8] and Fig [3-9]. The highest recorded temperature of 50°C occurred in 1989, while the lowest recorded temperature was 5.7°C as illustrated in Fig [3-8] and Fig[3-9].

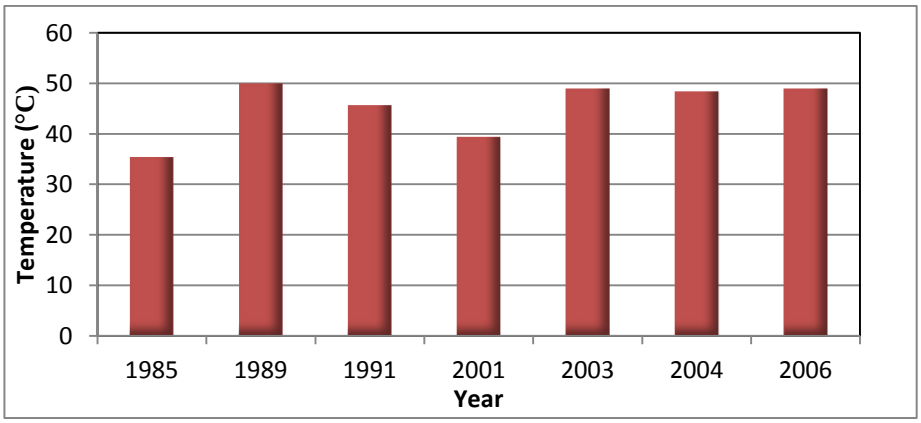

Fig[3-8], maximum temperature during years

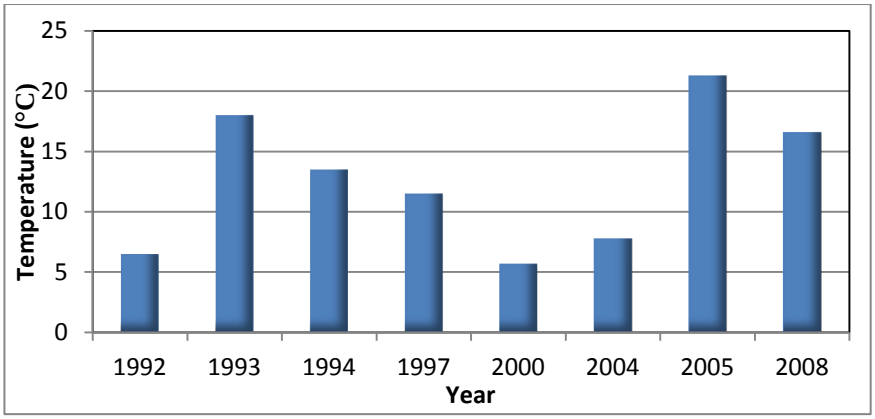

Fig [3-9], minimum temperature during years

The relative humidity data was also presented for the same period of time for both mornings and evenings. Table [3-2] shows the value of the mean maximum and mean minimum for the morning and evening. Fig [3-10] represents these values in the form of a chart. It can be calculated that, from 1985 to 2008, the relative humidity varies from a minimum mean value of 51% to a maximum mean value of 73%, while the mean value varies between 68.67% and 55.5%.

	Relative Humidity %	
Month	Mean Morning	Mean Evening
Jan	68	54
Feb	70	52
Mar	65	52
Apr	64	56
May	65	55
Jun	68	55
July	70	56
Aug	73	51
Sep	69	61
Oct	72	61
Nov	72	59
Dec	68	54
Max.	73	61
Min	64	51
Mean	68.67	55.5

Table [3-2], Relative humidity

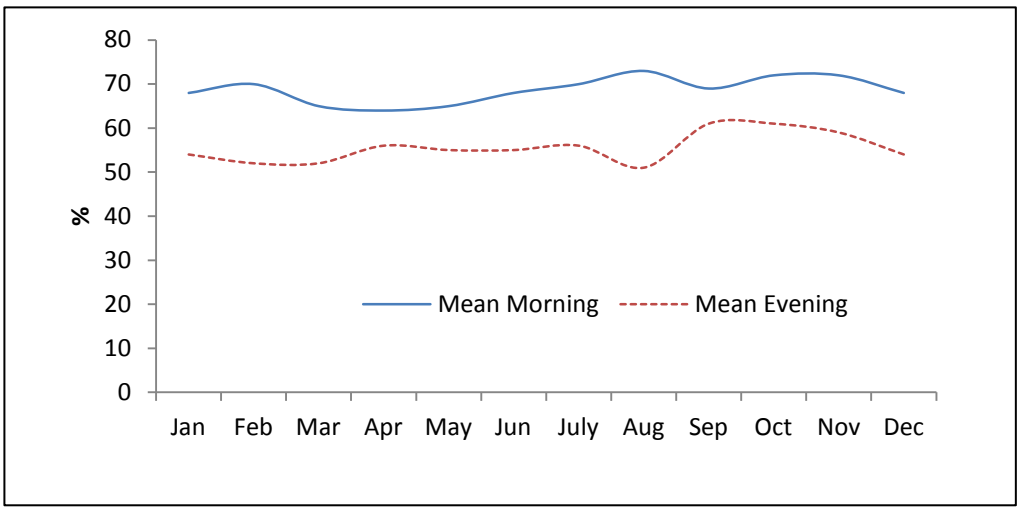

Fig [3-10], Relative humidity chart

In this study, the use of seawater is needed to provide the main input in supplying the desalination units (MED), (TVC-MED), ORC and also the absorption chiller for cooling purposes. Moreover, Jeddah City is located next to Red Sea, where its high surface temperatures are coupled with high salinities. This makes it one of the hottest and saltiest bodies of seawater in the world. The Red Sea surface temperature averages 26°C during the summer months, while during the winter, it averages 20°C. As the excising evaporation as well as scarcity rainfall and the absence of potable water sources reaches 205cm per year, the salinity of Red Sea varies from 0.03kg/kg to 0.04kg/kg,. These differences are considered in detail in this study [101].

3.7 Energy Analysis

Based on the first law analysis, energy analysis will be performed on a number of parameters on this study, to evaluate the performance of the base and proposed plants. A generic model was used in the power plant to simulate the microturbine, including its compressor and combustion chamber. According to the first law of thermodynamics, the amount of the net energy received through heat interaction is equal to the net energy transferred out in work interaction [75].

$$\sum \dot{Q}_{cyc} = \sum \dot{W}_{cyc} \qquad (3\text{-}3)$$

According to Bejan et al. [75], the thermal efficiency of a microturbine can be defined as the ratio of work generated to the total energy input put into the cycle, as follows:

$$\eta_{microturbine} = \frac{\dot{W}_{net}}{\dot{Q}_{net}} = \frac{\dot{W}_{microturbine} - \sum \dot{W}_{pump}}{\dot{m}_{Fuel} \times LHV} \qquad (3\text{-}4)$$

The efficiency of the power plant combined cycle can be identified as the ratio of the total electric power of the net to the energy input through the fuel [75]

$$\eta_{cc} = \frac{\dot{W}_{net,total.output}}{\dot{Q}_{in}} \quad (3\text{-}5)$$

Ways of calculating the carbon dioxide emission rate (CO_2) are also outlined in this study, and this was defined as being determined by the amount of carbon dioxide emitted in relation to the production of each kWh of electric power and useful heat energy.

$$CO_2\ Emission\ Rate = \frac{\dot{m}_{Fuel} \times \alpha}{\sum \dot{W}_{net,output} + \sum \dot{Q}_{net,output}} \quad (3\text{-}6)$$

where α is the amount (kg) of CO_2 produced for each ton of the consumed fuel. Natural gas was the only source of fuel for this study, which produces 3142 of CO_2 per ton [102].

An evaluation of the performance of the cogeneration plant was carried out by calculating the energy utilisation factor (EUF), which can be defined as the ratio of the total output work and the useful heat energy to the fuel energy supplied [103].

$$EUF = \frac{\dot{W}_{net,output} + \dot{Q}_{net,output}}{\dot{Q}_{in}} \quad (3\text{-}7)$$

The coefficient of performance (COP) was used to calculate the efficiency of the absorption chiller, excluding the electrical energy of the pumps, and was defined as the ratio of the cooling capacity generated from the evaporator to the heat energy provided to the generator [42].

$$COP = \frac{\dot{Q}_{Evaporator}}{\dot{Q}_{Generator}} \quad (3\text{-}8)$$

The performance of the desalination plant was considered in the evaluation. Desalination efficiency is measured by calculating the gain output ratio parameter (GOR), and is defined as the ratio of the potable water mass flow rate (kg/s) to the driving steam mass flow rate [59], and this can be expressed as an equation as follows:

$$GOR = \frac{\dot{m}_{potablewater}}{\dot{m}_{driving\ steam}} \quad (3\text{-}9)$$

Producing one kg of potable water requires a specific amount of heat energy, which is called the specific heat consumption and this was calculated as the amount of heat transferred in the first effect divided by the mass flow rate (kg/s) of the obtained potable water [71,74]:

$$specific\ heat\ consumption = \frac{\dot{Q}_{1^{st}\ effect}}{\dot{m}_{potable water}} \qquad (3\text{-}10)$$

The concentration factor parameter was calculated, and defined as the ratio of rejected brine salinity to the intake seawater salinity, as follows:

$$concentration\ factor = \frac{w_{rejected\ brine}}{w_{Intake seaawter}} \qquad (3\text{-}11)$$

where (w) is the salt mass friction in the seawater.

To ensure realistic and commercially available heat exchangers, the NTU method was needed in the process of making calculations. It was assumed that there was no heat generation in the heat exchanger and the study state and study flow, as well as negligible kinetic and potential energy differences and adiabatic processes and constant specific heat. The effectiveness of the process was defined as the ratio of the actual heat transfer to the maximum possible heat transfer [104,105].

$$\varepsilon = \frac{\Delta T_{actual}}{T_{h,in} - T_{c,in}} \qquad (3\text{-}12)$$

where ΔT_{actual} stands for the fluid with the larger difference in heat exchanger temperature . For a single phase heat exchanger, the NTU was defined by dividing the overall thermal conductance of the heat exchanger (UA) by the minimum heat capacity rate (C_{min}) [105].

$$NTU = \frac{UA}{C_{\min}} \qquad (3\text{-}13)$$

the C_{min} was found through a calculation of the heat capacity rate for both hot and cold streams in the heat exchanger, as shown in the following equation (3-14), while the UA was directly obtained from the simulation software.

$$C = \dot{m} \times C_p \qquad (3\text{-}14)$$

The C_{max} can be found in the heat exchanger stream that has one changing phase. This can be either located in the evaporator or the condenser.

3.8 Exergy analysis

The question of exergy analysis was discussed in the previous chapter. However, in this chapter the equations of the exergy destruction for each component in each plant will be presented. The method of entropy and enthalpy calculation is also focused on. Also, certain assumptions were made, such as the nuclear, electrical, surface tension, and magnetic effects being ignored [75, 76]. As there is no variation in the proposed plants' speed and elevation, the kinetic and potential exergy were neglected. The chemical exergy was considered for the stream of input fuel as an ideal natural gas, and was calculated as follows [79]:

$$E_{fuel} = \Theta \times \eta_{COM} \times \dot{m}_{fuel} \times LHV \qquad (3\text{-}15)$$

where the molar Gibbs function is represented by (Θ), which is equal to 1.04 for natural gas [79]. The chemical exergy for all other streams was neglected as it tended to be small, so that there was no change in its value in the system components, so it was not a significant factor in exergy destruction calculations [75-77].

The physical exergy (E^{ph}) was calculated as follows:

$$E^{PH} = (h - h_o) - T_o \times (s - s_o) \qquad (3\text{-}16)$$

where h and s denote the enthalpy and entropy respectively, and the subscript (o) is revered to the reference condition. The reference condition for all streams was assumed to be in ISO condition, for which the temperature is 15°C, and the pressure is 1.03 bars. The entropy of LiBr-H_2O mixture streams was calculated manually using the Kaita's method [106], whereby the enthalpy and entropy for all streams were directly read from the IPSEpro simulation software including air, water, and fuel composition, ORC working fluid, and exhaust gas composition.

In the desalination process the figures for the enthalpy and entropy of the seawater were calculated manually as they are not provided by the IPSEpro software [107-110]. The desalination process is basically a mixture of pure water and salt. The pure water's enthalpy and entropy were directly obtained from IPSEpro simulation software, while the salt water was calculated according to the following equations:

$$h_{salt} = h_{salt,o} + C_{p,salt}(T - T_O) \qquad (3\text{-}17)$$

$$s_{salt} = s_{salt,o} + C_{p,salt} In\left(\frac{T}{T_O}\right) \qquad (3\text{-}18)$$

where C_P is the salt specific heat, which is equal to 0.8368 kj/kg.K, and the enthalpy and the entropy of salt at the reference condition are represented by h_o and s_o respectively.

The heat of the solution can be considered through its enthalpy. The enthalpy of seawater is the sum of the enthalpy of its individual components including salt and water, as the seawater is an ideal dilute solution with a concentration of less than 5% [107-110], and this was calculated as follows:

$$h_{seawater} = (w_{salt} \times h_{salt}) + (w_{water} \times h_{water}) \quad (3\text{-}19)$$

where w_{salt} and w_{water} are the mass fractions of salt and water respectively. The entropy of the seawater solution has to be calculated separately for salt and water at the solution temperature and pressure level [107-110]. Due to this, the entropy of each individual component in the solution tends to be greater than the entropy of when it exists alone at the mixture's temperature and pressure, and this was calculated as follows:

$$s = s_{i,pure}(T_{solution}, P_{solution}) - \bar{R} \ln x_i \quad (3\text{-}20)$$

where $s_{i,pure}$ is the entropy of the (i) component at the solution pressure and temperature, which can be calculated by (s_{salt}) equation. The mole fraction (x_i) of the (i) component in the solution was calculated for salt and water as follows:

$$x_{salt} = 1 - x_{water} \quad (3\text{-}21)$$

$$x_{water} = w_{water} \frac{M_{solution}}{M_{water}} \quad (3\text{-}22)$$

where $M_{solution}$ is the molar mass of the solution, which can be found as follows:

$$M_{solution} = \frac{1}{\frac{w_{water}}{M_{water}} + \frac{w_{salt}}{M_{salt}}} \quad (3\text{-}23)$$

The molar mass of salt M_{salt} and water M_{water} were taken as 58.5 kg/kmol and 18 kg/kmol respectively [107-110]. The entropy of the seawater was calculated as follows:

$$s = w_{salt} \times s_{salt,pure}(T_{solution}, P_{solution}) + w_{water} \times s_{water,pure}(T_{solution}, T_{solution}) - \bar{R}(x_{salt} \ln x_{salt} + x_{water} \ln x_{water}) \quad (3\text{-}24)$$

the exergy and specific exergy can be calculated by finding the entropy and enthalpy for each stream of the proposed plant. Moreover, the exergy balance for each component of the plant was calculated, and this led to finding the exergy destruction and efficiency level of each proposed plant.

3.9 Modelling data of plants:

The real data of this study were collected from different sources for each plant. This supports the validation of the IPSEpro, which is the main tool used in this study. Also, the credibility and applicability of study was certified. However, according to the researcher's best knowledge, utilising the waste heat energy of a microturbine in the desalination process has not been covered in existing literature. Since thermal desalination technologies are not common in small-scale water production, the opportunity for modelling and simulating small-scale multi-effect distilled desalination (MED) and thermal vapour compression MED (TVC-MED) has been a great challenge in this study.

3.9.1 Microturbine:

The microturbine employed in this study was modelled according to the data collected from the C200 microturbine manufactured by the Capstone Company [111] as shown in Table [3-3]. This was commercially launched in 2008. The specification and performance of C200 microturbine data was obtained from Capstone Company via email [111].

Properties	Description
Manufacturer	Capstone
Model	C200
Shaft	One single Stage
Electrical Power Output	200kW
Voltage	400 to 480 VAC
Electrical Efficiency LHV	33%
Fuel	Natural Gas
Inlet pressure	75 psi
Exhaust Mass Flow	1.3 kg/s
Exhaust Gas Temperature	280°C
Exhaust Energy	1420 MJ/hr
Noise level	65 dbA

Table [3-3], microturbine specifications

3.9.2 Single-effect Absorption chiller

The absorption chiller used in this study is a single effect water cooling absorption chiller modelled on the collected data of a 105 kW absorption chiller obtained from Yazaki Energy Systems Inc. [112]. A Duhring P-T chart was used to validate this absorption chiller model. The specifications and technical data of the selected model are illustrated in table [3-4].

Properties	Description
Manufacturer	Yazaki Energy System, Inc
Model	SC30
Cooling Capacity	105 kW
Inlet Chilled water Temp.	12.5°C
Outlet Chilled water Temp.	7°C
Rated chilled Water Flow	48.4 gpm
Rated Cooling Water Flow	80.8 gpm
Inlet Cooling Water Temp.	31°C
Evaporator pressure drop	0.66 bar
Noise Level	49 dbA

Table [3-4], SC30 absorption chiller specifications

3.9.3 Organic Rankine Cycle

One of the waste heat energy applications of the microturbine is used to generate extra power from the ORC unit. This proposed model was based on the collected data obtained from the Infinity Turbine Company for the 2010 Model IT10 ORC that produces power from 10 kW up to 20kW [113]. The specifications and the technical date of selected model are shown in table[3-5].

Properties	Description
Manufacturer	Infinity Turbine
Model	IT10
Electrical Power	10kW-30kW
Working Fluid	R245fa
Application consideration	Direct Shaft Drive
Shaft speed	3000-1000 (RPM)
Waste Heat Application	Waste Heat
Noise Level	40 dbA

Table [3-5], IT10 ORC specification

3.10 Chapter Summary

The tools used in this study was introduced in this chapter including the simulation and modeling software IPSEpro and PSEconomy. The first and second law performance parameters were presented. Furthermore, the weather data of Jeddah city was also introduced followed by the real modeling data of the microturbine, ORC and the single effect absorption chiller.

Chapter 4

Base Models' Modelling and Results

4. Base Models Modelling:

The ways in which simulation, modelling and performance (including off-design study) were assessed for all the base models will be presented in this chapter. The modelling of base models focuses on microturbines, single-effect absorption chillers, organic Rankine cycles, multi-effect distillation desalination models and thermal vapour compression multi-effect distillation models. Using the collected real data, as presented in Chapter 3, the analysis of modelling performance is carried out with reference to the first and second law of thermodynamics.

4.1 Microturbine

The microturbine is a small-scale gas turbine. The gas turbine cycle method is used in the microturbine process, which can be described as a simple Brighton cycle. The effects of variations in the thermodynamic properties occurring in the gas turbine can also be applied to microturbine applications. The inlet air to the cycle can be set at an ISO or ambient condition according to the manufactured microturbine's design, which is equivalent to 15°C and pressure 1 bar. Fig [4-1] shows the main components in a C200 single-shaft microturbine model. This generates 200.3 kW of electricity, with an efficiency of 34.3% of the ISO condition. The off-design performance of the microturbine has been evaluated in a number of parametric studies that have examined the effect of the variation of environmental parameters on the model's overall performance. According to the weather data referred to in the previous chapter, the maximum and minimum readings of recorded temperatures in Jeddah City are 50°C and 5.7°C respectively, while the mean temperature is 28.1°C. The scale of ambient temperature variation ranges from 5°C to 50°C. Table [4-1], [4-2] shows the parameters of each of the streams of the microturbine cycle and the energy results of the ISO condition with a full load operation.

4.1.1 Ambient Temperatures Variation:

The energy results are listed in Tables [1] in the appendix A, while the most significant types of impact of ambient temperature variation on the proposed model's properties are presented and discussed here.

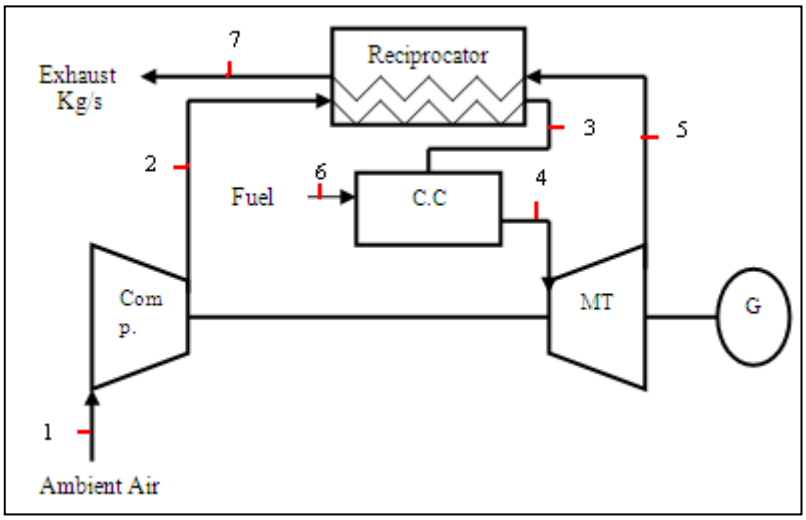

Fig [4-1], The base power plant microturbine 200kW

Stream No.	H (kj/kg)	S (kj/kgK)	M (kg/s)	T (C°)	P (bar)
1	15.1593	6.8494	1.2594	15	1.013
2	280.8973	6.9145	1.2594	274.4656	7.9
3	484.9455	7.2375	1.2594	465.3781	7.899
4	940.7473	7.8263	1.2711	850	7.889
5	495.1472	7.9381	1.2711	466.0535	1.0417
6	53.338	9.9618	0.0117	25	8
7	292.9837	7.6543	1.2711	280.9556	1.0407

Table [4-1], Microturbine's streams parameters

Parameters	Value
Emission Rate before Utilisation (g/kW)	652.64
Microturbine Power (kW)	200.32
Overall Electrical Efficiency (%)	34.3
Exhaust energy (kW)	372.4178
T4/T1	3.8993

Table [4-2], the microturbine energy properties

The density of the inlet air in the cycle decreases as its temperature increases, and this leads to a reduction in the microturbine cycle temperature ratio (T_4/T_1), which in turn results in a reduction in output power. This was discussed in more detail in the

previous chapter. Fig [4-2] shows that the microturbine temperature ratio decreased by an average of 12% for each 5°C increase in the ambient temperature.

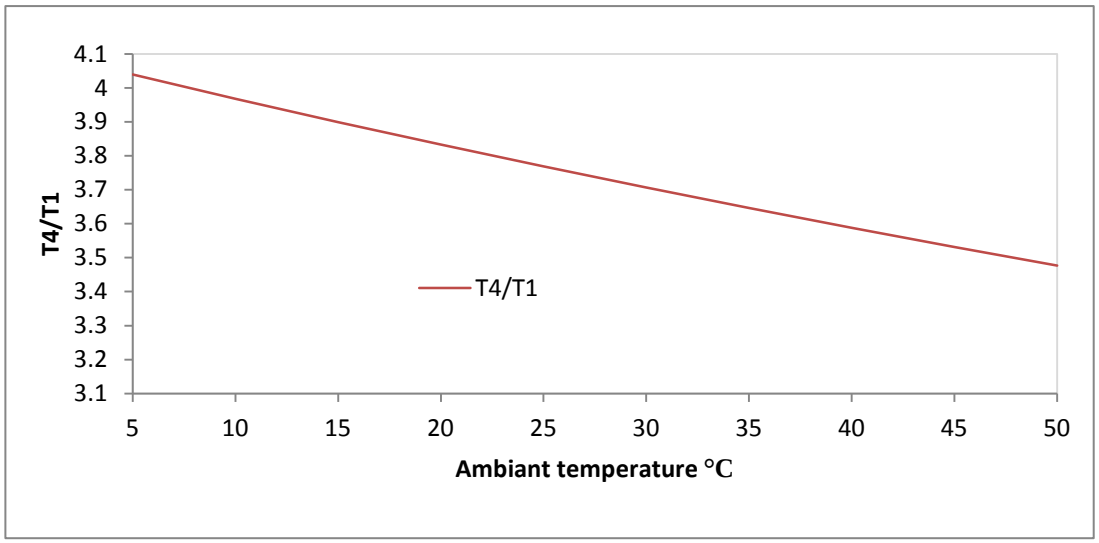

Fig [4-2], Microturbine temperature ratio relative to the ambient temperature variation

This causes a reduction in the microturbine's output power relative to the increase in the ambient temperature. The output power was reduced by a range of 3% for each 5°C increase in the ambient temperature, as shown in Fig [4-3].

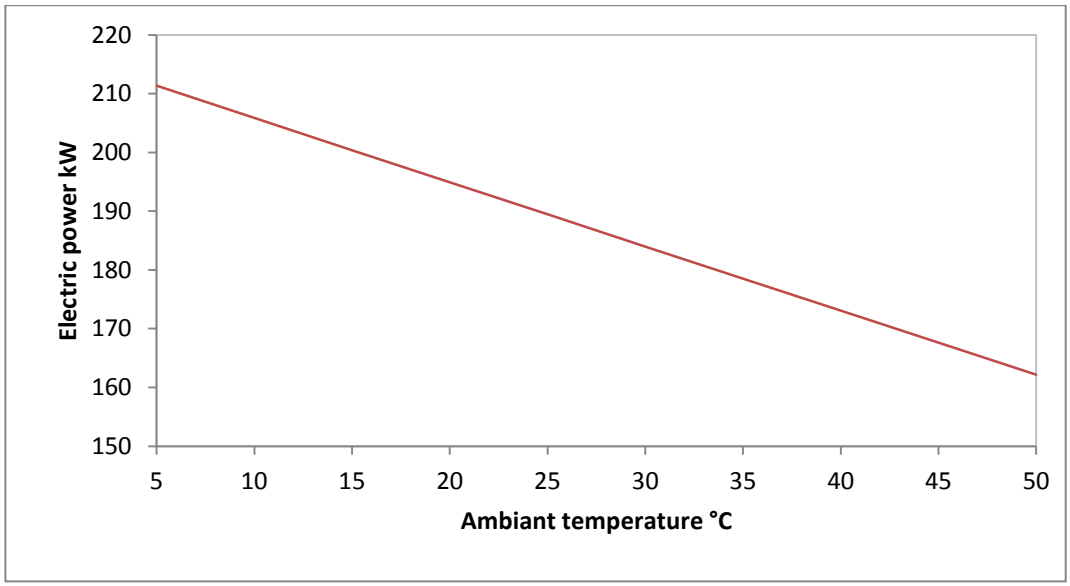

Fig [4-3], Power plant versus ambient temperature

A reduction in the microturbine output led to an increase in CO_2 emissions by 2.6 % for each 5°C increase in ambient temperature, and the stack exhaust gas temperature increased by a total of 31% relative to the variation of ambient temperature from 5°C to 50°C, as shown in Fig [4-4] and Fig [4-5] respectively.

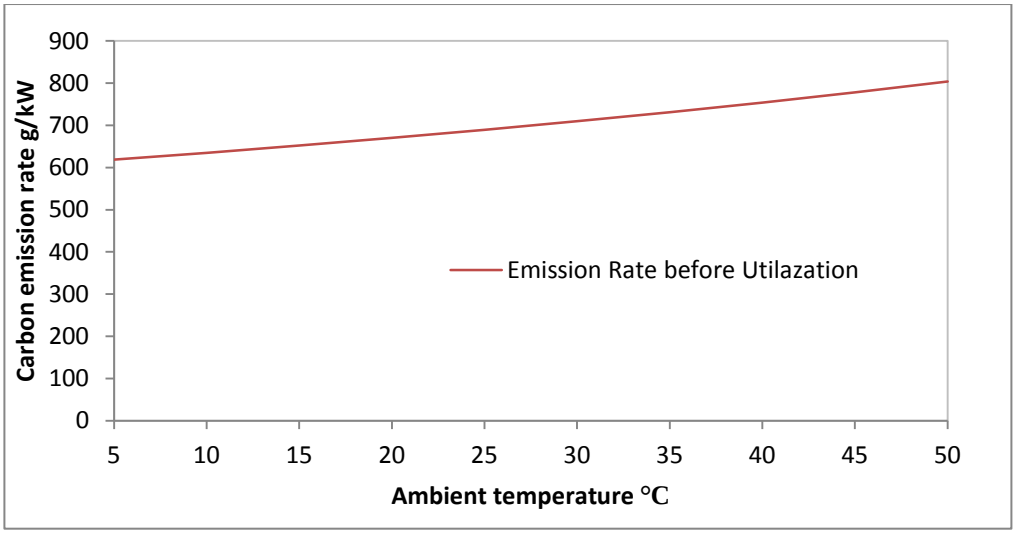

Fig [4-4], CO_2 emission rate versus ambient temperature

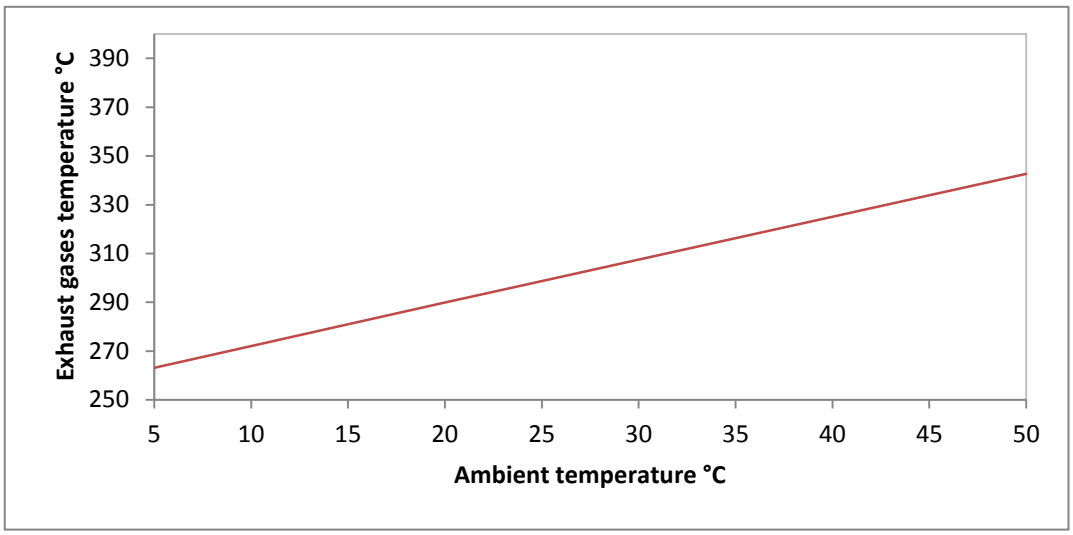

Fig [4-5], exhaust temperature versus ambient temperature

The exergy for each stream in microturbine cycle was calculated with reference to second law thermodynamic analysis. Subsequently, the exergy destruction for each component of the cycle was calculated according to the exergy balance equation presented in the previous chapter. In Fig [4-1], the exergy analysis and specific exergy of each stream in the model are listed in Table [4-3], while Fig [4-6] presents the exergy destruction of each component in a microturbine model.

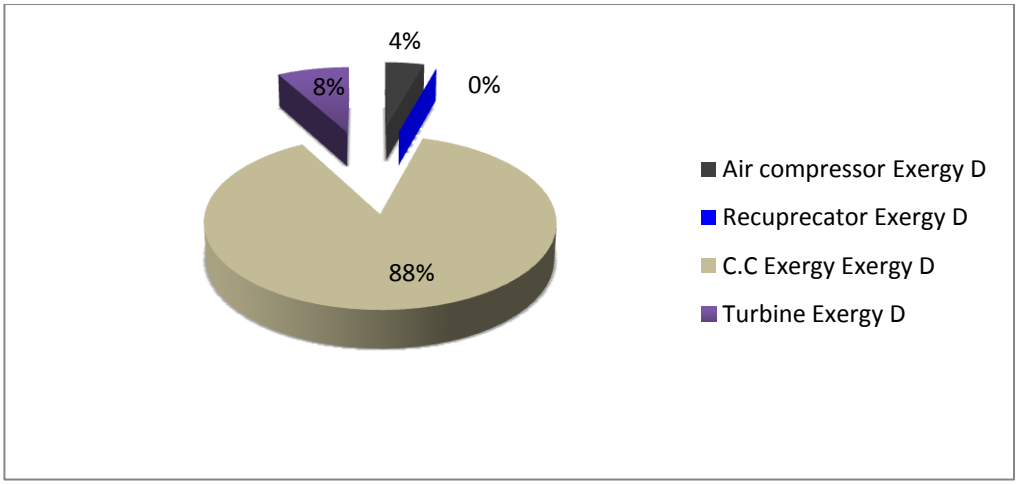

Fig [4-6], microturbine base plant components' exergy destruction

Stream No.	e	E
1	0	0
2	246.988	311.0521
3	358.0237	463.7362
4	669.5265	851.0495
5	191.7196	243.6989
6	50149.4	966.7762
7	71.2966	90.6266

Table [4-3], Microturbine's exergy and specific exergy for each stream

With an overall exergetic efficiency of 21.07% in the microturbine components including its air compressor, recuperator, turbine and combustion chamber, the main source of exergy destruction was found in the combustion chamber, where 585.55 kW was consumed, representing 59% of the total exergy input into the cycle, due to the high temperature heat transfer and mixing process that takes place with fuel (natural gas) and compressed air. However, the turbine consumed 5.4%of the total exergy input and formed 8.1% of the total exergy destruction because of the expansion process, while the exergy destruction of the recuprecator was insignificant and represented only 0.03% of the total exergy destruction of the cycle. This was due to controlling losses in the heat transfer process.

The ambient temperature variation has an effect on the overall exergetic efficiency of the microturbine model. With regard to increases in the system's exhaust temperature, as mentioned in Fig [4-5], and decreases in the microturbine power output while the ambient temperature was rising, Fig [4-7] shows that, the overall exergetic efficiency decreased by an average of 2.8% for each 5°C increase in the ambient temperature. These results are in agreement with [23-26,114,115], as reported previous studies.

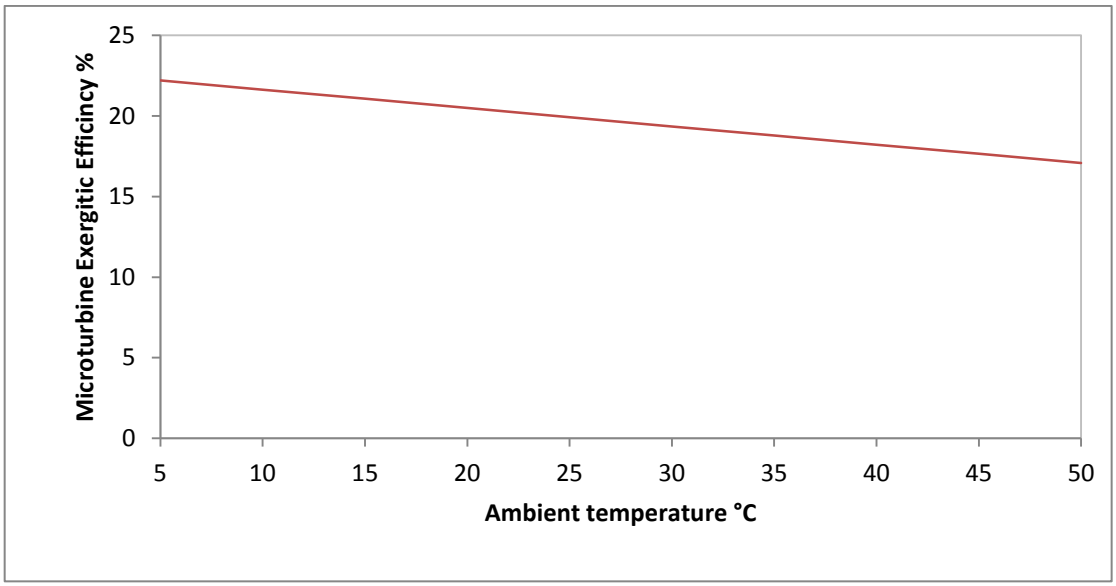

Fig [4-7], Microturbine's exergetic efficiency against the ambient temperature variations

As explained in the previous chapter, the mean relative humidity of Jeddah City varied from a minimum value of 4.7% to a maximum of 100% between 1985 and 2008. The mean humidity value was in the range of 50% to 60%. According to many studies, the variation in the air relative humidity had a minor effect on the output power and efficiency of the overall model, which is likely to be insignificant and can be ignored [23,50].

4.1.2 Partial load:

The partial load of the microturbine performance was investigated in order to monitor all the energy and exergy performance parameters. The load of the microturbine varied from 60% to a full load of 100%. This study was performed in ISO conditions of 15°C and 1 bar. All the results are listed in the appendix A in Table [2], while the most significant results are discussed in this chapter. Fig [4-8] shows the microturbine load variation in relation to the output electrical power. Adjusting the fuel supply of the microturbine to 60% caused a 67% reduction in the electric output power and in

overall electric efficiency in the range of 9% for each 10% decrease in the partial load, Fig [4-9].

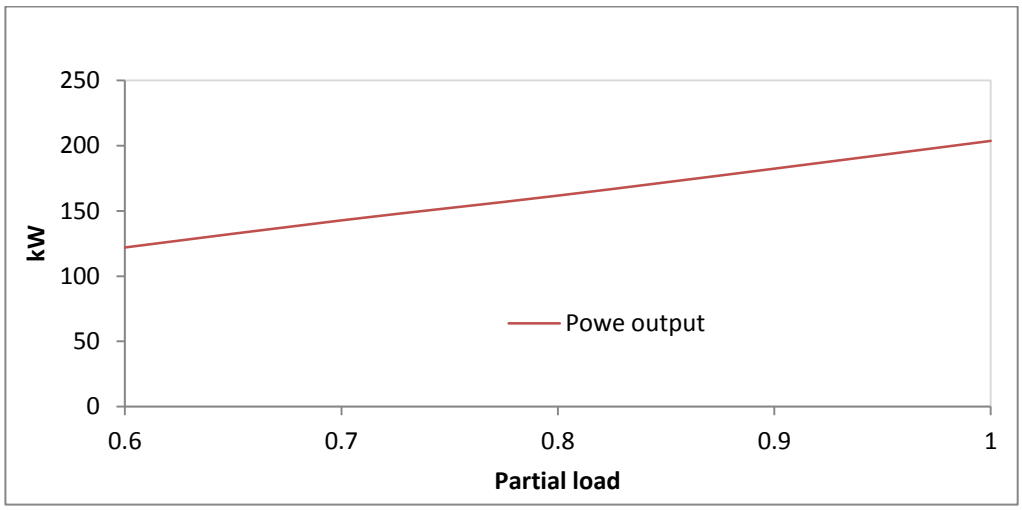

Fig[4-8], Partial load against the microturbine's output power

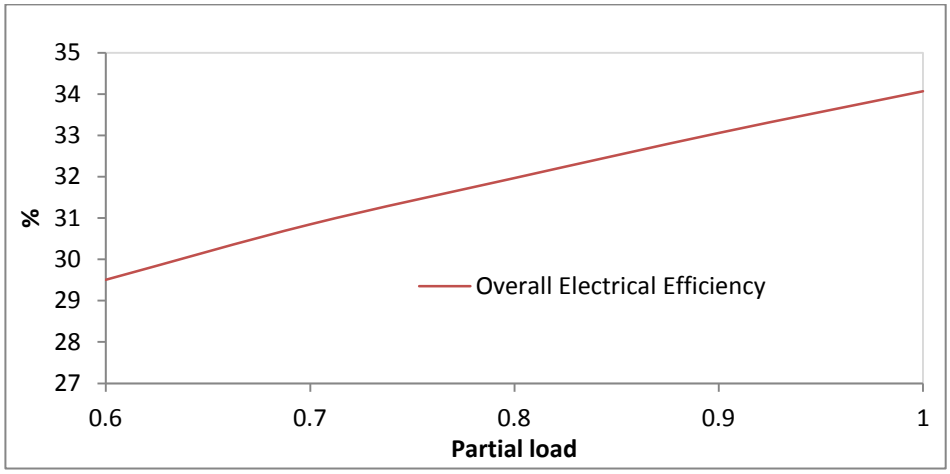

Fig [4-9], partial load against the microturbine's overall electric efficiency

Decreasing the partial load had an influence on the microturbine's CO_2 emission rate, which increased by 6% as the microturbine load decreased to 60%, due to a reduction of 67% in microturbine's output power. Fig [4-10] shows a comparison between the CO_2 emission rate and the fuel consumption with reference to the cycle's partial load.

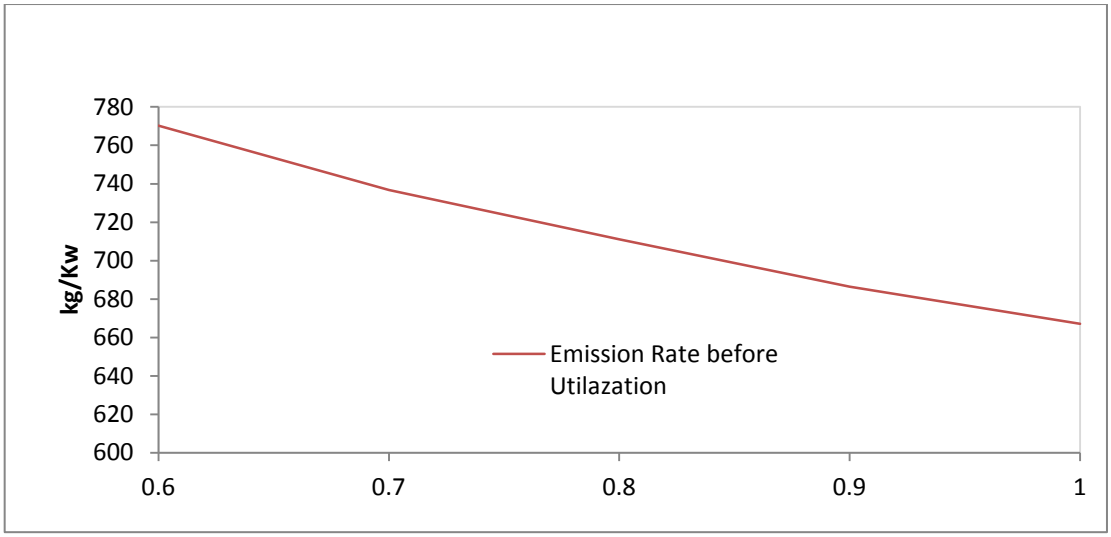

Fig [4-10], CO_2 emission rate and fuel consumption performance at partial load

Fig [4-9] represents the effect of the partial load on the overall efficiency. The overall exergetic efficiency was reduced by 6% as the microturbine partial load decreased to the minimum, as illustrated in Fig [4-11], due to the reduction in the fuel mass flow rate, which affected the output electric power and the electric efficiency.

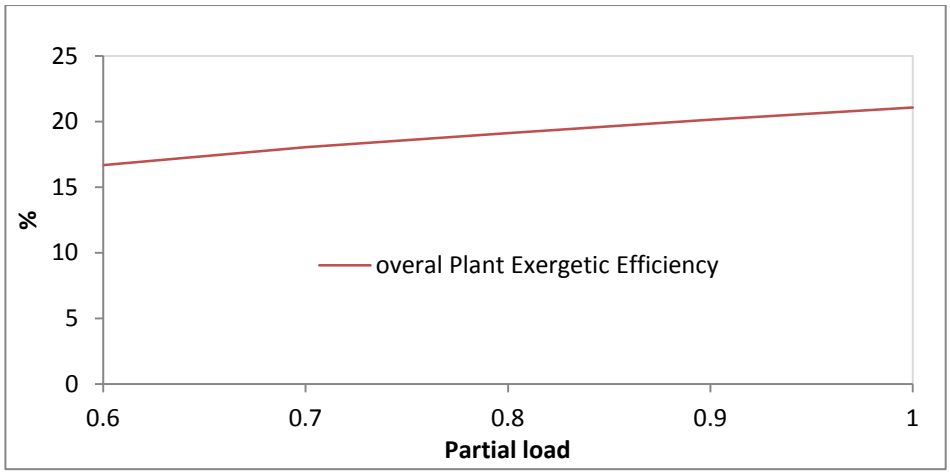

Fig [4-11], The microturbine exergetic efficiency against the partial load

The performance of this model indicates the amount of fuel required for any operation, allowing for adjustments of the proper load for the required amounts of electricity. The results of microturbine's behaviour under the partial load were found to be typical, as several similar studies had suggested they would be [26, 116,117].

4.2 Organic Rankine cycle (ORC):

An organic Rankine cycle (ORC) was employed in this study with an output of 16.88 kW of electricity, and the R245-fa refrigerant was used as working fluid to operate the cycle. It was modelled to resemble the IT10 organic Rankine cycle, as built by Infinity Turbine Co. [113], and as mentioned in the previous chapter. The ORC base plant model consists of four components: a heat supplier (evaporator), a power turbine, a condenser and a pump. The heat source needs to be an exhaust gas at a high temperature. Fig [4-12] shows the complete cycle of ORC, which begins when the working fluid is heated in the evaporator (heat exchanger) in order to reach a high temperature (3), and is then transferred to the turbine, where it is expanded to produce electrical energy (4). The working fluid then passes the condenser to cool and is turned into a liquid state (5) before being returned to the boiler to complete the cycle (D).

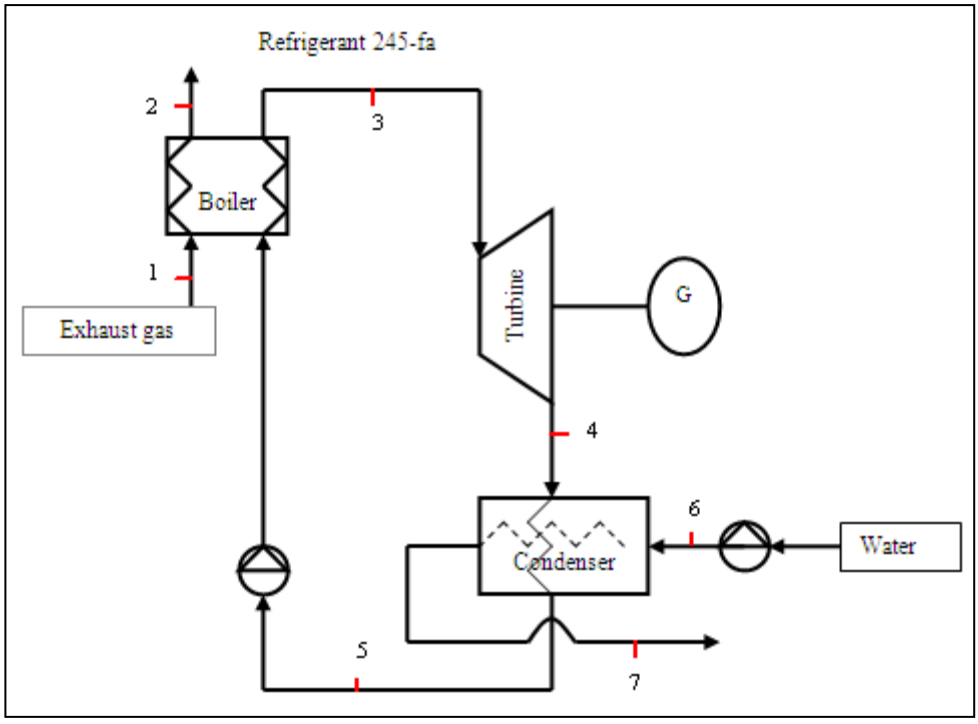

Fig [4-12], Organic rankine cycle (ORC) stand-alone

According to the refrigerant selection, a group of refrigerants were previously mentioned in the literature review. However, the most common refrigerants employed in the ORC were R-134a and R-245fa. Both refrigerants were recommended for use as they belong to the new refrigerant class because of their special thermodynamic properties such as a non-flammability and high molecular weight, no potential ozone depletion impact and less environmental damage. The comparison between R-134a

and R-245fa was considered as a part of the proposed ORC stand-alone, using each refrigerant separately as a working fluid in the proposed cycle. Table [4-4] shows the most significant output result between R-134a and R-245fa. Both refrigerants were applied separately under the same ORC conditions, when the heat source and intake cooling water temperature were the same.

Table [4-4] shows the different output parameters for each model, with the refrigerant R-245fa consuming less mass cooling water with an 18% lower refrigerant mass flow rate with a lower cycle pressure ratio compared to R-134a, thus resulting in lower values in the heat exchanger area. The net output electric power is slightly higher in the R-254fa refrigerant compared to R-134a, due to less power being consumed by the pumps, which will ultimately result in a need for to less equipment and lower operating costs. Also, as mentioned in the literature review, R-245fa provides a shorter atmospheric lifetime, a lower ASHRAE safety level (American Society of Heating, Refrigerating and Air-Conditioning Engineers), and less net greenhouse warming potential compared to R-134a [30-36]. Consequently, the refrigerant R-245fa was employed in this study as a working fluid for the proposed ORC stand-alone.

	R-134a	R-245fa
Net output electric power (kW)	13.6342	16.88
Refrigerant power turbine delta P (bar)	13.5646	4.3988
Cooling water mass flow (kg/s)	32.1411	4.0916
UA evaporator (kW)	1.0914	1.0834
Refrigerant mass flow rate (kg/s)	0.9434	0.7966
ORC pump power consumption (kW)	2.8814	0.5595

Table [4-4], The output results of R-245fa and R-134a refrigerants for ORC model

Table [4-5] and [4-6] show all the ORC parameters for each cycle's stream and the operating thermodynamic conditions of the cycle in ISO conditions, including a representation of the effectiveness and NTU to ensure a realistic picture of how the heat exchanger was used. However, in this section, the thermodynamic analysis is based on the first and second laws and has been used to evaluate different outputs and inputs into the cycle, including measures of the thermal efficiency, exergy efficiency and exergy destruction of each component. These parameters were examined with

reference to the variations in the ORC heat source temperature, the turbine inlet temperature and cooling temperature through the condenser.

Stream No.	H (kj/kg)	S (kj/kgK)	M (kg/s)	T (C°)	P (bar)
1	292.9406	7.6543	1.2419	280.9153	0.8966
2	149.6467	7.361	1.2419	145	0.8866
3	458.6986	1.7853	0.8024	70	6.0998
4	435.787	1.7892	0.8024	37.8278	1.6408
5	236.4771	1.1269	0.8024	27.3911	1.6308
6	92.3801	0.3253	5.4657	22	1
7	121.6743	0.4232	5.4657	29	1.24

Table [4-5], The ORC's parameter for each stream

Parameters	Value
R245a Thermal Efficiency (%)	9.3
ORC microturbine power (kW)	16.88
Evaporator Effectiveness	0.6
Evaporator NTU	0.9

Table [4-6], The ORC's energy properties

Table [4-7] shows the exergy and specific exergy as calculated for each stream, while Table [4-8], shows the exergy destruction for each component. In comparing ORC components, it was found that the total exergy destruction of the ORC was 48.4 kW, while the most significant source of exergy destruction rate occurred in the evaporator, representing 64% of the total heat input, which accounted for 94% of the total exergy destruction; as represented in Fig [4-13]. This was due to the heat transfer process between the high temperature heating source and the working fluid. The ORC turbine was responsible for 3.4% of the total exergy destruction with an exergy value of 1.76 kW. These results are in agreement with the literature [85, 29].

Stream No.	e (kW)	E (kW)
1	71.2516	88.4865
2	14.07	17.47
3	67.13	51.82
4	42.92	33.13
5	34.5	26.63
6	0.36	1.88
7	1.43	7.54

Table [4-7], the exergy and specific exergy for each stream of ORC

	Ed (kW)	y*D
Evaporator exergy destruction	45.8315	94.63198
Turbine exergy destruction	1.7619	3.637937
Cooling H.E exergy destruction	0.8379	1.73008
Overall exergy destruction	48.4313	100

Table [4-8], The exergy destruction of each component of ORC

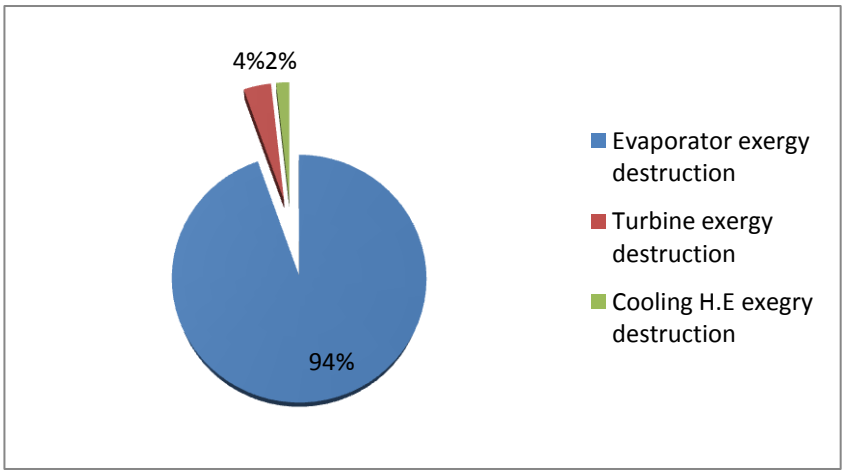

Fig [4-13], Pie chart for exergy destruction in all components

Fig [4-14] shows the effect of the difference in heat source on the output electric power. However, all results are listed in Tables [3] in the appendix A. As the difference in the heat source is increased, the output power increases. The generated power is then increased by about 6% for each 10°C increase in heat source temperature. This is because of releasing more heat to the working fluid passes

through the evaporator, which allows for increases in the temperature difference between the working fluid and heat source, so that the output power increases. In other words, the maximum use of the heat source leads to an improvement in the system output power. Thus, the thermal efficiency increased by about 2% for each 10°C increase in the heat source, as shown in Fig [4-15].

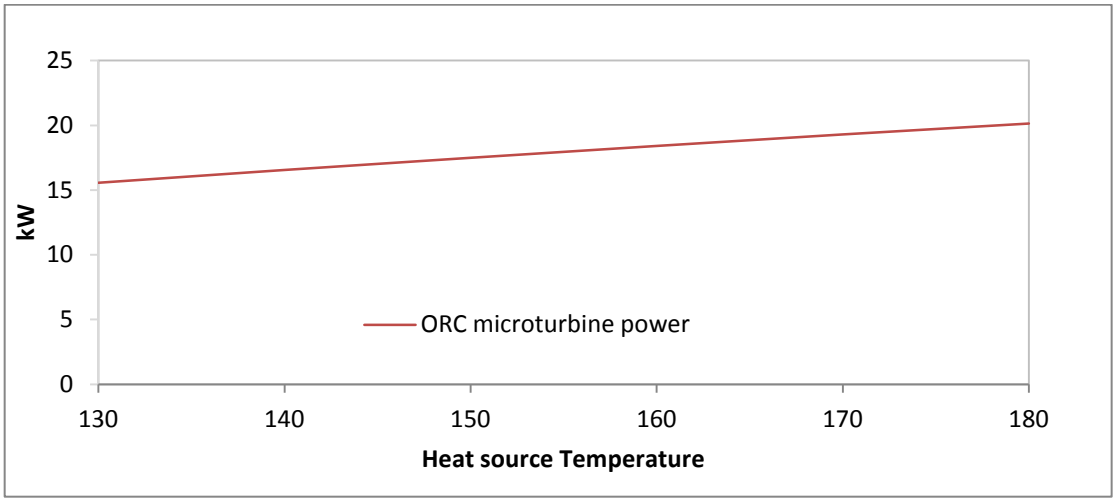

Fig [4-14], Heat source against output power

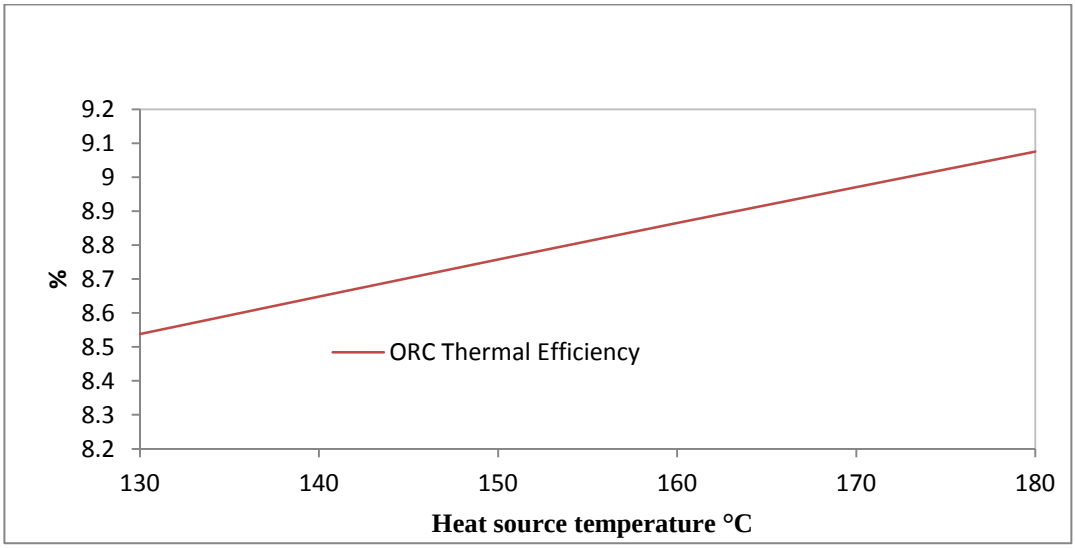

Fig [4-15], Heat source against thermal efficiency

Releasing more heat in the evaporator causes a reduction in heat source outlet, which increases the temperature of the working fluid going into the evaporator. This contributes to raising the rate of irreversibility efficiency of the ORC. Fig [4-16], illustrates the effect of the heat source on the exergy efficiency. The exergy efficiency shows only an insignificant increase with the increase in the heat source temperature.

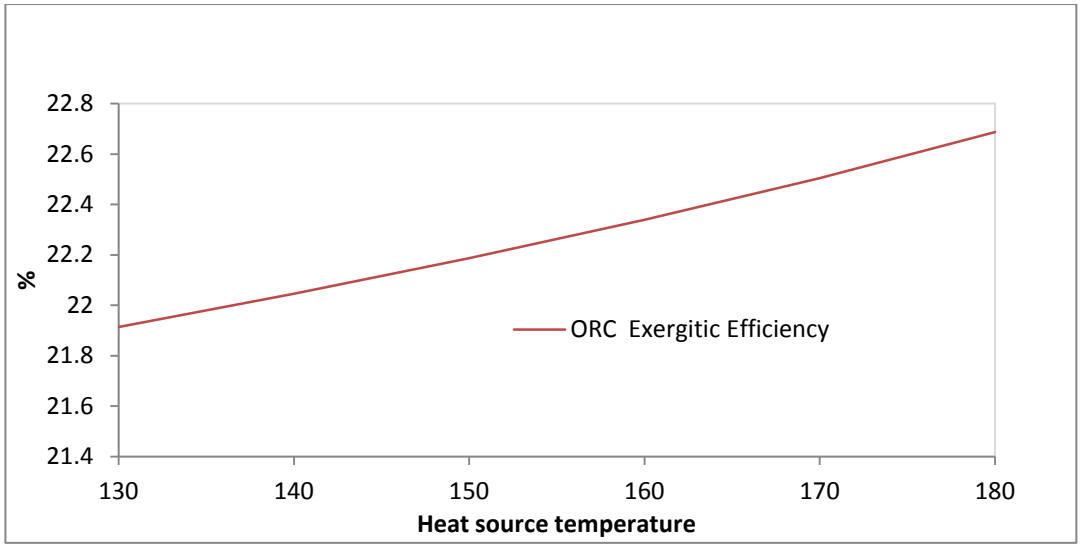

Fig [4-16], heat source versus exergy efficiency

A parametric study investigation was also carried out into the effects of turbine inlet temperature (T_3) which rose from 70°C to 82°C on the ORC parameters. All results are listed in Table [4] in the appendix A. Fig [4-17] shows the effect of the T_3 variation on the power output. The ORC generated power increased as the turbine inlet temperature increased. As the turbine pressure increased for 13%, the increasing average of output power was in the range of 0.4% for each 5°C, increasing in T_3. Fig [4-18] illustrates the impact of inlet temperature variations on the ORC thermal efficiency. As the output power increased, the results show that, the thermal efficiency was increased by 1% in the course of the increase of 15°C in T_3.

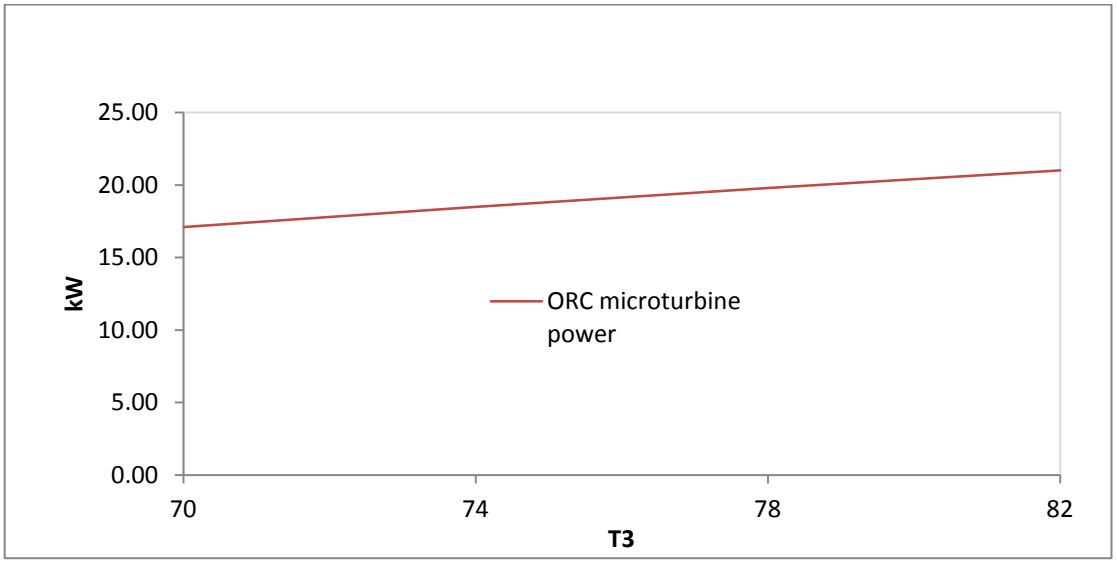

Fig [4-17], T_3 variation against output power

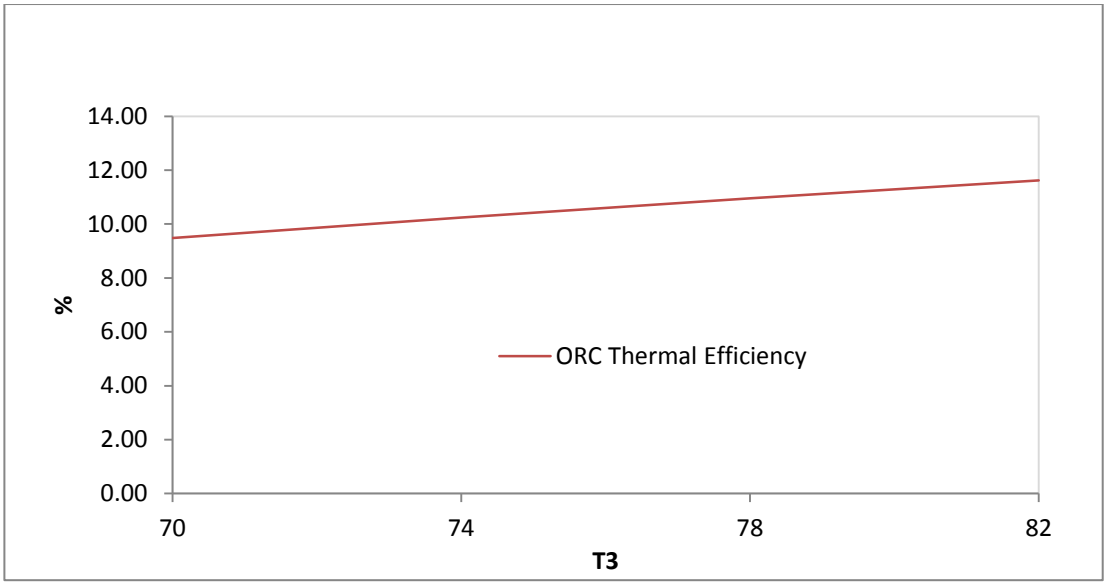

Fig [4-18], T_3 variation against thermal efficiency

Regarding the second thermodynamic biases, the behavior of the turbine inlet temperature variation on the ORC exergetic efficiency was addressed in Fig [4-19]. It was found that the exergetic efficiency increased by 0.3 % for each 5°C increase in turbine inlet temperature. This was due an increase in the enthalpy and entropy of the inlet working fluid to the turbine, which was associated with an increase of pressure rate. As the turbine inlet temperature and pressure increased, the exergy destruction decreased in the turbine, due to increases in the pressure difference of the turbine inlet and outlet. The evaporator exergy destruction decreased to about 4.5% for each 5°C increase in T_3, as the result of an increase in pumped working fluid to the evaporator, which in turn increased the difference in the working fluid temperature in the evaporator, as illustrated in Fig [4-20]. However, the working fluid coming out of turbine was cooled through the condenser, and a high drop in enthalpy had taken place. As a result, the exergy destruction of the condenser had increased by about 32% for each 5°C increase in turbine inlet temperature. In general, the variation of turbine inlet temperatures resulted in only insignificant changes in ORC thermodynamic energy and most of the exergy. As an increase in turbine inlet temperature is associated with increases in inlet pressure, operating the ORC at a lower turbine pressure and temperature can contribute to the required savings in total cost. These results are in agreement with [29,84,85].

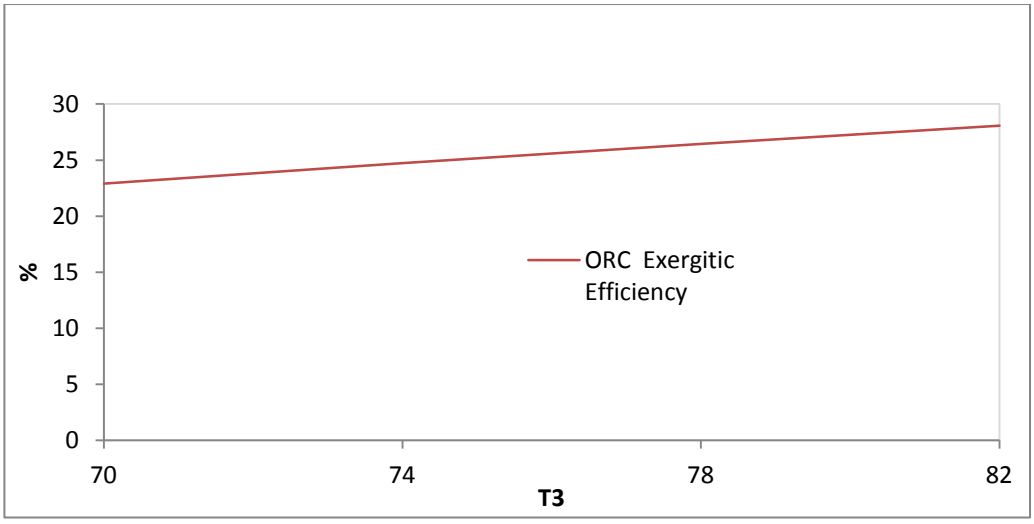

Fig [4-19], turbine inlet temperature against exergetic efficiency

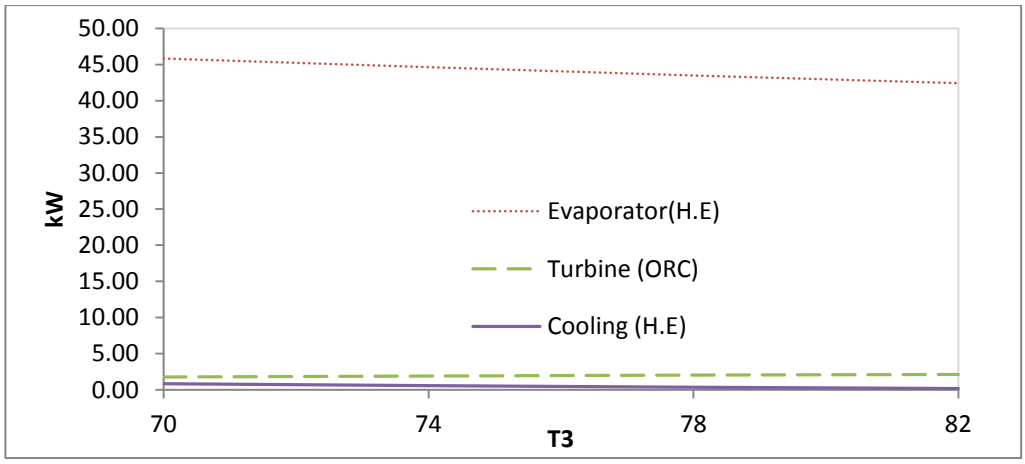

Fig [4-20], Turbine inlet temperature against exergy destruction

The condenser was used in ORC as cooling heat exchanger, and the seawater was assumed to be a cooling fluid at 22°C. However, the cooling water temperature was varied between 20°C and 28°C. All results are listed in Tables [5] in the appendix A. The main purpose of the condenser is to cool the refrigerant working fluid to a saturated state. From Fig [4-21] and Fig [4-22], it can be seen that the thermal efficiency and the system output power decreased with the increase of the cooling water temperature, causing less cooling of the working temperature going to the evaporator, which decreased the difference between the outlet and inlet temperature.

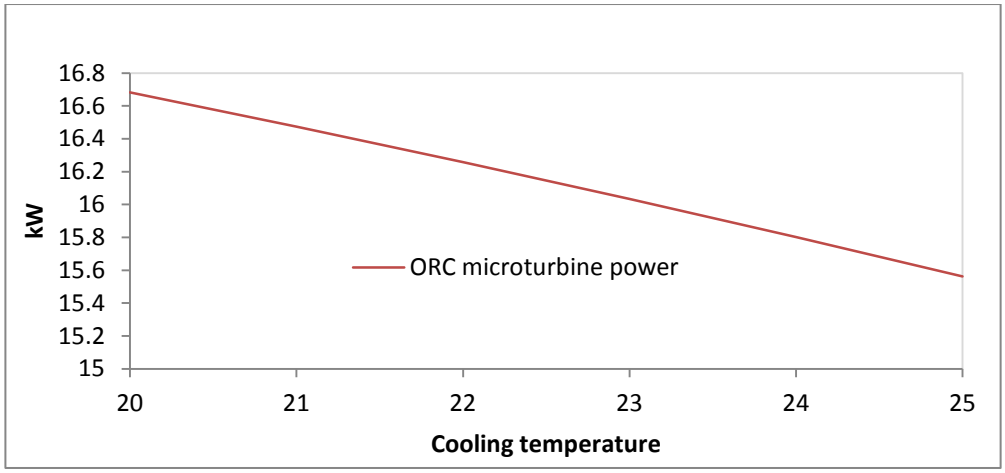

Fig [4-21], the thermal efficiency against water cooling temperature variation

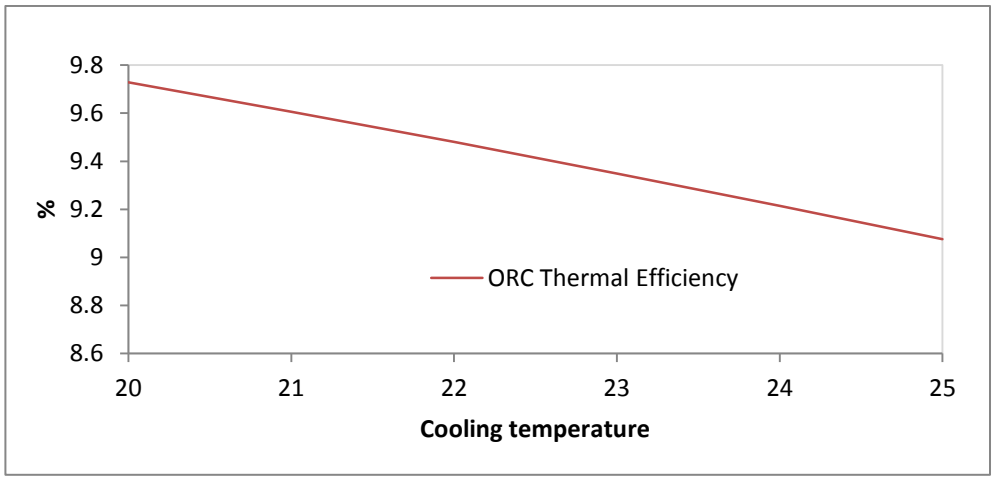

Fig [4-22], the power output versus water-cooling temperature variation

Fig [4-23], shows the exergy destruction of the evaporator, the turbine and the condenser. As the water becomes cooler, the evaporator's irreversibility and turbine increases, due to decreases in the amount of cooling water mass, which increases the difference of the working fluid temperature passing into the evaporator. The exergy destruction of the condenser is increased because of increases in the enthalpy difference of the condenser inlet and outlet that are associated with increases in the cooling water temperature. According to the exergy destruction of each component, exergetic efficiency decreased when the cooling temperature increased, as it can be seen on Fig [4-24]. These results are in agreement with [29,84,85]

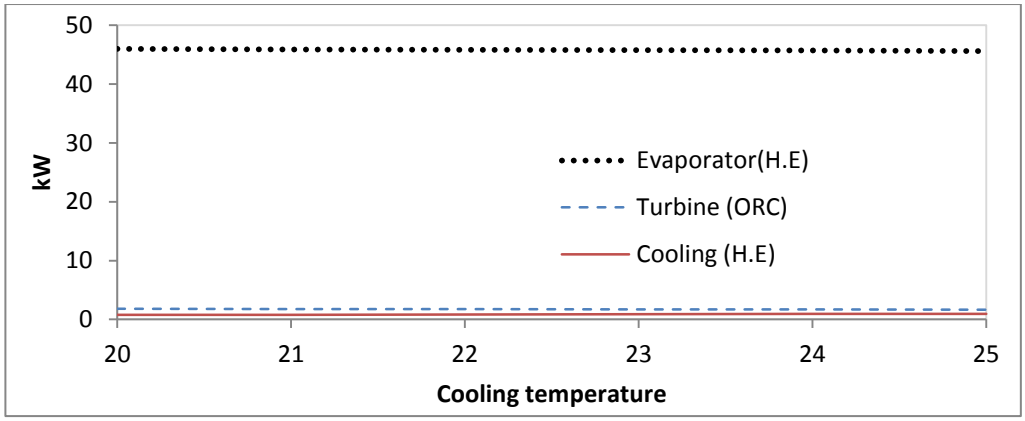

Fig [4-23], the exergy destruction versus water cooling temperature

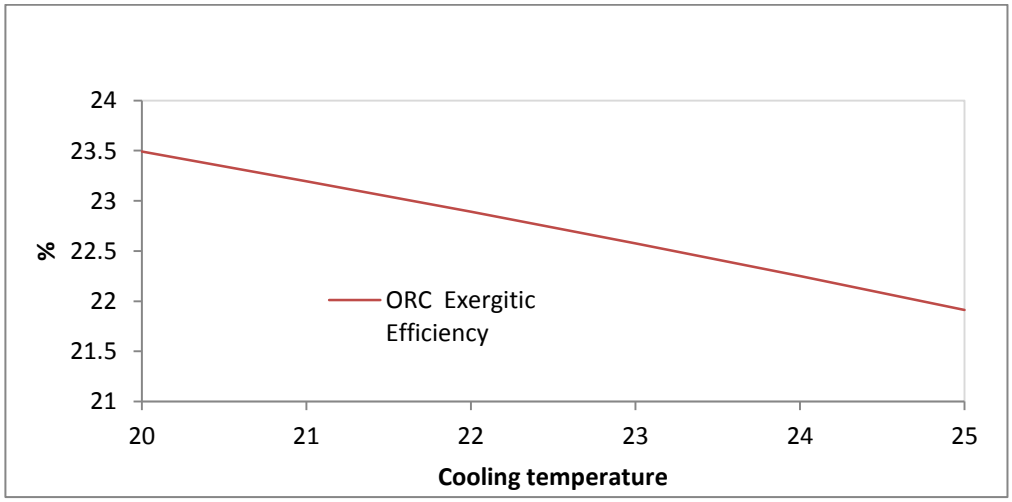

Fig [4-24], the exergy efficiency against water cooling temperature

4.3 Absorption chiller:

The model employed in this study is a water-cooled single-effect lithium-bromide/water absorption chiller with a cooling capacity of 105 kW. It is modelled on the collected data of a SC30 manufactured by Yazaki Energy Systems, Inc [112], which can generate 105 kW, as mentioned in the previous chapter. The model consists of a generator, absorber, evaporator and condenser, in addition to two expansion valves and a small pump and heat exchanger between the generator and the absorber, as illustrated in Fig [4-25].

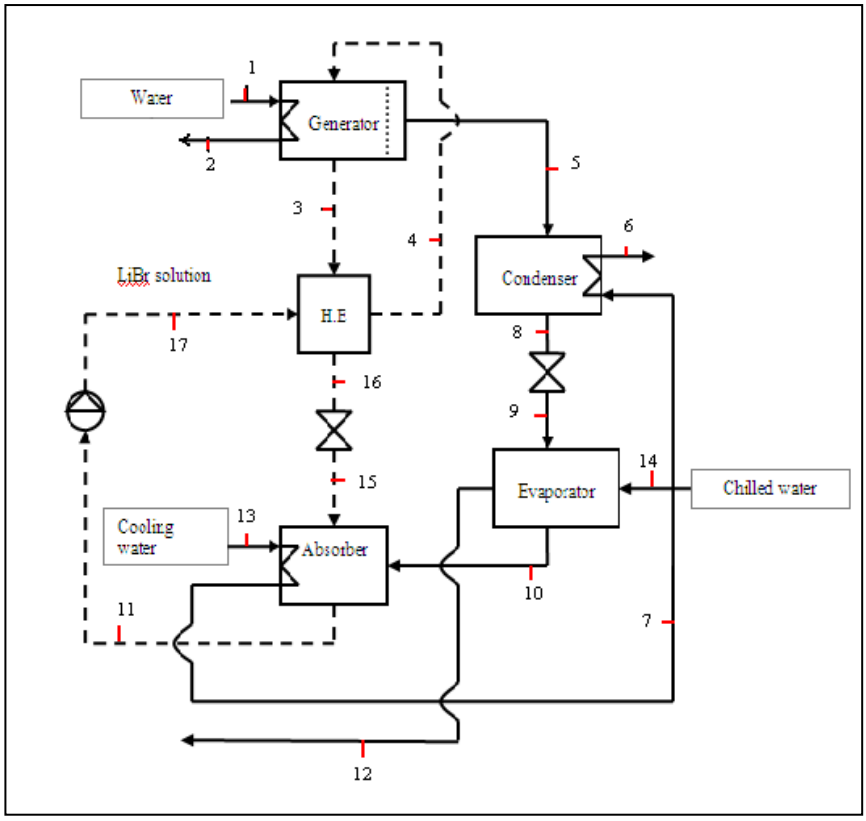

Fig[4-25], Single effect absorption chiller model

The performance of the absorption chiller is defined by the coefficient of performance (COP), which can be obtained by dividing the evaporator's heat transfer to the generator heat transfer. The COP of this model is 0.79. In the course of this investigation, an exergy analysis was performed. Regarding the crystallisation of lithium-bromide during the process, the absorption chiller model's cycle was plotted against the Duhring P-T chart and the line represented was not in contact with the crystallisation curve, as seen in Fig [4-26]. 7.64% of heat energy was consumed in the generator to produce the 105 kW cooling effect from the evaporator. The seawater was used as a cooling fluid to cool the absorber. It entered the cycle with an inlet temperature of 22°C, and then proceeded to cool the condenser.

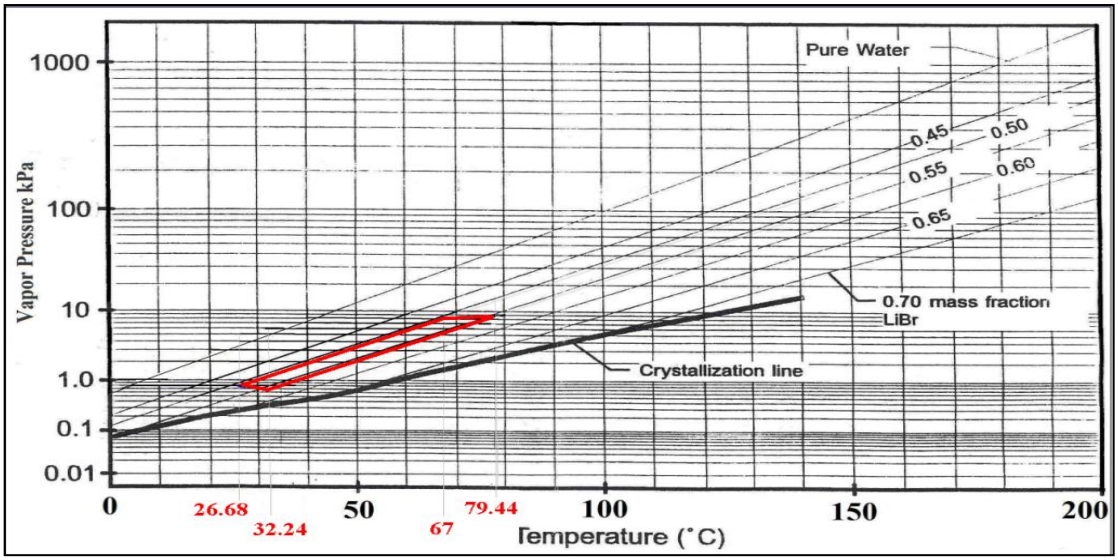

Fig [4-26], The Duhring P-T chart

On the basis of second law analysis, the entropy calculation for each LiBr/H_2O stream was obtained from the entropy curve that was reported by Kaita [106]. The results for the energy parameters for each stream and exergy and specific exergy were calculated and are represented in Table [4-9]. The negative exergies of streams 9 and 10 were justified by the thermodynamic conditions of negative streams which fell below the reference thermodynamic condition, and this was an indication of stored exergy in these two streams [87]. Moreover, based on the exergy balance that was reported in previous chapter, the exergy destruction of each component was calculated as illustrated in Table [4-10].

	H (kj/kg)	S (kj/kgK)	M (kg/s)	T (C°)	P (bar)	W	e(kW)	E(kW)
1	406.45	1.27	4.9	97	1.013	1	41.48	203.27
2	375.39	1.19	4.9	89.62	0.913	1	34.68	169.96
3	181.08	0.475	0.54	79.44	0.08	0.57	39.72	21.41
4	143.37	0.455	0.59	67	0.08	0.52	9.22	5.45
5	2639.02	8.42	0.05	74.4	0.08	1	216.52	11.44
6	166.315	0.58228	3.11	41	1.013	0.04	4.52	14.04
7	125.859	0.45151	3.11	30.99	1.113	0.04	1.75	5.43
8	173.85	0.59	0.05	41.51	0.08	1	4.74	0.25
9	173.85	0.63	0.05	3.76	0.008	1	-5.42	-0.29
10	2445.5	8.83	0.05	3.76	0.008	1	-97.68	-5.16
11	56.88	0.19	0.59	26.68	0.008	0.52	0.49	0.29
12	29.51	0.11	5.2	7	0.913	1	0.52	2.69
13	89.422	0.32997	3.11	22	1.013	0.04	0.33	1.03
14	52.6	0.19	5.2	12.5	1.013	1	0.06	0.29
15	86.12	0.2	0.54	32.24	0.008	0.57	25.4	13.69
16	56.89	0.19	0.59	26.69	0.08	0.52	0.49	0.29
17	86.12	0.19	0.54	32.24	0.08	0.57	25.4	13.69

Table [4-9], The energy and exergy and specific exergy parameter for each stream

Exergy destruction	Exergy destruction
Generator	5.914
Absorber	3.838
Evaporator	2.474
Condenser	2.58
Heat Exchanger	2.557
Exp. Valve	0.537
Overall System	17.9

Table [4-10], The exergy destruction of each component

A number of the absorption chiller's components, including the solution expansion valve in the middle of the heat exchanger, the absorber, and the model pumps, made a contribution of less than 1% to exergy destruction. The exergy destruction of these components was not considered in the calculations due to their insignificant

contribution to the absorption chiller model's total exergy destruction. The proportion of each component's exergy destruction is shown in Fig [4-27]. The largest amount of exergy destruction took place in the generator, representing 29.04% of the plant's total exergy destruction, and consuming 17.76% of the total input exergy into the model. This was generated as a result of the irreversibility, which was caused by the heat transfer between the heat energy source and the absorption chiller refrigerant fluid, as well as the separation process in $LiBr/H_2O$ in the generator. This result is in agreement with a number of previous studies [118].

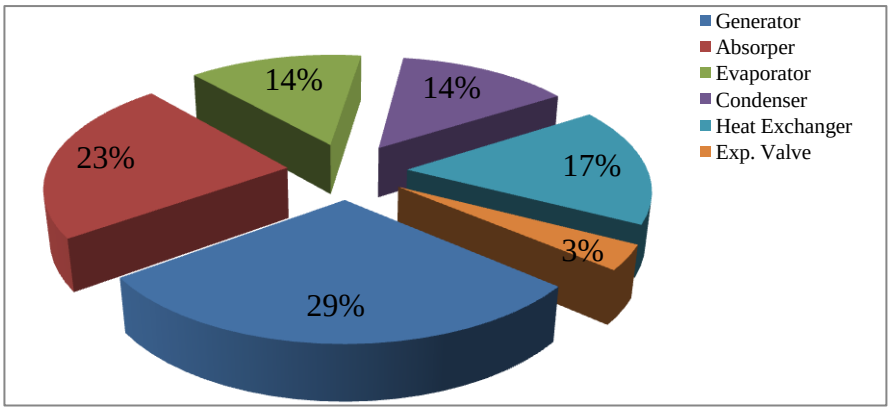

Fig [4-27], Absorption chiller's exergy destruction ratio

The second highest amount of exergy destruction value was found in the absorber, which used 3.83 kW, consuming 11.53% of the total input exergy and forming 23.44% of the total exergy destruction. The heat exchanger consumed 7.68% of the total input exergy, which represented 17.29% of the system's total exergy destruction, while the evaporator caused 13.82% of the system's total exergy destruction, consuming 7.43% of the input exergy. The condenser accounted for 14.41% of the cycle's total exergy destruction, and consumed 7.75% of the total input exergy. The refrigerant expansion valve, which was located in the middle of the evaporator and condenser, consumed 1.61% of the plant input exergy and accounted for 3% of the total exergy destruction.

One of this model's functions is to examine the behaviour of the effect of the evaporator's inlet temperature. Assuming that the inlet cooling water temperature was 22°C, the solution mass fraction at the generator outlet was 0.52%. At the absorber outlet it was 0.57%. The generator inlet mass flow rate and temperature were 4.9 kg/s and 97°C respectively. According to the real data of absorption chiller model, the evaporator mass flow rate was 9 kg/s and the outlet chilled water temperature was

7°C, while the inlet chilled water temperature was 12.5°C. The evaporator inlet temperature varied from 10°C to 22°C, while all the parameters of the first and second law were monitored. The results obtained from the evaporator inlet water temperature variation are listed in Table [6] in the appendix A. Fig [4-28] shows the heat transfer in the generator, absorber, condenser, heat exchanger and evaporator, in proportion to the increase in the evaporator inlet water temperature.

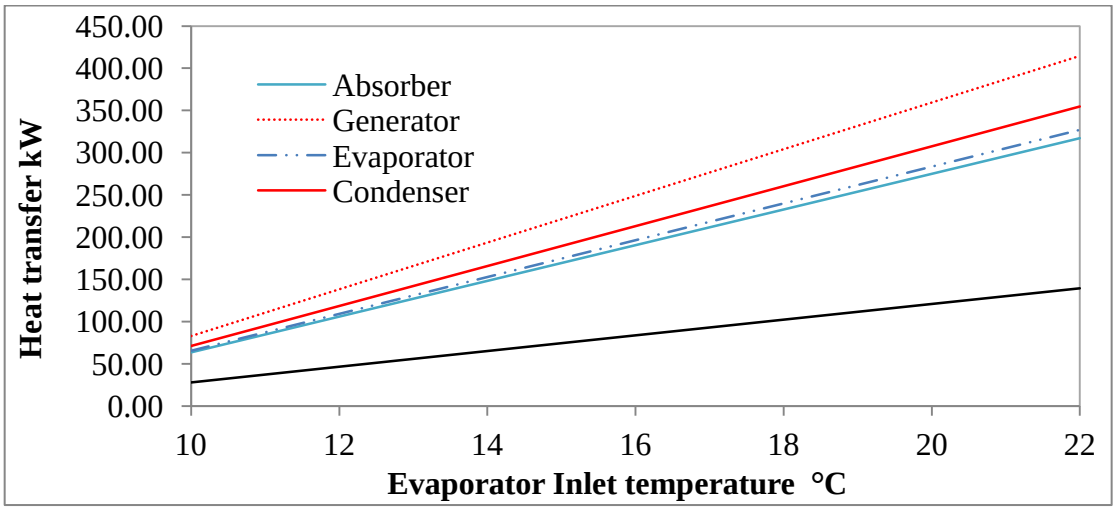

Fig [4-28], Heat transfer of absorption chiller component versus evaporator inlet water temperature

That average of heat transfer that occurred in all absorption chiller heat exchangers was increased in the range of 22.92% for each 2°C increase in the evaporator water inlet temperature, in order to overcome the increase in the evaporator inlet water temperature and meet the required chilled water temperature of 7°C. This increase was mainly driven by the increase in the mass flow rate of all cycle fluids, so that it could achieve the capacity for cooling the evaporator inlet water to a predefined temperature, as shown in Fig [4-29].

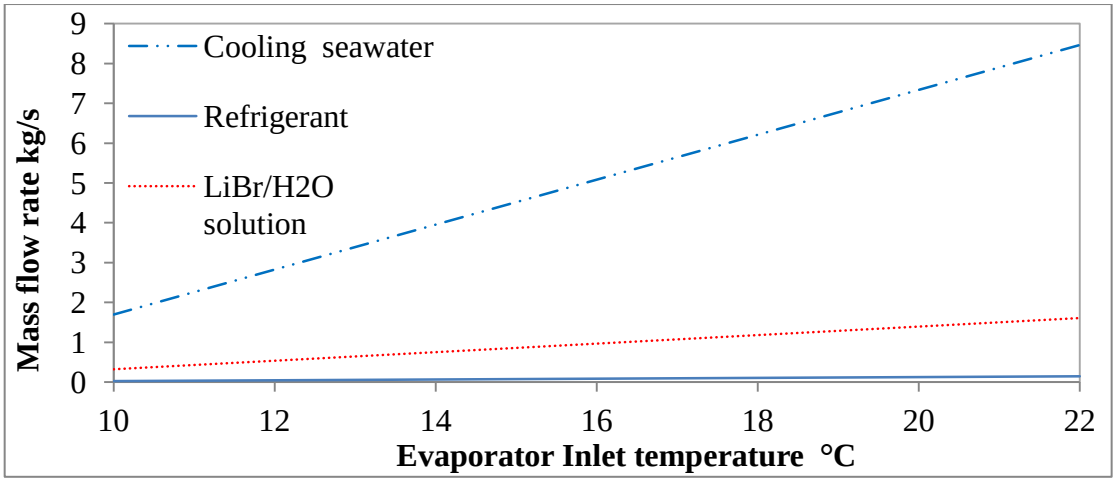

Fig [4-29], Absorption chiller fluid mass flow rate versus evaporator inlet water temperature

If, however, the set of the chilled water temperature was free, then the exergy destruction of the evaporator would be changed as well as the chilled water temperature; as illustrated in Fig [4-30]. The exergy evaporator would have increased by an average of 23.19% for each 2°C increase in the inlet water temperature, which would lead to an increase in the input exergy of the evaporator.

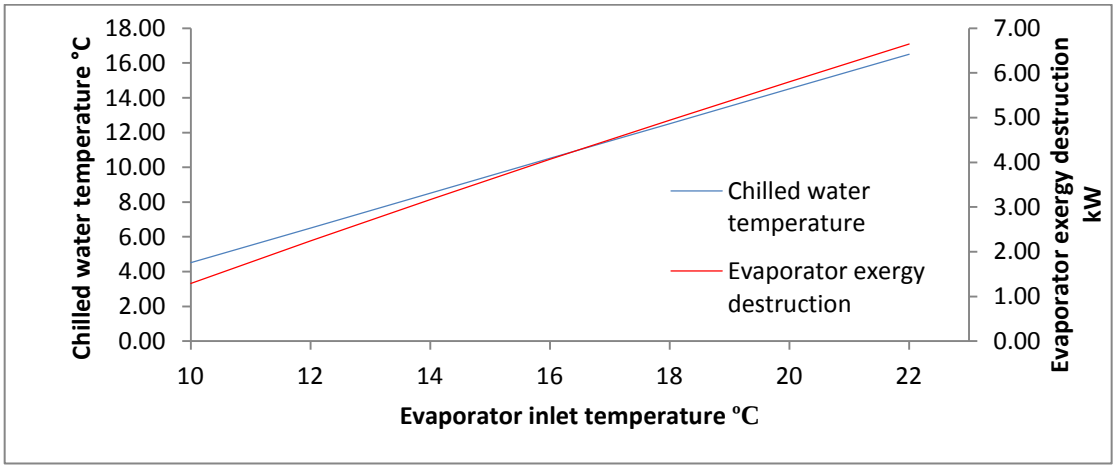

Fig [4-30], evaporator exergy destruction and chilled water temperature against evaporator inlet water temperature

As a result of increases in the evaporator's exergy destruction, the model's overall exergetic efficiency would decrease. This would lead to the chilled water being circulated between the cooling load and the evaporator in order to limit this effect and utilize the chilled water after the cooling load. This parametric study also confirmed the accuracy and reliability of the second-law analysis over the first law. The COP

was only a function of the exergy flow in both the evaporator and the generator. As a consequence, the COP showed no changes, while the exergy analysis reflected all the model's factual responses to any changes in its design variables. Fig [4-31] shows the exergy destruction increasing in all components including the generator, the absorber, the heat exchanger, the evaporator and condenser responding to an increase in the evaporator inlet water temperature as heat transfer increased, when the chilled water is set to manufactured temperature 7°C.

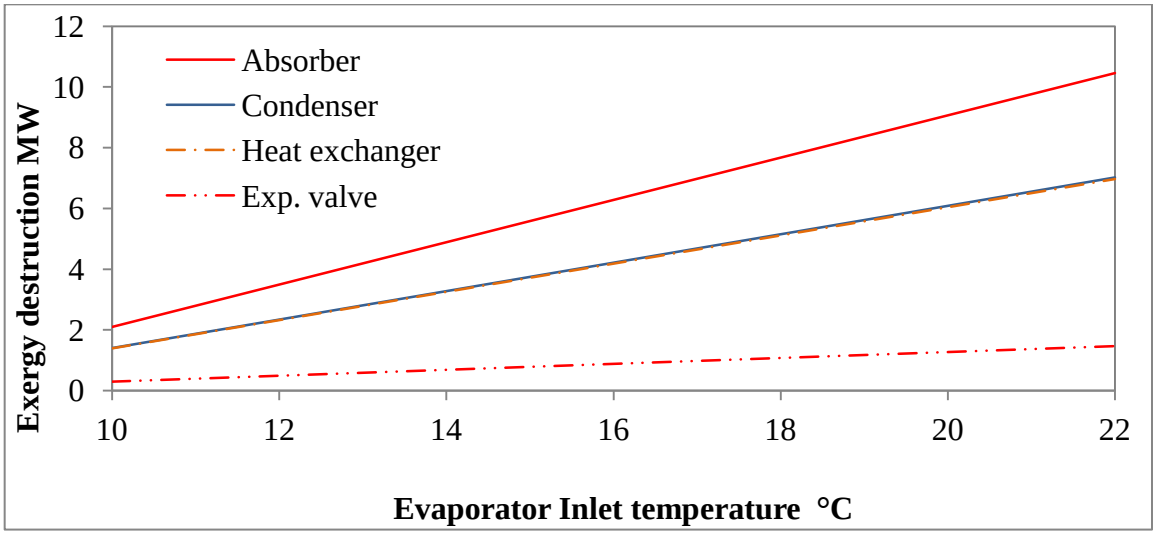

Fig [4-31], Exergy destruction of absorption chiller components versus evaporator inlet water temperature

The justification of this increase in the exergy destruction of model's components is related to the increase in the cycle fluid mass flow rate, as shown in Fig [4-27]. The trends of the generator and evaporator were different, as shown in Fig [4-32]. The evaporator exergy destruction increased in a nonlinear way, due to the nonlinear curve of its input exergy, which was driven by the increase in the evaporator inlet water temperature. The exergy destruction of the generator showed a temporary increase until it reached the maximum value at [20°C] of the inlet water temperature, and then dropped gradually to the value of a lower evaporator inlet water temperature.

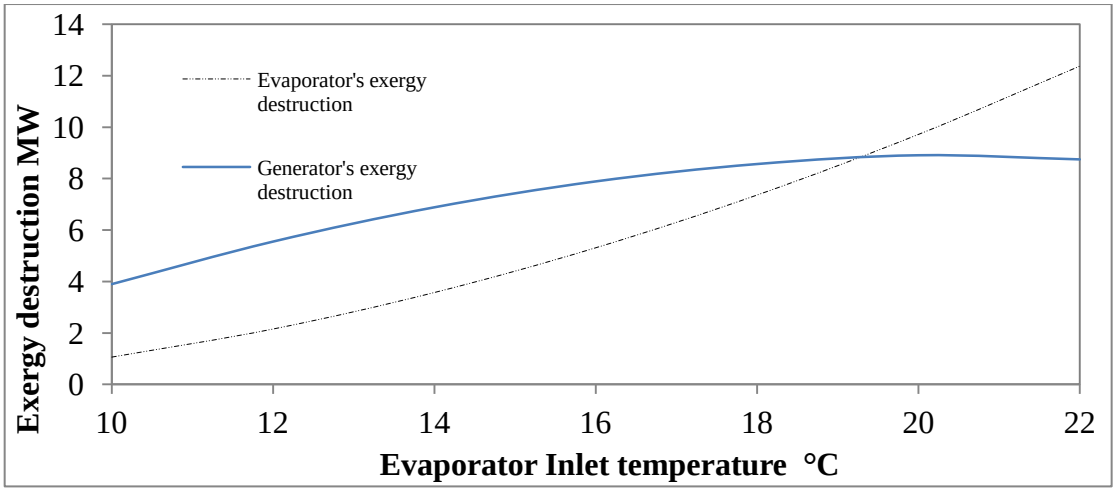

Fig [4-32], Evaporator and generator exergy destruction values against evaporator water inlet temperature

The reasons for this response were the relative temperature of the hot water stream rejected from the absorption chiller by the generator (T_2) and the LiBr/H_2O solution leaving the generator and going to the heat exchanger (T_3). The performance of the temperature ratio (T_2/T_3) is represented in Fig [4-33] against the variation of the evaporator inlet water temperature, which resulted in a decrease in T_2/T_3 as the evaporator inlet temperature increased. This was due to an increase in the cycle mass flow rate. Therefore, extra heat energy is required to maintain a separation process of the refrigerant from the LiBr/H_2O solution.

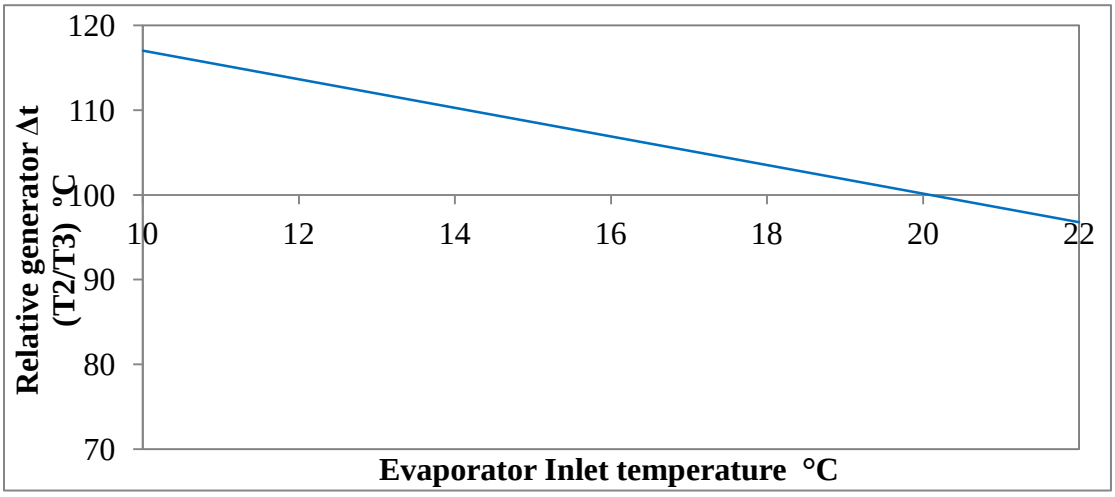

Fig [4-33],T_2/T_3 versus evaporator inlet water temperature

In the previous fig [4-30]-[4-32], it was shown that the exergy destruction of all cycle components increased with the raising of the evaporator's inlet water temperature. As a result of this effect, the exergetic efficiency declined. Fig [4-34] shows the

proportional relationship between the model's exergetic efficiency and the evaporator inlet water temperature.

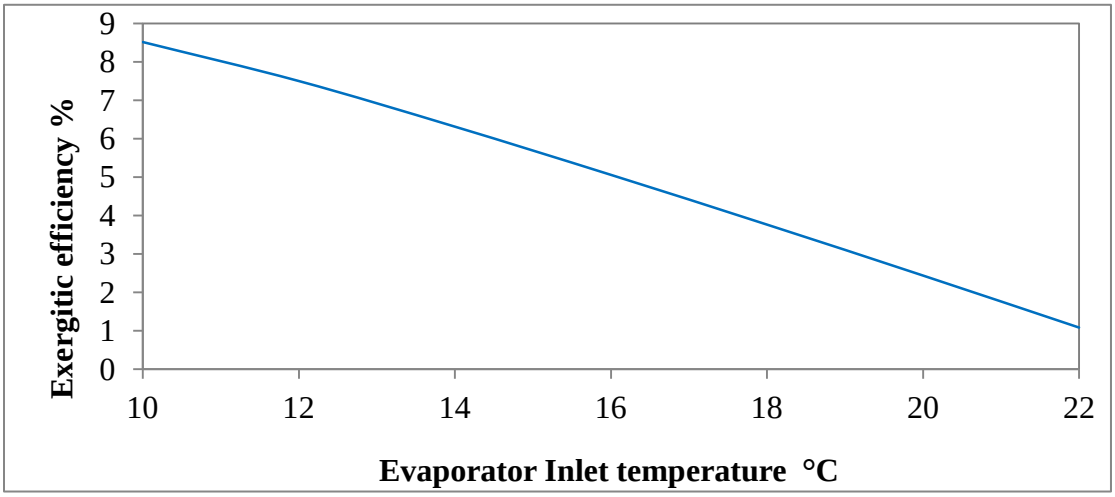

Fig [4-34], absorption chiller exergetic efficiency versus evaporator inlet water temperature

An investigation of the absorption chiller performance under the cooling water variation was employed in this study. The scale of cooling water temperature was set at between 20°C to 28°C, to match the variations in the temperature of the Red Sea. Many actions were taken within the absorption chiller model's parameters. Firstly, the $LiBr/H_2O$ solution concentration was set at the absorber and generator outlet, along with the energy mass flow rate of the energy source. Table [7] in the appendix A shows the results of this parametric study. However, the most significant result will be discussed in this section. It was found that, as shown in Fig [4-35], an increase of 11.88% in the cooling water mass flow rate resulted by a 2°C increase in the cooling water temperature. This was intended to cool the absorber and the condenser to the specific degree defined by the evaporator capacity for the condenser and by the $LiBr/H_2O$ solution concentration for the absorber.

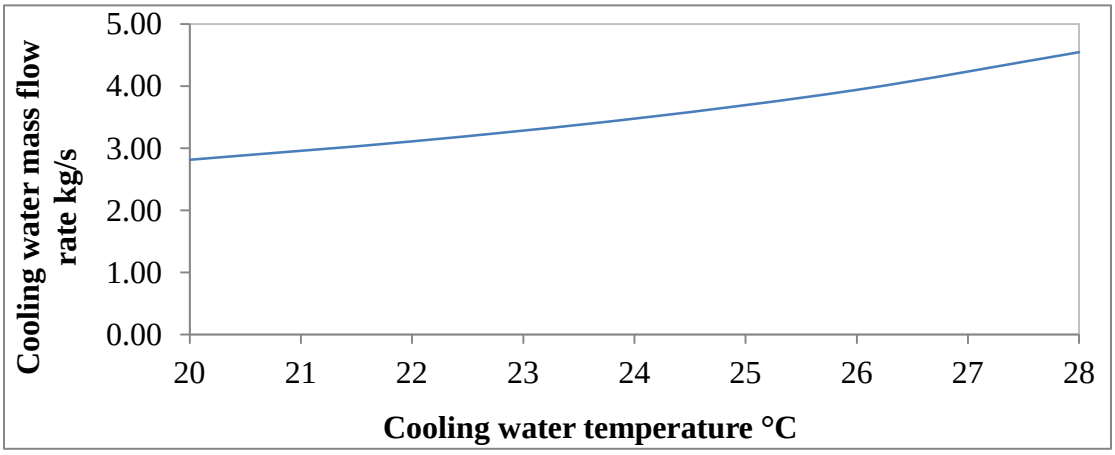

Fig [4-35], Cooling water mass flow rate against its temperature

The increase in the cooling water temperature had an effect on the exergy destruction of the absorber and condenser, as illustrated in Fig [4-36]. The absorber exergy destruction decreased by 14.36% and followed the same trend by 12.49% for the condenser for each 2°C increase in the cooling water temperature. This was due to the change in the input and output exergy rates. Also, the mass flow rate was maintained according to the cooling water temperature, in order to provide the required cooling capacity. However, if the cooling mass flow rate was set at a fixed amount, then the exergy destruction performance would have increased for both the absorber and condenser. This implies that changes in the cooling water mass flow rate can have a direct effect on the existing exergy destruction for both the condenser and the absorber, which result in reducing their exergy destruction. The effect of the variation in cooling water temperature on the absorber and condenser seemed to indicate no effect on the model's exergetic efficiency, as the latter was only a function of the evaporator and generator parameters.

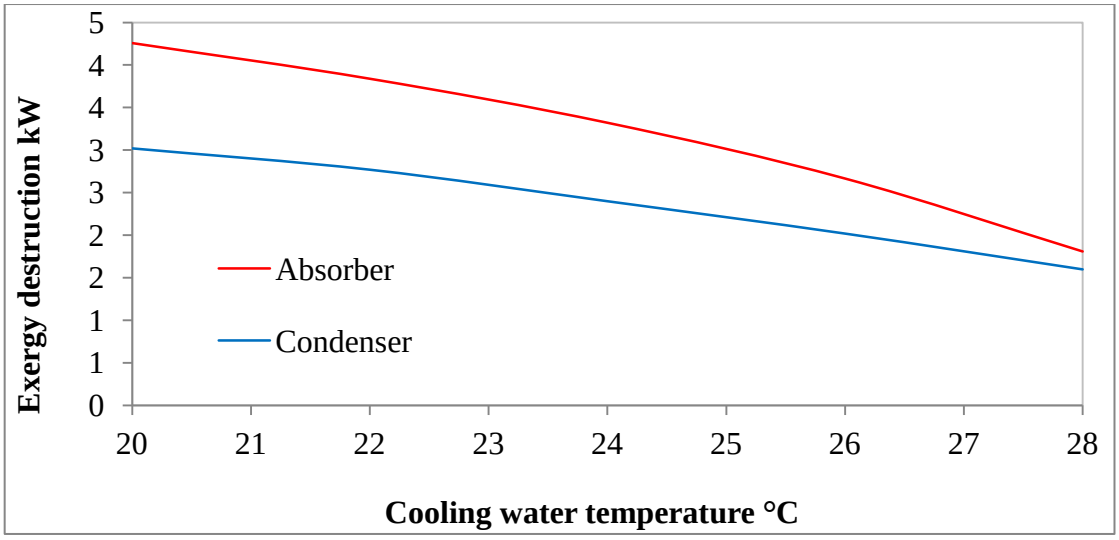

Fig [4-36], absorber and condenser exergy destruction versus cooling water temperature

Another examination also took place concerning this model, which tested the model performance under the variation of inlet water heat source temperatures. The same assumptions were adopted as in the previous study. In order to meet the real model data production, the variation in the heat energy source temperature was limited to 99°C to avoid the boiling point of hot water being reached. Fig [4-37] illustrates the changes in the generator mass flow rate and its exergy destruction when the generator inlet hot water temperature was varied. All the results are represented in Table [8] in the appendix A. The exergy destruction rate of the generator was increased, and the minimum value was found to be 87°C. However, when this temperature was lower, the exergy destruction and the hot water mass flow rate rapidly decreased, and an increasing in both parameters was recorded of 87°C. When the temperature varied by more than 87°C, the exergy destruction rate of the generator increased on average by 4.9% for each 2°C increase in its input hot water temperature. This due to the fact that, the system cannot used the extra heat as it is designed to a limited output power (kW), so extra heat will be destroyed which rise the exergy destruction of generator. Moreover, the average decrease by 18 % of input hot water mass flow rate typically occurred above this temperature.

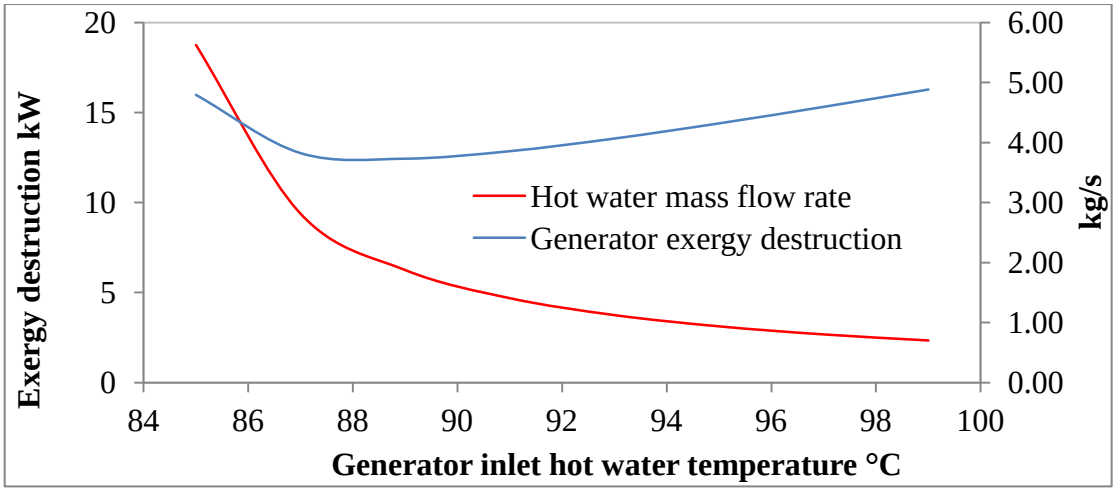

Fig [4-37], Generator inlet hot water temperature against mass flow rate and generator exergy destruction

Following to the investigation of the effect of the generator inlet hot water temperature on the cycle, the model's exergetic efficacy was also examined. Fig [4-38] shows how the exergetic efficiency started by increasing its value from 7.38% at 85°C of inlet hot temperature, and then dropping again to reach 7.36% at 99°C. The exergetic efficiency curve touched the maximum value of 7.63% at 89°C of inlet hot water temperature. This occurred mainly because of the behaviour of the exergy input curve, as shown in that same figure. This was affected by the decrease in the generator's hot water mass flow rate. The exergy analysis of this parametric study showed that the absorption chiller should be operated with an inlet hot water temperature of 87°C, in order to achieve a lower rate of exergy destruction in the generator. However, this finding can be added as a suggestion for the improvement of the real data.

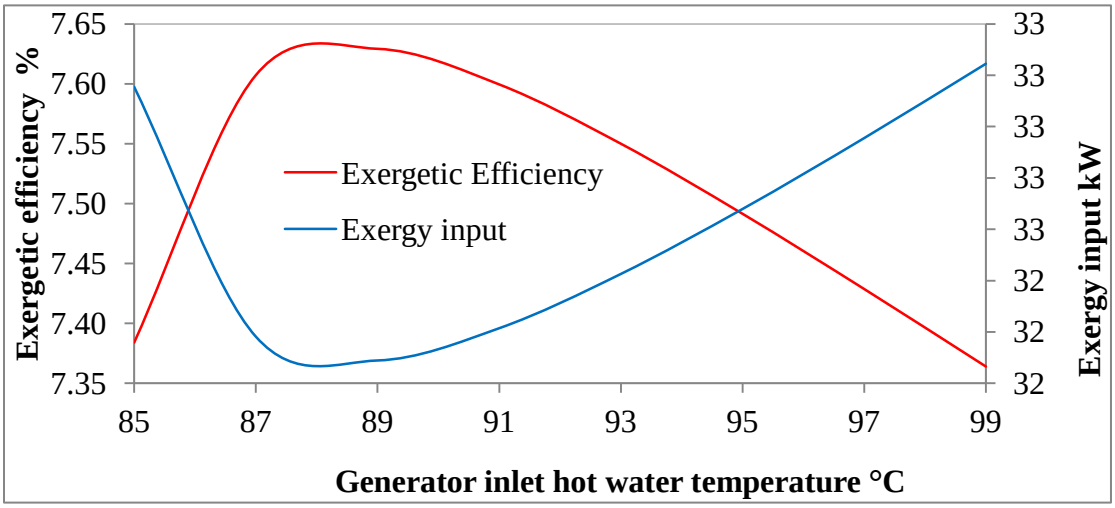

Fig [4-38], Exergetic efficiency and exergy inlet against generator inlet hot water temperature

4.4 MED Desalination Plant

The MED can be considered one of the most efficient thermodynamic methods. This type of thermal desalination has been included in this study. Since the thermal desalination technologies are not common in small-scale water production, it can be operated by the waste heat energy from high-grade heat. Therefore, the opportunity for modelling and simulating small-scale multi-effect distilled desalination (MED) is becoming a great challenge. Furthermore, TVC-MED desalination is another method of thermal desalination, which has also been employed in this study. The intention is to provide a better view of the comparison between these two methods. The proposed MED contains single-effect distillation cells (evaporator), a condenser and a pump; as shown in Fig [4-39]; while Table [4-11] lists the energy parameters of each stream in the proposed cycle.

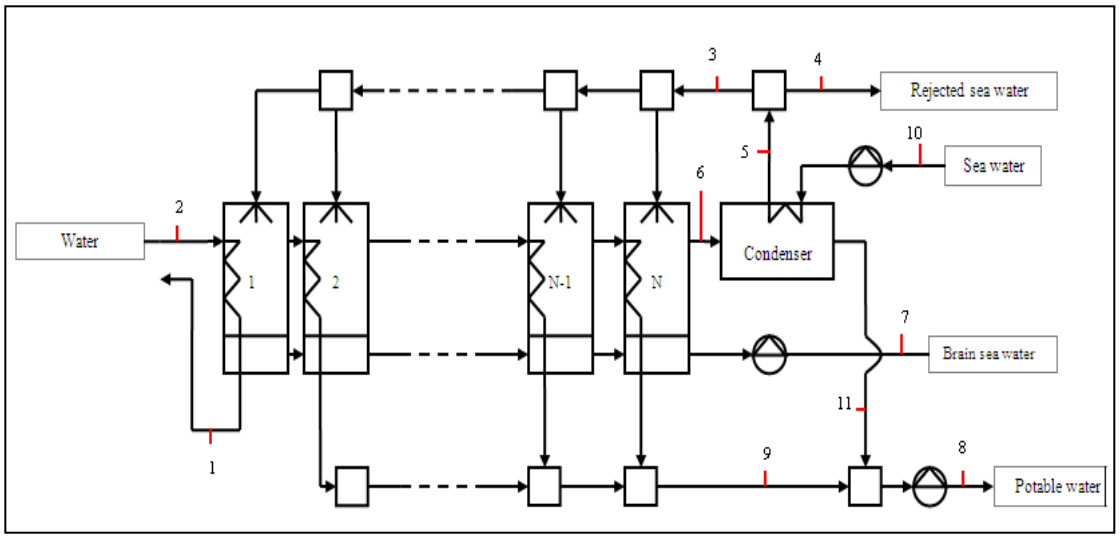

Fig [4-39], Proposed multi-effect desalination plant

	H (kj/kg)	S (kj/kgK)	M (kg/s)	T (C°)	P (bar)
1	295.1271	0.9611	0.0875	70.5034	0.319
2	2627.0000	7.7450	0.0875	70.5861	0.32
3	177.7352	0.6299	1.2936	44.7198	1.50
4	177.7352	0.6299	0.3771	44.7198	1.50
5	177.7352	0.6299	1.6708	44.7198	1.50
6	2592.054	8.0905	0.0633	50.3269	0.12
7	192.0341	0.6946	0.6936	50.3725	2.00
8	250.3753	0.8284	0.6000	59.7820	2.00
9	255.2233	0.8434	0.5367	60.9748	0.30
10	87.3632	0.3300	1.6708	22.0000	1.02
11	206.8845	0.6962	0.0633	49.4098	0.30

Table [4-11], The MED's energy parameters of each stream

The validated and reliable proposed model for MED can be obtained through IpsePro software. As well as facilitating the carrying out of a number of parametric studies, this may improve the quality of results by making possible investigations. The performance of the proposed model set against variations in thermodynamic properties. The number of effects was validated through a parametric study by examining the model, and varying a number of effects from two to nine. This study was performed at a seawater temperature of 22°C salinity of 0.04 kg/kg, according to the Red Sea data that was presented in the previous chapter. The results are listed in Table [9] in the appendix A. Also, the proposed model demonstrates the capability of producing a maximum amount of potable water of 53 m^3/day. However, the most significant result are represented and discussed in this chapter. Compared with other forms of desalination technology, the MED is considered to be a form that can be utilized by the microturbine's exhaust heat energy, which adds more effects to enhance its thermal performance. This should improve the gain output ratio (GOR) and reduce the specific heat consumption [70,74].

The GOR of the desalination plant is shown in Fig [4-40], which illustrates illustrated its behaviour in relation to a number of effects. This figure shows that in terms of occupying extra effects, the GOR would have improved by an average of 20.8% as a result of a reduction in the input energy by 16.4% for each additional effect required to produce the 53 m^3/day. The reason for this reduction in the input energy of the total heat transfer area is that each effect has the ability to evaporate a portion of the feed

seawater. Adding an extra effect with a lower pressure made it possible for the rejected brine to be evaporated once more, using the heat energy in the steam produced from the previous effect.

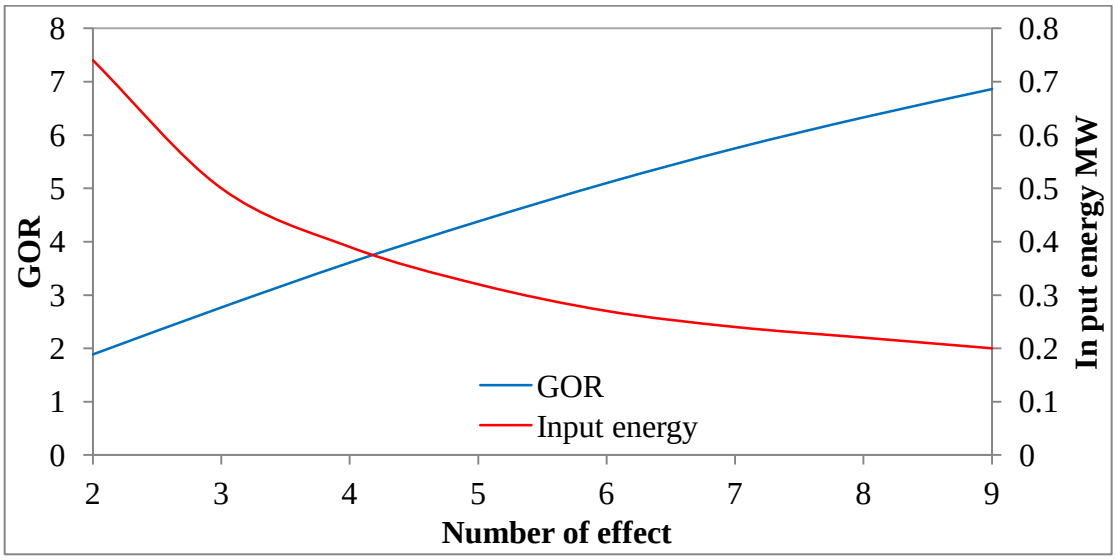

Fig [4-40], GOR and input energy versus number of effects

The behaviour of the specific heat consumption has been influenced by the increase in the number of effects, as shown in Fig [4-41], which indicated an average decrease of 16.4% for each additional effect. The concentration factor of the MED desalination showed a slight increase of 0.2% for each additional effect, due to an increase in the rejected brine water concentration associated with the exposure to more evaporation processes which occurred in the additional effect. The results obtained were in agreement with the literature [119,120].

As mentioned previously, the study of thermal desalination processes has included both MED, and TVC-MED methods. Therefore, as shown in Figures [4-40] and [4-41], GOR behaviour has only been investigated for the optimum number of nine effects, and this has been connected to the TVC-MED study, the results of which will be outlined in the next section of this chapter.

The salinity seawater in the proposed MED desalination was assumed to be 0.04 kg/kg and to have a temperature of 22°C. This plant consumed 340.08 kj/kg of heat energy to produce 53 m^3/day of potable water at a concentration factor of 1.86, and a gain output ratio (GOR) of 6.86. The modelled plant consumed 0.4 kW of electricity to drive three pumps at the seawater feed and drain, as well as at the water sink. Ensuring an economical size for the proposed condenser was achieved by calculating

the effectiveness and NTU. It was designed with an effectiveness value of 0.6 and 1.76 NTU, which is generally in agreement with the literature [104,105].

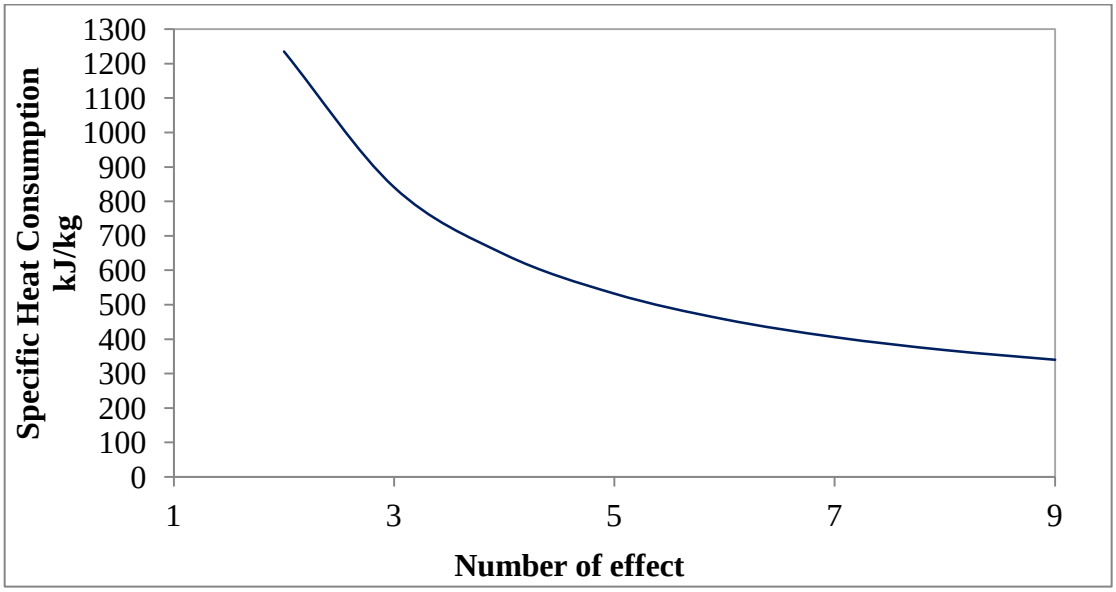

Fig [4-41], the effect of the number of effects on the specific heat consumption

The specific levels of energy and exergy were calculated for each stream in the proposed model on the basis of second law analysis. Then the exergy destruction in the evaporator (considered as one unit) and the condenser was carried out. The enthalpy and entropy of each seawater and brine water stream were calculated using the equations and methods presented in the previous chapter. The salt reference conditions were taken to be at ISO i.e temperature 15°C and at a pressure of 1.03 bar, where the enthalpy and entropy of salt in these conditions were h=12.552kJ/kg, and s=0.04473kJ/kgK respectively.

As the exergy and specific exergy are listed in Table [4-12] for each stream, as indicated in Fig [4-39]. The rejected brine streams of 4 and 7, as shown in Fig [4-39], indicated positive exergy, while other studies [107,108] showed different results, in which the exergy of the brine water was below zero. The negative exergy of rejected brine streams was justified by the fact that the salt concentration was higher than that considered in the reference conditions, which meant that more energy was required in the brine stream in order to dilute its concentration to meet the reference condition concentration. However, the salinity and temperature were controlling the exergy values in the brine water streams. The level of exergy was reduced by an increase in the brine water salinity, while it increased with the rise in temperature. This study presents positive exergy values of both brine water streams, due to the fact that the

designed reference condition was 15°C, a result which differs from those of previous similar studies, such as that of Kahrman, et al., in which the reference condition was 35°C [108]. With regard to the exergy balance presented in the previous chapter, the calculation of the evaporator exergy destruction values is shown in Table [4-12]:

	e (kJ/kg)	E (MW)
1	19.971	1.7476
2	398.087	34.8346
3	5.9003	7.6328
4	5.9003	2.2252
5	5.9003	9.858
6	263.6536	16.6779
7	4.5634	3.1653
8	12.2461	7.3476
9	12.7297	6.8326
10	0.3484	0.582
11	7.0466	0.4457

Table [4-12], Exergy and specific exergy results of proposed MED desalination

According to the exergy results, the most significant exergy destruction was found in the evaporator, with a value of 16.76 kW, which represented 70.6% of the plant's total exergy destruction. This result shows that a significant amount of exergy was destroyed in the evaporators. In addition to the destruction caused by the pump, the heat transfer process played a significant role with regard to the first effect that exposed the maximum heat energy input. Another source of irreversibility in the evaporator was that the pressure dropped from one effect to other [90]. The condenser formed 29.33% of the proposed model's total exergy destruction, with an exergy destruction of 6.95 kW, caused by the heat transfer process. This proposed model operated with a total exergy destruction of 23.71 kW, resulting in an overall exergetic efficiency of 29.68%. This performance was in agreement with existing studies [80, 90, 91].

The first and second laws of thermodynamic provided the guidance to investigate the off-design performance. An examination of the variations in the behaviour of the seawater on the plant performance is included in this study. This was carried out

through a parametric study that varied the seawater temperature from 20°C to 28°C with a seawater salinity of 0.04 kg/kg. Table [10] in the appendix A shows all the results of this study, and the most significant results are discussed in detail. Increasing in the seawater temperature resulted in raising the value of the GOR of the proposed MED model, due to the reduction in the input heat energy source mass flow rate, as presented in Fig [4-42].

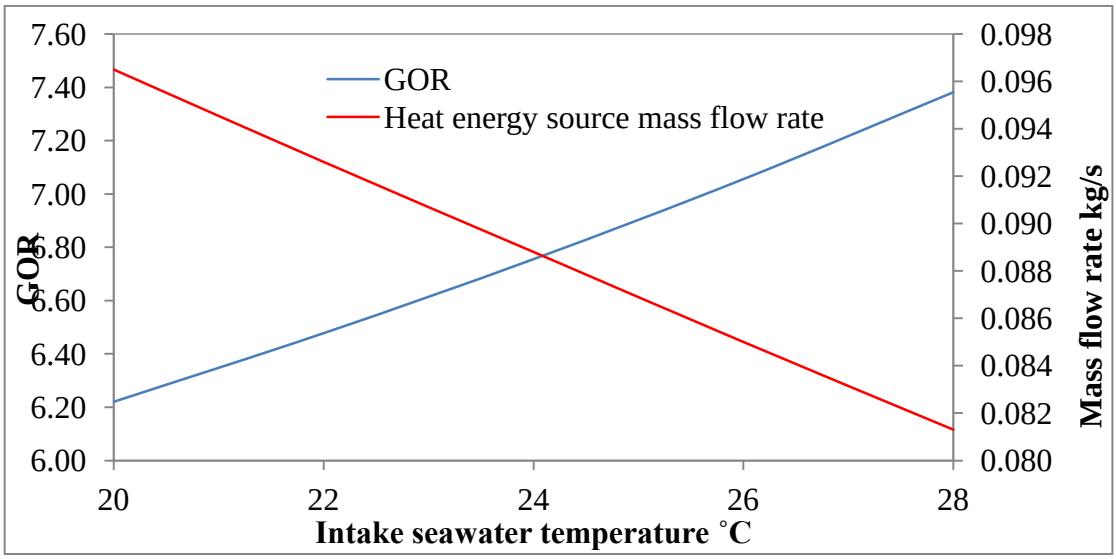

Fig [4-42], Intake seawater temperature variation against GOR and heat energy mass flow rate

The mass flow rate of the input heat energy source decreased, due to the fact that the first effect required low heat energy to raise the seawater temperature to boiling point, when evaporation occurs. Also, for each 2°C increase in the intake seawater temperature, the heat transfer in the first effect was reduced in the range of 0.3%. These findings for the performance of the intake seawater temperature variations were in agreement with Alasfour, et al [119]. The specific heat consumption decreased on average by 1.24% for each 2°C increase in the intake seawater temperature, which was caused by the reduction in the heat transfer in the first effect. As the temperature of the intake seawater increases, the heat transfer of the first effect decreases, when less heat input is required to obtain the evaporation. This effect of the intake seawater variation was illustrated in Fig [4-43].

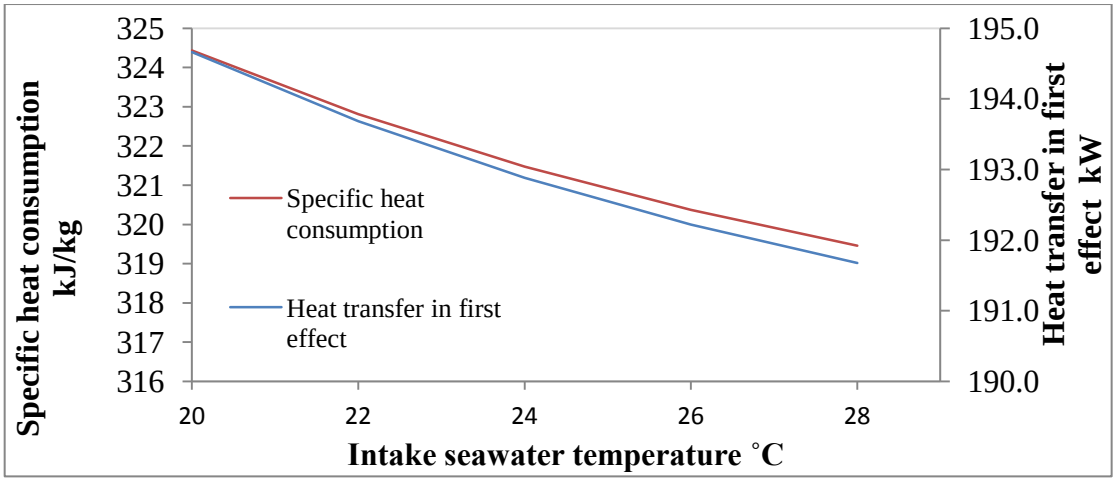

Fig [4-43], Heat transfer in the first effect and specific consumption versus intake seawater temperature

As the temperature of the intake seawater increased, the condenser input exergy decreased. This became a source for the dropping the exergy destruction of the condenser by an average of 11.47% for each 2°C increase in the intake seawater temperature. However, the exergy destruction of the evaporator showed an insignificant increase of an average of 1.2% for each 2°C increase in the intake seawater temperature, as a result of the reduction in input heat energy mass flow rate as presented in Fig [4-42]. The exergetic efficiency was a response to the reduction in the condenser exergy destruction, and showed an average increase of 0.5 for each 2°C increase in the intake seawater temperature. Fig [4-44] shows the proposed MED exergy results against the intake seawater temperature variation.

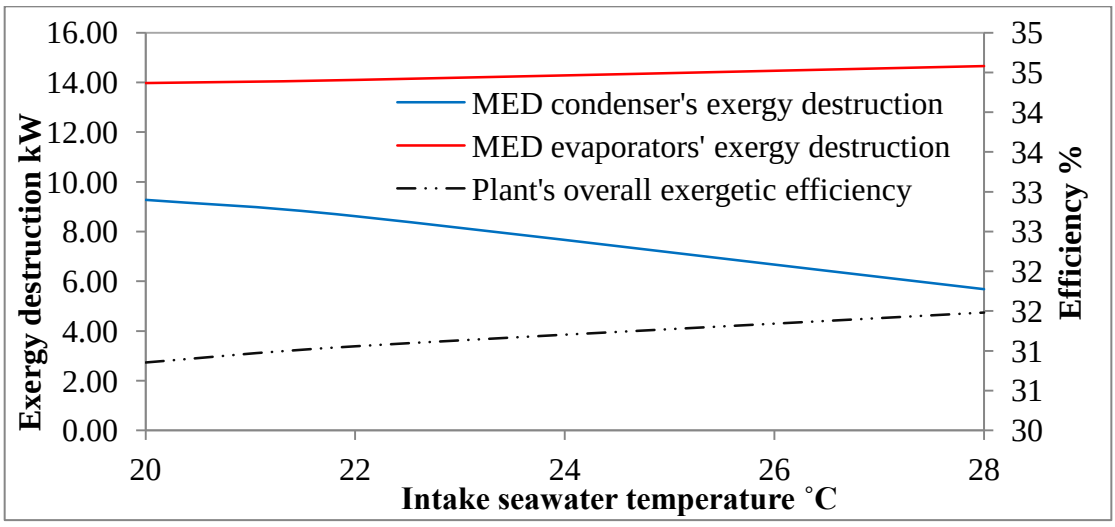

Fig [4-44], Exergy results versus intake seawater temperature

Investigating the proposed MED desalination plant's model performance against the variation in the seawater salinity was carried out as a part of the parametric study. The seawater salinity was varied from 0.036 kg/kg to 0.045 kg/kg at a seawater temperature of 22°C. The obtained results are listed in Table [11] in the appendix A. The GOR and the specific heat consumption were investigated against the variation of the seawater salinity as shown in Fig [4-45]. The results showed that the model GOR decreased slightly as a result of increasing the specific heat consumption. An increase in seawater salinity led to increases in its entropy and enthalpy, which require additional heat energy for the seawater to evaporate at the required pressure for each effect. This contributes to an increase in the input heat energy, which in turns causes an increasing in the specific heat consumption, and a reduction in the GOR value.

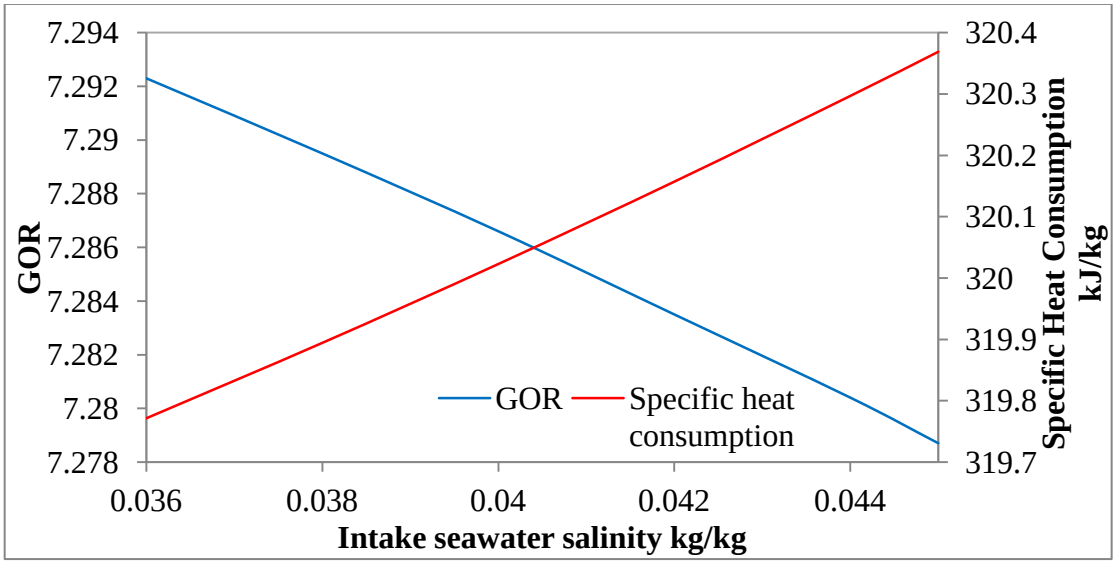

Fig [4-45], Specific heat consumption and GOR versus intake seawater salinity

The response of the exergy destruction of evaporator and condenser to the seawater salinity variation was insignificant. Fig [4-46] showed a very small increase in the exergy destruction of the evaporator, while the condenser's exergy destruction was relatively constant. However, the overall exergetic efficiency of this model was affected by the increase in the input heat energy.

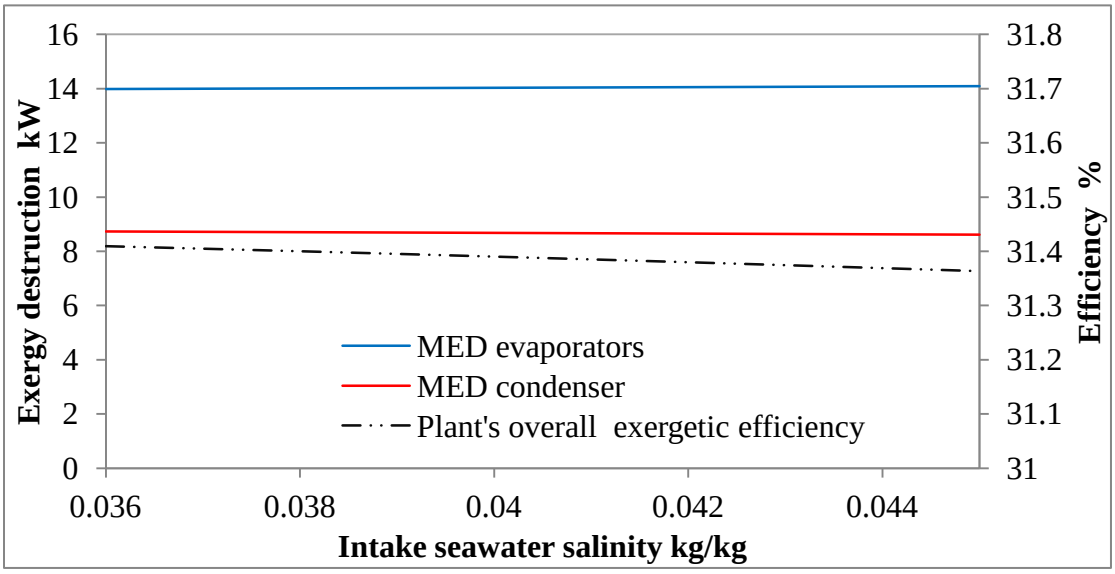

Fig [4-46], The result of exergy analysis against intake seawater salinity

4.5 TVC-MED Desalination

The thermal vapour compression multi-effect desalination model (TVC-MED) is a thermal desalination process that is considered to be the next generation of MED, and can be improved by employing a steam ejector, as illustrated in Fig [4-47], each stream in this figure has pointed with numbers and values are shown in Table [4-13]. A high-pressure steam is used by the ejector, which expands through the steam ejector nozzle at a height velocity known as the motive steam. During the last stage of the MED effects, an extraction of the part of the high velocity steam to the steam ejector occurs. Motive steam and suction steam are then pushed into a mixing chamber at the end of the steam ejector and combined, so transferring the requited heat to the brine heater (evaporator). Another part of the motive steam is extracted before it completes its cycle, in order to reheat the intake feed seawater at the condenser. The proposed steam ejector was designed according to available suction steam pressure, and the required steam properties include pressure, mass flow and temperature to provide the best thermodynamic results in order to validate this model. In the MED the pressure of the last effect was 2.8 bar, while the steam needed to drive the TVC-MED brine heater had to be 0.32 bar. According to the steam compression ratio C_R as shown in the following equation, the C_R was then 2.6.

$$C_R = \frac{P_d}{P_s}$$

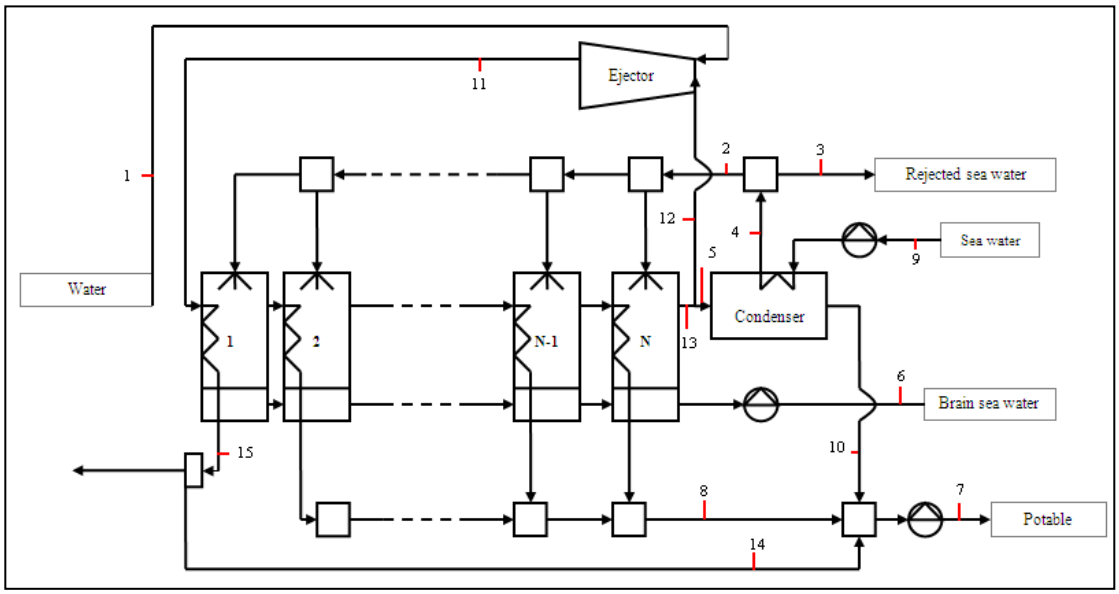

Fig [4-47], Proposed TVC-MED desalination process

The number of stages in the steam ejector is defined by the suction of the pressure steam. Moreover, the ratio of suction mass to motive mass is known as the entrainment ratio and was set to the minimum possible value in order to gain a better GOR value. The steam ejector properties were assumed to be in accordance with Hegazy [121].

The isentropic compression and expansion efficiency levels were set to 80% and 85% respectively. The evaporator and condenser were modelled exactly on the basic MED model mentioned in the previous section. The effectiveness and NTU of the condenser were 0.8 and 1.79 respectively. The figures for the optimum number of effects were obtained through a parametric study of the similar method to MED plant. The result of the GOR value and specific heat consumption showed that the nine effects provided the highest GOR value with the lowest specific consumption value. All the results are listed in Table [12] in the appendix A, while Table [4-13] presents the energy parameters of the TVC-MED's streams. The effect of the number of TVC-MED effects on the GOR and motive steam mass flow rate is presented in Fig [4-48]. The highest value of the GOR was achieved at nine effects, while the GOR begin to decline at ten effects. This is mainly due the increasing of motive steam flow by an average of 20% for each extra effect.

	H(kj/kg)	S(kj/kgK)	M(kg/s)	T(C°)	P(bar)
1	2631.908	6.6453	0.075	143.2203	3.95
2	177.7352	0.6299	1.2322	44.7198	1.50
3	177.7352	0.6299	0.1752	44.7198	1.50
4	177.7352	0.6299	1.4074	44.7198	1.50
5	2592.054	8.0905	0.0519	50.3269	0.12
6	192.0341	0.6946	0.6607	50.3725	2.00
7	248.3222	0.8222	0.6	59.2913	2
8	255.2233	0.8434	0.5113	60.9748	0.3
9	87.3632	0.33	1.4074	22	1.02
10	206.8845	0.6963	0.0887	49.4098	0.3
11	2627.923	7.7477	0.0833	71	0.32
12	2592.054	8.0905	0.0083	50.3269	0.12
13	2592.054	8.0905	0.0603	50.3269	0.12
14	295.1271	0.9611	0.0368	70.504	0.319
15	295.1271	0.9611	0.0833	70.5034	0.319

Table [4-13], The TVC-MED energy streams

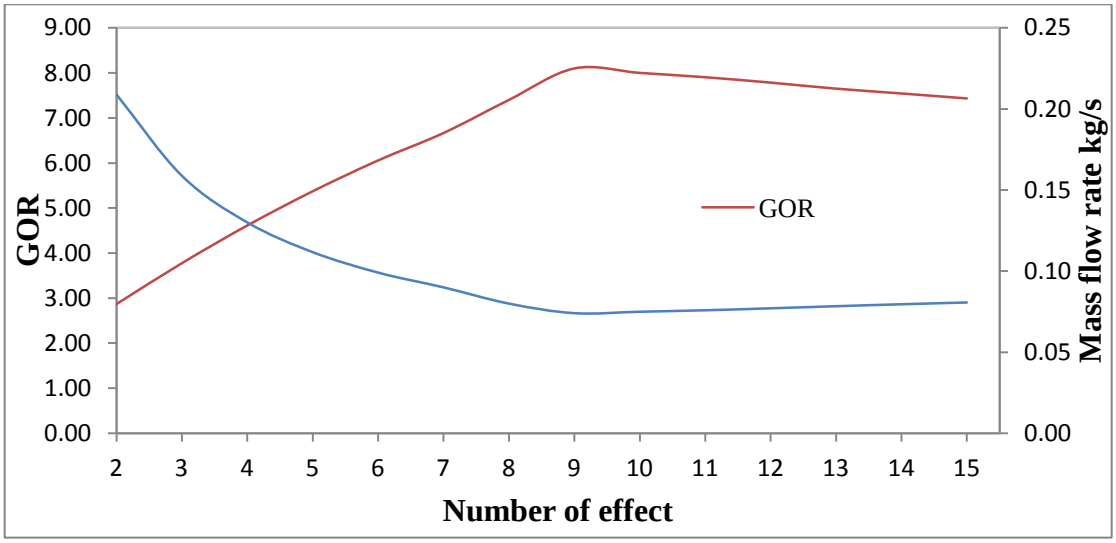

Fig [4-48], GOR and motive steam mass flow rate versus number of effects

It can be observed that, the GOR value has improved to 8.1, while it had been 6.68 in the MED, which is a 20 % improvement of the same potable water production rate of 53 m^3/day. Moreover, the specific heat consumption showed no significant change, as it was a function of the first-effect heat transfer. The extraction from the steam entering the condenser (12) causing a reduction in the amount of seawater rejected

after the condenser and before entering the brine water. This led to a slight increase in the concentration factor of TVC-MED compared to MED desalination.

On the basis of the second la-

w analysis, the exergy destruction values of the evaporator, condenser and steam ejector were calculated for the TVC-MED desalination process.

Following the similar methods used in MED, the entropy and enthalpy of each stream of the seawater and brine water were calculated. At the reference condition of 15°C and at a pressure of 1 bar, the exergy and specific exergy were also calculated for each TVC-MED stream, as illustrated in Table [4-14].

	e (kJ/kg)	E (kW)
1	504.4356	37.788
2	5.9003	7.2713
3	5.9003	1.0205
4	5.9003	8.2918
5	263.6536	13.6689
6	4.5634	3.0154
7	11.9825	7.1895
8	12.7297	6.509
9	0.3484	0.4896
10	7.0466	0.6248
11	398.2342	33.1843
12	263.6536	2.2192
13	263.6536	15.8881
14	19.971	0.7355
15	19.971	1.6642

Table [4-14], The exergy and specific exergy of Proposed TVC-MED desalination

According to the exergy destruction calculation, the highest amount of exergy destruction occurred in the steam ejector, which caused 22.98kW of exergy destruction, consumed 47%% of the total exergy input into the cycle, and accounted for 42.5% of the proposed model total exergy destruction. The TVC-MED effects consumed 3.62% of the total exergy input and accounted for 40.71% of the model's

total exergy destruction. 5.97kW of exergy destruction occurred in the condenser, which formed 16.78% of the model total exergy destruction by consuming 11.09% of the total exergy input to the cycle. Fig [4-49] shows the amount of exergy destruction for each component of TVC-MED. The overall results of the total exergy destruction of this proposed TVC-MED model was 48.80kW, while the exergetic efficiency was 26.66%. The performance of the condenser and the evaporator did not show a noticeable difference in comparison with MED desalination. The only difference was caused by employing the steam ejector, which added an extra 22.98 kW of exergy destruction.

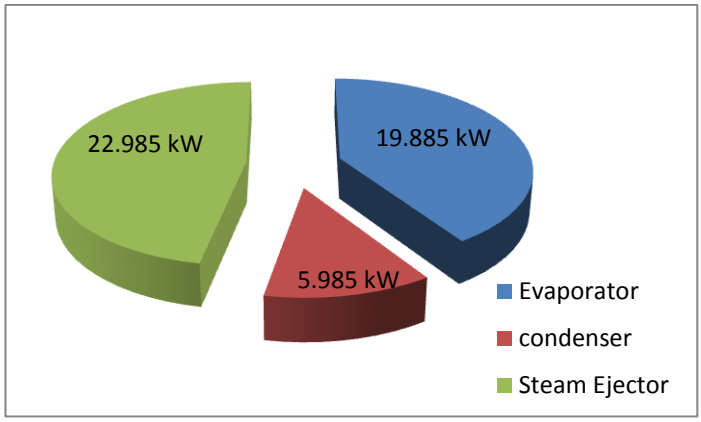

Fig [4-49], The exergy destruction of each component for TVC-MED

On the basis of the first and second laws, Table [4-15] shows the comparison between proposed MED and TVC-MED models. The GOR in TVC-MED was 20% higher than MED desalination process. However, The TVC-MED showed a higher value of the total exergy destruction, which in turn caused a drop in its exergetic efficiency from 29.68kW in MED to 26.66kW. The exergy of the input steam was increased from 34.83kW in MED to 53.9kW in TVC-MED. This was due to the extraction after leaving the last effect, which raised the entropy of the motive steam passing to the steam ejector. Furthermore, the effectiveness and NTU was higher in the TVC-MED, which led to a better cooling performance than MED.

		MED	TVC-MED
Evaporator exergy destruction	kW	16.76	19.887
Condenser exergy destruction	kW	6.95	5.97
Steam ejector exergy destruction	kW	-	22.98
Total exergy destruction	kW	23.71	35.62
Model's overall exergetic efficiency	%	29.68	26.66
GOR	-	6.85	8.01
Capacity	m^3/day	52.6	52.6
Specific heat consumption	kJ/kg	340.08	356.98
Concentration factor	-	1.86	1.87
Condenser effectiveness	-	0.6	0.8
Condenser NTU	-	1.76	1.76

Table [4-15], Comparison between the MED and the TVC-MED desalination model

The behaviour of the seawater temperature variations on the TVC-MED performance was investigated in a parametric study that varied the intake seawater temperature from 20°C to 28°C. All the results are listed in Table [13] in the appendix. The TVC-MED performance under the different seawater temperatures is illustrated in Fig [4-50], set against the GOR and the motive steam mass flow rate. The GOR increased in the range of 4.3%for each 2°C increase in the seawater temperature as a result of the reduction in the required motive steam mass flow rate in order to evaporate the high temperature of the intake seawater. This result is in agreement with existing studies [119-121].

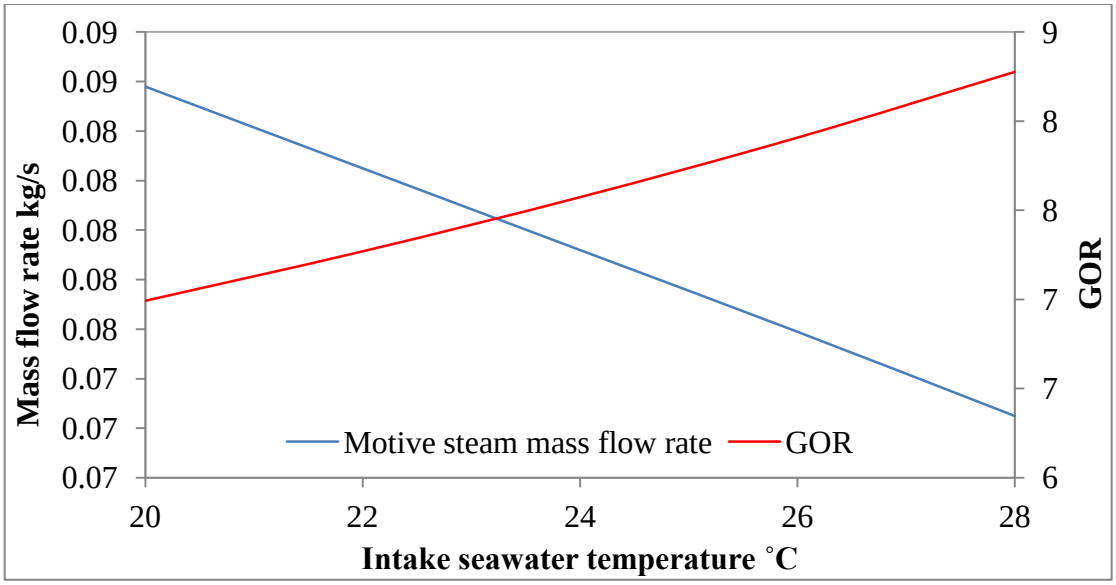

Fig [4-50], The variation of Intake seawater temperature against GOR and motive mass flow rate

The intake seawater variation was also performed to examine the value of specific heat consumption and the heat transfer in the first effect, which is the function of the latter, as shown in Fig [4-51]. As the intake seawater temperature increased, the input mass steam decreased, which in turn caused a reduction in the heat transfer in the first effect. This reduction was in the range of 4.12% for each 2°C increase of the seawater temperature, which led to another reduction in the specific heat consumption in the same range of 4.12% for each 2°C increase in the intake seawater temperature.

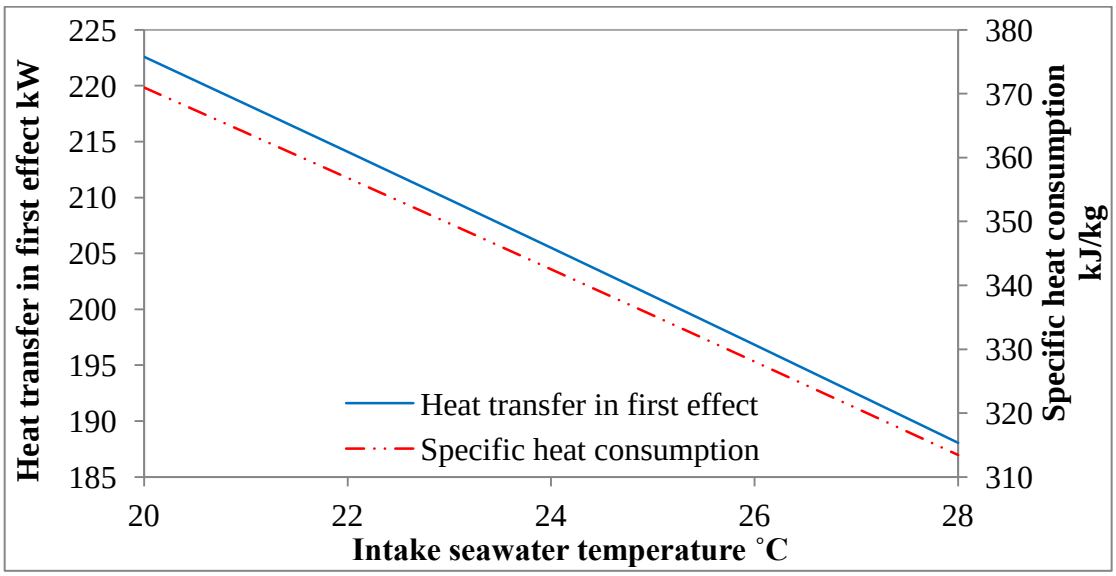

Fig [4-51], The effect of the intake seawater temperature on the specific heat consumption and the heat consumption

On the basis of second law analysis, it was found that for each 2°C increase in the intake seawater temperature, the exergy destruction of the condenser decreased on average by 17%, as shown in Fig [4-52]. This reduction was due to the fact that, the input exergy of the condenser was influenced by the seawater temperature variation, while its output showed no response to this variation. The evaporator exergy destruction increased on average by 10% for each 2°C increase in the intake seawater temperature. This was due to a reduction in specific heat consumption, as illustrated in Fig [4-51]. The exergy destruction of the steam ejector was increased by 4.1% for each 2°C increase in the intake seawater temperature, due to a reduction in the steam ejector output. Since the steam mass flow rate decreased as shown in Fig [4-50], the model exergetic efficiency increased by 4.16% for each 2°C increase in the intake seawater temperature.

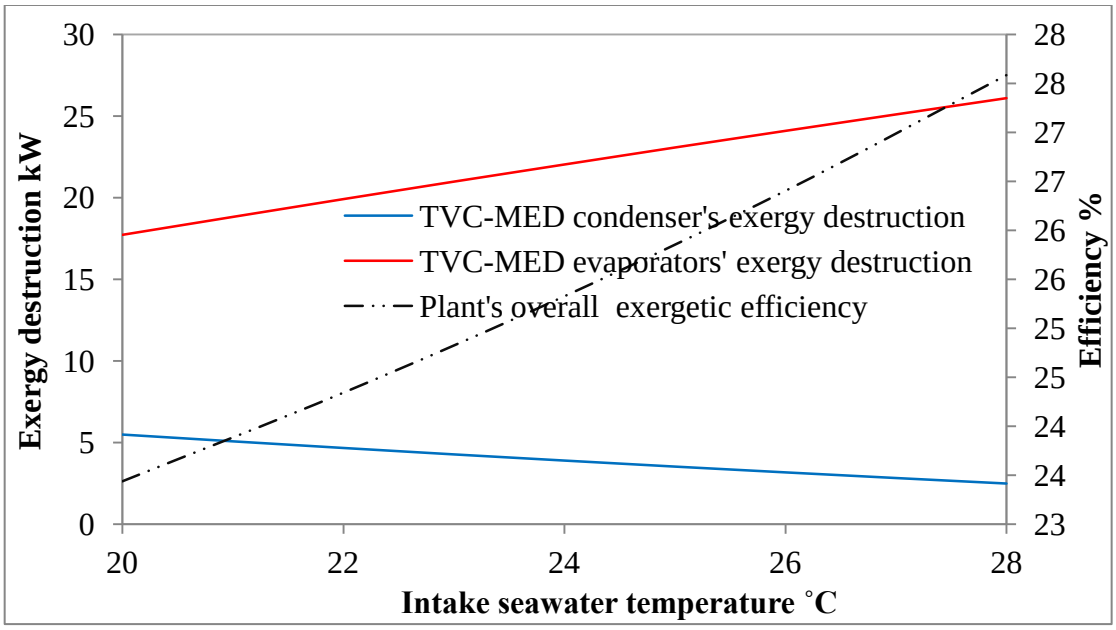

Fig [4-54], TVC-MED exergy destruction and efficiency versus intake seawater temperature

4.6 Chapter Summary:

All models including microturbine, ORC, single effect absorption chiller, TVC-MED and MED desalination were presented as stand-alone unit. Moreover, a number of parametric studies have applied for each model including the ambient temperature variation and inlet seawater temperature variation.

The microturbine was operated at different ambient condition and partial load.

Regarding to ORC, a comparison between R-134fa and R-254fa was performed, and then the latter was chosen as a working fluid for the proposed model. Then the ORC was operated at different: heat source temperature, intake seawater temperature and inlet stream temperature to the turbine.

The single effect absorption chiller was operated at different: inlet water temperature to the generator, chilled water temperature and intake seawater temperature.

Furthermore, another comparison took place between MED and TVC-MED, the results showed that TVC-MED is more efficient and therefore it was selected for the proposed model.

Chapter 5

Microturbine CHP's Modelling and Results

5. Proposed modelling plant (Complete models):

This chapter presents the modelling, simulation and performance of the microturbine combined with each base plant, as outlined in the previous chapter, excluding the multi-effect distilled desalination (MED). Performances assessment and off-design studies were carried out. A number of parametric studies and partial load performance of each proposed model were performed. The results of each proposed combined model will be presented and compared with the base plant before utilisation. All the results of proposed combined plants will be introduced and compared according to the energy and exergy outcome, in order to draw a satisfactory conclusion related to each proposed model.

5.1 Proposed plant modelling:

This study aims to establish the most effective low-grade heat energy model to be utilised with the C200 microturbine. A comparison between three models will focus on finding the minimum CO_2 emission rate and the best energy utilisation factor (EUF) of the combined cycle performance. Also, the second law analysis results will be presented, including exergy destruction and exergetic efficiency.

5.2 Microturbine cascaded with organic rankine cycle (ORC):

The first proposed model simulates the C200 microturbine cascaded with an [IT10] organic Rankine cycle (ORC), while the refrigerant R245-fa was used as a working fluid. The utilization in this proposed cycle took place through a heat exchanger. The point of this was to transfer the heat energy of the microturbine exhaust to evaporate the working fluid used to operate the ORC. The microturbine utilised [48%] of heat energy of the high temperature exhaust gas. The first operating mode is modelled on the ISO condition, with an inlet air temperature of 15°C and 1 bar at full load. The results are shown through the operating mode on the basis of the first law of energy and second law of energy of the proposed combined cycle.

Fig [5-2] shows the complete proposed model of microturbine cascaded with ORC. The microturbine is presented as a block shape as previously addressed in Chapter 4, and is shown in Fig [5-1], where the ambient air enters to the microturbine with a temperature of 15°C at I bar and mass flow rate of 1.2 kg/s, to generate 200.3 kW of the electric power. The working fluid is heated and evaporated by 48% of the

microturbine's exhaust heat energy. Then the working fluid enters the ORC turbine at 70°C to generate an electric power of 17 kW, which represents 12% of the microturbine total power.

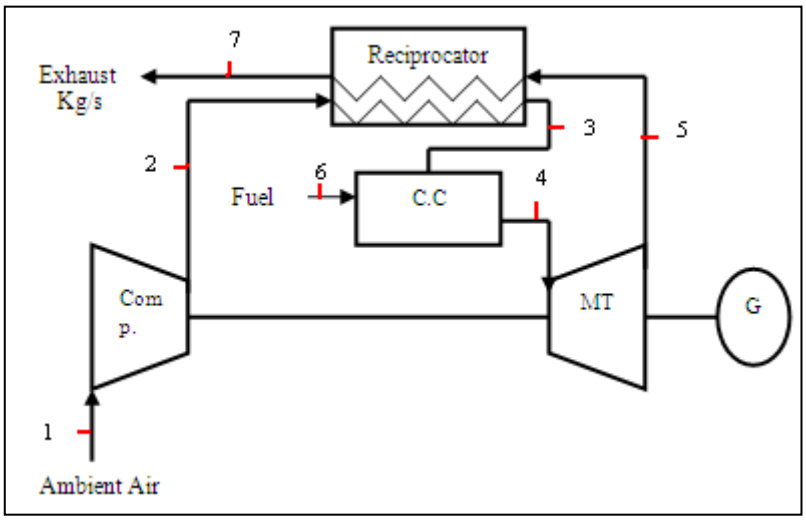

Fig [5-1], Microturbine stand-alone

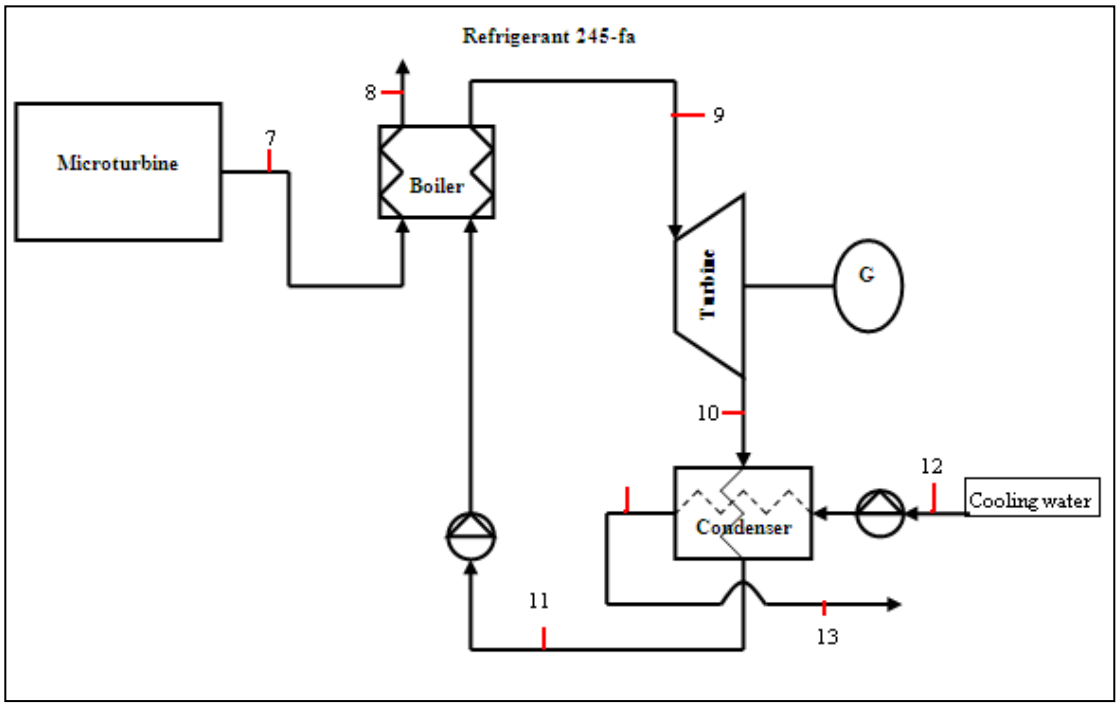

Fig [5-2], Microturbine cascaded with ORC

The plant's behaviour was evaluated by the energy utilisation factor (EUF), which was defined previously in Chapter 3. This is considered here in order to evaluate the performance of the cogeneration plant and is defined as the total of the ratio of the total output work and the useful heat energy divided by the fuel energy supplied. The amount of CO_2 emission rate is also calculated to obtain a comparison with the CO_2 emitted from the base plant in relation to the cogeneration model. Table [5-1] shows

the energy and exergy results of the cogeneration proposed plant at ISO conditions, and full load operation.

	H(kj/kg)	S(kj/kgK)	M(kg/s)	T(°C)	P(bar)	e (kW)	E (kW)
1	15.1593	6.8494	1.2594	15	1.013	0	0
2	280.8973	6.9145	1.2594	274.4656	7.9	246.988	311.0521
3	484.9455	7.2375	1.2594	465.3781	7.8999	358.0237	463.7362
4	940.7473	7.8263	1.2711	850	7.8899	669.5265	851.0495
5	495.1472	7.9381	1.2711	466.0535	1.0418	191.7196	243.6989
6	53.338	9.9618	0.0117	25	15	50149.4	966.7762
7	292.9837	7.6543	1.2711	280.9556	1.0417	71.2966	90.6266
8	149.6467	7.3609	1.2711	145	1.0317	12.4478	15.8226
9	458.6986	1.7853	0.8225	70	6.0998	67.1309	55.213
10	435.8992	1.7892	0.8225	37.9724	1.6514	43.2185	35.5458
11	236.7244	1.1277	0.8225	27.5716	1.6414	34.5305	28.4002
12	92.3813	0.3253	5.5984	22	1.013	0.3581	2.0045
13	121.6743	0.4232	5.5984	29	1.24	1.4321	8.0174

Table [5-1] shows the energy and exergy results of the cogeneration proposed plant at ISO conditions operated at full load.

In general, the energy properties of both models of microturbine and ORC showed insignificant differences to the base plant model. However, the amount of CO_2 emission rate decreased by 9% compared to the microturbine stand-alone. The energy utilisation factor was 38.17%, with an evaporator effectiveness of 0.53, and a NTU of 0.8. The overall efficiency was 37. 32%, due to increase the total power generation to 216.88kW, represented by the microturbine and ORC. On the basis of second law analysis, no significant results occurred compared to the base plant models. The largest amount of exergy destruction took place in the combustion chamber due to the heat transfer and mixing process, and represented 80% of the model's total exergy destruction, which accounted for 60% of the total exergy input to the combined cycle. The evaporator's exergy destruction represented 6.2% of the total exergy destruction, and formed 4.6% of the total exergy input. Furthermore, the turbine of the microturbine unit represented 5.6% of the total exergy destruction, and shaped 4.2% of the total exergy input. However, the stack exergy destruction was reduced in the

combined proposed model from 90 kW to 12 kW, which represents a reduction of 13.3% in exergy destruction. This drop in the stack's exergy was due to the amount of the exhaust gas utilised in the evaporator of the ORC cycle. Furthermore, the overall exergetic efficiency of the combined cycle, including microturbine and ORC, had decreased by 34% compared to the microturbine stand-alone model. This is because of the extra exergy destruction generated from the ORC.

5.2.1 Parametric studies:

The proposed plant performance under varying ambient temperatures was investigated by varying the compressor inlet-air temperature from 5°C to 50°C. The combined proposed cycle for the microturbine and the ORC was operated at full load, with an inlet cooling water temperature of 22°C, which used in purpose of cooling the working fluid of ORC at the condenser. The results of this proposed model are listed in Table [1] in the appendix B.

The variation of ambient temperature showed an effect on the output electric performance. According to Fig [5-3] the microturbine with ORC output power decreased by 3% for each 5°C increasing in the ambient temperature. This showed the same performance as the microturbine standing alone, as previously introduced. However, as the power generated by microturbine decreased with reference to the higher amount of electricity, the total net output power also decreased by an average of 3% for each 5°C increase in the ambient temperature, as presented in Fig [5-3].

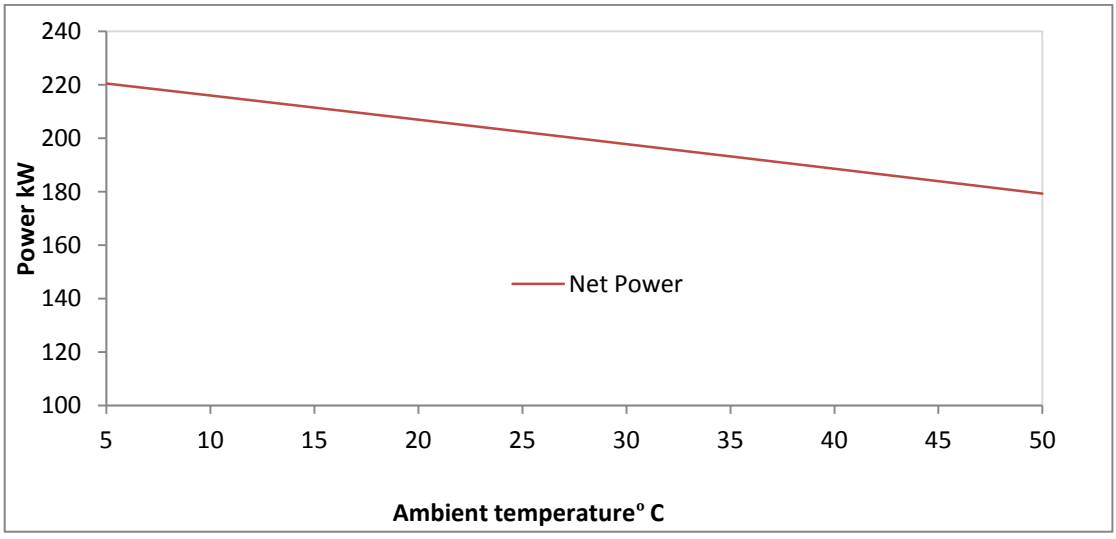

Fig [5-3], The ORC and microturbine output power versus the ambient temperature variation

As the increase in the ambient temperature resulted in a decrease in the output power of the overall proposed model, and the temperature of the waste exhaust gas increased by 31%, the overall electric efficiency also faced an average reduction of 3% for each 5°C increase in the ambient temperature. This was driven by the decrease in the output of electrical power. Fig [5-4] shows the relation between the ambient temperature and the overall efficiency for the proposed combined cycle.

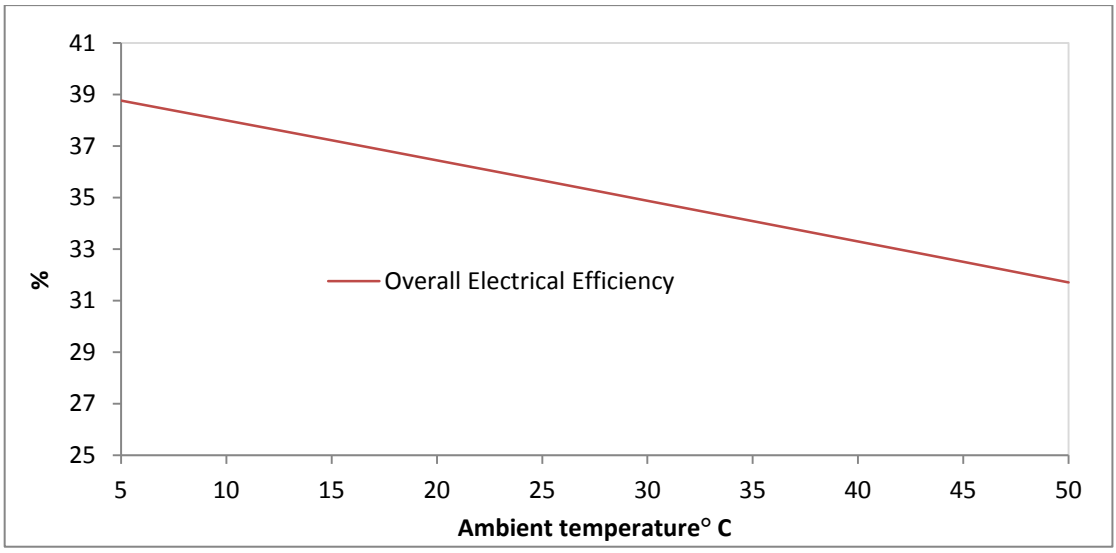

Fig [5-4], Ambient temperature against the overall efficiency

As the CO_2 emission rate decreased by utilising the microturbine waste heat energy, the ambient temperature variation had an effect on the CO_2 emission rate. Fig [5-5] shows that the CO_2 emission rate increased by an average of 2.2% for each 5°C increase in ambient temperature. This was due to increases in the stack temperature and enthalpy of the microturbine, caused by increases in the air inlet temperature of the compressor of the microturbine. However, increases in the emission rate can be directly influenced by the energy utilisation factor, which caused a decline in the EUF by an average of 2.1% for each 5°C increase in the ambient temperature, as presented in Fig [5-6].

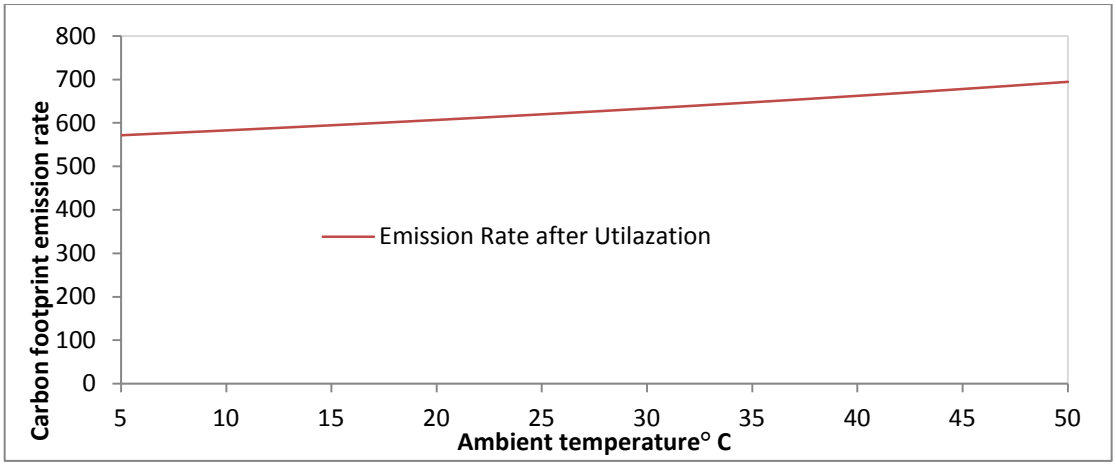

Fig[5-5],Combined model's CO_2 emission rate for verses the ambient temperature variation

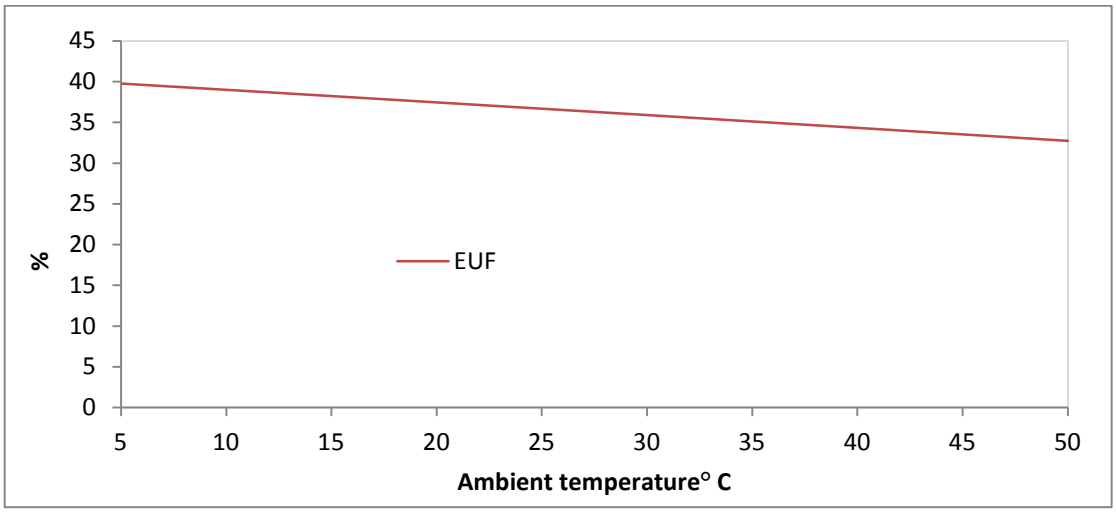

Fig [5-6], EUF against the ambient temperature variation

On the basis of second law analysis, the component most affected by the increasing in the ambient temperature was the evaporator. The exergy destruction of the evaporator increased by an average of 7.5% for each 5°C increase in the ambient temperature. This increase resulted in an increase in the exhaust gas temperature of the microturbine of around 31%, and increased its exergy content, which maximised the exergy destruction of the evaporator. However, increasing the ambient temperature resulted in a reduction in the overall exergetic efficiency by an average of 2.1% for each 5°C increase in ambient temperature, as shown in Fig [6-7].

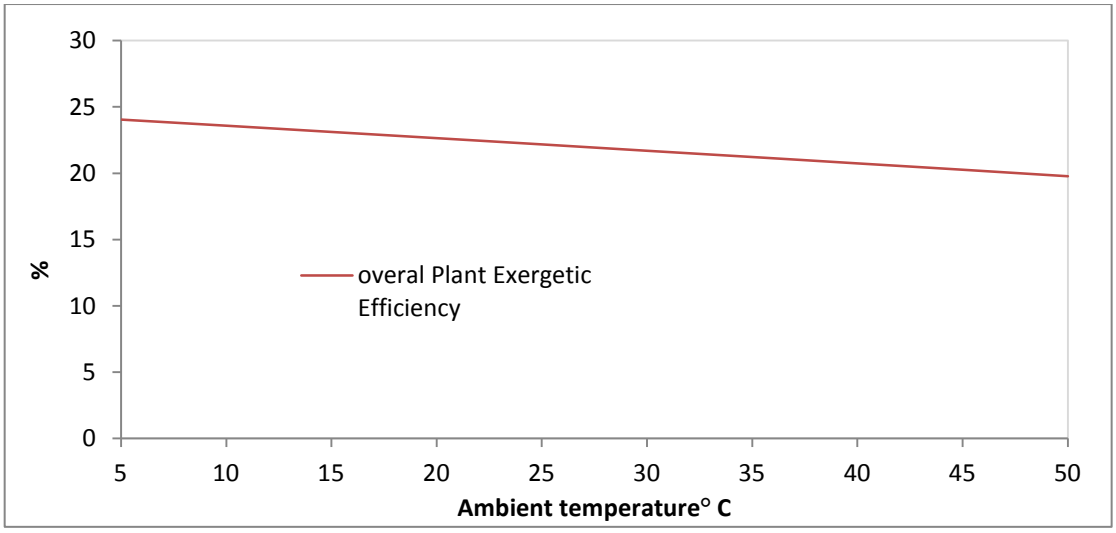

Fig [5-7], Ambient temperature variation verses overall exergetic efficiency

5.2.3 Partial loads:

The behaviour of the partial load for the microturbine cascaded with the ORC was investigated by operating the combined cycle at a different load operation. This method was considered in order to monitor all the energy and exergy performance parameters. The load of this combined cycle was varied from 60% to the full load at 100%. However, the lowest limit of operation load was 60%, because the mass flow rate of the fuel consumption was not enough to operate the combined cycle below this load. Operating at partial load is usually carried out when the need for reducing the fuel consumption is required to be a specifically lower electrical demand, such as in winter season. The study was performed in ISO condition, with a cooling water temperature of 22°C. All the results of this study are listed in Table [2] in the appendix B.

Fig [5-8] shows the model's net output of electric power with the microturbine load variation. The model's net electric power generation decreased by 44.3% when it was operated at 60% of the load, which generated 122.49 kW, and produced 217.15 kW at the full load. This was because of the reductions in the fuel consumption mass flow rate, which in turn affected the exhaust gas mass flow rate required for the utilisation process. The reduction of microturbine output power in the gas turbine improved by 5% compared to the stand-alone model.

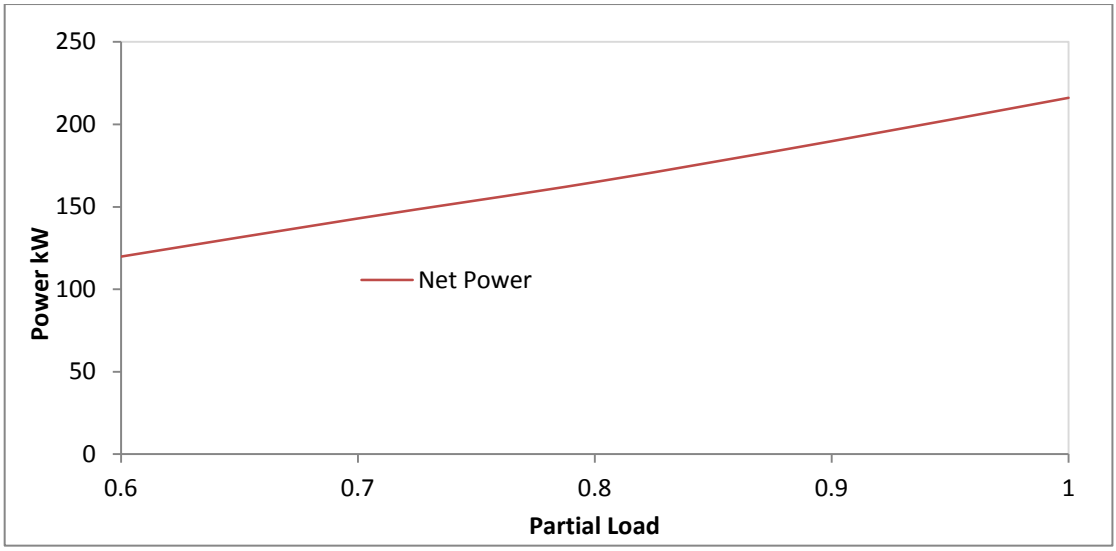

Fig [5-8], Net output power versus the partial load variation

As net output power declined by 44.3%, the overall efficiency for the combined cycle also dropped, as the proposed model operated at 60% of the load. The overall electrical efficacy declined by 13% to reach a value of 30.5%, while it increased at the full load to reach 35% as illustrated in Fig [5-9].

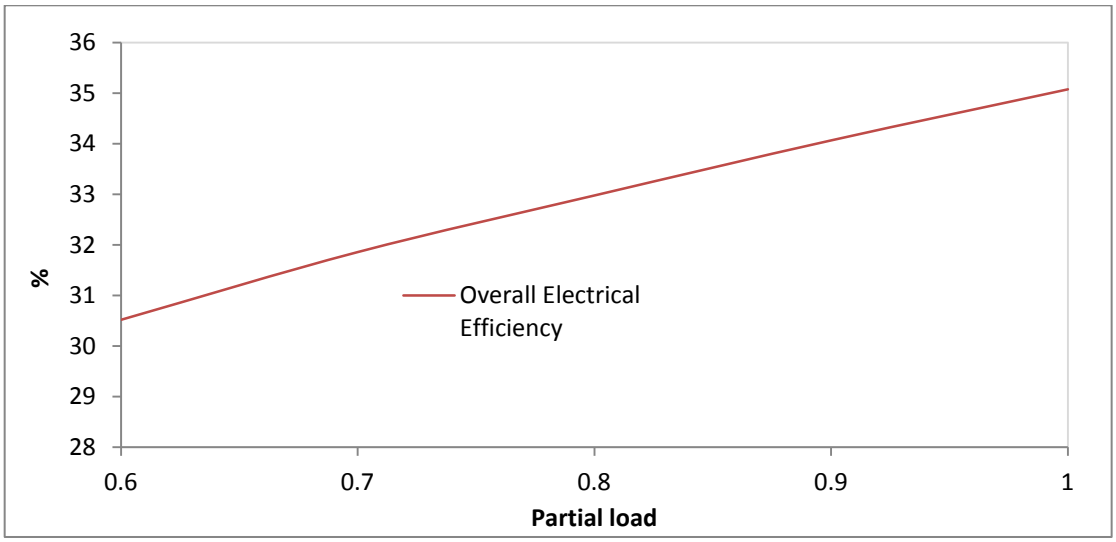

Fig [5-9], The overall efficiency against the partial load variation

The CO_2 emission rate was influenced by the reduction in the partial load. Fig [5-10] shows that the combined cycle's CO_2 emission rate decreased by an average of 1.7% for each 10% increase in the partial load, which concluded in a total reduction of 7% at the full load, driven by a higher reduction in the combined model's output of

electric power by 44.3%. Consequently, the EUF was increased by an average of 2.1% for each 10% increase in the operating load, as showed in Fig [5-11].

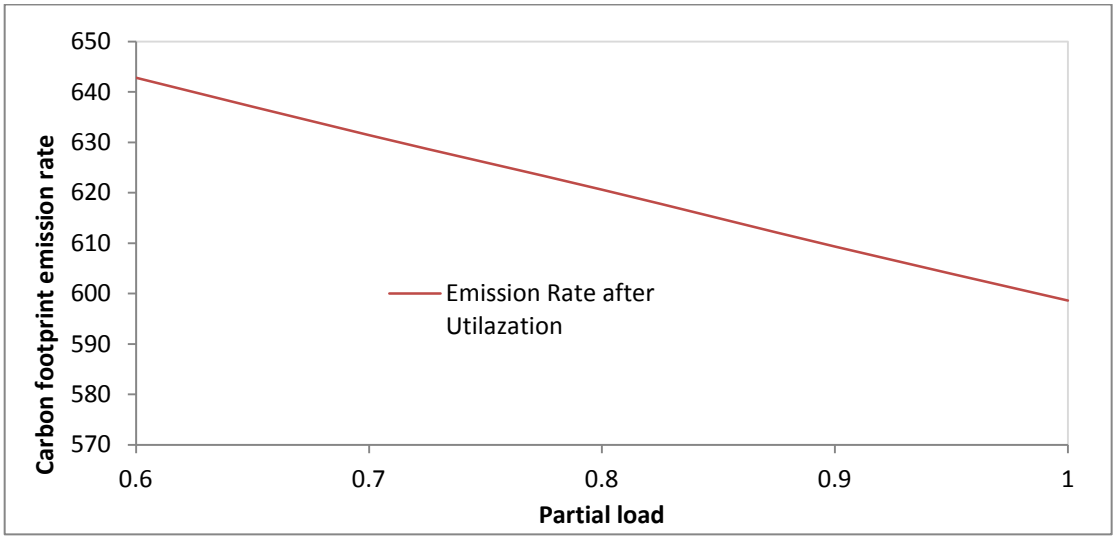

Fig [5-10], CO_2 emission rate against the model's partial load variation

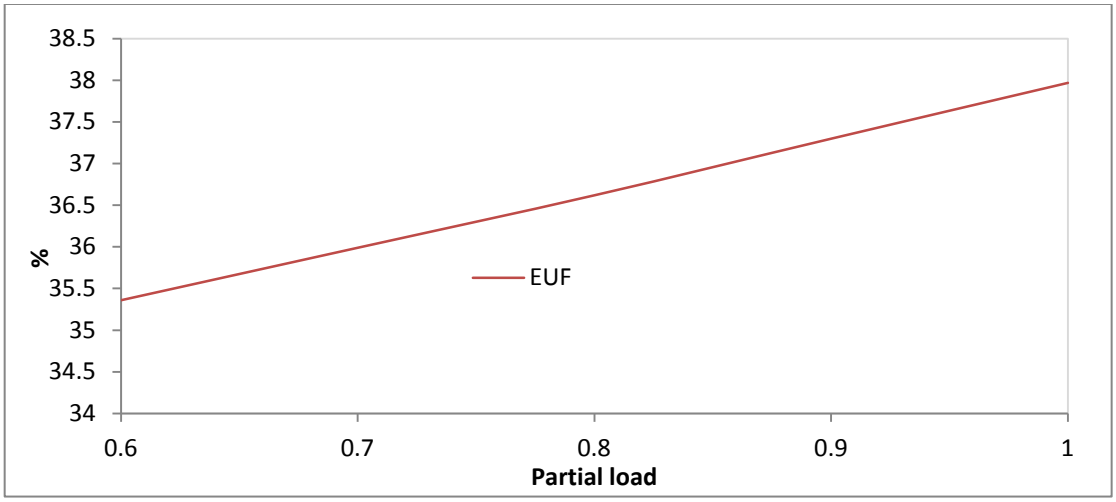

Fig [5-11], EUF against the model's partial load variation

On the basis of exergy analysis, the exergy destruction for all components was increased insignificantly in response to increasing in the partial load from 60% to the full load. However, the exergy destruction of the evaporator dropped by 26.5% as the load decreased to the lower limit. The exergetic efficiency was affected by the reduction in the partial load, which declined by 27.5% at the load of 60%. The increase in the exergetic efficiency averaged 8.3% for each 10% increase in the amount of load, as shows in Fig [5-12]. The reason for the exergy reduction occurring at low load in this combined cycle is linked to the reduction in the supplied fuel mass,

which also reduced the exhaust gas mass flow rate by 35.43% for the lowest load that was equivalent to 60%.

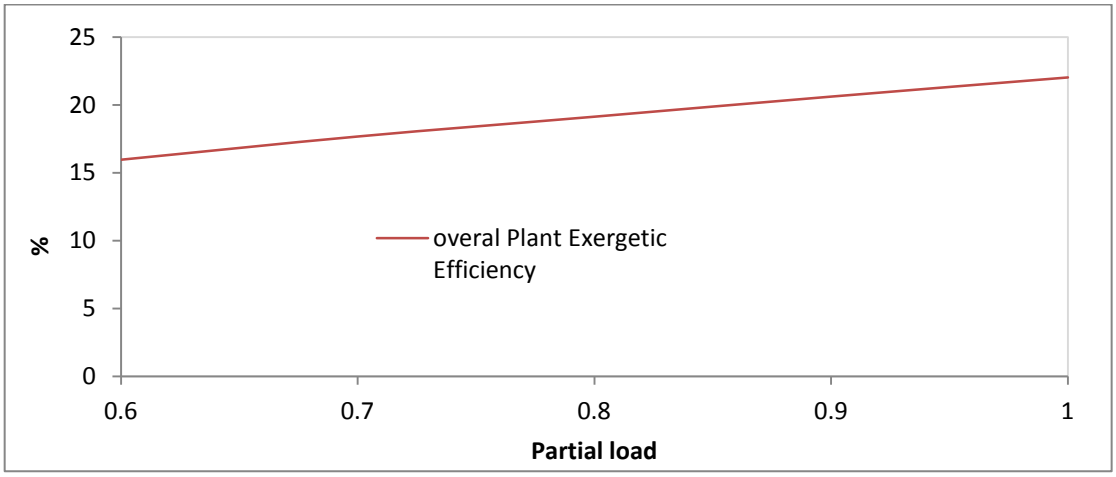

Fig [5-12], The exergetic efficiency versus the model's partial load variation

5.2.4 Intake water temperatures:

The performance of the combined cycle of microturbine utilised in ORC was monitored under variations of seawater temperatures ranging from 20°C to 28°C. The proposed model was operated at full load, and the parametric study was considered at ISO condition. The obtained results are listed in Table [3] in the appendix B.

Fig [5-13] shows the effect of the cooling water temperature on the net output electric power. For each 2°C increase in the intake cooling water temperature, the net output power decreased insignificantly by an average of 0.4%. This insignificant reduction was mainly caused by the reduction in the ORC thermal efficiency, which decreased by an average of 3% for each 2°C increase in the intake cooling temperature, as shown in Fig [5-13]. This was because of the fact that higher intake cooling temperature provided extra heat to the R245-fa refrigerant in heat transfer process, which raised its temperature to an average of 5% for each 2°C increase in the cooling water. This in turns resulted in increasing the temperature at the expansion process, which led to losing some output electric power. The CO_2 emission rate was insignificantly increased by an average of 0.2% for each 2°C increase in the intake cooling temperature, as illustrated in Fig [5-14].

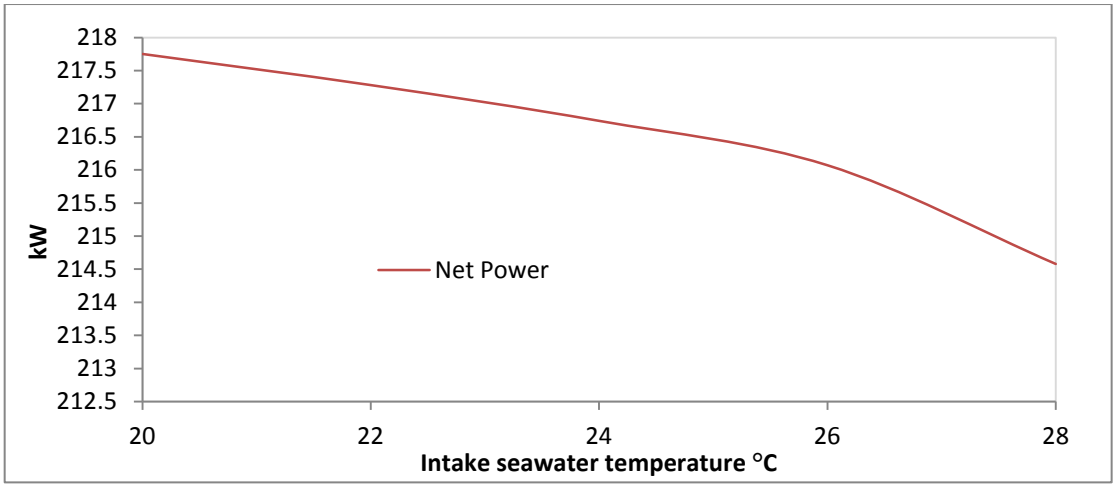

Fig [5-13], The net output power and ORC thermal efficiency versus the intake cooling temperature.

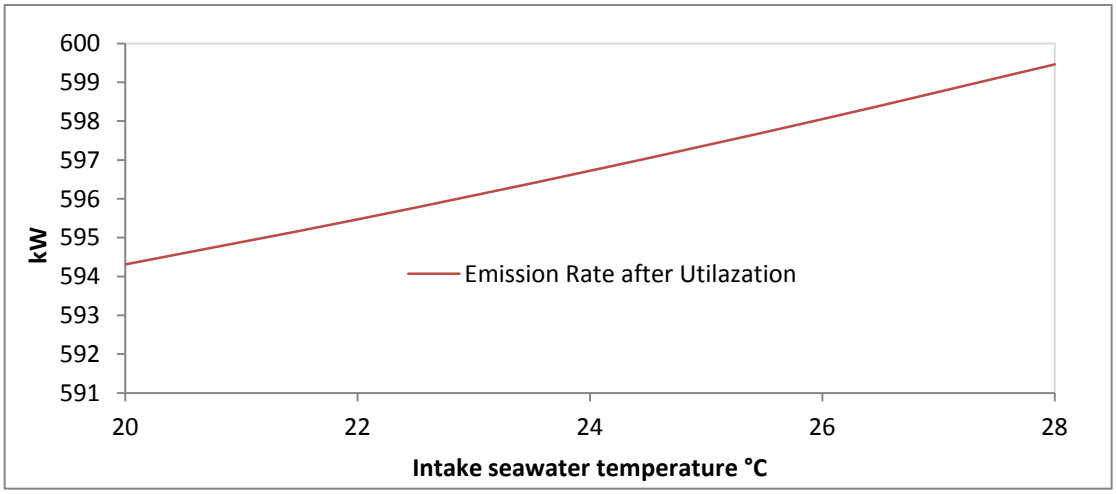

Fig [5-14], The CO_2 emission rate against the intake cooling water temperature

On the basis of exergy analysis, the component most affected by the increase in the intake cooling temperature was the condenser, while the other components showed insignificant increases. As the intake cooling temperature increased by 2°C, its entropy increased in the average of 8.3%, causing an average increase of 7.8% in the condenser's exergy destruction, as shown in Fig [5-15].

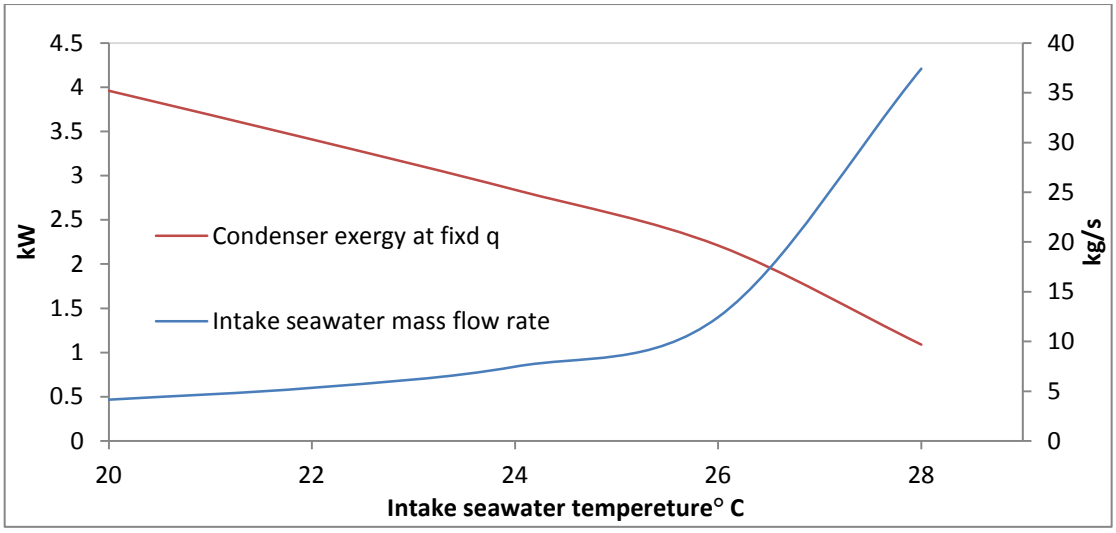

Fig [5-15], The condenser's exergy destruction versus the intake cooling temperature

5.3 Microturbine cascaded with single effect cooling absorption chiller:

The second proposed plant was cascade the microturbine C200 as a high grade heat energy with a water-cooling single effect absorption chiller [SC30] as a low grade heat energy which was manufactured by Yazaki. This would provide 105 kW of cooling capacity. The utilisation process was adopted in this combined cycle through a heat exchanger, which transferred [40.79%] of the waste heat energy of the microturbine to reheat the absorption chiller's lithum bromide in the generator. The first operating mode was modelled at ISO conditions, with an inlet air temperature of 15°C and 1 bar at full load, and a cooling water temperature of 22°C. The results are shown in the operating mode on the basis of the first and second laws of energy in relation to the proposed combined cycle.

The integration of the microturbine with a single effect absorption chiller is illustrated in Fig [5-16], which describes the proposed combined cycle. The ambient air intakes to the cycle are cooled down by the chilled water provided from the evaporator of the absorption chiller through the heat exchanger. It then mixes with a fuel in the combustion chamber, producing a high temperature exhaust gas to operate the gas turbine and generates 208.21 kW, which is higher than the stand-alone model due to decreasing the input air temperature passing through the compressor to 8°C. 40.97% of the microturbine waste heat energy is utilised through the boiler to operate the single effect absorption chiller. The evaporator of the absorption chiller generates 105kW of cooling capacity, according to the collected data, which cooled the chilled water by up to 7°C in order to cool the intake ambient air to the microturbine cycle.

The coefficient of performance (COP) of the single effect absorption chiller was 0.79, defined previously in Chapter 3 as the ratio of the cooling capacity generated from the evaporator to the heat energy provided to the generator.

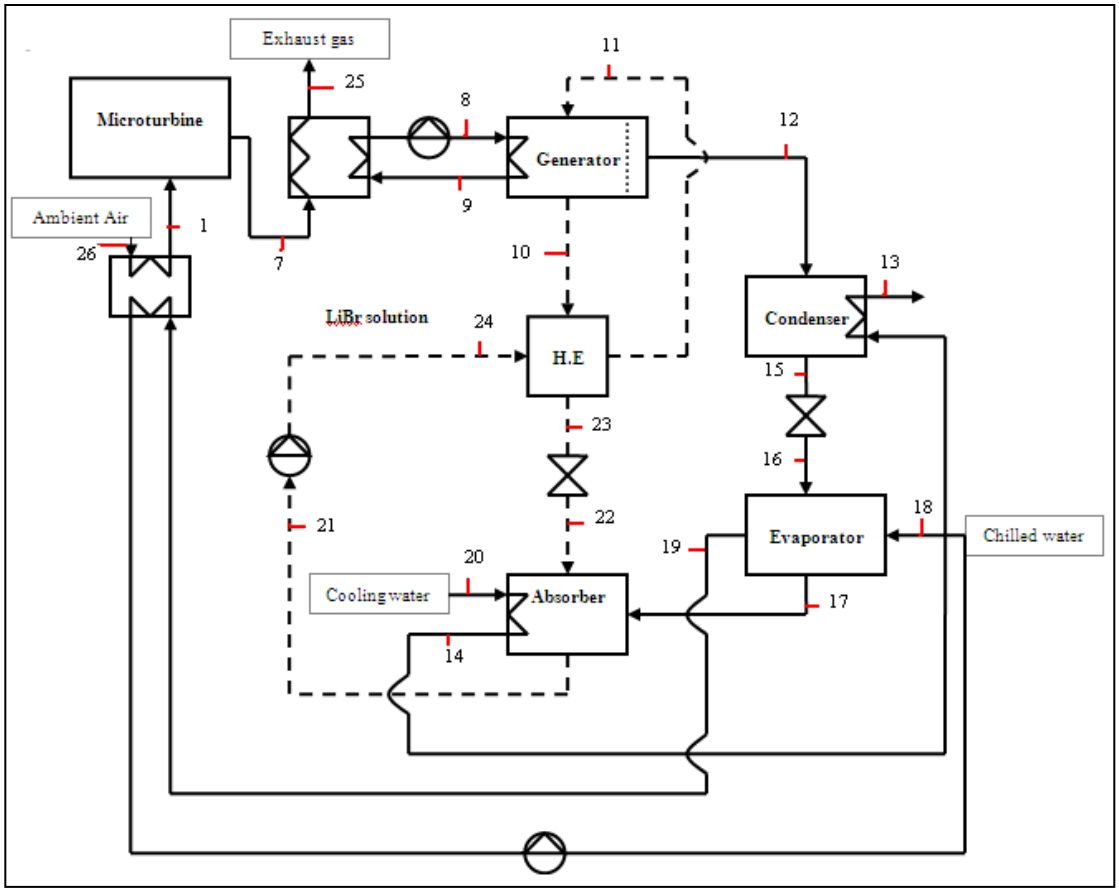

Fig [5-16], Microturbine cascaded with single effect absorption chiller

As considered in the first proposed model, the behaviour of this proposed combined cycle was obtained through the EUF values, and the CO_2 emission rate. The normal mode of operation of this proposed cycle was investigated under the ISO condition and full load operation. Table [5-2] shows the obtained results for both the first and second law thermodynamic effect on the system. The energy utilisation factor was 52.43% with a boiler effectiveness of 60% and an NTU of 0.8. While the CO_2 showed a significant decrease, which was represented 31% of the reduction caused to the utilisation process. However, the overall output electric power has been insignificantly increased, compared to the microturbine stand-alone, because of the electrical requirements of the combined cycle such as operating pumps, while the utilisation process involved inserting a waste heat exhaust stream into the boiler heat exchanger. The overall electric power efficiency was 35.63%, which was also

increased slightly. On the exergy basis, the proposed combined cycle shows insignificant differences compared to the microturbines and single effect absorption chillers in both models. However, the exergy destruction of the microturbine cycle's components was slightly decreased, due to decreasing the ambient air temperature.

Most of the exergy destruction took place in the combustion chamber due to the heat transfer and mixing process, and this represented 79.14% of the model total exergy destruction, accounting for 58.62% of the total exergy input to the combined cycle. The gas turbine of the microturbine exergy destruction represented 7.20% of the total exergy destruction, and formed 5.42% of the total exergy input. Furthermore, the boiler heat exchanger represented 4.49% of the total exergy destruction, and shaped 3.33% of the total exergy input. As regards the single effect absorption chiller, the highest exergy destruction occurred in the generator with a value of 4.53 kW, which represented 0.63 of the total exergy destruction and accounted for 0.46 of the total exergy input. However, the stack exergy destruction was reduced by 71.81% in the combined proposed model from a value of 90.28 kW to one of 25.41 kW.

5.3.1 Parametric studies:

The performance of the proposed combined cycle was investigated under varying ambient temperatures by varying the compressor inlet-air temperature from 5°C to 50°C. The microturbine as a high-grade heat energy was operated at full load. The single effect absorption chiller's inlet cooling water temperature was 22°C, which was used in cooling the LiBr solution in the absorber, and again at the condenser. The results of this proposed model are listed in Table [4] in the appendix B.

As previously explained, the ambient temperature variation had an effect on the performance of the microturbine stand-alone. However, using the single-effect absorption chiller has contributed to the generation of the chilled water with [5.2kg/s], [7°C].

	H(kJ/kg)	S(kJ/kgK)	M(kg/s)	T(°C)	P(bar)	W	e (kW)	E (kW)
1	8.0806	6.8198	1.2594	8	1.0299	-	1.4556	1.8331
2	280.325	6.9134	1.2594	273.9187	7.9	-	246.717	310.7108
3	484.9455	7.2375	1.2594	465.3781	7.8999	-	358.0237	463.7388
4	940.7473	7.8263	1.2711	850	7.8899	-	669.5265	851.0495
5	495.1493	7.9381	1.2711	466.0553	1.0422	-	191.7219	243.7018
6	53.338	9.9618	0.0117	25	15	-	50149.4	966.7762
7	292.4187	7.6533	1.2711	280.4271	1.0421	-	71.0265	90.2833
8	409.4175	1.2809	2.464	97.7	1.19	1	42.1562	103.8717
9	347.5881	1.1108	2.464	83	1.09	1	29.1861	71.9139
10	181.0801	0.475	0.5393	79.4438	0.08	0.571	39.7232	21.4239
11	143.3726	0.455	0.5922	67	0.08	0.52	9.2157	5.4578
12	2639.016	8.4172	0.0529	74.4015	0.08	1	216.5196	11.453
13	166.315	0.58228	3.9389	37	1.013	0.04	4.5198	17.8029
14	125.859	0.45151	3.9389	29.0984	1.113	0.04	1.748	6.8853
15	173.8518	0.5927	0.0529	41.5101	0.08	1	4.7419	0.2508
16	173.8518	0.6282	0.0529	3.7614	0.008	1	-5.4212	-0.2868
17	2445.5	8.8317	0.0529	3.7614	0.008	1	-97.6803	-5.1669
18	31.2279	0.1126	5.2045	12.5	1.013	1	0.0552	0.2873
19	29.515	0.1065	5.2045	7	0.913	1	0.5171	2.6913
20	89.422	0.32997	3.9389	22	1.013	0.04	0.3328	1.3107
21	31.2279	0.17	0.5922	24.544	0.008	0.52	0.2327	0.1378
22	81.0932	0.2	0.5393	29.744	0.008	0.571	20.3763	10.9896
23	52.3162	0.17	0.5922	24.5471	0.08	0.52	0.2393	0.1417
24	81.0932	0.17	0.5393	29.744	0.08	0.571	20.3763	10.9896
25	172.589	7.4144	1.2711	1.2711	1.0321	-	19.9917	25.4118
26	15.1593	6.8446	1.2594	15	1.03	-	0	0

Table [5-2], the energy and exergy results of the microturbine integrated with single effect absorption chiller

The chilled water provided can be used to recover on-site demand, which pre-cools the inlet air for the proposed combined cycle, or off-site for the purpose of external cooling. In this study, the cooler heat exchanger was placed to provide the pre-cooling process to intake ambient air from the chilled water in the absorption chiller. This

cooling heat exchanger achieved an effectiveness of 88.75%, and a NTU of 2.15 at ISO conditions. Fig [5-17] shows the effect of the ambient temperature variation on the proposed cycle's output electric power. The output of electric power remained steady with no changes in its values, as the ambient temperature increased. This was because of the heat transfer in the cooler caused by the chilled water, which stabilised the ambient temperature fluctuation by pre-cooling the intake air temperature to 8°C. This also affected the overall net output efficiency in Fig [5-18], which shows no reaction toward ambient temperature variation. As the ambient air is pre-cooled to 8°C, Fig [5-17] and Fig [5-18] show a stable performance when the temperature varies from 10°C to 50°C. However, if the ambient air becomes less than 8°C, then no need to operate the absorption chiller unit, as it is only used for in-site cooling purpose in this study. Generally speaking, in comparison to the microturbine stand-alone, this utilisation process allows the output electric power of the microturbine stand-alone to increase by 18% while the ambient temperature varies from 10°C to 50°C, and its electric efficiency increased by 18%. Therefore, utilising absorption chiller led to improvements in microturbine performance.

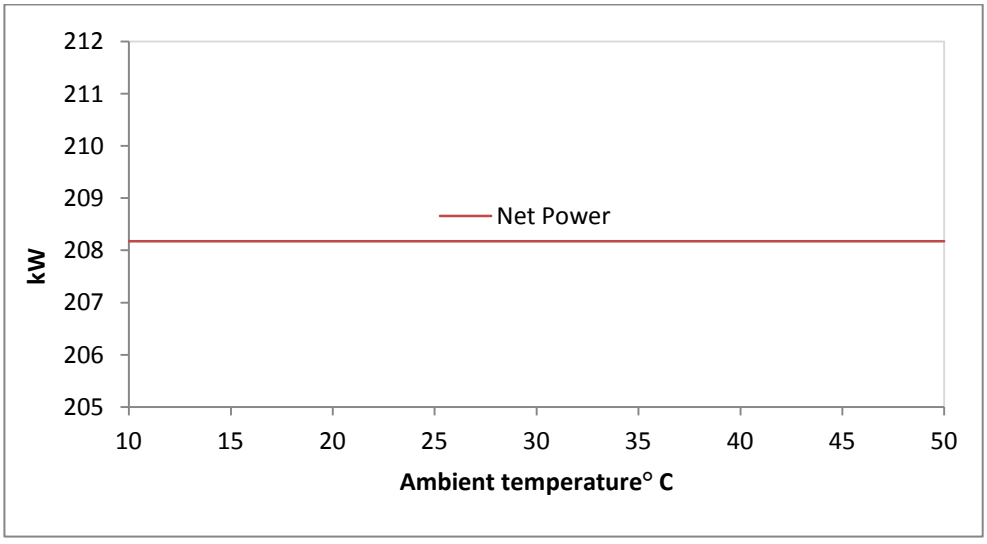

Fig [5-17], Ambient temperature variation versus the output electric power

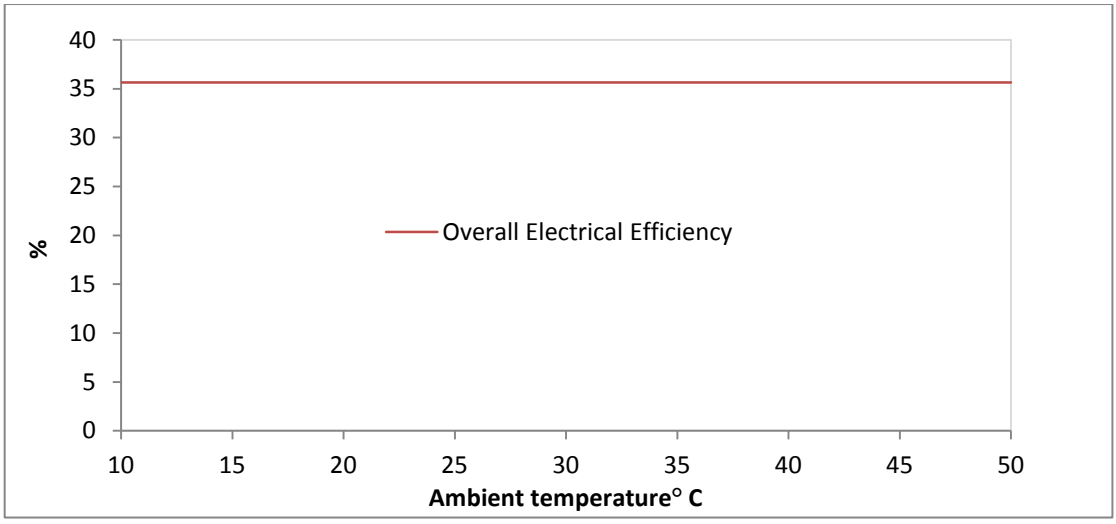

Fig [5-18], Ambient temperature variation versus overall efficiency

The energy utilisation factor (EUF) showed an influence by increasing the intake ambient temperature. The utilisation amount of the waste heat energy of the microturbine decreases by an average of 4.7% for each 5°C increase in the ambient temperature. Fig [5-19] illustrates the effect of ambient temperature variation on EUF. The EUF decreases by an average of 2.1% for each 5°C increase in the ambient temperature. This is because of increases in ambient temperature caused by a reduction in the cooling capacity load of the absorption chiller. This is effected in order to pre-cool the inlet air to 8°C, which in turn increases the heat transfer rate of the cooler heat exchanger by 41.6% for each 5°C increase in the ambient temperature. According to this process, the CO_2 emission rate decreased by an average of 2.2% for each 5°C increase in the ambient temperature, as illustrated in Fig [5-20].

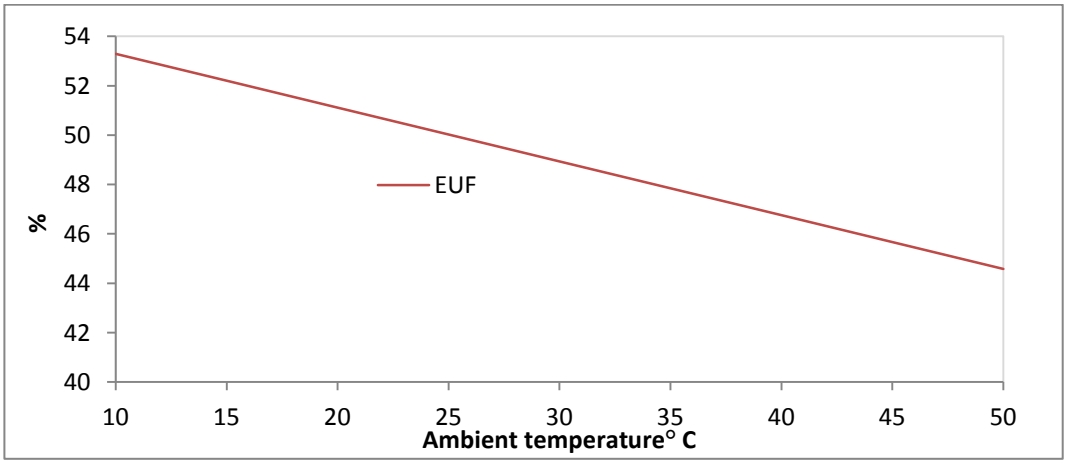

Fig [5-19], Ambient temperature variation versus EUF

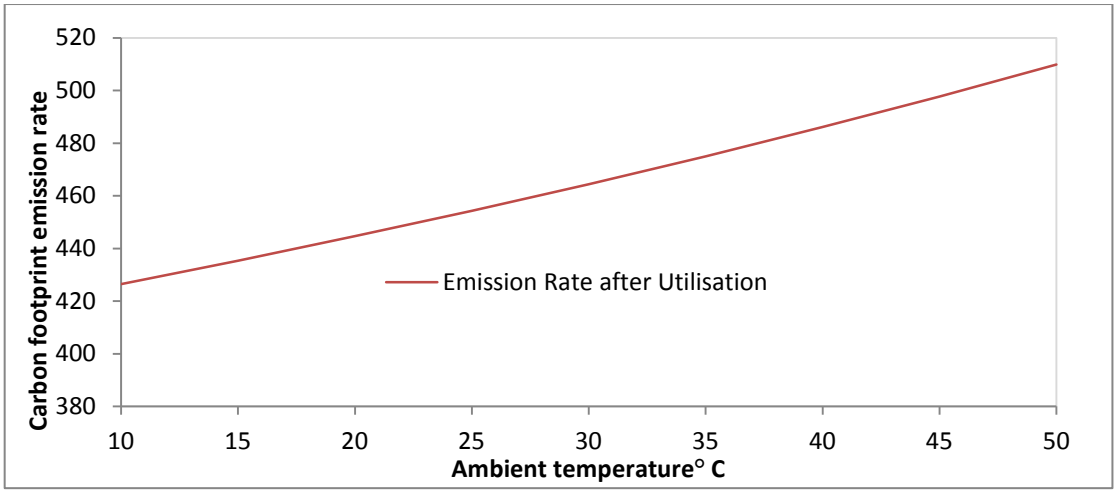

Fig [5-20], Ambient temperature variation versus CO_2 emission rate

The second law analysis of components showed no reaction while the ambient temperature is varied. This confirms the benefit of using the cooling provided by the absorption chiller for an on-site purpose, which stabilises the intake ambient temperature to the system and causes constant exergy destruction. Fig [5-21] shows that, as the ambient temperature increases, overall exergetic efficiency will remain steady compared to the microturbine stand-alone, whose exergy efficiency decreased by 22.3% when the ambient temperature increased from 5°C to 50°C. Furthermore, with regard to the pre-cooled the inlet ambient temperature, the generator exergy destruction and the exergetic efficiency of single effect absorption chiller remained steady, while both of them fluctuated in the stand-alone model due to heat source variation.

All the results were in agreement with what had been reported in the literature [52, 26].

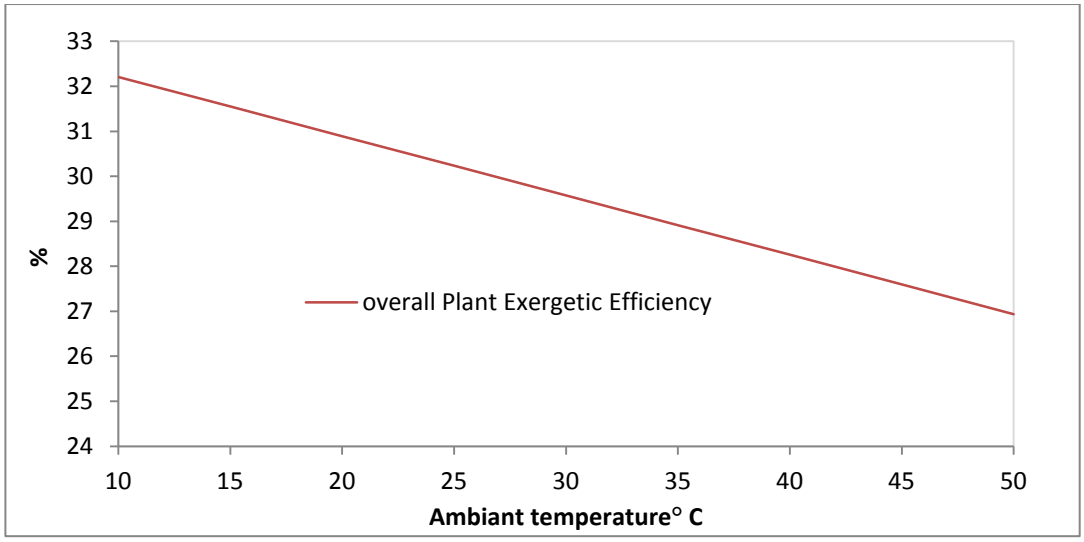

Fig [5-21], Ambient temperature variation versus overall exergetic efficiency

5.3.2 Partial load

Operating the proposed combined cycle of the partial load was carried out in order to monitor the energy and exergy behaviours of the microturbine cascaded with the single effect absorption chiller at the different load operation. The load was operated under a different percentage of intake fuel. It varied from 60% to the full load at 100%. The study was performed in ISO conditions, with a cooling water temperature of 22°C. All the results of this study are listed in Table [5] in the appendix B.

Operating the proposed combined cycle at different partial load has an effect on a number of energy parameters. Fig [5-22] shows the effect on the overall output of electric power when the load is varied. As the load decreased to 60%, the net output power decreased by 45.3%. This was mainly due to the reduction in the fuel consumption mass flow rate, which was reduced to meet the required operating load. Accordingly, the overall efficiency had also reduced in average of 2.29% for each 10% decrease in the partial load, as illustrated in Fig [5-23].

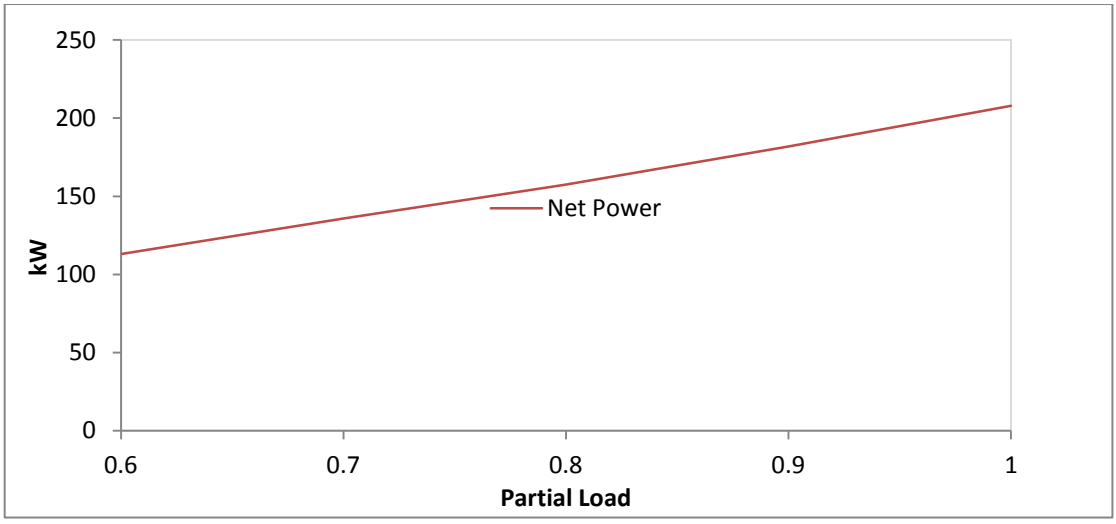

Fig [5-22], The partial load variation against the total output electric power

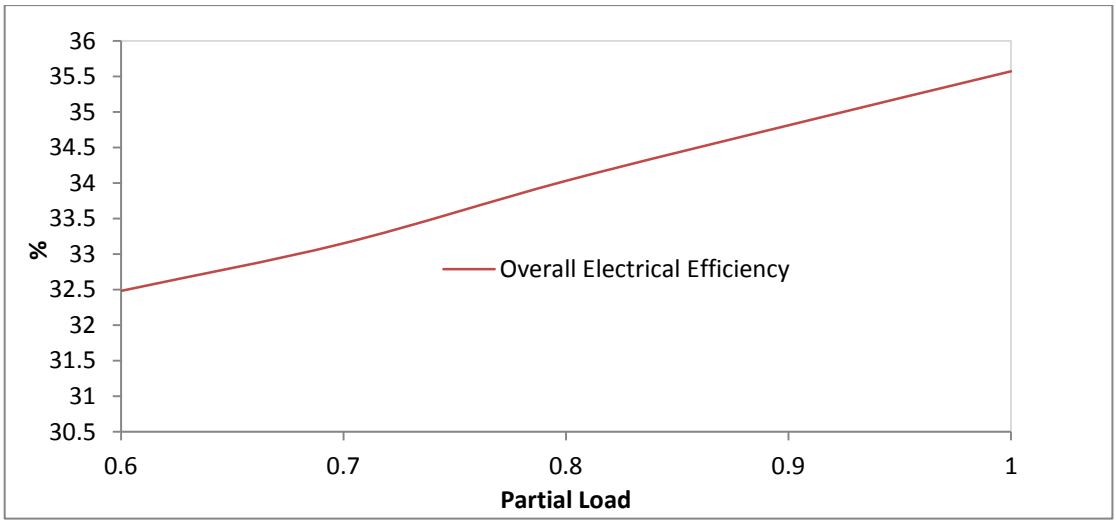

Fig [5-23], the partial load variation against the overall electric efficiency

The EUF was influenced by the reduction in the partial load. Fig [5-24] shows that the combined cycle's EUF increased by an average of 0.9% for each 10% increase in the partial load, which resulted in a total increase of 3.78% at the full load, driven by the higher reduction in the combined model's output electric power by 45.3% and increasing the cooling capacity of the absorption's chiller evaporator by 37.18% at full load. The CO_2 emission rate decreased by 3.77%, increasing the operating load from 60% to full load, as shown in Fig [5-25].

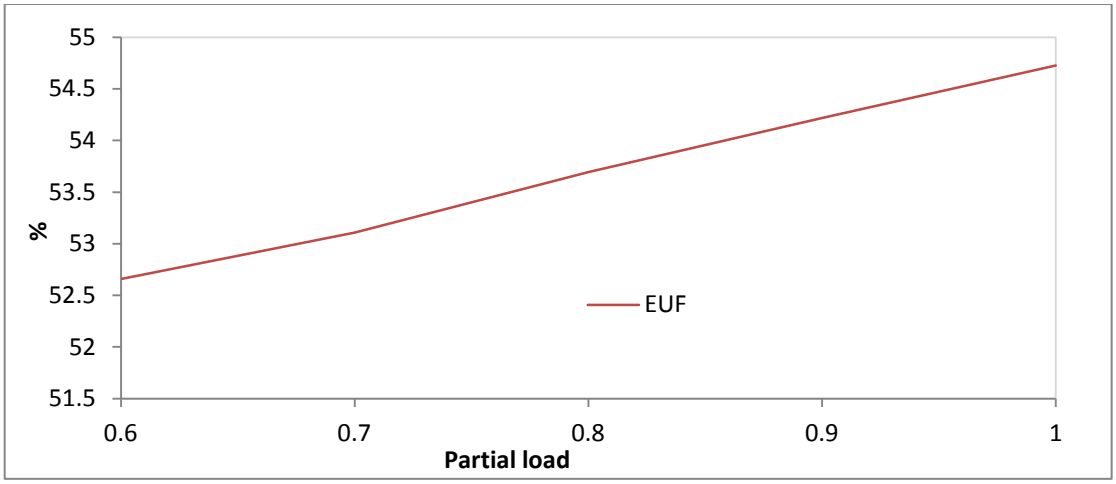

Fig [5-24], The partial load variation versus EUF

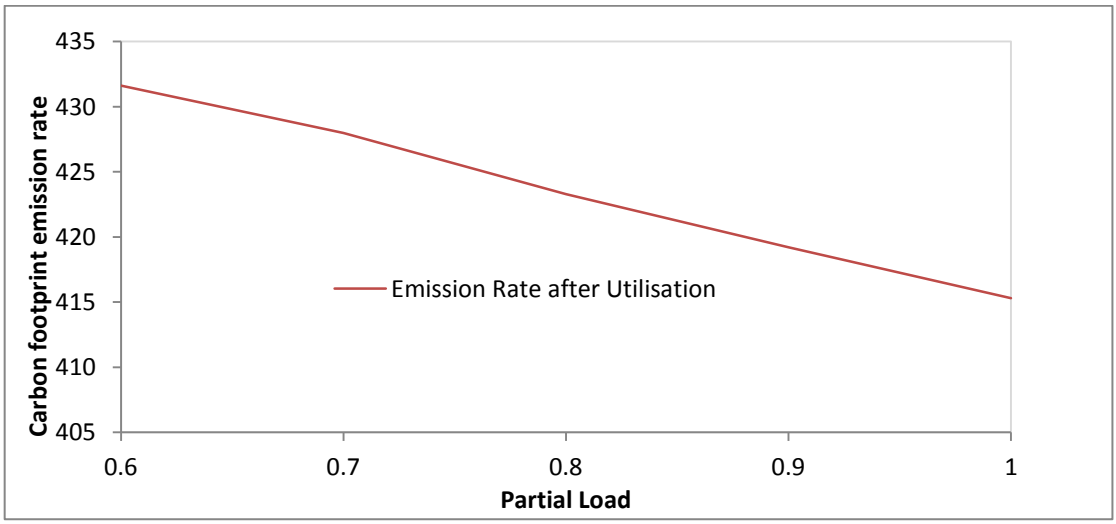

Fig [5-25], The partial load variation versus Co_2 emission rate

On the basis of exergy analysis, the combined cycle's exergy destruction of all components increased in response to the increasing in the partial load from 60% to the full load. This was essentially caused by increasing the fuel mass flow rate, which increased the input exergy by an average of 3.6% for each 10% increase in the operating load, as well as the exergy input for the absorption chiller by an average of 12.34% when the cycle ran from 60% to full load, which took place at the stack stream. The exergetic efficiency was affected by the reduction in the partial load, which dropped by 24.09% at the load of 60%. The increase in exergetic efficiency was at an average of 8.3% for each 10% increase in the amount of load, as shown in Fig [5-26]. The reason for the exergy reduction at a low load in this combined cycle was linked to the fact that the reduction in the supplied fuel, which also reduced the exhaust gas mass flow rate by 36.88% at the lowest load, was equivalent to 60%.

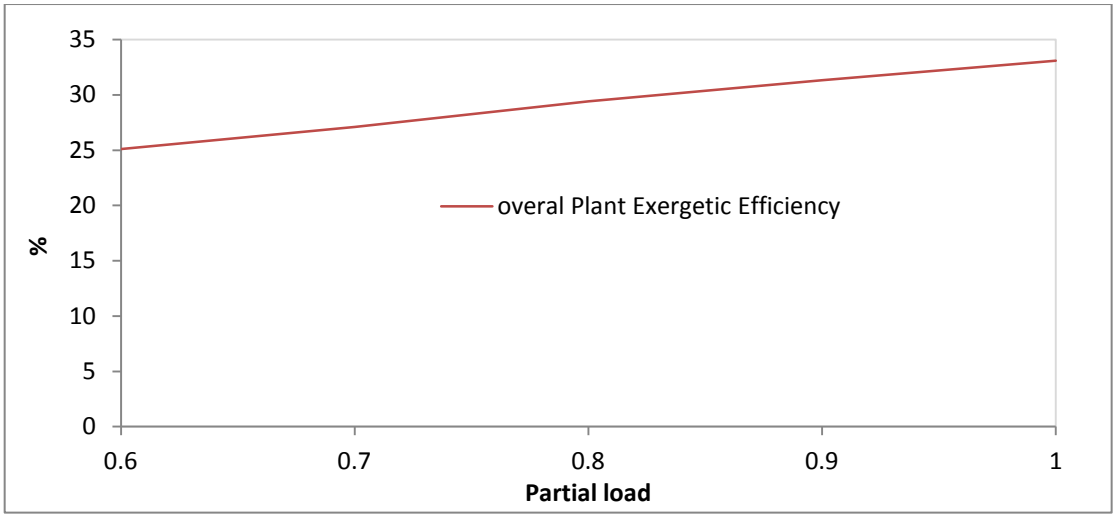

Fig [5-26], The partial load variation versus the overall exergetic efficiency

5.3.3 Intake cooling water

The performance of the combined cycle of the microturbine utilised in the single effect absorption chiller was monitored under seawater temperatures varying from 20°C to 28°C. The proposed model was operated at full load, and the parametric study was considered under ISO conditions. The results are listed in Table [6] in the appendix B.

As the cooling seawater is a part of the absorption chiller model, the overall power and efficiency of the proposed combined model showed no influence when the cooling water temperature was varied. However, the cooling water mass flow rate increased by an average of 18.6% for each 2°C increase in the cooling water temperature, as shown in Fig [5-27]. This increase took place in order to cool the absorber and the condenser to a specific degree, as defined by the evaporator's capacity load for the condenser and by the LiBr/H_2O solution concentration for the absorber.

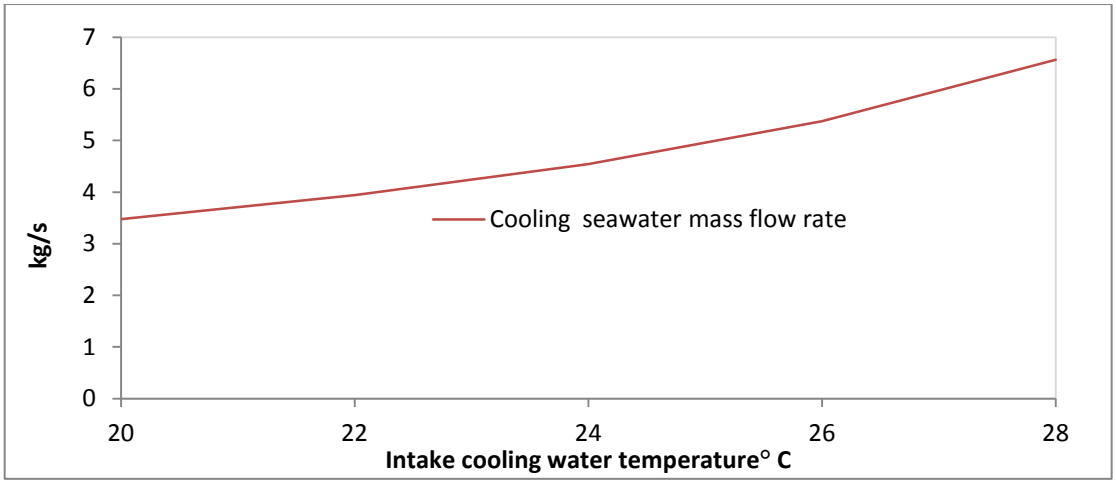

Fig [5-27], The cooling water temperature versus the water cooling mass flow rate

On the basis of second law analysis, the exergy destruction of the absorber was affected by the increasing of the cooling water temperature. Fig [5-28] shows that the exergy destruction of the absorber decreased by 21.8% for each 2°C increase in the water-cooling temperature. This was mainly due to an increase in the input exergy rate of the cooling water stream, which was associated with increases in its temperature and mass flow rate needed to provide the required cooling capacity. Accordingly, the exergy destruction of the condenser was also increased as a result of the cooling water increase, as illustrated in Fig [5-29]. Therefore, the change in the cooling water mass flow rate has a direct effect on the existing exergy destruction for both the absorber and condenser, which results in reducing their exergy destruction. As no exergy destruction was changed in the components of microturbine's model, and the evaporator and generator had specific functions in the absorption chiller model, the overall exergetic efficiency shows a steady value while the cooling water temperature varied.

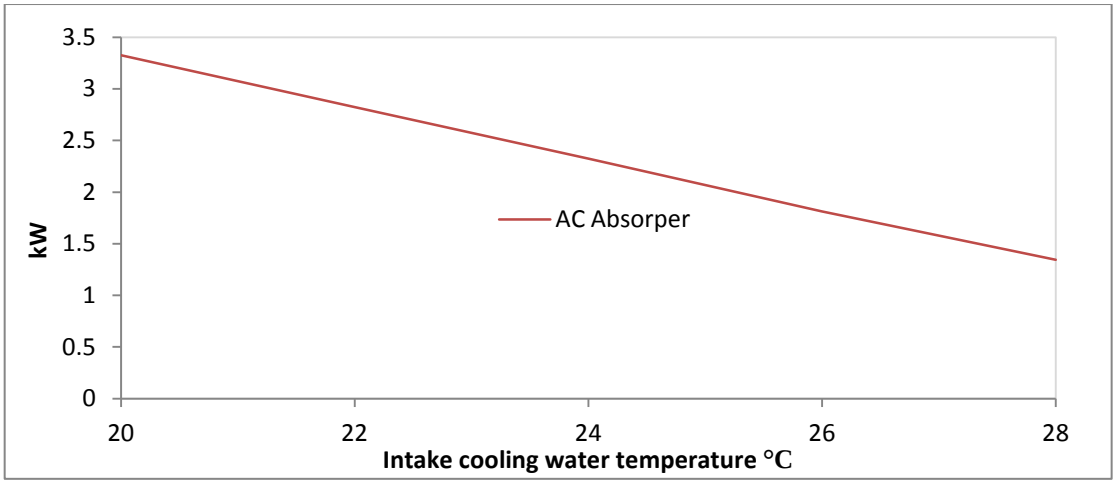

Fig [5-28], Cooling water temperature variation against the absorber exergy destruction

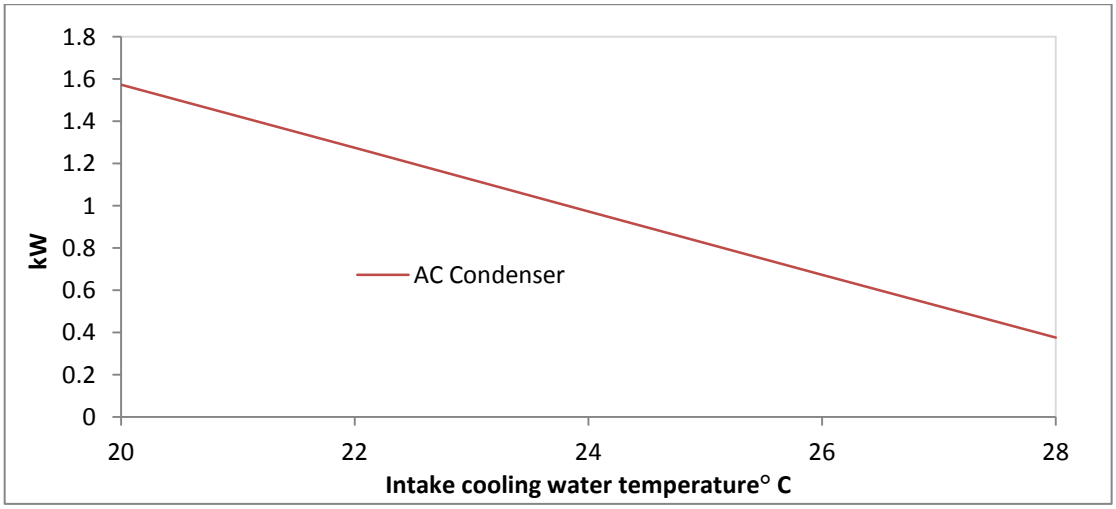

Fig [5-29], Cooling water temperature variation against the condenser exergy destruction

5.4 Microturbine cascaded with thermal vapour compression multi-effect distillation desalination (TVC-MED):

Since thermal desalination technologies are not commonly used in small-scale water production, the opportunity for modelling and simulating small-scale thermal vapour compression multi-effect distilled desalination (TVC-MED) is a great challenge.

As previously discussed, there are two types of the thermal desalination process, MED and TVC-MED. The results of these two stand-alone models showed that the TVC-MED had gained a higher GOR than MED as illustrated in Table [4-15]. The steam ejector was considered to be an improvement to the TVC-MED desalination. The steam ejector in the proposed combined cycle was designed according to available suction steam pressure, and the required steam properties including pressure, mass flow and temperature that provide the best thermodynamic results in order to have a reliable validation of this model.

Utilising the waste heat energy of the microturbine to operate the TVC-MED desalination process is considered in this study as the third proposed combined cycle. The C200 microturbine manufactured by Capstone was employed in this proposed combined model. The utilisation process was adopted in this combined cycle through a heat exchanger called the evaporator, which recovered 48.9% of the waste heat energy of the microturbine used to reheat the motive steam coming from the ejector. The TVC-MED desalination produces a 53m^3/day of potable water, according to the proposed model. The maximum capacity of 53 m^3/day is validated by the reliability of the energy and exergy results. The first operating mode is modelled in ISO conditions, with an inlet air temperature of 15°C and 1 bar at full load. The results are shown in the operating mode on the basis of the first and second laws of energy with reference to this proposed combined cycle. Fig [5-30], illustrates the third proposed combined cycle, using a microturbine cascaded with TVC-MED desalination. The microturbine generates 200.3 kW, with an efficiency of 36.43%, while the TVC-MED desalination produces 53 m^3/day of potable water. The performance of the TVC-MED desalination model was evaluated by using the gain output ratio (GOR), which was 7.7, defined in Chapter 3 as the ratio of the potable water mass flow rate to the driving steam mass flow rate. However, the GOR of MED-TVC stand-alone was slightly higher than the combined cycle. This is due to the fact that the driving steam's temperature of the combined model is 5% lower than that in the TVC-MED stand alone, which caused

an increase in its mass flow rate in order to recover the heat energy amount needed to provide a desire potable water of 53m^3/day, and this in turn affects the value of the GOR.

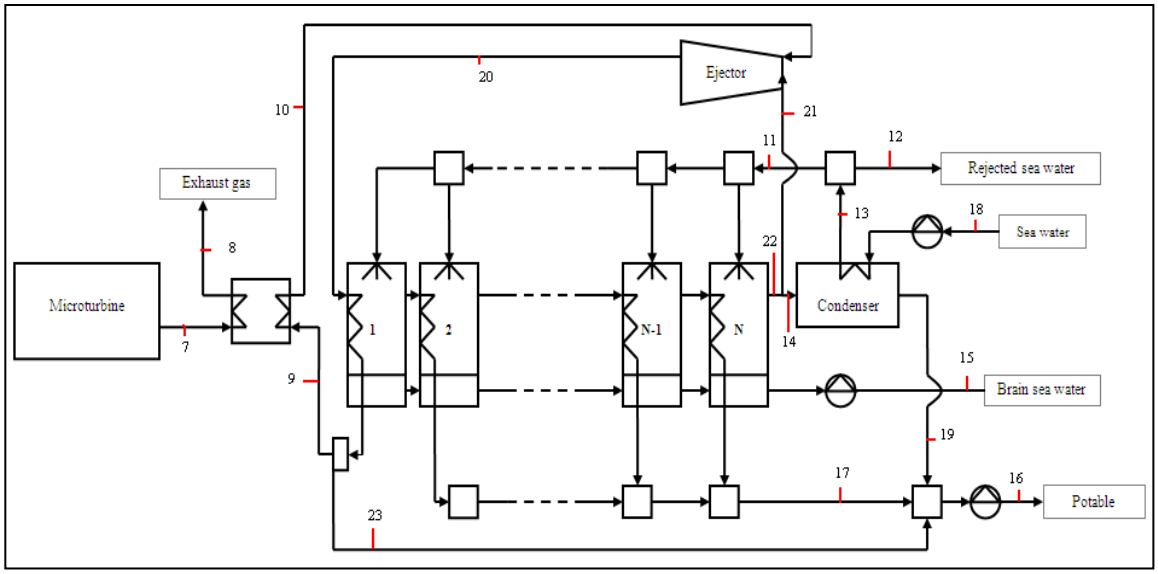

Fig [5-30], Microturbine cascaded with TVC-MED desalination

A measure of the effects of the behaviour of this proposed combined cycle was obtained through the EUF values, and the CO_2 emission rate. The normal mode of operation of this proposed cycle was investigated under the ISO condition and full load operation. Table [5-3] shows the results for both the first and second laws' thermodynamic effect on the system. The energy utilisation factor was 67.2%, with evaporator and condenser effectiveness of 65% and 82% and NTU of 1.0 and 1.9 respectively. The emission rate of the CO_2 indicated a significant decrease, which was extended by 46.8% compared to the stand-alone model, concluding a 341.99 kg/kW of the CO_2 emission rate after the utilisation process, with a specific heat consumption of 336.48 kg/kW, and a concentration factor of 1.86. However, the overall output electric power had been insignificantly reduced compared to the microturbine stand-alone, because of the electrical needs in the combined cycle such as pumps. Furthermore, the overall electric power efficiency was 34.21%, which was also slightly reduced.

On the exergy basis, the proposed combined cycle showed an insignificant difference compared to the microturbine in both models and the TVC-MED desalination. However, the exergy destruction of the microturbine cycle's components indicated no difference from the stand-alone model. In contrast, the TVC-MED desalination

showed no significant difference to the stand-alone model that was introduced in Chapter 3. Most of the exergy destruction had taken place in the combustion chamber, as the main exergy input source passes through it, due to the heat transfer and mixing process. This represented 75.7% of the model's total exergy destruction, which accounted for 59.9% of the total exergy input to the combined cycle. The gas turbine of the microturbine exergy destruction represented 6.8% of the total exergy destruction, and formed 5.3% of the total exergy input. Furthermore, the boiler heat exchanger represented 6.6% of the total exergy destruction, and shaped 5.3% of the total exergy input. Also, the stack exergy destruction was reduced by 84%. However, on the basis of thermal desalination exergy, the main exergy destruction in the TVC-MED desalination model occurred in the evaporator between the first and the ninth effect with a value of 22.37, which represented 2.9% of the total exergy destruction and accounted for 2.3% of the total exergy input.

5.4.1 Parametric studies:

The performance of the proposed combined cycle was investigated under varying ambient temperatures by varying the compressor inlet-air temperature from 5°C to 50°C, while the pressure remained constant at 1 bar. The microturbine was operated at full load, while the TVC-MED was operated as low-grade heat energy. The inlet seawater temperature of the TVC-MED desalination was 22°C, and was operated to produce a maximum amount of potable water of 53 m^3/day. The results of this proposed model are listed in Table [7] in the appendix B.

The variation in ambient temperature had an effect on the output electric performance. According to Fig [5-31] the output power of the microturbine decreased by 2.8% for each 5°C increase in the ambient temperature. This showed the same relative performance as the microturbine stand-alone, which was mentioned previously.

	H(kj/kg)	S(kj/kgK)	M(kg/s)	T(°C)	P(bar)	e(kW)	E(kW)
1	15.1593	6.8494	1.2594	15	1.013	0	0
2	280.8973	6.9145	1.2594	274.4656	7.9	246.9841	311.0472
3	484.9455	7.2375	1.2594	465.3781	7.8999	358.0197	463.7313
4	940.7473	7.8263	1.2711	850	7.8899	669.5265	851.0495
5	495.1472	7.9381	1.2711	466.0535	1.0418	191.7196	243.6989
6	53.338	9.9618	0.0117	25	15	50149.4	966.7762
7	292.9837	7.6543	1.2711	280.9556	1.0417	71.2966	90.6266
8	149.8242	7.3614	1.2711	145.1705	1.0317	12.503	15.8929
9	295.4953	0.9613	0.0779	70.5355	3.2	20.2788	1.5801
10	2630.883	6.7342	0.0779	135.6319	3.19	693.0891	54.0054
11	180.369	0.6299	1.2937	45.3812	1.5	5.9003	7.6333
12	180.369	0.6299	0.13	45.3812	1.5	5.9003	0.767
13	180.369	0.6299	1.4237	45.3812	1.5	5.9003	8.4003
14	2592.054	8.0905	0.0552	50.3269	0.12	263.6536	14.5418
15	192.0348	0.6946	0.6937	50.3724	2	4.5634	3.1657
16	250.2375	0.828	0.6	59.7491	2	12.2283	7.337
17	255.1192	0.8431	0.5362	60.9499	0.3	12.7159	6.8181
18	87.3632	0.33	1.4237	22	1.02	0.3484	0.496
19	206.8845	0.6963	0.0638	49.4098	0.3	7.0466	0.4497
20	2627	7.745	0.0866	70.5861	0.32	398.087	34.4654
21	2592.054	8.0905	0.0087	50.3269	0.12	263.6536	2.2827
22	2592.054	8.0905	0.0638	50.3269	0.12	263.6536	16.8244
23	295.1271	0.9611	0.0087	70.504	0.319	19.971	0.1729
24	295.1271	0.9611	0.0866	70.5034	1.013	19.971	1.729

Table [5-3], The energy and exergy properties of the microturbine cascaded with the TVC-MED desalination.

Moreover, as the output electric power decreased when the ambient temperature increased, the overall electrical efficiency decreased by an average of 2.8% for each 5°C increase in the ambient temperature, as illustrated in Fig [5-32].

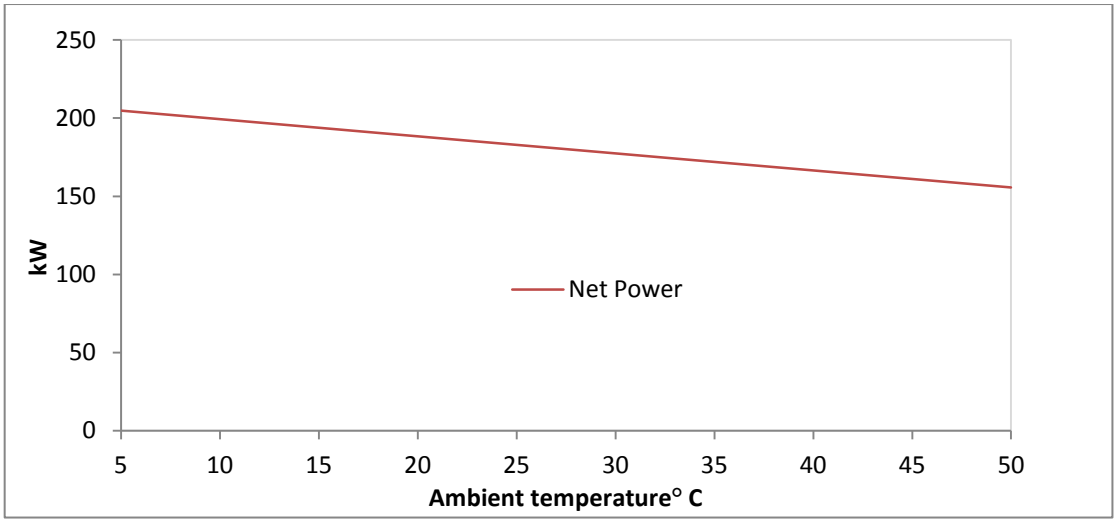

Fig [5-31], The output electric power versus ambient temperature variation

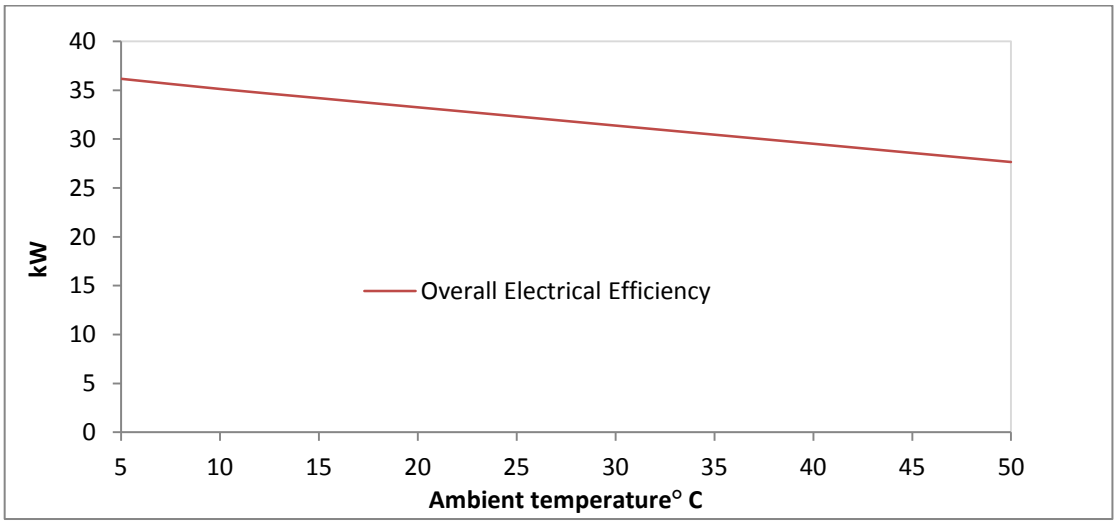

Fig [5-32], The overall efficiency versus ambient temperature variation

Following to the reduction in the output of electrical power, Fig [5-33] shows that the CO_2 emission rate increased by an average of 1.4% for each 5°C increase in the ambient temperature variation. This was due to changes in the heat transfer value of the heat exchanger when the utilisation process was taking place. The temperature of the stack was influenced by an increasing in the ambient temperature of 31% when the ambient temperature increases from 5°C to 50°C. Furthermore, in order to meet the energy requirements, including temperature and pressure and enthalpy, for the required amount of potable water, which were 53 m^3/day, the heat transfer value of the heat exchanger had to be varied when the ambient temperature was changed. Also,

the amount needed to recover the waste heat energy of the microturbine to operate the TVC-MED desalination model was reduced by an average of 2.9% for each 5°C increase in the ambient temperature. The ambient temperature variation has an effect on the heat transfer rate of the boiler, where motive steam is heated by the microturbine waste heat energy. The heat transfer rate decreased by an average of 16% for each 5°C increase in the ambient temperature. As the amount of recovered waste heat energy was reduced, the energy utilisation factor was reduced by an average of 1.4% for each 5°C increase in the ambient temperature, as illustrated in Fig [5-34].

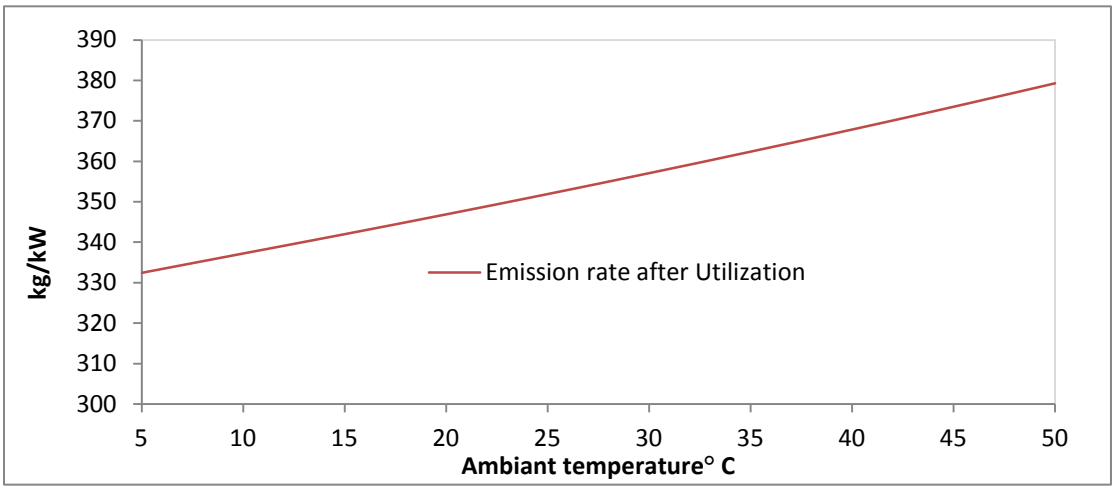

Fig [5-33], The CO_2 emission rate versus the ambient temperature variation.

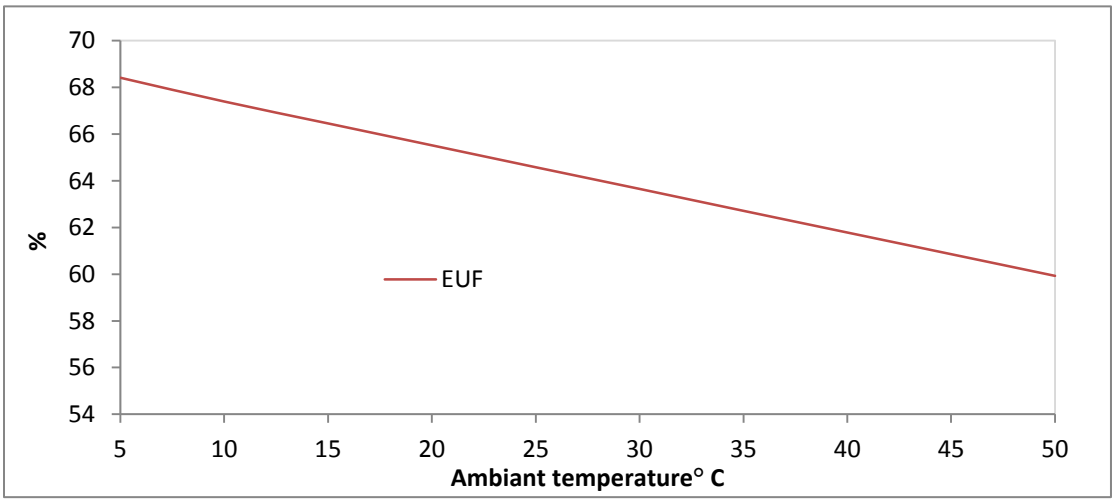

Fig [5-34], EUF versus the ambient temperature variation

Regarding the second law biases, variations in the ambient temperature showed no significant effect on the exergy destruction of the proposed model components. However, the highest exergy destruction effect had taken place in the boiler, and had

increased by the average of 7% for each 5°C increase in the ambient temperature. This was due to an increase in the waste heat energy temperature, and 82% of the stack exergy which was used in the heat exchanger process. As Fig [5-35] shows, the overall exergetic efficiency decreased by the average of 2.6% for each 5°C increase in the ambient temperature.

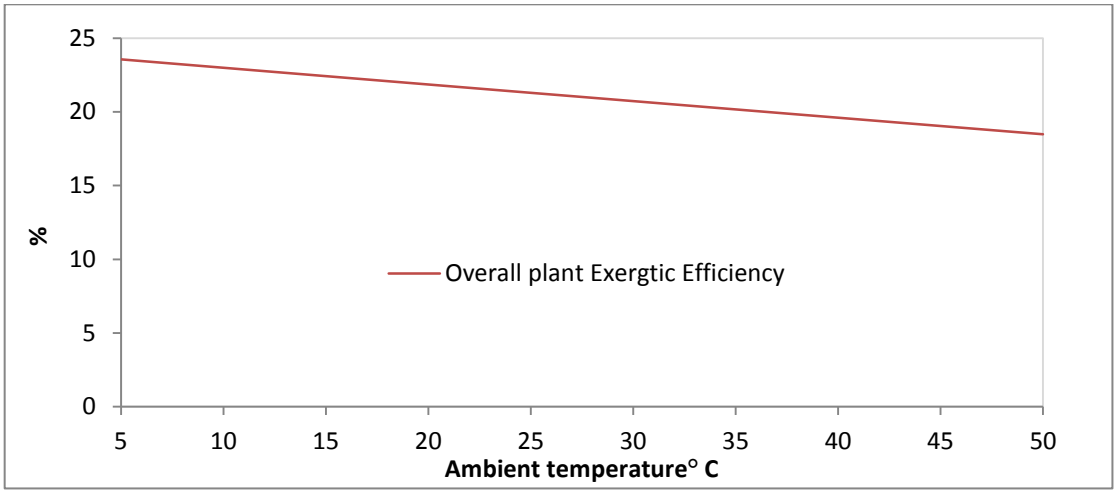

Fig [5-35], The exergetic efficiency versus the ambient temperature variation

5.4.2 Partial load

The operation the proposed combined model was investigated by operating the microturbine being cascaded with the TVC-MED desalination at a different load operation. The energy and exergy performance parameters were monitored when the operating load was varied between 60% to full load 100%. However, the TVC-MED desalination process produced 53 m^3/day of potable water, and it was found that, the waste heat energy of the microturbine could not handle the production of TVC-MED desalination when the load became less than 100%. Therefore, the operation of the proposed model at a partial load was designed for the half production of potable water, which was 26.5 m^3/day. Table [5-4] provides a full energy and exergy comparison between full and the half production of potable water with TVC-MED desalination at 22°C of inlet seawater temperature when the microturbine operates at full load in ISO conditions.

Thermodynamic properties	0.6 kg/s	0.3 kg/s
Air compressor (kW)	26.9989	26.9989
Recuprecator (kW)	0.3882	0.3882
C.C (kW)	579.4581	579.4581
Turbine (kW)	52.267	52.267
Evaporator (kW)	22.3084	16.09
Boiler (kW)	51.2346	26.8796
Condenser (kW)	6.3607	2.4384
Steam Ejector (kW)	21.8226	11.4639
Microturbine Power (kW)	200.32	200.32
GT Efficiency (%)	36.43	36.43
EUF	66.46	51.67
Fresh Water production (m^3/day)	53	26.5
GOR	7.7	7.33
Waste energy utilization (%)	48.8626	25.6685
Emission rate after Utilization (kg/kW)	341.9965	439.8447

Table [5-4], Comparison of energy and exergy analysis between TVC-MED desalination operation modes

As Table [5-4] shows, operating the TVC-MED desalination process at half load led to the production of 26.5 m^3/day of potable water. This increased the CO_2 emission rate by 13%, due to the decrease in the heat transfer rate of the boiler heat exchanger, while the electric power of the microturbine remained constant at 200.31 kW, which caused an increase in the stack temperature. The EUF also decreased by 22.7%. The GOR showed a very small reduction as the production of potable water decreased. The main exergy reduction was raised in the evaporator and boiler as there was a reduction in both intake seawater mass flow rate of 45%, and in the motive steam mass flow rate by 50%. According to this, the overall exergetic efficiency increased insignificantly by 0.05% as the input and output exergy of the microturbine remained steady.

Operating at a partial load was carried out, in order to examine the performance of the proposed combined cycle with different operating load patterns ranging from 60% to

100%. This study was performed in ISO conditions, with a seawater temperature of 22°C, and the TVC-MED desalination model was operated at half load, producing 26.3 m^3/day of potable water. All the results of this study are listed in Table [8] in the appendix B.

Fig [5-36] shows that the effect of operating a partial load on the net output of electrical power. As the partial load increases, the fuel consumption is increased, which leads to an increase by an average of 17.8% for each 10% increase in the microturbine load. Consequently, as Fig [5-37] shows, the overall efficiency dropped by 13% when the load was reduced from 100% to 60%.

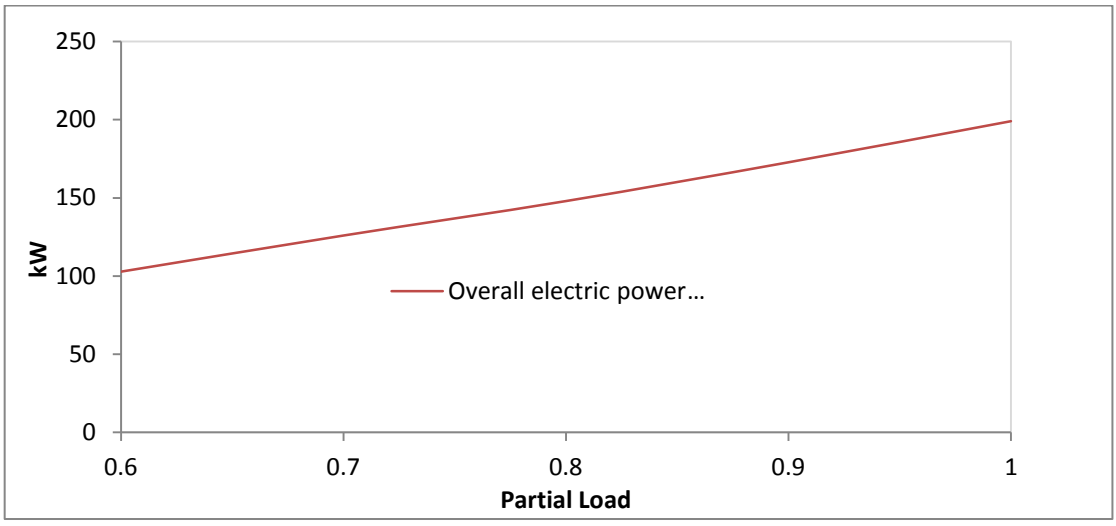

Fig [5-36], The overall electric power versus the partial load

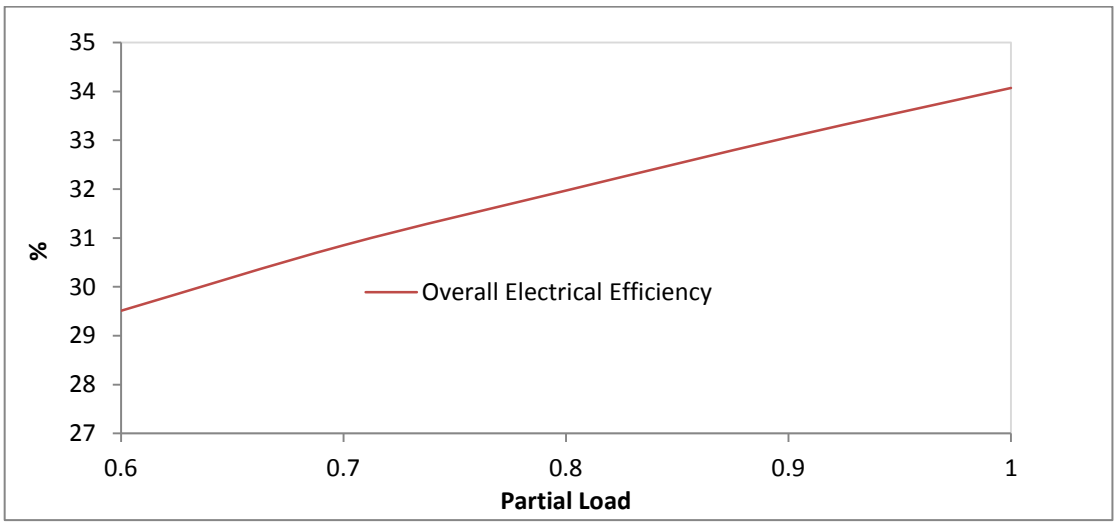

Fig [5-37], The overall electric efficiency versus the partial load

Fig [5-38], shows the CO_2 emission rate performance at partial load. Operating the proposed model from the full load to 60% caused a reduction in the CO_2 emission rate

of 11.2%. This is because of the increase in the heat transfer rate in the boiler of 25.7% in order to provide the required amount of heat for water production, as the amount of potable water production was stable when the load is decreased. According to this, the EUF was increased by an average of 2.9% for each 10% decrease in microturbine load, as illustrated in Fig [5-39]. This means operating microturbine at partial load is recommended at half water production when the electric demand is low.

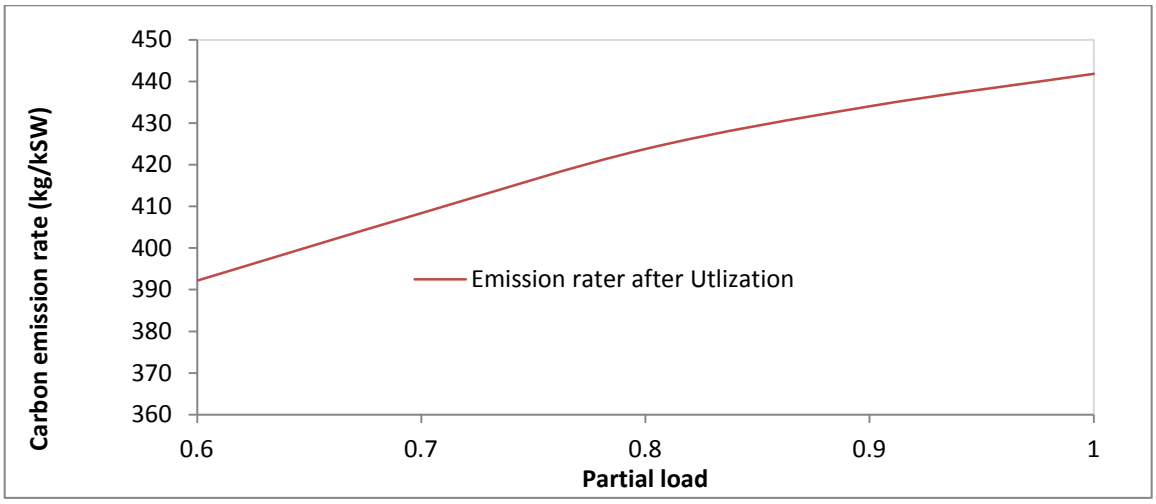

Fig [5-38], The CO_2 emission rate versus the partial load

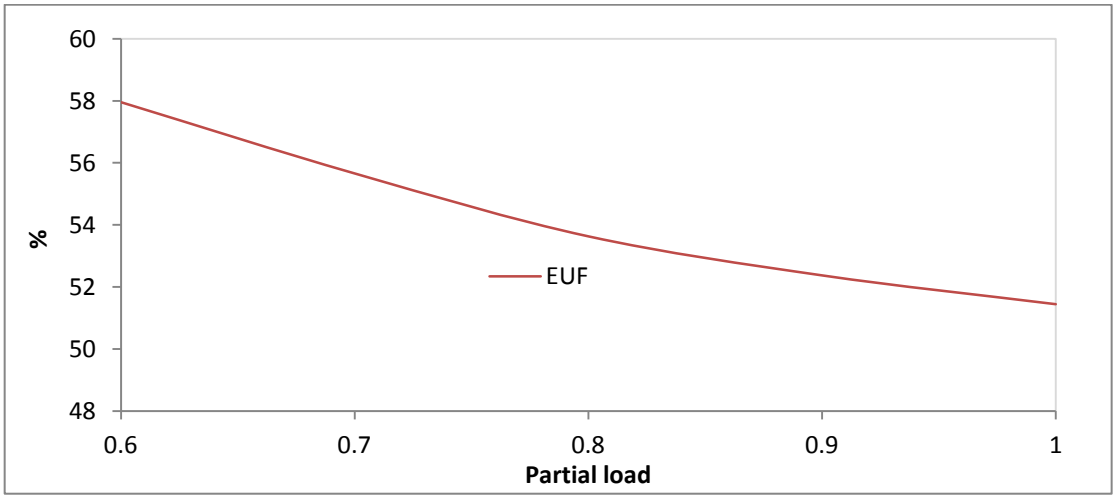

Fig [5-39], The EUF versus the partial load

On the basis of exergy analysis, the total exergy destruction decreased to a 60% operating load. This was driven by the reduction in the amount of fuel consumption, which caused a reduction of 35.3% in the exhaust mass flow rate at a 60% load. The main reduction in the exergy destruction was produced by the microturbine components by an average of 8.6% for each 10% decrease in its load, and the exergy

destruction of TVC-MED desalination remained constant due to the stable production of the potable water. Fig [5-40] shows the proposed combined model's overall exergetic efficiency at a partial load. The overall exergetic efficiency was inversely proportional to the operating load, which decreased by 30% at 60% of the operating load.

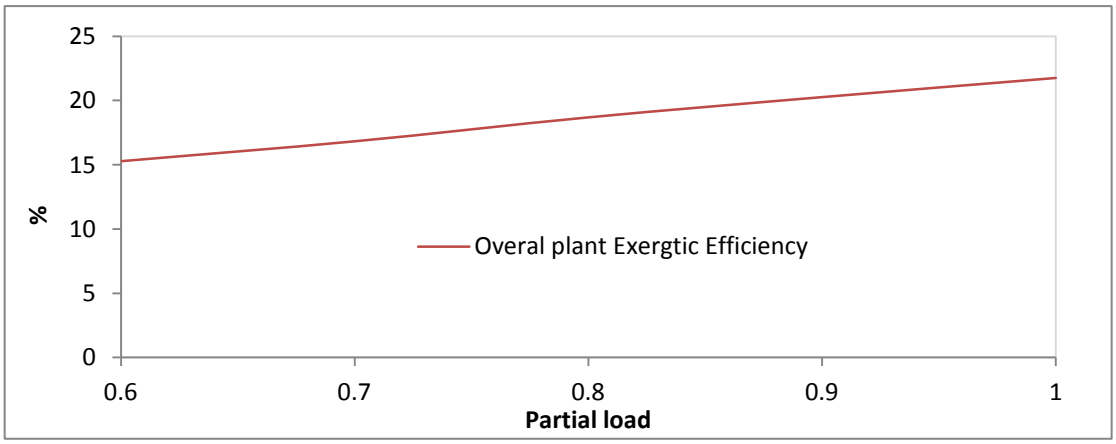

Fig [5-40], The overall exergetic efficiency versus the partial load

5.4.3 Intake of seawater:

The behaviour of the proposed combined cycle of the microturbine utilised in TVC-MED desalination was monitored by varying the intake seawater temperature to between 20°C to 28°C. The proposed model operated at full load, and the parametric study was considered at ISO condition. The obtained results are listed in Table [9] in the appendix B.

As the intake seawater is a part of the TVC-MED desalination model, the overall power and efficiency of the proposed combined model showed no influence when the intake seawater temperature was varied. However, the seawater water mass flow rate increased by an average of 10% for each 2°C increase in the seawater water temperature, as shown in Fig [5-41]. This increase took place in the intake seawater in order to be re-heated in the condenser to the specific temperature required for the first evaporator. After this, the extra amount of mass flow rate was rejected. As the production of the potable water was fixed, the suction mass flow rate decreased by an average of 9% for each 2°C increase in the intake seawater temperature.

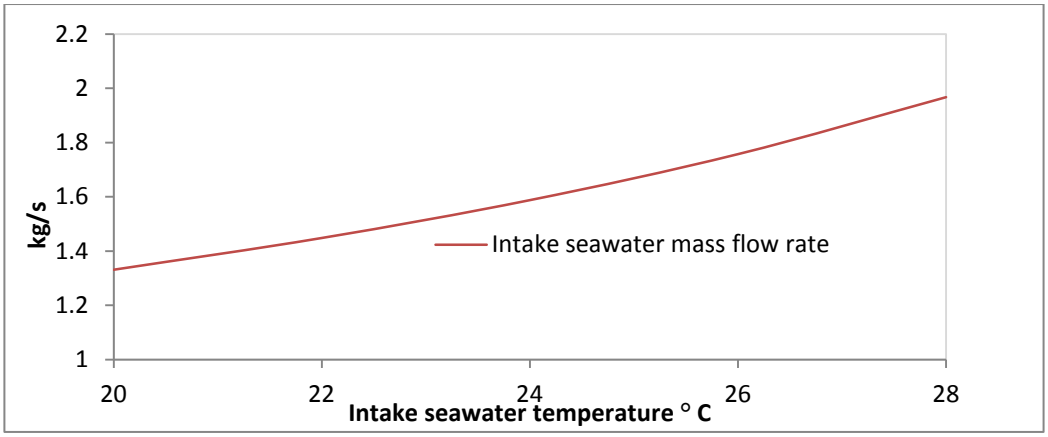

Fig [5-41], The intake seawater mass flow rate versus its temperature variation

The effect of the intake seawater temperature variation was also examined in this model with regard to exergy destruction. As the intake seawater temperature increased by 2°C, the condenser exergy destruction decreased by an average of 17%, as illustrated in Fig [5-42]. This was because that, the influence of the seawater temperature only occurred in the inlet stream to the condenser while the temperature of the outlet stream remained constant, in order to inter the first desalination effect. According to this effect, the overall exergetic efficiency increased slightly by 1% when the intake seawater varied from 20°C to 28°C.

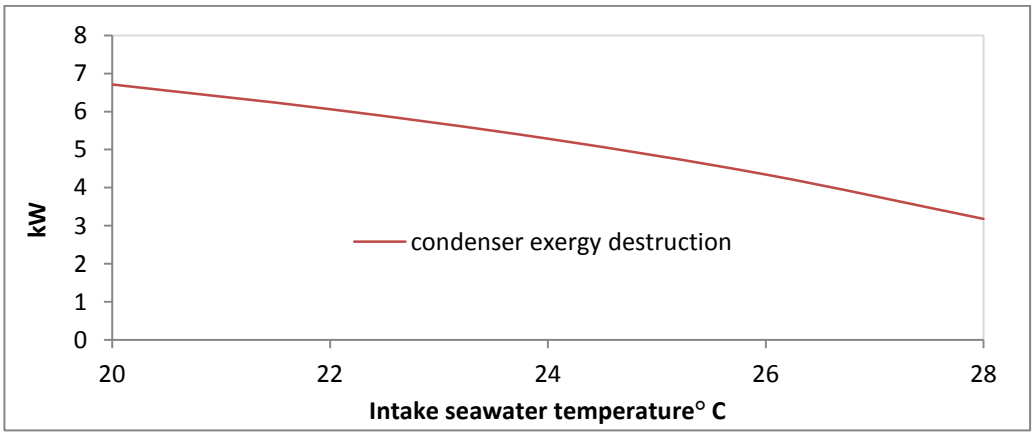

Fig [5-42], The condenser exergy destruction versus intake seawater temperature's variation

5.5 The energy and exergy comparison of all microturbine combined models:

The microturbine unit C200 manufactured by the Capstone Company has been widely used as high-grade heat energy to simulate and model the low-grade heat energy. Each proposed model, including the organic Rankine cycle (ORC), single effect cooling water absorption chiller and thermal vapour compression desalination (TVC-MED) was simulated separately with microturbine stand-alones. Then, the energy and exergy analysis were obtained for each model, as previously mentioned in this chapter.

The comparison has been performed for all proposed combined models powered by a microturbine's waste heat energy, based on first and second law analysis, in order to illustrate a clear thermodynamic view of all models. Fig [5-43], and Fig [5-44] summarise the results of each proposed combined cycle, including the overall output of electrical power, overall efficiency, carbon foot print reduction, energy utilisation factor (EUF), stack exergy destruction, and overall exergetic efficiency as shown in Table [5-5]. Furthermore, all models were monitored under ISO conditions, and operated at full load with a cooling water temperature of 22°C.

	ORC+microturbine	Absorption chiller +microturbine	TVC-MED +microturbine
Net Power (kW)	216.88	208.21	199.89
Overall Electrical Efficiency (%)	37.23	35.63	34.21
Emission Rate before Utilisation (g/kW)	667	667	667
Emission Rate after Utilisation (g/kW)	594.35	433.49	341.99
EUF (%)	38.24	52.43	66.46
Overall Plant Exergetic Efficiency (%)	23.11	31.68	22.42
Waste energy utilisation (%)	48.01	40.70	48.90

Table [5-5], The energy and exergy results for all proposed combined cycles

Fig [5-43] demonstrates the energy effect on each model, showing that integrating the microturbine with the ORC unit led to the generation of an extra 4.1% of electric power compared to that produced by the absorption chiller, and 7.8% for TVC-MED desalination. This was because the ORC stand-alone was producing an extra 16.88 kW of electric power, causing a higher output power than other models. This also led to a relatively higher overall efficiency of 37.23% among other proposed combined models. Utilising the microturbine in the absorption has raised the overall electric power to 208.21 kW because of cooling the inlet air temperature to the microturbine's

compressor to 8°C, which in turn caused a constant efficiency and output power rate of 35.63% and 208.21 kW respectively, while the ambient temperature of other combined models was 15°C and it could be changed according to the ambient condition. However, the lowest carbon emission rate among all models took place when utilising the microturbine with TVC-MED desalination, with a reduction of 46.8% compared to a microturbine stand-alone. This is because producing the desire amount of potable water of 53m^3/day requires a high amount of heat rate at the heat exchanger where the utilising process between microturbine and TVC-MED desalination is taking place. Accordingly, the EUF of the TVC-MED desalination was 9.2% higher than utilised in the absorption chiller, and 42.4% higher than utilised in ORC. ORC gained a lowest EUF due to lower rates of production compared to other models, in order to meet the specification and the production range of the real manufactured ORC unit.

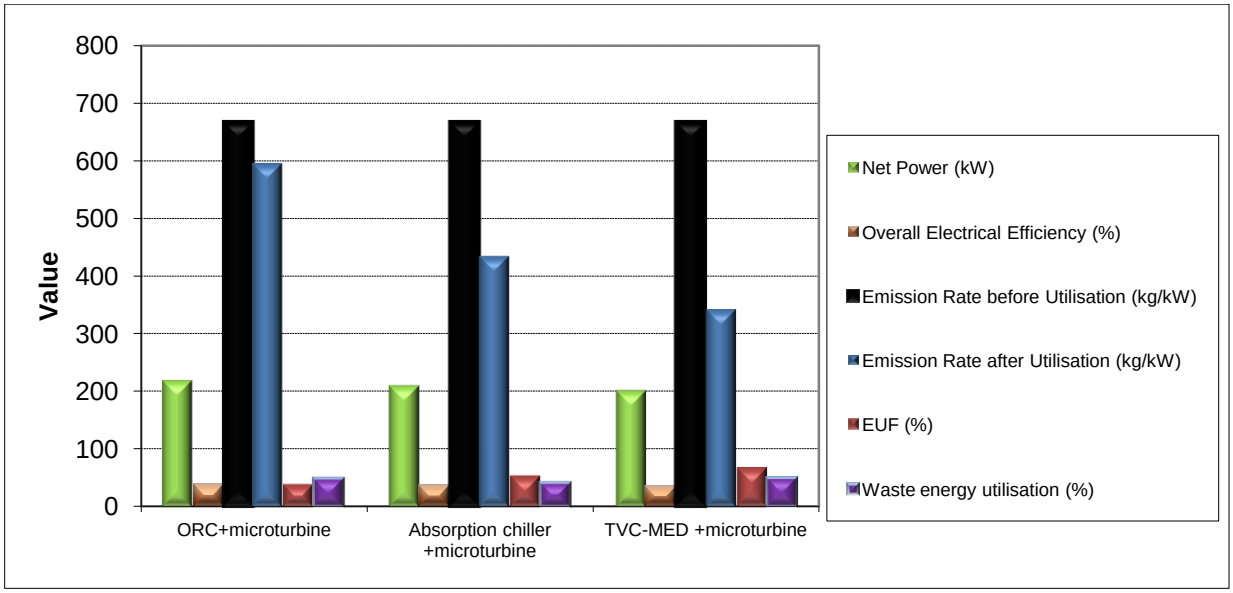

Fig [5-43], The energy results for all proposed combined cycles

Regarding the second law analysis, Fig [5-44] shows a comparison of the overall exergetic efficiencies for all proposed models. The higher rate of exergetic efficiency was presented by utilising the microturbine with the single effect absorption chiller with a value of 31.68%, while ORC and TVC-MED produced rates of 23.11%, and 22.42% respectively. The absorption chiller was providing a 105 kW of cooling capacity, which counted as a model's output product added to the power generated from the microturbine. However, the lowest stack exergy destruction was presented in

the microturbine combined with the ORC, with a value of 15 kW. Utilising the absorption chiller led to the highest rate of stack exergy destruction. However, the benefits of utilising microturbines in the absorption chiller were that the model's energy and exergy remained constant against the ambient temperature variation due to pre-cooling process of the intake air provided from the absorption chiller's chilled water, while the other combined models including ORC and TVC-MED were influenced and their energy and exergy parameters affected.

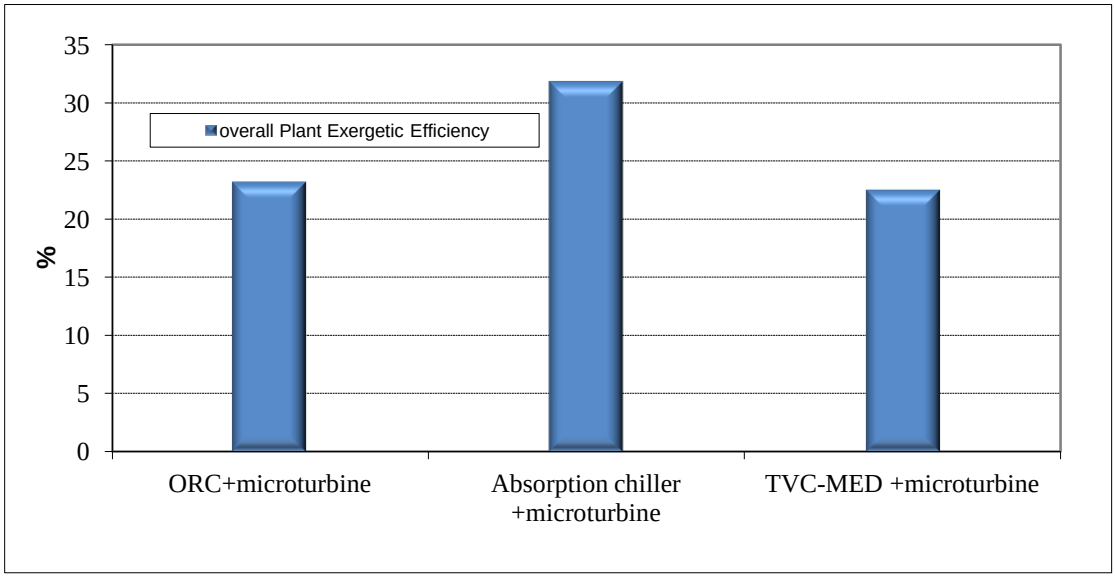

Fig [5-44], The exergy results for all proposed combined cycles

5.6 Chapter Summary

The effect of ambient conditions, operating at partial load and intake seawater temperature were discussed and explained for each CHP model in this chapter. Then, the overall comparison was performed between all proposed CHP models based on the first and second law of thermodynamic.

Chapter 6

Economic Study

6.1 Introduction:

This chapter aims to provide an economic assessment of all the models that were previously simulated and studied. Furthermore, each model provides a different source of energy. For example the microturbine and organic Rankine cycles supply electricity, while the absorption chiller and TVC-MED supply cooling and potable water respectively. However, the microturbine is considered to be a main part of each model in that its waste heat energy is used to operate the other proposed model. Therefore, considerations of economic feasibility were applied for the following models:

1- Microturbine stand-alone.
2- Microturbine + organic rankine cycle (ORC).
3- Microturbine + single effect absorption chiller.
4- Microturbine + thermal desalination process (TVC-MED).

The fuel price is widely known to vary greatly, which has an influence on the accuracy of any economic result. The fuel price was assumed to be constant in this study, as it is subsidised by the government against any increase in its value.

The economic analysis was carried out by evaluating three profit factors for each proposed model: the payback period (PBP), the net present value (NPV), and the average rate of return (ARR). However, the initial cost of each unit, including its equipment, was obtained from official sources or past studies, or manually calculated, and then was used to complete a part of the capital cost. The annual cash inflow was calculated according to both the unit's operation and maintenance (O&M), and the fuel costs. The annual cash outflow was calculated according to the product's selling prices for energy and potable water. The sensitivity study was conducted to find the selling price for energy and potable water in order to illustrate the effect of fluctuations in these variables within the unit's lifetime.

The economical feasibility results of all proposed models were carried out using PSEconomy [122], part of the IPSE pro software previously explained in chapter 3. The software was used in a simple form that was similar to the MS excel spreadsheet, in order to gather all the component cost of units for either inflow and outflow cash, including the initial cost and the operation and maintenance cost, as well as the annual revenues. The Microsoft Excel model was used to calculate the cost of the heating and cooling heat exchanger employed as part of this study.

6.2 Initial Cost Estimate:

The initial cost gives a clear idea of the cost of the purchased equipment. Obtaining these data can be carried out directly through the company's database, or by searching the most recent studies which provide some initial costs or, alternatively, by calculating the cost using the extensive cost databases maintained by the engineering company. The initial cost of each model was obtained to give a wide understanding of the economic feasibility of this study by finding the total cost of the microturbine unit, the ORC, the TVC-MED and single effect absorption chiller. According to Bejan, et al [75], the contingency factors which represent the sudden prices changing and the transportation difficulties were added as an extra 5% to the fixed capital investment, while the equipment installation cost was 33% of the capital equipment cost; electrical equipment and materials were 13%, and lastly 12% of instrumentation and controls were added to total equipment cost for all units.

The proposed model of the microturbine was combined with the single effect absorption chiller containing two heating and cooling heat exchangers and it was very difficult to obtain the direct quotation of their initial cost from the supplier company, as well as, the microturbine with TVC-MED, whose heat exchanger was used for heating. However, the cost of the heat exchanger was obtained by using the HIS ESDU international costing technique [123]. The UK'S major manufacturer of heat exchangers, IMI Marston was assisted by ESDU in order to provide the C-values required for calculating the cost of heat exchangers. Calculating the final cost of the heat exchanger was carried out using a Microsoft Excel model by inserting the required data from ESDU tables.

The required data for both heating and cooling heat exchanger including the hot and cold side temperature can be observed using the IPSEpro simulation software, while the other data is calculated by the Microsoft Excel model as there are a number of equations used in MS Excel to perform automatic calculation.

The inlet and outlet hot and cold temperatures (T_h, T_c) for each stream were used as input data to calculate the mean temperature difference in the following equation:

$$\Delta T_{lm} = \frac{\left[\left(T_{h,in} - T_{c,out}\right) - \left(T_{h,out} - T_{c,in}\right)\right]}{\log_e\left[\left(T_{h,in} - T_{c,out}\right)/\left(T_{h,out} - T_{c,in}\right)\right]} \qquad (6\text{-}1)$$

The value of $\left(\dot{Q}/\Delta T_{lm}\right)$ was calculated to obtain the value of C_1 and C_2 by reading directly from the ESDU tables. As the value of $\left(\dot{Q}/\Delta T_{lm}\right)$ is found between two scales, as shown in table 9.3 of double pipe heat exchangers [123], the C-value is then calculated by the logarithmic interpolation as follows [123]:

$$C = \exp\left\{\log_e C_1 + \frac{\log_e (C_1/C_2)\log_e\left[(\dot{Q}/T_{lm})_1\right]}{\log_e\left[(\dot{Q}/\Delta T_{lm})_1/(\dot{Q}/T_{lm})_2\right]}\right\} \qquad (6\text{-}2)$$

Multiplying the C-value by $\left(\dot{Q}/\Delta T_{lm}\right)$ will bring the final cost of the employed heat exchanger. Fig [6-1] shows a screenshot for the heat exchanger calculation. The capital cost was updated by using the GB pound retail price index (RPI), while the instillation cost is added to the final unit cost. Table [6-1] represents the final cost of each added heat exchanger to the proposed combined cycles.

The estimation cost for all proposed models including electricity, cooling and potable water are presented in Table [6-2] and Table [6-3]. The former shows the particular cost estimation for each unit, while the latter illustrates the initial estimate for the combined model

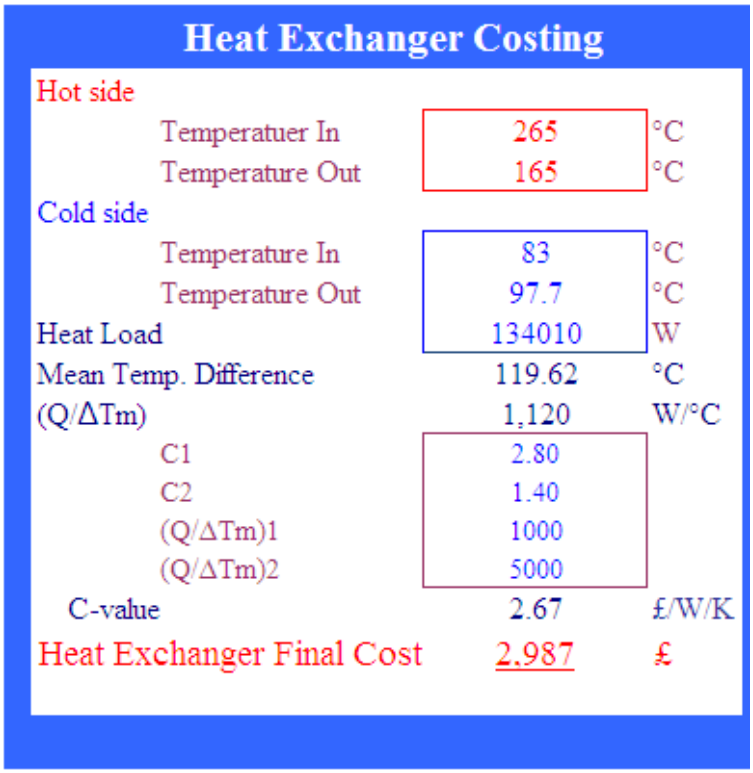

Fig [6-1], Screenshot of MS Excel model for heat exchanger calculation

Absorption chiller heating H.E	£4,300
Absorption chiller air cooled H.E	£6,000
TVC-MED (H.E)	£5,090

Table [6-1], Heat exchanger cost estimate

Moreover, the equipment instillation, electrical material, instrumentation and control, contingencies and savage value were added as onsite and indirect costs. The microturbine cost was obtained from the Capstone Company, where the microturbine originally was manufactured by an electronic letter [124]. The cost of the organic Rankine cycle was provided by the Infinity Turbine Company [125]. It was very difficult to obtain the price of the single effect absorption chiller. Therefore, the absorption chiller cost was directly obtained from a recently published study by Boonnasa and Namprakai [126]. Furthermore, there was concern over TVC-MED desalination unit's price. The Australian Government, represented by the National Water Commission, published a review which provided the cost of TVC-MED desalination [127]. Fig [6-2] shows the PSEconomic window where each unit's capital cost, onsite cost, and indirect cost were inserted.

Unit	**Unit cost**
Microturbine	£1134.39/kW=£**226879**
ORC	£9,396
Single effect absorption chiller	£78.21/kW=**£8212.05+£10300 (H.E)=£18512**
TVC-MED desalination	£594.5/m^3-**£31512+5090(H.E)=£36602**

Table [6-2], The initial cost estimation for each unit

	Microturbine	Micro+ORC	Micro+AC (on-site)	Micro +TVC-MED
Combined unit cost	£226,879.00	£236,275	£245,391	£263,481.00
Purchased equipment instillation	£74,870	£77,971	£80,979	£86,949
Instrumentation and Controls	£27,225.48	£28,353.00	£29,446.92	£31,617.72
Electrical equipment and materials	£29,494.27	£30,715.75	£31,900.83	£34,252.53
Total capital investment	**£358,468.82**	**£373,314.50**	**£387,717.78**	**£416,299.98**

Table [6-3], The initial cost estimation for each combined model

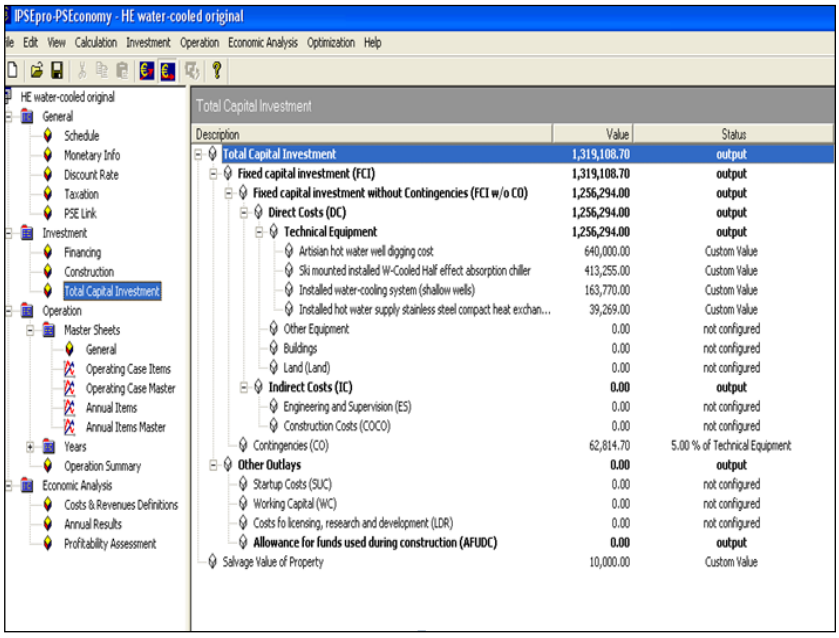

Fig [6-2], PSEconomy window where the estimated value of each unit are inserted

6.3 Annual Cash Outflow:

The annual cash outflow is defined by the cost decided on by the investor. In this study, the cost of fuel, operation and maintenance are considered as annual cash flow. The calculation was based on the assumption that all proposed units were assumed to operate for 8760 hours per year. According to the Capstone Company, the operating

fuel was natural gas and its cost is estimated to be £0.12/kg [127]. However, the natural gas price was highly subsidised in Saudi Arabia for industrial and petrochemical use, and was set by the Ministry of Water and Electricity at £0.02/kg.
The other factor in the outflow cost is operation and maintenance (O&M), which was considered separately in each model. Table [6-4] shows the total outflow cost of the fuel, and the O&M cost for each model. The microturbine O&M was obtained from SWANA Research foundation [128], while the ORC's O&M was gained from published paper by Ingwald and Peter etc al. [129], and the absorption chiller's O&M cost was obtained according to Boonnasa and Namprakai [126]. Moreover, the TVC-MED O&M acquired from the National Water Commission [127].

	Annual Fuel price	**Operation and maintenance cost**
Microturbine	**£8515**/year	£0.0093/kW-5000hr=**£9300**/year
ORC	-	**£2125**/year
Absorbtion chiller	-	£0.39/kW-12hr=**£491.4**/year
TVC-MED	-	£0.075/m3-260hr/year=**£1033.5**

Table [6-4], The annual fuel, O&M cost for each proposed unit

6.4 Annual Cash Inflow:

The revenue or the sales income profit is represented by the annual cash inflow. In this study, the energy electric power and the potable water are considered to be selling products. According to the Saudi Electricity Company [130], the electricity tariff in Saudi Arabia is £0.023/kWh, which is highly subsidised in addition to the monthly fixed rate for example maintenance and insurance, while the potable water tariff is £0.047/m^3 according to the Saline Water Conversion Corporation [131]. The energy power and potable power selling price are taken as they have been defined by Saudi government, which are £0.023/kWh and £0.47/m^3 for electricity and potable water respectively. However, the revenue for each model was calculated according to the Saudi tariff. In order to investigate the effect of different selling prices on the annual revenue, the variation of the selling electricity and potable water price was performed from £0.02/kWh to £0.1/kWh and £0.4/m^3 to £1.2m^3 respectively as illustrated in Table [6-5] and Table [6-6].

(£/kWh)	Revenue of Selling Electricity power (£)			
	Microturbine	Micro+ORC	Micro+AC (on-site)	TVC-MED (water £0.47/m^3)
0.02	35,040.00	38,018.40	35,040.00	44,132.00
0.023	40,296.00	43,721.00	40,296.00	49,388.15
0.04	70,080.00	76,036.80	70,080.00	79,172.00
0.06	105,120.00	114,055.20	105,120.00	114,212.00
0.08	140,160.00	152,073.60	140,160.00	149,252.00
0.1	175,200.00	190,092.00	175,200.00	184,292.00

Table [6-5], The annual revenues at energy power price variation

Revenue of Selling potable water (£)	
(£/m^3)	TVC-MED (Energy £0.023/kWh)+microturbine
0.4	48,034
0.6	51,903
0.8	55,772
1	59,641
1.2	63,510

Table [6-6], The annual revenues at potable water price variation

6.5 Profitability Evaluation:

It is very important to estimate the expected profit regarding the proposed project before it is invested. Therefore, a number of profit measures were employed in this evaluation for each model that either provides electric power or power with potable water.

The profitability evaluation criteria can be defined as follows:

6.5.1 Payback period (PBP):

The payback period is defined as the length of time required for cash inflows from a project to recover the original cash outlays as required by the initial investment [75] The payback period can be defined by the following equation [122]:

$$TCI = \sum_{j=1}^{PBP} CFN_j \quad (6\text{-}3)$$

Where:

TCI: Total capital Investment

CFN: Cash Flow Net

6.5.2 Net Present Value (NPV):

The net present value method is defined as the difference between the sum of all the net cash flows and the initial total capital investment. According to Adrian B. [75], it is highly recommended to accept any project for which the net present value is positive. However, the project with negative present value should be rejected. Furthermore, the project with the highest present value is more likely to be preferred economically among various alternatives.

The net present value is calculated as the following equation [122]:

$$NPV = \sum_{j=1}^{t} \frac{CFN_j}{(1+r)^j} - TCI \quad (6\text{-}4)$$

where CFN_j is the net cash flow at time (j), and r is the discount rate (the rate of return that could be earned).

6.5.3 Net-Benefit Cost Ratio (NBCR):

The benefit ratios are defined as the ratio of the net present value of future net cash flow to the total capital investment, which is explained by the cost efficiency of the proposed project. It is also defined as a profitability index (PI). It is calculated as follows [122]:

$$NBCR = \frac{NPV}{TCI} \quad (6\text{-}5)$$

However, Bejan, et al. reported that [75], using net benefit-cost ratio over the net present value adds no particular advantage to the profitability evaluation as the negative value of net-benefit cost ratio indicates that the project's net present value is less than the initial investment, which specified the same result. Moreover, the net present value calculation is straightforward and simpler.

6.5.4 Average rate of return (ARR):

The average rate of return is defined as the ratio of the average annual net profit to the total capital investment. It is calculated as follows [122]:

$$ARR = \frac{\overline{NP}}{TCI} \quad (6\text{-}6)$$

where $\overline{NP}$ is the average annual net profit.

The payback period, net present value and average rate of return are considered as an evaluation and comparison method in this study of all proposed models, while the net benefit cost ratio method is excluded, according to the recommendations of the literature [75].

6.6 Case Study:

The economic case study was applied for each proposed model, to give an indication of the profitability of each unit. This evaluation took place by calculating the payback period, net present value and average rate of return according to the governmental electricity and potable water-selling price, which are £0.023/kWh and £0.47/m^3 respectively. Firstly, each model was assumed to operate at full load and in ISO conditions, with seawater at a temperature of 22°C. The microturbine stand-alone generated 200.3kW of electricity, while the microturbine combined with ORC generated 217kW. The microturbine with a single effect absorption chiller produced 208.2kW, while the absorption chiller is only used for the on-sit cooling purpose, reducing the ambient inlet air to 8°C. However, the microturbine combined with the TVC-MED desalination is generating an energy power that comes from the microturbine's generator, and 53 m^3/day of potable water produced by the TVC-MED desalination.

The project lifetime was assumed to be 20 years, according to the manufacturing company [132], with zero taxation and interest rate. Table [6-7] shows the results obtained by the PESeconomic software, which indicates the economic acceptability and profitability of each proposed model.

Selling energy power and potable water price at £0.023/kWh-0.47/m3			
units	Pay Back Period year	Net Present Value	Average Rate of Return (%)
Microturbine	16.743	95708.81	3.82
Microturbine+ORC	16.483	107420	3.91
Microturbine+Absorbtion chiller	18.23	60770	3.33
Microturbine+TVC-MED (full)	14.036	212672	4.97

Table [6-7], Economic evaluation results for each model

The evaluation results show that the higher payback period was found in the micro turbine, combined with an absorption chiller of 21% more than the lowest rate of the microturbine with TVC-MED desalination, which means that the latter model would payback all the capital investment in 14.034 years. Also, the net present value and the average rate of return showed that the less profit rate could be found in the absorption chiller, while the highest rate was obtained in the TVC-MED combined with the microturbine. It also can be seen that investing in microturbine with TVC-MED desalination adds an extra 54% of the net present value compared to the microturbine stand-alone, indicating that using the microturbine with TVC-MED desalination can lead to an extra gain of £116,963. Furthermore, the profitability evaluation results of the microturbine with ORC were in the range of the microturbine stand-alone, with a less payback period of 1.5% and more net present value of 11%. Therefore, the most profitable model is combined TVC-MED desalination with the microturbine due to obtaining the higher net present value and an average rate of return with the lowest payback period compared to the other proposed models. However, although investing in the microturbine with an absorption chiller achieved the higher value of the payback period and the lower average rate of return, it could be economically stable when the ambient temperature is varied, which keep the generated electricity from the microturbine constant as the absorption chiller is used for on-site cooling. Generally speaking, the profitability evaluation results showed that all proposed models can recuperate their capital costs over a period of 14 years, and according to [75], this period may be sharply exceeded by the least preferred payback period of six years. Therefore, carrying out a sensitivity study is needed to figure out the economic evaluation of each model, when the selling electricity price varies, as does the selling price of potable water.

Secondly, according to previous assumptions, another comparison was performed on the microturbine with TVC-MED desalination, where the desalination model was operated to produce only half of its nominal capacity, which is 26.5 m^3/day of potable water. According to Table [6-8], the payback period for the TVC-MED operated at a full load was 13% lower than operating the unit at half load, which also affected the value of the average rate of return. Furthermore, it also achieved a higher net present value of 39.7% compared to producing half potable water.

Selling energy power and potable water price at £0.023/kWh-0.47/m3			
units	Pay Back Period year	Net Present Value	Average Rate of Return (%)
Microturbine+TVC-MED (full)	14.036	212672	4.97
Microturbine+TVC-MED (half)	16.17	128060	4.03

Table [6-8], Economic evaluation with full and half TVC-MED desalination

As a result, the evaluation criteria indicated that operating the TVC-MED desalination at full load was relatively more profitable than the TVC-MED desalination with half water production, due to providing a higher amount of potable water with the same amount of generated electricity, and the O&M cost showed a small difference to the TVC-MED when operated at half load.

6.7 Sensitivity Study:

A sensitivity study was performed in order to investigate the effect of the variations of the both electricity selling and potable water prices on the profitability measures. All the proposed models were assumed to operate at full load in ISO conditions, and the seawater was set at a temperature of 22°C.

6.7.1 Electricity selling prices:

The electricity-selling prices were chosen to be in line with Saudi Arabian electricity prices, which were significantly subsidized by the government. The aim of performing this sensitivity study at a different electricity selling price was to define the minimum price at which the model can become economically viable, and to measure the how increasing this price may be affected by the use of selected economic evaluation methods. Using PESeconomy software, the electricity selling price variation was created in steps of £0.02/kWh, from £0.02/kWh to £0.1/kWh, while in the course of TVC-MED desalination, the potable water price was fixed at the subsidised rate of £0.47/m^3. The previous operating assumption was also considered, in which all models operated at full load in ISO condition, and the seawater temperature was 22°C, while the TVC-MED desalination produced the full capacity of potable water as shown in Table [6-5]. All results are listed in the appendix C at Table [1]. Furthermore, the lifetime of this project was assumed to be 20 years. The effect of the selling price variation was examined by considering the following criteria:

6.7.1.1 Payback period (PBP):

The effect of the variation of the selling electricity prices on the payback period profitability was illustrated in Fig [6-3]. At the selling price of £0.02/kWh, all models were found to be non-viable due to exceeding the 20 year life of the project, while recovering the capital costs cannot be achieved within the project's lifetime. However, the microturbine with TVC-MED desalination was found to be the only profitable model at this electricity-selling price, with a payback period of 16 years and nine months.

Increasing the selling price to £0.04/kWh decreased the value of the payback period over the range of 7 years in all proposed models, while the lowest value was obtained in the microturbine with ORC, because of generating the higher electric energy sold for £0.04/kWh against its initial capital cost. However, the payback period was still beyond the minimum-preferred rate [75].

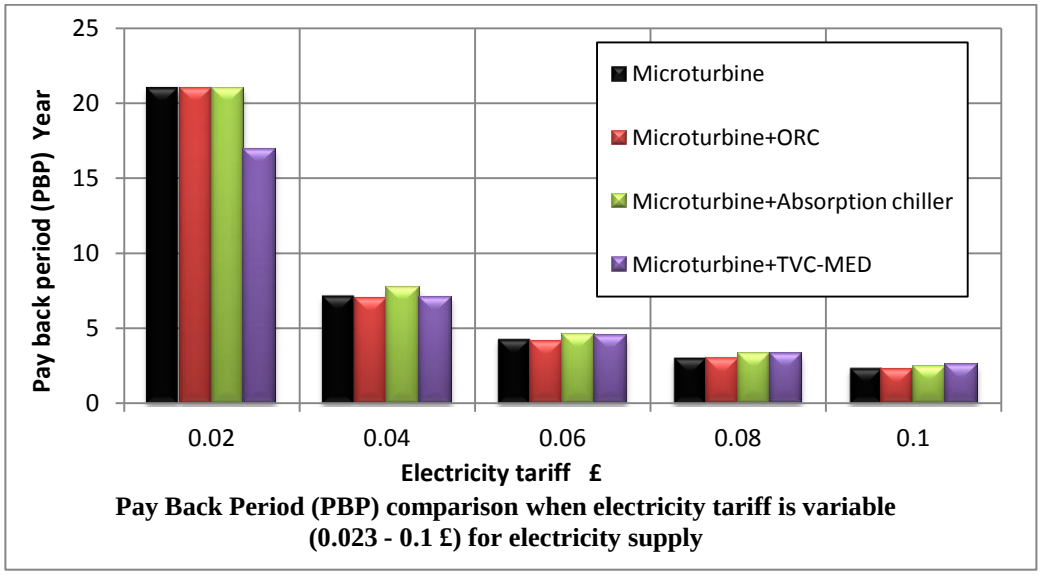

Fig [6-3], The payback period against the selling electricity price variation

For the selling price of £0.06/kWh to £0.1kWh, the payback period was steeply reduced and achieved the required value of recovering the capital cost for all models, which encouraged investing at the selling price of £0.06/kWh.

6.7.1.2 Net Present Value:

The variation of electricity selling prices against the net present values of the simulated models is shown in Fig [6-4]. At the selling price of £0.02/kWh, the net present value for the microturbine stand-alone, (microturbine+ORC), and (microturbine + absorption chiller) were economically unprofitable as their NPV was

at a negative value due to high initial and operation costs. In other words, the total cash flows were less than the total initial and operation costs for each unit when the selling price was equal to £0.02/kWh.

Moving the selling electricity price above £0.02/kWh has increased the NPV of all models. The (microturbine + ORC) has gained the highest NVB compared to other models. This is mainly because of receiving a high cash flow from the extra electricity that was generated by the ORC. The (microturbine + absorption chiller) gained the lowest rate of NPV because of the high cost of absorption chiller and the cooling water used on-site. It seems clear that, as the electricity selling prices increase, the net present value of all the proposed models will increase, and become viable for the (microturbine + ORC) and (microturbine + TVC-MED) due to providing extra electricity and potable water respectively.

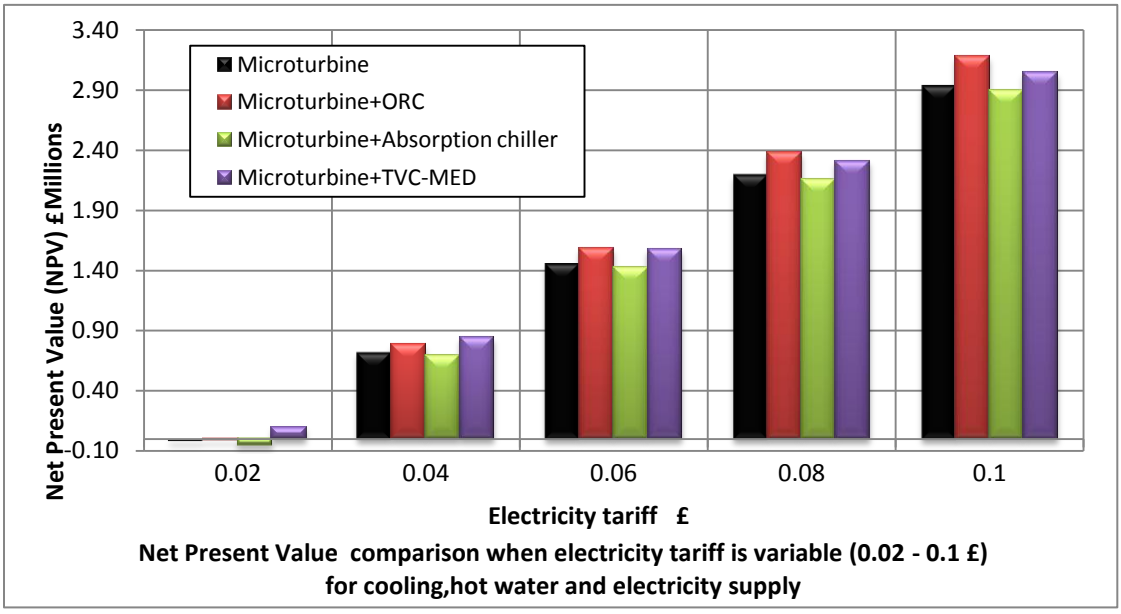

Fig [6-4], The NPV versus the selling electricity price variation

6.7.1.3 Average Rate of Return:

The effect of the variation in selling electricity prices on the ratio of the average annual net profit to the total capital cost is illustrated in Fig [6-5]. At the selling price of £0.02/kWh, all models were found to be non-viable, due to the low average rate of return, and recovering the capital costs cannot be achieved within the project's lifetime. However, the microturbine with TVC-MED desalination was found to be the only profitable model at this electricity-selling price, whereby the highest average of

return took place. This is mainly due to providing an extra product (potable water), which was added to the total annual revenues.

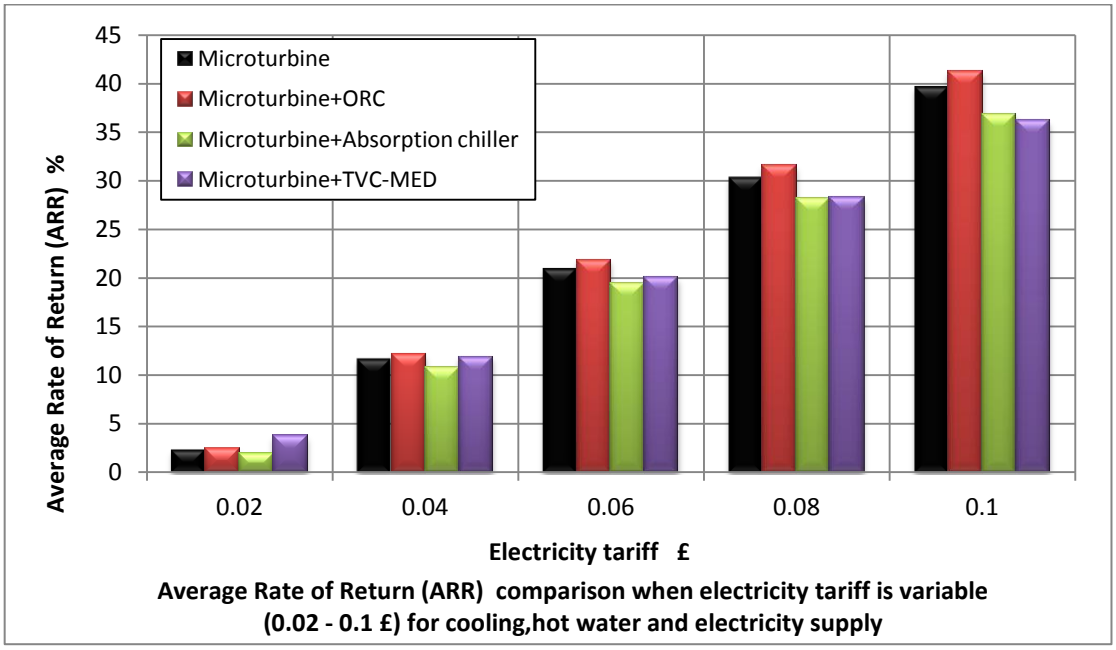

Fig [6-5], The average rate of return versus the electricity price variation

Raising the electricity-selling price from £0.04/kWh to £0.1/kWh demonstrated a great improvement in the ARR value of all proposed models, which leads to a high annual profit. Moreover, the (microturbine + ORC), and (microturbine + TVC-MED) were the most profitable models. It could be concluded that adding extra electricity revenue or potable water revenue to the original electricity revenue provided by the microturbine has led to a great deal of profit improvement.

6.7.2 Potable Water Selling Price:

A sensitivity study was also carried out to investigate the variation of the potable water selling price in order to measure its influence on the economic feasibility of the microturbine, combined with TVC-MED desalination. Using the PSEconomic software a variation in the potable water-selling price was made from £0.4/m^3 to £1.2/m^3, with a step of £0.2/m^3 as shown in Table [6-6]. A previous comparison was performed on (microturbine + TVC-MED) being operated in two modes to produce a full capacity of potable water, Table [6-8]. It was found that the TVC-MED desalination at full water production had led to higher revenues than the half water capacity mode. Therefore, performing the economic feasibility at variation of the potable water price could only be carried out (microturbine + TVC-MED) for the full

potable water production. All the results are listed in Table [2] Appendix C. This was performed under the same conditions: fuel cost, O&M cost and the electric energy selling price was £0.023/kWh, which met the subsidised tariff of the Saudi government, while the microturbine was operated at full load, in ISO conditions and the seawater temperature was 22°C. The project life was assumed to be 20 years.

Fig [6-6] shows the variation of potable water price versus the payback period. Increasing the selling price from £0.4/m^3 to £1.2/m^3 would have only shortened the payback period by two years. This was due to the small amount of potable water production compared with the generated electricity. The improvement in the net present value was limited to an annual average of £8000 for each £0.2 increase in the selling price as illustrated in Fig [6-6].

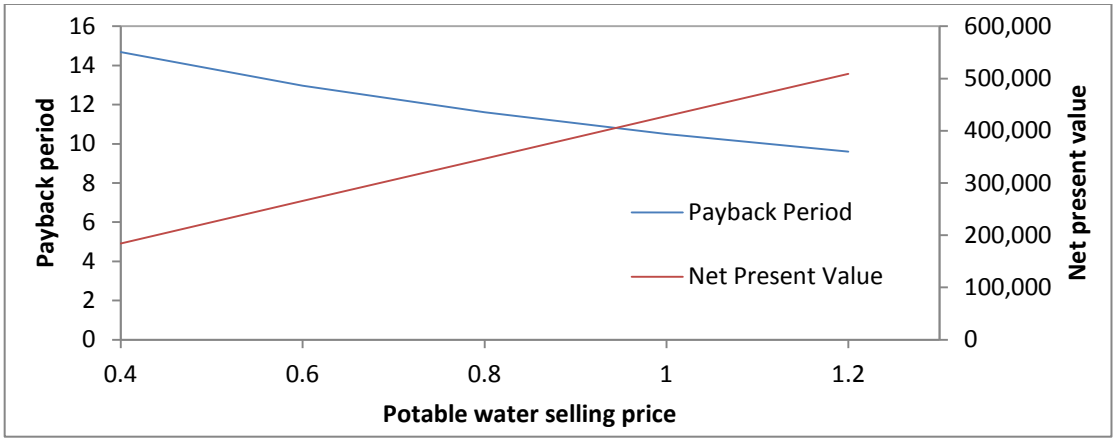

Fig [6-6], The effect of the potable water price variation versus PBP and NPV

Similarly, Fig [6-7] shows that the average rate of return has only increased by 1% for every £0.2 rise in the potable water-selling price. From the profitability evaluation results, it could be concluded that adjusting the potable water price demonstrated a limited effect on the model's economic acceptability. Thus, discounting the selling price of the potable water is recommended for competing with the subsidised Saudi tariff of £0.47/m^3, which showing no effect on economic performance.

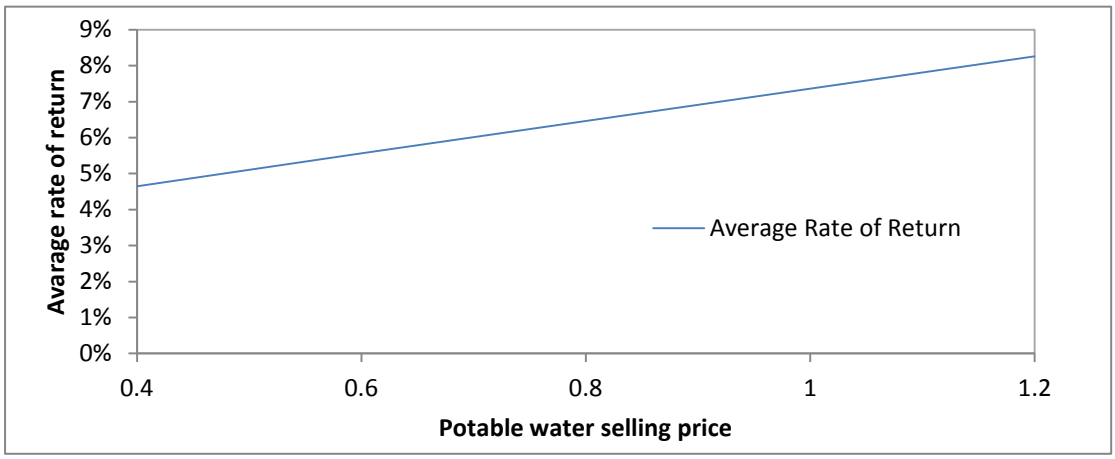

Fig [6-7], The effect of the potable water price variation versus the average rate of return

6.8 Chapter Summary:

The economic impact on each proposed model was presented in this chapter. Three economic evaluation criteria were employed, which are payback period (PBP), average rate of return (ARR) and net present value (NPV), in order to assess the economic acceptability of each model.

The initial cost of each equipment or sub-plant was presented or calculated, and all other capital cost of each unit was defined.

The annual cash outflow and inflow was introduced for each proposed model. A case study was performed in which each model was evaluated in accordance with the subsidised tariff. Furthermore, two different operating modes in the produced potable water of the TVC-MED were preformed, and then the profitability evaluation criteria were obtained by using the PSEcnomic software.

A sensitivity study including the economic evaluation criteria was performed for each proposed model in accordance with different electricity and potable water selling price.

Chapter 7

Conclusion and Recommendations

7-1 Introduction:

The meeting of consumer and market requirements is usually carried out through reliable research studies, which encourage technological development. Effective solutions can be brought to introduce the best product with competitive prices. However, this study's main aims were to bring about a reliable solution to the following issues:

- The shortage of the electricity and potable water in arid and semi-arid zones
- The increase in the prices of fossil fuels
- The need to minimize and control the rate of greenhouse gas production
- The effect of climate conditions on power plant performance

The small-scale power microturbine C200, designed by the Capstone Company, was chosen because of its capability of generating the maximum power of 200.3kW by one stand-alone unit. The single effect absorption chiller was employed in this study to generate an on-site cooling effect, since it can be powered by low-grade heat energy. The thermal vapour compression multi-effect distillation desalination was chosen as the potable water producer, due to its ability to be operated by thermal energy. Also, the organic Rankine cycle was powered by low-grade heat energy to provide extra electrical power without consuming fuel. Each model was simulated and investigated on a stand-alone basis under both ISO conditions and off-design. The ORC, absorption chiller and TVC-MED desalination were separately powered by the microturbine's waste heat energy with the same amount of fuel consumption. A number of parametric studies were performed in order to investigate the performance of both stand-alone and proposed combined models under the effect of variations in the ambient conditions and seawater temperatures.

All models were modelled and simulated on the basis of real data obtained from the commercially available units. The weather data for Jeddah City was obtained from the Presidency of Metrology and Environment in Saudi Arabia. All the base and proposed models were simulated through a software package called IPSEpro, using its advance power plant, refrigeration and desalination libraries to combine each proposed model. The energy and exergy analysis were then obtained, while the effectiveness-NTU methods were used to validate the heat exchanger units.

The economic accessibility and profitability of all the proposed models was clearly demonstrated. Each combined model was evaluated economically using three criteria;

the payback period, the net present value, and the average rate of return. The initial capital cost and the indirect cost represented by the auxiliary equipment for each proposed model were either obtained from the vendors' quotations or recent published studies. A Microsoft Excel model was employed to calculate the initial cost of the heat exchanges, while PSEconomic was used to carry out the annual mathematical economic calculations for each proposed model. A number of sensitivity studies were carried out to illustrate the influence of variations of electricity and potable water selling prices on each model's economic performance. Subsequently, the results of each model were analysed and compared.

7-2 Conclusion

7-2-1 Microturbine Combined with ORC:

The first proposed model simulates the C200 microturbine with ORC. However, two organic fluids (R245fa and R-134a) were chosen to be the working fluids for the proposed ORC model, because they belong to the new class of refrigerants developed to be reliable and environmentally safe and which have thermodynamic properties that make them suitable for use with low temperature heat sources. A comparison between the results of the two-modelled refrigerants showed that refrigerant R-245fa brought better results and performance than R-134a.

The energy properties of both microturbine and ORC models showed insignificant differences with the base plant model. However, the amount of the CO_2 emission rate decreased by 9%, compared to the microturbine stand-alone. The energy utilisation factor was 38.17%. The overall efficiency was 37.23%, due to increasing the total power generation to 216.8kW, because of the use of the microturbine and ORC. On the basis of second law analysis, no significant results were shown, compared to the base plant models. The largest amount of exergy destruction took place in the combustion chamber due to the heat transfer and mixing process, which represented 80% of the model's total exergy destruction, accounting for 60% of the total exergy input into the combined cycle. The overall exergetic efficiency of the combined cycle, including the microturbine and the ORC decreased by 34% compared to the microturbine stand-alone model. This is because of the extra exergy destruction generated from the ORC.

7-2-2 Microturbine Combined with Single effect absorption chiller:

The integration of the microturbine with the single effect absorption chiller took place as a second proposed model for this study. As with the first proposed model, a picture of the behaviour of this proposed combined cycle was obtained through the EUF values, and the CO_2 emission rate. The normal mode of operation of this proposed cycle was investigated under ISO conditions and full load operation. The energy utilisation factor was 52.43%. The CO_2 showed a significant decrease, which represented 31.00% of the reduction due to the utilisation process. However, the overall output electric power was 208.21 kW, which is higher than the stand-alone model due to using the cooling on-site that provided from absorption chiller, which decreased the input air temperature passing through the compressor to 8°C. Furthermore, the overall electric power efficiency was 35.63%. Regarding the exergy basis, the proposed combined cycle showed insignificant differences compared to the microturbine and single-effect absorption chiller in both models. The largest amount exergy destruction took place in the combustion chamber, due to the heat transfer and mixing process, and represents 79.14% of the model's total exergy destruction, accounting for 58.60%of the total exergy input to the combined cycle.

7-2-3 Microturbine Combined with TVC-MED Desalination:

Since thermal desalination technologies are not common for small-scale water production, the opportunity for modelling and simulating small-scale thermal vapour compression multi-effect distilled desalination (TVC-MED) provided a great challenge.

Two types of thermal desalination process were discussed: MED and TVC-MED desalination. The results of these two stand-alone models showed that the TVC-MED had gained a higher GOR than MED. Also, a number of comparisons were made to facilitate the conclusion that TVC-MED is more efficient in the combination process with a microturbine. As the steam ejector was considered as an improvement to the TVC-MED desalination, the steam ejector of the proposed combined cycle was designed according to available suction steam pressure, and the required steam properties including pressure, mass flow and temperature provided the best thermodynamic results in order to create a reliable validation of this model.

Utilising the waste heat energy of the microturbine to operate the TVC-MED

desalination process was considered as the third combined cycle for this study. The results showed that the energy utilisation factor was 67.2%, while the emission rate of the CO_2 showed a significant decrease of 46.8% compared to the microturbine stand-alone model, reaching 341.99 kg/kW of the CO_2 emission rate after the utilisation process, with a specific heat consumption of 336.48 kg/kW, and concentration factor of 1.86. However, the overall output of the electrical power was insignificantly reduced in comparison to the microturbine stand-alone because of the requirements for electricity in the combined cycle such as pumps. Furthermore, the overall electrical power efficiency was 34.21%, which was also slightly reduced in comparison to the microturbine stand-alone.

On the exergy basis, the proposed combined cycle showed insignificant differences when compared to both models' use of microturbine and TVC-MED desalination. However, the exergy destruction of the microturbine cycle's components showed no difference to the stand-alone model. Also, the TVC-MED desalination showed no significant difference to the stand-alone model. The largest amount of exergy destruction took place in the combustion chamber, as the main exergy input source passes through it due to the heat transfer and mixing process. This represented 75.7% of the model's total exergy destruction, which accounts for 59.9% of the total exergy input into the combined cycle.

7-2-4 The Energy and Exergy Comparison of All Microturbine Combined Models:

The comparison has been performed for all proposed combined models that were powered by the microturbine's waste heat energy, which was based on the analysis of the first and second laws, in order to illustrate a clear thermodynamic view of all the models in this study as shown in Table [5-5]. Furthermore, all models were monitored under ISO conditions, and operated at full load with a cooling water temperature of 22°C. Integrating the microturbine with the ORC unit led to the generation of an extra 4.1% of electric power compared to that produced by the absorption chiller, and 7.8% for TVC-MED desalination. This was because the ORC stand-alone was producing an extra 16.88 kW of electric power, causing a higher output power than other models. This also led to a relatively higher overall efficiency of 37.23% among other proposed combined models. Utilising the microturbine in the absorption has raised the overall electric power to 208.21 kW because of cooling the inlet air temperature to the

microturbine's compressor to 8°C, which in turn caused a constant efficiency and output power rate of 35.63% and 208.21 kW respectively, while the ambient temperature of other combined models was 15°C and it could be changed according to the ambient condition. However, the lowest carbon emission rate among all models was found when using a microturbine with TVC-MED desalination with a reduction of 46.8% compared to a stand-alone microturbine. To reach the required amount of potable water of 53m^3/day, a high amount of heat rate is needed at the heat exchanger, where the utilising process between microturbine and TVC-MED desalination occurs. Accordingly, the EUF of the TVC-MED desalination was 9.2% higher than when utilising the absorption chiller, and 42.4% higher than when utilising the ORC. Utilising ORC demonstrated the lowest EUF due to the lower rate of production as compared to other models, which meets the specification and the production range of the real manufactured ORC unit.

Regarding the second law analysis, a higher rate of exergetic efficiency was presented by utilising the microturbine with the single effect absorption chiller with a value of 31.68%, while ORC and TVC-MED had rates of 23.11%, and 22.42% respectively. This was due to the fact that the absorption chiller was providing 105 kW of cooling capacity, which counted as the model's output product when generated power was added from the microturbine. However, the lowest stack exergy destruction was presented in the microturbine, combined with the ORC, with a value of 15 kW. The utilisation of the absorption chiller led to the highest rate of the stack exergy destruction.

It can be clearly seen from these results that all the proposed models can help to reduce the carbon emission rate, and that this can play significant role in tackling the issue of global warming. While the benefit of utilising a microturbine in the absorption chiller is that the model's energy and exergy remains constant against the ambient temperature variation due to pre-cooling process of the intake air that provided from the absorption chiller's chilled water, as the other combined models including ORC and TVC-MED are influenced and their energy and exergy parameters are affected. In contrast, combining the microturbine with ORC will give extra electric power that can be useful for many purposes. In addition, integrating the TVC-MED desalination with the micro-turbine will produce potable water that can tackle the issue of water shortages, especially in remote coastal areas.

7-2-5 Economic Study Conclusion:

All the proposed models were compared economically according to their economic evaluation results. The obtained results show that, if the electricity selling price was selected to be £0.023/kWh, which is in line with the Saudi domestic electricity price, then the profitability evaluation results would not be attractive for investment as the capital cost of all units could not be recovered within the desirable duration, as reported by Began [75]. However, the stand-alone microturbine, including the proposed combined models, was manufactured for the purpose of the commercial investment that could be brought to the society, either to serve individual needs or to invest in the private sector. Therefore, the selling price of electricity could vary, depending on the provider's electric tariff. On the other hand, this study's aim is partly to encourage the supply for electricity and potable water for people who live in the remote coastal area, where the electricity supply is deficient and may not be enough for all the daily needs. Hence, providing the microturbine with the governmental electric tariff is the best choice for this situation. However, if the microturbine is used for the purposes of investment, such as operating a resort village located the coastal area, then the electricity selling price could be set at £0.04/kWh or £0.06/kWh, which should provide a desirable payback period, net present value and average rate of return for all the combined models. Accordingly, the proposed models' economic performance indicates profitability and viable investment. However, adjusting the potable water price has produced a limited effect on the model's economic acceptability. Thus, discounting the selling price of the potable water is recommended in order to compete with the subsidised Saudi tariff of £0.47/m^3, showing no effect on economic performance.

7-2-6 Conclusion Summary:

To summaries the energy, exergy and economic comparison of each proposed model, Table [7-1] shows all results of proposed combined models including microturbine stand-alone. Furthermore, Table [7-2] illustrates the economic finding of each proposed model in this study.

	Microturbine	ORC+microturbine	Absorption chiller +microturbine	TVC-MED +microturbine
Net Power (kW)	200.30	216.88	208.21	199.89
Overall Electrical Efficiency (%)	34.30	37.23	35.63	34.21
Emission Rate before Utilisation (kg/kW)	667	-	-	-
Emission Rate after Utilisation (kg/kW)	-	594.35	433.49	341.99
EUF (%)	-	38.24	52.43	66.46
overal Plant Exergetic Efficiency (%)	21.07	23.11	31.68	22.42
Waste energy utilisation (%)	-	48.01	40.7	48.9

Table [7-1], Energy and exergy results of all proposed models

Selling energy power and potable water price at £0.023/kWh-0.47/m3			
units	Pay Back Period year	Net Present Value	Average Rate of Return (%)
Microturbine	16.74	95708	3.82
Microturbine+ORC	16.48	107420	3.91
Microturbine+Absorbtion chiller	18.23	60770	3.33
Microturbine+TVC-MED (full)	14.03	212672	4.97

Table [7-2], Economic evaluation of all proposed models

7-3 Recommendations for Future work:

With regard to all the results of the proposed models presented in this study, the following recommendations are suggested for future work:

- All proposed models were modelled separately, according to the microturbine's limited load, when the microturbine's waste heat energy can only power one combined cycle. However, if more than one microturbine is installed, then the opportunity to operate more than one sub-model could be achieved, which is recommended for future work.
- Although most of the recent published work in this research file is based on modelling and simulation software, the experimental research work is likely to be more precise and accurate. Therefore, creating a test rig is recommended for the proposed techniques used in this study, which contains small scale elements of all proposed models mentioned in this research work.
- The purpose of employing the single effect absorption chiller in this study was to use its cooling product on-site in order to stabilize the fluctuations in ambient temperature. Therefore, another study could be conducted based on energy and exergy analysis, in which the cooling product could be used for off-site purposes.
- All the proposed models were assumed to be under ISO conditions and were operated at a full load in the economic study. However, it was suggested that another economy study could be carried out under the conditions of ambient temperature variation, as well as when a partial load was in operation.

References

1- Kolanowski, B. F., 2004, Guide to Microturbine, New York: Marcel Dekker.

2- Shah, R.K., 2005, Compact Heat Exchangers for Microturbines. In Micro Gas Turbines (pp. 2-1 – 2-18). Educational Notes RTO-EN-AVT-131, Paper 2. Neuilly-sur-Seine, France.

3- Soares, C., 2007, Microturbines Applications for Distributed Energy System, California: Elsevier .

4- Capstone Corporation, 2009, Capstone C200 Microturbine, USA: Capstone Technical Support.

5- Energy Nexus Group, 2002, Technology Characterization: Microturbine, [online]. Available at: http://epa.gov/chp/documents/microturbines.pdf [Cited 24 November 2010].

6- Ho, J. C., Chua, K. J. and Chou, S. K., 2004, Performance study of a Microturbine system for cogeneration application, Renewable Energy, 29 (7), pp. 1121-1133.

7- Appendix B: Microturbines and heat pumps, [online]. Available at: http://etd.rau.ac.za/theses/available/etd-05092005-124454/restricted/AppendixB.pdf [cited 24 November 2010].

8- Energy Solution System, 2004, Microturbine CHP System, [online]. Available at: http://www.energysolutionscenter.org/distgen/AppGuide/Chapters/Chap4/4-2_Microturbines.htm#Introduction [Accessed 24 November 2010].

9- McDonald, C. F., Low-cost, 2000, *Compact primary surface recuperator concept for microturbines*, Applied Thermal Engineering, Volume 20, issue 5, pp. 471-497.

10- McDonald, C.F., 1996, *Heat recovery exchanger technology for very small gas turbines*. Int. Journal of Turbo and Jet Engines 13 4 pp. 239–261.

11- Kaikko, J. and Backman, J.,, 2007, *Technical and economic performance analysis for a microturbine in combined heat and power generation*, *Energy* **32**, pp. 378–387.

12- Gomes, E. E. B. et al., 2004, *Performance evaluation and case studies of microturbines fuelled with natural gas and diesel*. Processing of the institution of mechanical Engineers, Part A: Journal of Power and Energy. 218(8).

13- McDonald, C.F., 2000, *A low cost recuperator concept for microturbine applications*, ASME Paper No. 2000-GT-167, ASME, New York, NY.

14- Moore, M. J., 2002, *Microturbine Generators*, UK: Professional Engineering.

15- Rouse, M., 2008, *Turbine Talk*, Capstone Turbine Corporation, p.p 1-6, California.

16- Traverso, A. and Massardo, A.F., 2005, *Optimal design of compact recuperators for micro-turbine application*, Applied Thermal Engineering **25**, pp. 2054–2071.

17- Schwarzacher, W., 1993, *Cyclostratigraphy and the Milankovitch theory. Amsterdam*: Elsevier Science.

18- Keepin, B. and Kats, G., 1988, *Greenhouse warming: comparative analysis of nuclear and efficiency abatement strategies*. Energy Policy, 16 (6), pp. 538561.

19- Mathews, J., 2007, *Seven steps to curb global warming*. Energy Policy, 35 (8), pp. 4247- 4259.

20- Chae, S. Kim, S. Yoon, S. and Park, S., 2010, *Optimization of a waste heat utilization network in an eco-industrial park.* Applied Energy, In Press.

21- Peacock, A.D. and Newborough, M., 2005, *Impact of micro-combined heat-and-power systems on energy flows in the UK*, ESI. Energy.

22- Delattin, F. Bram, S. Knoops, S. et al., 2008, *Effects of steam injection on microturbine efficiency and performance*; Energy 33; 241-247.

23- Kehlhofer, R. Bachmann, R. Nielson, H. and Warner, J., 1999, *Combined-cycle gas and steam turbine power plants*. 2 ed. Oklahoma: PennWell Publishing Company.

24- Felipe, R. Arrieta, P. Electo, E. and Lora, S., 2005, *Influence of ambient temperature on combined-cycle power-plant performance*. Applied Energy, 80 (3), pp. 261272.

25- Hosseini, R. Beshkani, A. and Soltani, M., 2007. *Performance improvement of gas turbines of Fars (Iran) combined cycle power plant by intake-air cooling using a media evaporative cooler*. Energy Conversion and Management, 48 (4) pp. 10551064.

26- Hwang, Y., 2004, *Potential energy benefits of integrated refrigeration system with microturbine and absorption chiller,* International Journal of Refrigeration, 27 (8), pp. 816-829.

27- Quoilin, S., 2007, *Experimental study and modeling of a low temperature Rankine cycle for small scale cogeneration*, Master Thesis, Université de Liège, Belgium

28- Tchanche, B. Lambrinos, G. R. Frangoudakis, A. and Papadakis., 2010, *Exergy analysis of micro-organic Rankine power cycles for a small scale solar driven reverse osmosis desalination system*, Applied Energy, 87 (4), pp. 1295-1306.

29- Wei, D. Lu, X. Lu, Z. and Gu, J., 2007, *Performance analysis and optimization of Organic Rankine Cycle (ORC) for waste heat recovery*, Energy Conversion and Management, 48 (4), pp. 1113-1119.

30- Schuster, A. Karellas, S. Kakaras, E. and Spliethoff, H., 2009, *Energetic and economic investigation of Organic Rankine Cycle applications*, Applied Thermal Engineering, 29 (8-9), pp. 1809-1817.

31- Drescher, U. and Brüggemann. D., 2007, *Fluid selection for the organic Rankine cycle (ORC) in biomass power and heat plants*, Applied Thermal Engineering **27**, pp. 223–228.

32- Saleh, B. Koglbauer, G. Wendland, M and Fischer, J., 2007, *Working fluids for low-temperature organic Rankine cycles*, Energy **32**, pp. 1210–1221.

33- Liu, B.-T. Chien, K.-H. and Wang, C.-C., 2004, *Effect of working fluids on organic Rankine cycle for waste heat recovery*, Energy **29**, pp. 1207–1217.

34- Hung, T.C., 2001, *Waste heat recovery of organic Rankine cycle using dry fluids*, Energy Convers Manage **42** 5, pp. 539–553.

35- Larjola, J., 1995, *Electricity from industrial waste heat using high-speed organic Rankine cycle (ORC)*. Int J Prod Econ **41** 3, pp. 227–235.

36- David J. et al., 2010, *Organic Rankine cycle working fluid considerations for waste heat to power applications*, ASME, ASHRAE Transactions.

37- Lemort, V., 2006, *Testing and modeling scroll compressors with a view to integrating them as expanders into a Rankine cycle*, DEA thesis, Université de Liège.

38- Fluorocarbons and sulphur hexafluoride, 2010, *Maijor HFC molecules*, [online]. Available at: http://www.fluorocarbons.org/en/families/hfcs/products_applications.html [cited 24 November 2010].

39- Abrahamsson, K. Gidner, A. and Jernqvist, A., 1995, *Design and experimental performance evaluation of an absorption heat transformer with self-circulation*. Heat Recovery Systems and CHP, 15 (3), pp. 257272.

40- Occhionero, A. J. Hughes, P. J. and Reid, E. A., 1991, *Absorption chillers: part of the solution. In International CFC and Halon Alternatives Conference*. 35/12/1991. The alliance for responsible atmospheric policy. Washington.

41- Garland, P., 1998, *A history of U.S. market share in commercial chillers*. U.S. Department of Energy, USA.

42- The Trane Company, 2000, *Air Conditioning Clinic: absorption water chillers, one of the equipment series*. La Crosse: American Standard Inc.

43- Sun, Z. G., 2007, *Experimental investigation of integrated refrigeration system (IRS) with gas engine, compression chiller and absorption chiller*, Energy 33, pp. 413-436.

44- Sun, Z. G. Wang, R. Z. and Sun, W. Z., 2004, *Energetic efficiency of a gas-engine-driven cooling and heating system*, Applied Thermal Engineering, 24 (5-6), pp. 941-947.

45- Axelsson, H. Harvey, S. Asblad, A. and Berntsson, T., 2003, *Potential for greenhouse gas reduction in industry through increased heat recovery and/or integration of combined heat and power*, Applied Thermal Engineering, 23 (1), pp. 65-87.

46- El-Din, M. M. S., 1999, *Optimal utilization of waste heat from heat engines by use of a heat pump*, Energy Conversion and Management, 40, pp. 937-949.

45- Herold, K. Klein, S. and Radermacher, R., 1995, *Absorption chillers and heat pumps*. London: CRC Press.

46- Keith, E. Herold, R. R. a. S. A. K., 1996. *Absorption Chillers and Heat Pumps*, United States of America: Taylor and Francis.

47- Ameri, M. and Hejazi, S., 2004, *The study of capacity enhancement of the Chabahar gas turbine installation using an absorption chiller*. Applied Thermal Engineering, 24 (1) pp. 5968.

48- Adel, E. Nasser, M. and El-Kalay, M., 1991, *A heat-recovery cooling system to conserve energy in gas-turbine power stations in the Arabian Gulf*. Applied Energy, 38 (2), pp. 133- 142.

49- Boyce, M., 2006, *Gas Turbine Engineering Handbook*, 3rd ed. USA Gulf Professional Publication.

50- Kakaras, E. Doukelis, A. and Karellas, S., 2004, *Compressor intake-air cooling in gas turbine plants*. Energy, 29 (1215), pp. 23472358.

51- Medrano, M. Mauzey, J. McDonell, V. Samuelsen, S. and Boer, D., 2006, *"Theoretical Analysis of a Novel Integrated Energy System Formed by a Microturbine and an Exhaust Fired Single-Double Effect Absorption Chiller"*, *Int. J. of Thermodynamics*, Vol. 9, No.1, pp. 29- 36.

52- Bruno, J.C. Ortega-López, V. and Coronas, A., 2009, *Integration of absorption cooling systems into micro gas turbine trigeneration systems using biogas: case study of a sewage treatment plant,* Apply Energy **86** (6), pp. 837–847.

53- Alhazmy, M. and Najjar, Y., 2004, *Augmentation of gas turbine performance using air coolers.* Applied Thermal Engineering, 24 (23), pp. 415429.

54- Wang, F. Chiou, J. and Wu, P., 2007, *Economic feasibility of waste heat to power conversion.* Applied Energy, 84 (4), pp. 442454.

55- Kakaras, E. Doukelis, A. Prelipceanu, A. and Karellas, S., 2006, *Inlet-air cooling methods for gas turbine based power plants*. Journal of Engineering for Gas Turbines and Power, 128 (2), pp. 312317.

56- Birkett, J.D., 1994, *A brief illustrated history of desalination: From the Bible to 1940.* Desalination, **50**: p. 17-52.

57- Glater, J., 1998, *The early history of reverse osmosis membrane development*. Desalination, **117**(1-3): p. 297-309.

58- Al-Sahlawi, M., 1999, *Seawater desalination in Saudi Arabia: economic review and demand projections*. Desalination, 123, pp. 143147.

59- United Nations, 2001, *Water desalination technologies in the ESCWA member countries.* New York: United Nations.

60- Miller, J., 2003, *Review of water resources and desalination technologies.* California: Sandia National Laboratories.

61- Banat, F., 2007, *Economical and technical assessment of desalination technology*. Jordan University of Science and Technology.

62- Khawaji, A. Kutubkhanah, A. and We, J., 2008, *Advances in seawater desalination technologies*. Desalination 221 (13), pp. 47–69.

63- Al-Rawajfeh, A. Glade, H. and Ulrich, J., 2003, *CO2 release in multiple-effect distillers controlled by mass transfer with chemical reaction*. Desalination, 156 (1-3), pp.109123.

64- Kronenberg, G. and Lokiec, F., 2001, *Low-temperature distillation processes in single- and dual-purpose plants*. Desalination, 136 (13), pp. 189197.

65- Glater, J., 1998, *The early history of reverse osmosis membrane development*. Desalination, 117 (13), pp. 297309.

66- Fritzmann, C. Lowenberg, J. Wintgers, T. and Melin,T., 2007, *State-of-the-art of reverse osmosis desalination*, Desalination **216**, pp. 1–76.

67- Clayton, R., 2006, *Desalination for water supply*. UK: Foundation for Water Research.

68- Tidball, R. and Kadaj, R., 1981, *Waste heat powered reverse osmosis plants*. Desalination, 39, pp. 137145.

69- Aybar, H., 2004, *Desalination system using waste heat of power plant*. Desalination, 166, pp. 167170.

70- Henry, S. and Teresa, S., 2007, *Utilization of waste heat in the desalination process*. Desalination, 204 (13), pp. 464470.

71- Shih, H., 2005, *Evaluating the technologies of thermal desalination using low-grade heat*. Desalination, 182 (13), pp. 461469.

72- Methnani, M., 2007, *Influence of fuel costs on seawater desalination options*. Desalination, 205 (13), pp. 332339.

73- Nisan, S. and Benzarti, N., 2008, *A comprehensive economic evaluation of integrated desalination systems using fossil fuel and nuclear energies and including their environmental costs*. Desalination, 229 (13), pp. 125146.

74- Kamali, R. and Mohebinia, S., 2008, *Experience of design and optimization of multi- effects desalination systems in Iran.* Desalination, 222 (13), pp. 639645.

75- Bejan, A. Tsatsaronis, G. and Moran, M., 1995, *Thermal design and optimization*. New York: John Wiley and Sons.

76- Ameri, M. Ahmadi, P. and Hamidi, A., 2009, *Energy, exergy and exergoeconomic analysis of a steam power plant: a case study*. International Journal of Energy Research. 33 (5), pp. 499512.

77- Kopac, M. and Hilalci, A., 2007, *Effect of ambient temperature on the efficiency of the regenerative and reheat Çatalagzı power plant in Turkey.* Applied Thermal Engineering, 27 (89), pp. 13771385.

78- Rivero, R. and Garfias, M., 2006, *Standard chemical exergy of elements updated.* In: *17th International Conference on Efficiency, Costs, Optimization, Simulation, and Environmental Impact of Energy on Process Systems*. Energy, 31 (15) pp. 33103326.

79- Shi, X. and Che, D., 2007, *Thermodynamic analysis of an LNG fuelled combined cycle power plant with waste heat recovery and utilization system*. International Journal of Energy Research, 31, pp. 975998.

80- Sayyaadi, H. and Saffari, A., 2010, *Thermoeconomic optimization of multi effect distillation desalination systems.* Applied Energy, 87 (4), pp.11221133.

81- Dincer, I. Al-Muslim, H., 2002, *Thermodynamic analysis of reheat cycle steam power plants.* Fuel and Energy Abstracts, 43 (4), pp.01406701.

82- Ameri, M. Ahmadi, P. and Khanmohammadi, S., 2008, *Exergy analysis of a 420 MW combined cycle power plant*. International Journal of Energy Research, 32 (2), pp. 175- 183.

83- Hepbasli, A., 2008, *A key review on exergetic analysis and assessment of renewable energy resource for a sustainable future*, Renew Sust Energy Rev 12, pp. 593–661.

84- Al-Sulaiman, F. Hamdullahpur, F. and Dincer, I., 2011, *Greenhouse gas emission and exergy assessments of an integrated organic Rankine cycle with a biomass combustor for combined cooling, heating and power production*, Applied Thermal Engineering, Volume 31, Issue 4, Pages 439-446.

85- Al-Sulaiman, F. Dincer, I. and Hamdullahpur, F., 2009, *Exergy analysis of an integrated solid oxide fuel cell and Organic Rankine Cycle for cooling, heating and power production,* Journal of power sources, 195 (8), pp. 2346-2354.

86- Kaushik, S. and Arora, A., 2009, *Energy and exergy analysis of single effect and series flow double effect water–lithium bromide absorption refrigeration systems. International Journal of Refrigeration*, 32 (6), pp. 12471258.

87- Misra, R. Sahoo, K. Sahoo, S. and Gupta, A., 2003, *Thermo economic optimizations of a single-effect water/LiBr vapour absorption refrigeration system*. International Journal of Refrigeration, 26 (2), pp. 158169.

88- Talbi, M. and Agnew, B., 2000, *Exergy analysis: an absorption refrigerator using lithium bromide and water as the working fluids*. Applied Thermal Engineering, 20 (7), pp. 619- 630.

89- Sencan, A. Yakut, K. and Kalogirou, S., 2005, *Exergy analysis of lithium bromide/water absorption systems*. Renewable Energy, 30 (5), pp.645657.

90- Choi, H. Lee, T. Kim, Y. and Song, S., 2005, *Performance improvement of multiple-effect distiller with thermal vapour compression system by exergy analysis.* Desalination and the Environment, 182 (13), pp. 239249.

91- Mabrouk, A. Nafey, A. and Fathc, H., 2007, *Thermo economic analysis of some existing desalination processes*. Desalination. 205 (13), pp. 354373.

92- Hamed, O. Zamamiri, M. Aly S. and Lior N., 1996, *Thermal performance and exergy analysis of a thermal vapour compression desalination system*. Energy Conversion and Management, 37 (4), pp. 379387.

93- Kurzfassung. 2001. Comparison of Software for Thermodynamic Process Calculation. VGB PowerTech.

94- SimTech Simulation Technology, 2003. IPSEpro process simulator manuals: process simulation environment. SimTech Simulation Technology.

95- SimTech Simulation Technology, 2003. IPSEpro process simulator manuals: Process Simulator. SimTech Simulation Technology.

96- SimTech Simulation Technology, 2003. IPSEpro process simulator manuals: Model Development Kit. SimTech Simulation Technology.

97- SimTech Simulation Technology, 2003. IPSEpro process simulator manuals: Advanced Power Plant Library. SimTech Simulation Technology.

98- SimTech Simulation Technology, 2003. IPSEpro process simulator manuals: Refrigeration Process Library. SimTech Simulation Technology.

99- SimTech Simulation Technology, 2003. IPSEpro process simulator manuals: Desalination Process Library. SimTech Simulation Technology.

100- Jeddah municipality. Saudi Arabia. [cited 20-4-2011]; Avilable at: http://www.jeddah.gov.sa/english/index.php

101- Presidency of Meteorology and Environment, 2009. Surface annual climatologically report. Saudi Arabia: Ministry of Defense and Aviation

102- Construction information Service, 2007. Construction products industry key performance indicators handbook. UK: Construction Products Association.

103- Horlock, J. 2003. Advanced gas turbine cycles. Oxford: Elsevier Science Ltd.

104- Cengel, Y. and Turner, R., 2001. Fundamentals of thermal-fluid sciences. 2ed ed. New York: McGraw-Hill Higher Education.

105- Logan, E., 1999. Thermodynamics: processes and applications. USA: CRC Press.

106- Kaita, Y., 2001. Thermodynamic properties of lithium bromide-water solutions at high temperatures. International Journal of Refrigeration, 24 (5), pp. 374390.

107- Banat, F. and Jwaied, A., 2008. Exergy analysis of desalination by solar- powered membrane distillation units. Desalination, 230 (13), pp. 2740.

108- Kahraman, N. and Cengel, Y., 2005. Exergy analysis of a MSF distillation plant. Energy Conversion and Management, 46 (1516), pp. 26252636.

109- Cerci, Y., 2002. Exergy analysis of a reverse osmosis desalination plant in California. Desalination, 142 (3), pp. 257266.

110- Kahramana, N. Cengelb, Y. Woodb, B. and Cercic, Y., 2005. Exergy analysis of a combined RO, NF, and EDR desalination plant. Desalination, 171 (3), pp. 217232.

111- Capstone Turbine Corporation, 2009. *C200 Microturbine High-pressure Natural Gas*. California.

112- Yazaki Energy System INC, 2008. SC10 *Water fired single effect chiller*. WFC-S Series. Texas.

113- Infinity Turbine LLC, 2010. *Model IT10 Organic Rankine Cycle*. Madison,USA.

114- W. Wang, R. Cai and N. Zhang, 2004, *General characteristics of single shaft microturbine set at variable speed operation and its optimization*, Appl Thermal Engineering, **24**, pp. 1851–1863.

115- P. Gomatom and W. Jewell (2002), *Fuel parameter and quality constraints for microturbine distributed generators*, Wichita State University.

116- A. Bolcea, G.Chicco and P.Mancarella, 2011, *Optimal operation of a 30kW microturbine natural gas cluster*, U.P.B. Sci. Bull., Series C, Vol. 73, Iss. 1.

117- T.S. Kim and S.H. Hwang, 2006, *Part load performance analysis of recuperated gas turbines considering engine configuration and operation strategy*, Energy **31**, pp. 260–277.

118- Khaliq, A., 2009. Exergy analysis of gas turbine regeneration system for combined cycle production of power heat and refrigeration. International Journal of Refrigeration, 32, pp. 435545.

119- Alasfour, F. Darwish, M. and Amer, A., 2005. *Thermal analysis of ME TVC+MEE desalination systems*. Desalination, 174 (1), pp. 3961.

120- Kamali, R. Abbassi, A. and Vanini, S., 2009. *A simulation model and parametric study of MED–TVC process*. Desalination, 235 (13), pp 340351.

121- Hegazy, A., 2007. *Possible waste heat recovery in the condenser of a regenerative steam cycle. Journal of Thermal Science and Technology*, 2 (1), pp.112.

122- SimTech Simulation Technology, 2003. *IPSEpro process simulator manuals: PSEconomy Library*. SimTech Simulation Technology.

123- Gregory, E. Lamb, B. Marsland, Johnston, R. and Summers, C., 1994. *Selection and costing of heat exchangers ESDU 92013*. London: Engineering Sciences Data Unit.

124- An email received from Sven. Fransen, C., Microturbine *Sales & Applications - Europe, Russia, Middle East & Africa*, dated: 21- 10-2010, http:// www.capstonmicroturbine.

125- An email received from Gregory. Giese, C., Infinity Turbine *President of Global Energy and Infinity Turbine* LLC, dated: 06- 07-2011, http://www.infinityturbine.com.

126- Boonnasa, S. and Namprakai, P., 2008. *Sensitivity analysis for the capacity improvement of a combined cycle power plant* (100-600 MW). Applied Thermal Engineering, 28 (1415), pp. 1865-1874.

127- UNESCO Centre for Membrane, 2008. *Emerging trends in desalination: A review*. National Water Commission, Waterlines Report Series No 9.

128- SWANA Applied Research Foundation, 2003. *Economic Feasibility Considerations Regarding Landfill Gas Microturbine System*. Solid Waste Assciation of North America.

129- Obernberger, I. Thonhofer, P. and Reisenhofer, E., 2002. *Description and evaluation of the new 1,000 kW_{el} Organic Rankine Cycle process integrated in the biomass CHP plant in Lienz, Astria*. *Euroheat & Power*.

130- Al-Zahrani, S. Al-Ajlan, A. M. and Al-Jardan, A. M., 1994. *Using different types of anti-scalant at the Al-Jubail power and desalination plant in Saudi Arabia*. *Desalination*, 97 (13) pp. 1728.

131- Saline Water Conversion Corporation, 2008. Projects: Working Plants, Al-Riyadh: Saline Water Conversion Corporation.

132- An email received from Sven. Fransen, C., Microturbine *Sales & Applications - Europe, Russia, Middle East & Africa*, dated: 11- 07-2011, http:// www.capstonmicroturbine

Published Work

- B. Makhdoum, B. Agnew (2011), *An Energy and Exergy Analysis of a Microturbine CHP System*, Journal of Environmental Science and Engineering, vol.5, (4), pp. 508-518.

Appendix

-Appendix A (Base Models)**:**

	Ambiant Tempreture C									
Parameter	5	10	15	20	25	30	35	40	45	50
CO2 Emission Rate (kg/kW)	618.44	634.8	652.03	670.2	689.39	709.69	731.19	754.01	778.27	804.11
Net Power (kW)	211.36	205.88	200.39	194.92	189.45	183.98	178.52	173.07	167.62	162.18
Microturbine Efficiency (%)	37.91	36.93	35.96	34.98	34	33.03	32.05	31.08	30.11	29.14
Overall Electrical Efficiency (%)	36.18	35.24	34.3	33.36	32.42	31.49	30.55	29.62	28.69	27.76
Microturbine Exergetic Efficiency (%)	22.21	21.64	21.07	20.49	19.92	19.35	18.79	18.22	17.65	17.08
overal Plant Exergetic Efficiency (%)	22.21	21.64	21.07	20.49	19.92	19.35	18.79	18.22	17.65	17.08
Air compressor Exergy destruction (%)	28.1196	28.3564	28.479	28.4913	28.3969	28.1994	27.9022	27.5083	27.0208	26.4425
Recuprecator Exergy destruction (%)	0.4661	0.4194	0.3797	0.3464	0.3193	0.2981	0.2822	0.2716	0.2659	0.2649
C.C Exergy destruction (%)	579.5402	579.4966	579.4531	579.4095	579.3658	579.322	579.2782	579.2342	579.1902	579.146
Turbine Exergy destruction (%)	52.2563	52.2624	52.2684	52.2745	52.2805	52.2866	52.2927	52.2988	52.3049	52.311
T3/T1	4.03	3.96	3.89	3.83	3.76	3.7	3.64	3.58	3.53	3.46

Table [1], Parametric study of the microturbine stand-alone’s ambient temperature

	Partial Load %				
Parameters	0.6	0.7	0.8	0.9	1
CO2 Emission Rate (kg/kW)	691.03	682.6	674.25	665.13	652.03
Net Power (kW)	102.79	125.9	147.95	172.75	199.04
Overall Electrical Efficiency (%)	24.12	26.97	29.58	32	34.23
Microturbine Exergetic Efficiency (%)	16.67	18.04	19.12	20.15	21.07
Overall Plant Exergetic Efficiency (%)	16.67	18.04	19.12	20.15	21.07
Air compressor Exergy destruction (%)	16.9807	19.8917	22.5601	25.471	28.479
Recuprecator Exergy destruction (%)	0.6417	0.6583	0.6267	0.5368	0.3797
C.C Exergy Exergy destruction (%)	499.4912	519.6453	538.1703	558.4393	579.4531
Turbine Exergy destruction (%)	31.2273	36.5666	41.4539	46.7772	52.2684

Table [2], Parametric study of the microturbine stand-alone's partial load

	Heat Source Temperatures (ºC)					
Parameters	130	140	150	160	170	180
ORC Thermal Efficiency (%)	8.5379	8.6482	8.7573	8.8649	8.971	9.0754
ORC microturbine power (kW)	15.5632	16.544	17.4925	18.4087	19.2926	20.1438
Evaporator (H.E) destruction (%)	45.6148	47.6646	49.4849	51.0655	52.3957	53.4637
Turbine (ORC) destruction (%)	1.6822	1.787	1.8881	1.9857	2.0796	2.1698
Cooling (H.E) destruction (%)	0.9685	1.3135	1.7005	2.1295	2.6007	3.1142
ORC Exergetic Efficiency (%)	21.9141	22.0462	22.1869	22.3389	22.5047	22.687

Table [3], Heat source parametric study of the ORC stand-alone

	T_3 temperature (ºC)			
Parameter	70	74	78	82
ORC Thermal Efficiency (%)	9.48	10.24	10.95	11.62
ORC microturbine power (kW)	17.10	18.50	19.80	21.00
Evaporator (H.E) destruction (%)	45.83	44.63	43.49	42.40
Turbine (ORC) destruction (%)	1.76	1.90	2.03	2.15
Cooling (H.E) destruction (%)	0.84	0.59	0.38	0.19
ORC Exergetic Efficiency (%)	22.8914	24.7225	26.4461	28.069

Table [4], T_3 parametric study of the ORC stand-alone

	Cooling Temperature (°C)					
Parameters	20	21	22	23	24	25
ORC Thermal Efficiency (%)	9.7283	9.6064	9.4801	9.3494	9.2145	9.0754
ORC microturbine power (kW)	16.6829	16.4739	16.2573	16.0332	15.8018	15.5632
Evaporator (H.E) destruction (%)	45.9691	45.9011	45.8315	45.7605	45.6882	45.6148
Turbine (ORC) destruction (%)	1.811	1.7868	1.7619	1.7361	1.7095	1.6822
Cooling (H.E) destruction (%)	0.7657	0.7982	0.8379	0.8825	0.9284	0.9685
ORC Exergetic Efficiency (%)	23.4907	23.1965	22.8914	22.5759	22.25	21.9141

Table [5], Cooling temperature parametric study of the ORC stand-alone

	Evaporator Inlet temperature °C						
Parameter	10	12	14	16	18	20	22
Generator's exergy destruction (kW)	3.89	5.55	6.88	7.89	8.57	8.91	8.75
Absorber exergy destruction (kW)	2.10	3.49	4.88	6.28	7.67	9.06	10.45
Evaporator's exergy destruction (kW)	1.06	2.15	3.57	5.31	7.36	9.72	12.37
Condenser exergy destruction(kW)	1.41	2.35	3.28	4.22	5.15	6.09	7.03
Heat exchanger exergy destruction (kW)	1.40	2.33	3.25	4.18	5.11	6.04	6.96
Exp. valve	0.29	0.49	0.68	0.88	1.07	1.27	1.46
Exergy in put	18.85	30.46	41.74	52.69	63.30	73.58	83.51
Absorption chiller's exergetic efficiency	8.51	7.50	6.31	5.06	3.76	2.44	1.08
Heat transfer of Evaporator (kW)	65.54	109.16	152.75	196.31	239.86	283.39	326.90
Heat transfer of Generator (kW)	83.09	138.39	193.66	248.90	304.11	359.30	414.47
Heat transfer of Absorber (kW)	63.60	105.92	148.22	190.50	232.75	274.99	317.22
Heat transfer of Condenser (kW)	71.12	118.46	165.76	213.04	260.29	307.53	354.75
Heat transfer of Heat exchanger (kW)	27.94	46.53	65.11	83.68	102.24	120.79	139.34
Cooling seawater (kg/s)	1.70	2.83	3.95	5.08	6.21	7.33	8.46
Chilled water temperature (°C)	7.00	7.00	7.00	7.00	7.00	7.00	7.00
Refrigerant (kg/s)	0.03	0.05	0.07	0.09	0.11	0.12	0.14
LiBr/H2O solution (kg/s)	0.32	0.54	0.75	0.97	1.18	1.40	1.61
Relative generator Δt (T_2/T_3) (°C)	117.0314	113.6539	110.2764	106.8987	103.5208	100.1424	96.7635
Evaporator inlet exergy (kW)	1.0845	0.4052	0.0547	0.0244	0.3069	0.8954	1.7835
Evaporator outlet exergy (kW)	2.689	2.689	2.689	2.689	2.689	2.689	2.689

Table [6], Evaporator inlet temperature parametric study of the Absorption chiller stand-alone

	Cooling water temperature °C				
AC Generator	20	22	24	26	28
Generator exergy destruction (kW)	5.91	5.91	5.91	5.91	5.91
Absorber exergy destruction (kW)	4.26	3.84	3.32	2.67	1.81
AC Evaporator exergy destruction (kW)	2.47	2.47	2.47	2.47	2.47
Condenser exergy destruction (kW)	3.02	2.77	2.40	2.02	1.60
Cooling water mass flow rate (kg/s)	2.81	3.11	3.47	3.94	4.54

Table [7], Cooling temperature parametric study of the Absorption chiller stand-alone

		Generator inlet hot water temperature °C							
Parameter	Unit	85	87	89	91	93	95	97	99
Generator exergy destruction (kW)	kW	4.79	3.82	3.73	3.85	4.07	4.32	4.59	4.88
Exergy input (kW)	kW	33.15	32.18	32.09	32.21	32.43	32.68	32.96	33.24
Exergetic Efficiency (%)	%	7.38	7.61	7.63	7.60	7.55	7.49	7.43	7.36
Cooling seawater mass flow rate (kg/s)	kg/s	3.22	3.22	3.22	3.22	3.22	3.22	3.22	3.22
Refrigerant mass flow rate (kg/s)	kg/s	0.05	0.05	0.05	0.05	0.05	0.05	0.05	0.05
LiBr/H2o mass flow rate (kg/s)	kg/s	0.61	0.61	0.61	0.61	0.61	0.61	0.61	0.61
Generator outlet temperature (°C)	°C	104.48	104.48	104.48	104.48	104.48	104.48	104.48	104.48
Chilled water temperature (°C)	°C	6.70	6.70	6.70	6.70	6.70	6.70	6.70	6.70
Hot water mass flow rate (kg/s)	kg/s	18.75	9.38	6.25	4.69	3.75	3.12	2.68	2.34

Table [8], Generator inlet water temperature parametric study of the Absorption chiller stand-alone

	No of Effects							
Thermodynamic properties	2	3	4	5	6	7	8	9
Potable water prodction (m^3/day)	53	53	53	53	53	53	53	53
GOR	1.89	2.77	3.61	4.38	5.1	5.75	6.33	6.86
Specific Heat Consumption (kJ/kg)	1235.49	840.95	646.55	532.09	457.54	405.76	368.19	340.08
Input energy (kW)	0.74	0.5	0.39	0.32	0.27	0.24	0.22	0.2
Seawater intake mass (kg/s)	7.86	5.2	3.87	3.07	2.55	2.17	1.89	1.67
Rejected brine water (kg/s)	0.72	0.71	0.71	0.71	0.7	0.7	0.7	0.69
Rejected seawater (kg/s)	6.540	3.890	2.560	1.770	1.240	0.870	0.590	0.380
Concentration factor	1.838	1.842	1.847	1.851	1.854	1.858	1.862	1.865

Table [9], Number of effects's parametric study of the MED desalination stand-alone

	Intake seawater temperature ˚C				
Parameter	20	22	24	26	28
MED evaporators' exergy destruction (kW)	21.38	19.43	17.47	15.48	13.48
MED condenser's exergy destruction (kW)	4.39	4.91	5.47	6.05	6.66
Plant's overall exergetic efficiency (kW)	27.16	28.16	29.23	30.39	31.63
GOR	6.22	6.48	6.76	7.06	7.38
Specific heat consumption (kJ/kg)	374.89	359.99	345.19	330.49	315.91
Heat transfer in first effect (kW)	224.93	215.99	207.11	198.30	189.55
Heat energy source mass flow rate (kg/s)	0.10	0.09	0.09	0.09	0.08

Table [10], Intake seawater temperature parametric study of the MED desalination stand-alone

	Intake seawater salinity kg/kg					
Component	0.036	0.038	0.04	0.042	0.044	0.045
MED evaporators exergy destruction (kW)	13.9842	14.0079	14.0323	14.0574	14.0832	14.0964
MED condenser exergy Destruction (kW)	8.7329	8.7076	8.6821	8.6567	8.6312	8.6185
Plant's overall exergetic efficiency (%)	31.4094	31.4	31.3901	31.3797	31.3688	31.3632
Potable water (m^3/day)	52.5969	52.5969	52.5969	52.5969	52.5969	52.5969
GOR	7.2923	7.2895	7.2866	7.2835	7.2804	7.2787
Specific heat consumption (kJ/kg)	319.7714	319.8943	320.0228	320.157	320.2967	320.3687
Concentration factor	1.8647	1.8645	1.8644	1.8643	1.8642	1.8641
feed seawater mass flow rate (kg/s)	1.50	1.51	1.51	1.51	1.51	1.51
Heat energy source mass flow rate (kg/s)	0.08	0.08	0.08	0.08	0.08	0.08

Table [11], Intake seawater salinity parametric study of the MED desalination stand-alone

	No of Effects													
Parameters	2	3	4	5	6	7	8	9	10	11	12	13	14	15
GOR	2.87	3.78	4.62	5.37	6.06	6.67	7.40	8.10	8.00	7.90	7.78	7.65	7.54	7.43
Specific Heat Consumption (Kj/kg)	970.10	730.41	592.48	504.03	443.02	399.00	366.16	325.16	323.08	322.20	322.47	323.42	324.81	326.25
Energy in (kW)	549.77	417.90	342.20	293.88	260.68	236.88	219.26	194.99	197.36	199.71	202.75	206.25	209.16	212.24
Seawater intake mass (kg/s)	5.32	3.90	3.07	2.52	2.13	1.84	1.62	1.31	1.30	1.30	1.29	1.29	1.28	1.27
motive steam mass flow (kg/s)	0.21	0.16	0.13	0.11	0.10	0.09	0.08	0.07	0.08	0.08	0.08	0.08	0.08	0.08
Suction mass flow rate (kg/s)	0.03	0.03	0.02	0.02	0.01	0.01	0.01	0.01	0.01	0.01	0.01	0.01	0.01	0.00
Concentration factor	1.84	1.84	1.85	1.85	1.85	1.86	1.86	1.87	1.87	1.87	1.88	1.88	1.88	1.89

Table [12], Number of effects parametric study of the TVC- MED desalination stand-alone

	Intake seawater temperature ˚C				
Component	20	22	24	26	28
TVC-MED steam ejector's exergy destruction (kW)	7.8154	7.5172	7.22	6.91	6.6034
TVC-MED evaporators' exergy destruction (kW)	17.7189	19.91	22.03	24.0882	26.0909
TVC-MED condenser's exergy destruction (kW)	5.4866	4.67	3.90	3.1767	2.4968
Plant's overall exergetic efficiency (kW)	23.4368	24.3414	25.33	26.4025	27.584
GOR	6.99	7.2695	7.57	7.91	8.28
Specific heat consumption (kJ/kg)	370.97	356.8174	342.51	328.05	313.44
Concentration factor	1.87	1.8659	1.87	1.86	1.86
Heat transfer in first effect (kW)	222.5822	214.0905	205.5074	196.8323	188.065
feed seawater mass flow rate (kg/s)	1.70	1.7	1.7	1.70	1.70
Motive steam mass flow rate (kg/s)	0.09	0.0825	0.0792	0.0759	0.0725

Table [13], Intake seawater temperature’s parametric study of the TVC- MED desalination stand-alone

-Appendix B

Complete combined proposed models results

	Ambint tempereture (Micro+ORC)									
Parameters	5	10	15	20	25	30	35	40	45	50
CO2 Emission Rate (kg/kW)	571.290	582.570	594.350	606.690	619.610	633.150	647.370	662.310	678.030	694.600
R134a Thermal Efficiency (%)	9.590	9.490	9.390	9.290	9.180	9.080	8.980	8.870	8.760	8.660
ORC microturbine power (kW)	15.159	16.147	17.109	18.043	18.950	19.830	20.682	21.507	22.303	23.072
Net Power (kW)	225.980	221.440	216.880	212.290	207.690	203.070	198.420	193.750	189.060	184.350
Microturbine Power (kW)	211.360	205.880	200.390	194.920	189.450	183.980	178.520	173.070	167.620	162.180
EUF	39.780	39.010	38.240	37.460	36.680	35.900	35.110	34.320	33.520	32.720
Overall Electrical Efficiency (%)	38.770	38.000	37.230	36.450	35.670	34.880	34.090	33.300	32.510	31.710
Air compressor exergy destruction (kW)	26.636	26.872	26.994	27.006	26.911	26.713	26.415	26.020	25.532	24.953
Recuprecator exergy destruction (kW)	0.477	0.429	0.388	0.354	0.325	0.303	0.286	0.274	0.267	0.265
C.C exergy destruction (kW)	579.550	579.506	579.463	579.420	579.376	579.333	579.289	579.245	579.201	579.157
Turbine exergy destruction (kW)	52.255	52.261	52.267	52.273	52.279	52.285	52.291	52.297	52.303	52.310
Evaporator(H.E) ORC exergy destruction (kW)	40.252	44.074	47.991	51.999	56.094	60.274	64.534	68.874	73.289	77.777
Turbine (ORC) exergy destruction (kW)	1.644	1.750	1.853	1.953	2.050	2.143	2.234	2.322	2.406	2.487
Cooling ORC exergy destruction (H.E)	0.519	0.803	1.125	1.484	1.881	2.315	2.786	3.295	3.842	4.427
ORC 245fa Exergitic Efficiency (%)	23.910	23.380	22.870	22.370	21.880	21.410	20.950	20.490	20.050	19.620
overal Plant Exergetic Efficiency (%)	24.040	23.580	23.110	22.640	22.170	21.690	21.220	20.740	20.260	19.770

Table [1], Ambient temperature parametric study of the Microturbine+ORC

	Partial load (Micro+ORC)				
Parameters	0.6	0.7	0.8	0.9	1
CO2 Emission Rate (kg/kW)	642.84	631.46	620.64	609.36	598.65
Net Power (kW)	191.79	142.9	164.95	189.75	216.04
Microturbine Efficiency (kW)	35.36	35.99	36.62	37.3	37.97
EUF	30.52	31.86	32.98	34.07	35.08
Overall Electrical Efficiency (%)	30.52	31.86	32.98	34.07	35.08
Air compressor exergy destruction (kW)	17.4614	20.0048	22.2649	24.6694	27.1
C.C exergy destruction (kW)	539.065	559.4185	578.1904	598.7792	620.1622
Turbine exergy destruction (kW)	30.0016	35.4922	40.6018	46.2493	52.1573
Evaporator(H.E) ORC exergy destruction (kW)	2.8192	2.8192	2.8192	2.8192	2.8192
Turbine (ORC) exergy destruction (kW)	1.797	1.797	1.797	1.797	1.797
Cooling ORC exergy destruction (H.E)	30.26	31.59	32.7	33.79	34.79
ORC 245fa Exergitic Efficiency (%)	25.83	23.98	22.92	22.12	21.51
overal Plant Exergetic Efficiency (%)	15.96	17.67	19.13	20.61	22.02

Table [2], Partial load parametric study of the Microturbine+ORC

	Intake cooling temperature (ºC)				
Parameters	20	22	24	26	28
CO2 Emission Rate (kg/kW)	594.31	595.47	596.72	598.05	599.46
R134a Thermal Efficiency (%)	9.73	9.48	9.21	8.93	8.63
ORC microturbine power (kW)	16.6829	16.2573	15.8018	15.3178	14.8072
Net Power (kW)	217.75	217.28	216.74	216.07	214.58
EUF	38.24	38.17	38.09	38	37.91
Evaporator(H.E) ORC exergy destruction (kW)	45.9691	45.8315	45.6882	45.5405	45.3898
Turbine (ORC) exergy destruction (kW)	1.811	1.7619	1.7095	1.6541	1.596
Cooling ORC exergy destruction (H.E)	0.7657	0.8379	0.9284	0.9869	0.5861
ORC 245fa Exergitic Efficiency (%)	23.49	22.89	22.25	21.57	20.85
overal Plant Exergetic Efficiency (%)	22.9	22.85	22.81	22.76	22.7

Table [3], Intake cooling water temperature parametric study of the Microturbine+ORC

Paramters	10	15	20	25	30	35	40	45	50
Emission Rate (kg/kW)	424.6676	433.4951	442.6974	452.2991	462.3273	472.8115	483.7838	495.2795	507.3374
Air compressor exergy destruction (kW)	39.1459	39.1459	39.1459	39.1459	39.1459	39.1459	39.1459	39.1459	39.1459
C.C exergy destruction (kW)	566.6151	566.6151	566.6151	566.6151	566.6151	566.6151	566.6151	566.6151	566.6151
Turbine exergy destruction (kW)	52.2667	52.2667	52.2667	52.2667	52.2667	52.2667	52.2667	52.2667	52.2667
Boiler H-E exergy destruction (kW)	32.9137	32.9137	32.9137	32.9137	32.9137	32.9137	32.9137	32.9137	32.9137
AC Generator exergy destruction (kW)	4.5386	4.5386	4.5386	4.5386	4.5386	4.5386	4.5386	4.5386	4.5386
AC Absorper exergy destruction (kW)	2.6688	2.6688	2.6688	2.6688	2.6688	2.6688	2.6688	2.6688	2.6688
AC Evaporator exergy destruction (kW)	2.4762	2.4762	2.4762	2.4762	2.4762	2.4762	2.4762	2.4762	2.4762
AC Condenser exergy destruction (kW)	0.2846	0.2846	0.2846	0.2846	0.2846	0.2846	0.2846	0.2846	0.2846
AC Heat Exchanger exergy destruction (kW)	2.5599	2.5599	2.5599	2.5599	2.5599	2.5599	2.5599	2.5599	2.5599
Absorption chiller Exergetic Efficiency (%)	7.5223	7.5223	7.5223	7.5223	7.5223	7.5223	7.5223	7.5223	7.5223
COP	0.7887	0.7887	0.7887	0.7887	0.7887	0.7887	0.7887	0.7887	0.7887
Net Power (kW)	208.2114	208.2114	208.2114	208.2114	208.2114	208.2114	208.2114	208.2114	208.2114
EUF	53.5204	52.4305	51.3406	50.2507	49.1608	48.0707	46.9804	45.89	44.7993
Overall Electrical Efficiency (%)	35.6366	35.6366	35.6366	35.6366	35.6366	35.6366	35.6366	35.6366	35.6366
overall Plant Exergetic Efficiency (%)	32.3446	31.6859	31.0273	30.3686	29.7099	29.0511	28.3922	27.7332	27.0741

Table [4], Ambient temperature parametric study of the Microturbine+Absorption chiller

	Partial Load (Micro+AC)				
Paramters	0.6	0.7	0.8	0.9	1
CO2 Emission Rate (kg/kW)	431.6172	427.9742	423.2841	419.1992	415.3041
Air compressor exergy destruction (kW)	23.7255	26.8079	30.6957	34.1861	37.7122
Recuprecator exergy destruction (kW)	7.689	8.9223	10.5962	12.21	13.9442
C.C exergy destruction (kW)	491.5951	507.5522	528.4389	547.8458	568.0125
Turbine exergy destruction (kW)	30.9425	35.5596	41.6513	47.3551	53.3218
Boiler H-E exergy destruction (kW)	20.3428	23.0195	26.4123	29.4737	32.5809
AC Generator exergy destruction (kW)	2.8589	3.2313	3.7015	4.124	4.5512
AC Absorper exergy destruction (kW)	2.0945	2.3673	2.7118	3.0213	3.3343
AC Evaporator exergy destruction (kW)	1.4037	1.5866	1.8175	2.025	2.2347
AC Condenser exergy destruction (kW)	0.9889	1.1177	1.2804	1.4265	1.5743
AC Heat Exchanger exergy destruction (kW)	1.6125	1.8225	2.0877	2.3261	2.567
Net Power (kW)	113.1349	131.9642	157.4786	181.8846	207.8047
EUF	52.6586	53.1069	53.6953	54.2185	54.7271
Overall Electrical Efficiency (%)	32.4831	33.1529	34.0322	34.8141	35.574
overall Plant Exergetic Efficiency (%)	25.1122	27.0979	29.4117	31.3169	33.0868

Table [5], Partial load parametric study of the Microturbine+Absorption chille

	Cooling temperature (ºC) (Micro+AC)				
Componants	20	22	24	26	28
CO2 Emission Rate (kg/kW)	433.4951	433.4951	433.4951	433.4951	433.4951
Air compressor exergy destruction (kW)	39.1459	39.1459	39.1459	39.1459	39.1459
Recuprecator exergy destruction (kW)	13.2409	13.2409	13.2409	13.2409	13.2409
Turbine exergy destruction (kW)	52.2667	52.2667	52.2667	52.2667	52.2667
AC Absorper exergy destruction (kW)	3.3251	2.823	2.323	1.814	1.346
AC Condenser exergy destruction (kW)	1.5724	1.2745	0.9726	0.6729	0.3757
Net Power (kW)	195.0452	195.0452	195.0452	195.0452	195.0452
EUF	52.4305	52.4305	52.4305	52.4305	52.4305

Table [6], Cooling temperature parametric study of the Microturbine+Absorption chiller

	Ambint Temperaturre (°C) (Micro+TVC-MED)									
	5	10	15	20	25	30	35	40	45	50
CO2 Emission Rate (kg/kW)	332.430	337.215	341.997	346.889	351.918	357.089	362.409	367.883	373.518	379.322
Air compressor exergy destruction (kW)	26.629	26.864	26.999	27.011	26.916	26.717	26.420	26.025	25.537	24.958
C.C exergy destruction (kW)	579.652	579.502	579.458	579.415	579.371	579.328	579.284	579.240	579.196	579.152
Turbine exergy destruction (kW)	52.255	52.261	52.267	52.273	52.279	52.285	52.291	52.297	52.303	52.310
Evaporator exergy destruction (kW)	18.060	20.225	22.308	24.306	26.226	28.073	29.851	31.565	33.218	34.812
Boiler exergy destruction (kW)	51.235	51.235	51.235	51.235	51.235	51.235	51.235	51.235	51.235	51.235
condenser exergy destruction (kW)	6.361	6.361	6.361	6.361	6.361	6.361	6.361	6.361	6.361	6.361
Steam Ejector exergy destruction (kW)	21.823	21.823	21.823	21.823	21.823	21.823	21.823	21.823	21.823	21.823
Net Power (Kw)	210.860	205.400	199.890	194.410	188.940	183.480	178.020	172.570	167.120	161.680
EUF	68.420	67.400	66.460	65.520	64.580	63.650	62.710	61.780	60.850	59.920
Overall Electrical Efficiency (%)	36.190	35.150	34.210	33.270	32.340	31.400	30.470	29.540	28.600	27.670
Ejector Exergtic Efficiency (%)	19.846	29.563	29.563	29.563	29.563	29.563	29.563	29.563	29.563	29.563
Overal plant Exergtic Efficiency (%)	23.568	22.996	22.427	21.861	21.295	20.729	20.165	19.601	19.038	18.475

Table [7], Ambient temperature parametric study of the Microturbine+TVC-MED

	Partial Load (Micro+TVC-MED)				
	0.6	0.7	0.8	0.9	1
CO2 Emission Rate (kg/kW)	392.1532	408.3582	423.7744	434.0252	441.8213
Air compressor exergy destruction (kW)	17.4646	19.5907	22.269	24.6739	27.105
C.C exergy destruction (kW)	498.2722	515.2236	537.3967	557.985	579.3676
Turbine exergy destruction (kW)	30.0016	34.5708	40.6018	46.2493	52.1573
Evaporator exergy destruction (kW)	13.2938	14.1142	14.9425	15.5585	16.0994
Boiler exergy destruction (kW)	26.8796	26.8796	26.8796	26.8796	26.8796
condenser exergy destruction (kW)	2.4384	2.4384	2.4384	2.4384	2.4384
Steam Ejector exergy destruction (kW)	11.4639	11.4639	11.4639	11.4639	11.4639
Net Power (Kw)	102.29	125.4	147.45	172.25	198.54
EUF	57.96	55.66	53.63	52.37	51.44
Overall Electrical Efficiency (%)	29.51	30.85	31.97	33.06	34.07
(MED+Ejc) exergetic Efficiency (%)	7.9007	7.9007	7.9007	7.9007	7.9007
Overall plant exergetic Efficiency (%)	15.2676	16.8162	18.6803	20.2553	21.7466

Table [8], Partial load parametric study of the Microturbine+TVC-MED

	Cooling water temperature (°C) (Micro+TVC-MED)				
	20	22	24	26	28
Emission rate after Utilization (kg/kW)	340.2882	340.2882	340.2882	340.2882	340.2882
Air compressor exergy destruction (kW)	26.9989	26.9989	26.9989	26.9989	26.9989
Recuprecator exergy destruction (kW)	0.3882	0.3882	0.3882	0.3882	0.3882
C.C exergy destruction (kW)	579.4581	579.4581	579.4581	579.4581	579.4581
Turbine exergy destruction (kW)	52.267	52.267	52.267	52.267	52.267
Evaporator exergy destruction (kW)	22.3518	22.3518	22.3518	22.3518	22.3518
Boiler exergy destruction (kW)	51.7685	51.7685	51.7685	51.7685	51.7685
condenser exergy destruction (kW)	6.7092	6.0595	5.2844	4.3436	3.1777
Steam Ejector exergy destruction (kW)	22.0564	22.0564	22.0564	22.0564	22.0564
Microturbine Power (Kw)	206.32	206.32	206.32	206.32	206.32
EUF	66.79	66.79	66.79	66.79	66.79
Overall Electrical Efficiency (%)	35.31	35.31	35.31	35.31	35.31
(MED+Ejc) exergetic Efficiency (%)	19.6685	19.6535	19.6357	19.6141	19.5873
Overall plant exergetic Efficiency (%)	21.253	21.2522	21.2511	21.2499	21.2484
Intake seawater mass flow rate (kg/s)	1.3312	1.4482	1.5878	1.7573	1.9673

Table [9], Cooling water temperature parametric study of the Microturbine+TVC-MED

-Appendix C

The sensitivity study for all proposed models

Units		Pences	Average rate of return %	Pay Back period Year	Net Present value
1	Microturbine	0.02	2.42	21	-14667
		0.04	11.73	7.202	721172.81
		0.06	21	4.311	1457012.81
		0.08	30.35	3.076	2192852
		0.1	39.66	2.392	2928692
2	Microturbine+ORC	0.02	2.46	21	-12342
		0.04	12.16	6.988	786052
		0.06	21.86	4.165	1584434
		0.08	31.56	2.967	2382825
		0.1	41.25	2.304	3181211
3	Microturbine+Absorption chiller	0.02	2.02	21	-49605
		0.04	10.76	7.743	686234
		0.06	19	4.61	1422074
		0.08	28.2	3.29	2157914
		0.1	36.9	2.5	2893754
4	Microturbine+TVC-MED	0.02	3.74	16.954	102243
		0.04	11.92	7.106	838133
		0.06	20.09	4.495	1573973
		0.08	28.27	3.287	2309813
		0.1	36.2	2.607	3042940

Table [1], The sensitivity study of the proposed models at electricity selling price variation

Microturbine+TVC-MED	100% potable water	**Electric price fixed at £0.023**			
Water selling price(£)	**0.4**	**0.6**	**0.8**	**1**	**1.2**
Average Rate of Return	4.65%	5.56%	6.46%	7.36%	8.26%
Pay Back Period	14.688	12.968	11.61	10.508	9.598
Net Present Value	184,235.33	265,484.33	346,733.33	427,982.33	509,231.33

Table [2], The sensitivity study of the proposed models at potable water selling price variation

Journal of Environmental Science and Engineering, 5 (2011) 508-518

An Energy and Exergy Analysis of a Microturbine CHP System

B.M.A. Makhdoum[1] and B. Agnew[2]

1. School of Mechanical and Systems Engineering, Newcastle University, Newcastle NE1 7RU, United Kingdom

2. School of the Built Environment, Northumbria University, Newcastle NE1 8ST, United Kingdom

Received: November 8, 2010 / Accepted: December 21, 2010 / Published: April 20, 2011.

Abstract: The micro-turbine is known as a producer of high-grade energy (work) and also low energy (heat). The following low grade heat energy have been modeled under ISO ambient conditions (international standard organization), i.e. 15 ℃ and 1 bar, to utilize the waste heat energy of a 200 kW micro-turbine combined with a single effect absorption chiller, an organic ranking cycle using R245fa (ORC-R245 fa) as a working fluid, a multi-effect distillation desalination (MED) and a thermal vapor compression MED Desalination unit (TVC-MED). The thermal comparison was carried out based on an energy and exergy analysis in terms of electric efficiency, exergetic efficiency, carbon footprint, and energy utilization factor (EUF). The software package IPSEpro has been used to model and simulate the proposed power plants. As a result, utilizing the exhaust waste heat energy in single-effect absorption chillier has contributed to stabilize ambient temperature fluctuation, and gain the best exergetic efficiency of 39%, while the EUF has reached 72% and the carbon footprint was reduced by 75% in MED and TVC-MED Desalination respectively. The results also reveal that TVC-MED is more efficient than traditional MED as its gain output ratio (GOR) is improved by 5.5%. In addition, ORC-245fa generates an additional 20% of the micro-turbine electricity generation.

Key words: Micro-turbine, absorption chiller, energy, exergy, ORC, MED, TVC-MED.

1. Introduction

Many applications and advantages of micro-turbines help create a rapidly increasing market. A handful of these advantages are highlighted as follows. First, the environmental performance of the micro-turbine is very impressive, thanks to decades of intensive research. In fact, micro-turbines can now operate with fuels, which produce much lower NOx emissions than previously possible, surprisingly with even higher reliability and energy efficiency. Therefore, micro- turbines can be considered as an environmentally friendly alternative. The environmental dimension is especially important when it comes to the current environmental legislation. Secondly, another very important factor is the availability of gas as a fuel of choice for smaller scale industrial and cogeneration application. Other reasons to encourage employing micro-turbines are they are quick to install, easy to maintain, and also have a short payback period [1].

Generally speaking, a micro-turbine consists of the same major components as a normal gas turbine, but to a considerably smaller scale: the air compressor, the combustor and the turbine (see Fig. 1) [2]. From a technical point of view, a micro-turbine can be used with a single shaft, and all the components can be found on the same shaft that drives the generator [3].

A variety of distributed generation applications are well suited with a micro-turbine. This is due to a high range of flexibility in connection methods of the micro-turbine, and it has the ability to be installed

B. Agnew, professor, research fields: thermal power systems, refrigeration, combined cycles, internal combustion engines. E-mail: brian.agnew@northumbria.ac.uk.

Corresponding author: B.M.A. Makhdoum, MSc, Ph.D. candidate, research fields: micro-turbine CHB system, thermal analysis, environment. E-mail: basim.makhdoum@ncl.ac.uk.

in parallel to provide lager loads. The exhaust waste energy

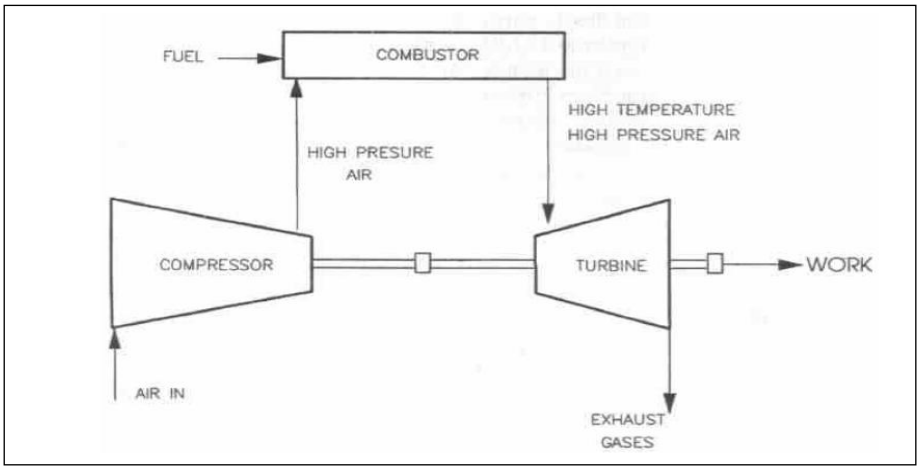

Fig. 1 Micro-turbine components.

heat of a micro-turbine can be utilized to supply other thermal energy needs in building or industrial process such as heating building space, producing domestic hot water and driving single effect absorption chillier. Also, a micro-turbine application can be targeted by customers in light industrial facilities and in financial services; for instance, schools, hospitals and other commercial or institution structures [4]. A micro-turbine produces high-grade energy (work), however, it also can be used as low- grade energy (heat) source that can be recovered for a useful purpose. This paper presents an overview of several low-grade heat energy powered systems that have been modeled under ISO conditions (international standard organization), i.e. 15 ℃and 1 bar to utilize the waste heat energy of a 200 kW micro-turbine. These are: a single effect absorption chiller, an organic ranking cycle using R245 fa as the working fluid (ORC-R245 fa), a multi-effect distillation desalination (MED) and a thermal vapor compression MED desalination plant (TVC-MED). These components of the combined system are described below.

1.1 Absorption Chillers

There are many types of chillers such as ammonia/water chillers and ammonia/water/hydrogen refrigerators; however, using lithium bromide as a working fluid in these types is considered one of the best choices among hundreds of working fluids [5]. According to many authors [6-8], the main operating factor of an absorption chiller is the waste heat that is obtained from a micro-turbine or gas turbine. It has been stated that driving lithium bromide by the waste heat of the gas engine leads to many benefits; for instance, increasing the efficiency of the plant, reducing both operating costs and energy requirements and environmental pollution will be produced at a low level [6, 9, 10].

A single-effect water/lithium bromide chiller has been integrated in this study and it is powered by the micro-turbine's waste heat energy. Fig. 2 shows the complete cycle of a single-effect absorption chiller. The arrows on this figure show the direction of the energy that is transferred into and from the cycle. The cycle of the absorption chiller starts when the desorber receives heat to evaporate the water that is in solution with lithium bromide. The strong solution (low concentration of water) leaves the desorber and enters the absorber. Then, the solution is weakened by the absorption of water vapor coming from the evaporator. Then, the weak solution is pumped from the absorber to the desorber via the solution heat exchanger. The evaporated water produced in the desorber is condensed and then flows by way of an

expansion valve to the evaporator where, because of the low pressure, it is evaporated and transferred to the absorber. The desired refrigeration effect is produced by the evaporation of the water.

1.2 Organic Rankine Cycle (ORC)

The use of an Organic Rankine power cycle to recover low grade thermal energy is becoming widely recognized as a major technology in power engineering [11]. The simple Rankine Cycle contains four components: a heat supplier (evaporator), power turbine, condenser and pump. The cycle begins when the refrigerant is heated in the boiler (heat exchanger) to a high temperature, and then transferred to the turbine where it is expanded to produce electrical energy. The refrigerant then passes to the condenser where it is turned to liquid before being returned to the boiler to complete the cycle (Fig. 3). Typical ORCs are reliable flexible, have a good safety record and require low maintenance. The use of an ORC can result in a decrease in the emission of environment pollutants such as carbon dioxide due to no additional fuel being consumed [12]. Many studies have been carried out to operate ORC as part of a power system, for example, with solar heat energy and geothermal energy [11, 13].

1.3 Multi Effect Distilled (MED) Desalination

Utilizing the waste heat energy of a micro-turbine in the desalination process has not been covered through the literature. Since the thermal desalination technologies are not common for small scale water production, the opportunity of modeling and simulating small scale multi-effect distilled desalination (MED) is becoming a great challenge, by a small-scale unit; however, it consumes electricity that is provided by high grade energy [11]. Multi Stage Flash

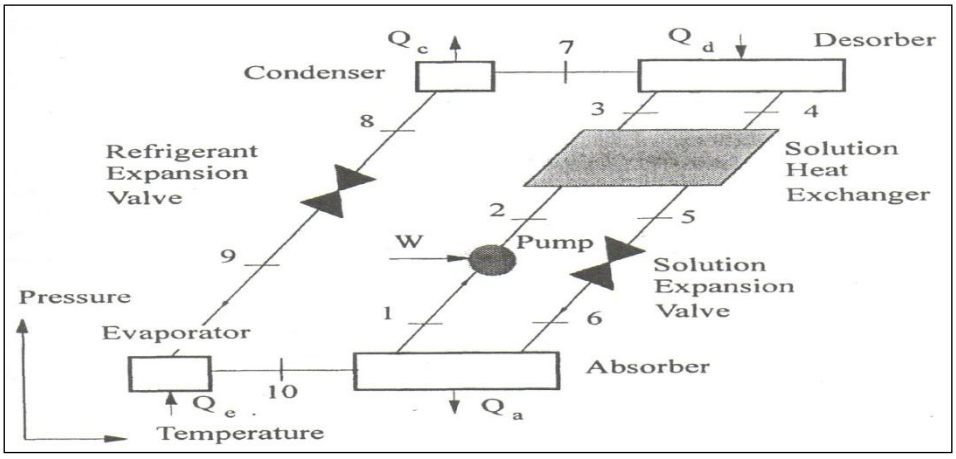

Fig. 2 Single-effect water/lithium bromide absorption chiller [7].

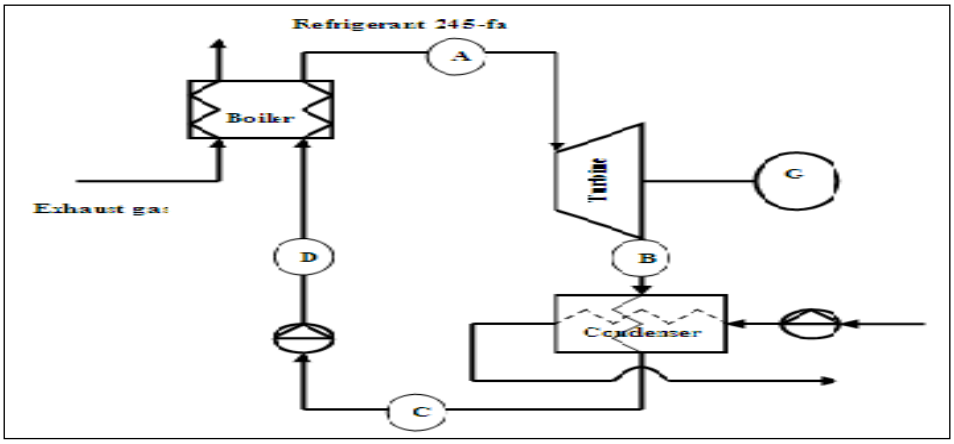

Fig. 3 The ORC process.

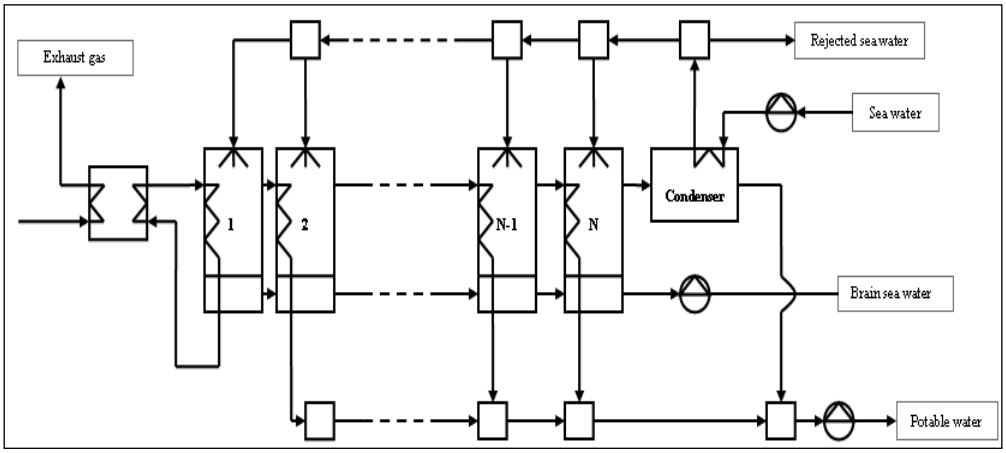

Fig. 4 The MED desalination process.

(MSF) has not been considered in this study as it needs too high a source temperature to operate well [14]. Among these and other desalinations systems, MED is considered the most efficient thermodynamic method (Fig. 4). MED takes place in a number of evaporators called effects, and uses the principle of producing low pressure in the various effects in order to boil seawater to the desired temperature [15]. Nonetheless, this technology can be improved by installing a steam ejector to reduce the quantity of motive steam requirement, which also raises the Gain Output Ratio (GOR).

2. Tools

The proposed model of this study has been modeled by using the IPSEpro software. This software is a complete set of modules used to create process models, and the life cycle of a process plant can be simulated and investigated according to the given thermodynamic properties. Firstly, PES, which is IPSEpro's process simulation environment, and the system of equations, is solved by using two-phases: firstly, checking the model for errors in the process conditions and then calculating the optimum solution method; secondly, PSExcel, which can be installed in Microsoft Excel (MS-Excel), allows the data in the PSE project to be put together with an MS-Excel worksheet. Thus, the result from IPSEpro simulations can be transferred to the Ms-Excel in order to investigate the process situation at many picked points, such as carrying out a parametric study. Besides, the proposed model has been created by using two libraries: advance power plant and refrigeration library. IPSEpro's simulation has also

provided an approach that supplies the explanation of equations with numerical methods that were previously defined by the analysis phase. Hence, the proposed model can be created and analyzed either according to selected icons from a given standard library or by creating a new icon with the other module. This is called the IPSEpro Model Development Kit (MDK), which creates new models and then converts them into a shape that can be simply used by IPSEpro [16].

2.1 Energy Analysis

The first low energy analysis is used in order to evaluate the thermodynamic performance in each model, including:

The thermal efficiency of the micro-turbine cycle that can be defined as the ratio of work obtained to the input total energy into the cycle [17] as follows:

$$\eta_{microturbine} = \frac{\dot{W}_{net}}{Q_{in}} = \frac{\dot{W}_{microturbine} - \sum \dot{W}_{pump}}{\dot{m} \times LHV} \quad (1)$$

Where, LHV is low heating value of the fuel, W is work generated, Q is the unit of heat input and $\dot{m}$ is mass flow rate kg/s.

The production of carbon dioxide (CO_2) is also calculated to act as a measure of the global warming impact of the plant for each kWh of useful energy.

$$CO_2 \text{ Emission Rate} = \frac{\dot{m} \times \alpha}{\sum W_{net,output} + \sum Q_{net,output}} \quad (2)$$

Where α the amount in (kg) of CO_2 produced for each ton of the consumed fuel.

The Energy Utilization Factor (EUF) is calculated to evaluate the performance of co-generation plant. This is defined as the ratio of the sum of total work and useful heat energy to the energy supplied in the fuel.

$$EUF = \frac{W_{net,output} + Q_{net,output}}{Q_{in}} \quad (3)$$

The Coefficient of Performance (COP) of the absorption chillers is calculated to measure its thermodynamic performance as follows:

$$COP = \frac{\dot{Q}_{Evaporator}}{Q_{Desorber}} \quad (4)$$

The performance of the desalination plant was evaluated by using the Gain Output Ratio (GOR), which defined as the ratio of the potable water mass flow rate (kg/s) to the driving steam mass flow rate. Furthermore, gaining a useful understanding to compare GOR was calculated for both MED and TVC-MED desalination models as follows:

$$GOR = \frac{\dot{m}_{potablewater}}{\dot{m}_{drivingsteam}} \quad (5)$$

2.2 Exergy Analyses

Exergy analysis is considered a part of this study. According to Tchache [11], the most exergy destruction in the ORC occurres in the turbine, while Al-sulimani [18] claimed that the evaporator has a significant source of exergy distraction.

Recently the exergy analysis has recently gained more credibility among published work. It is considered a powerful thermodynamic technique for assessing and monitoring the performance of a thermodynamic process.

The following equations were used to calculate the exergy of the system:

$$E = E^{KN} + E^{PT} + E^{CH} + E^{PH} \quad (6)$$

Where, E^{KN} kinetic exergy, E^{PT} potential exergy, E^{CH} chemical exergy, and E^{PH} physical exergy. However, in this study both kinetic and potential exergy are neglected.

The fuel exergy is calculated as follow:

$$E_{fuel} = \Theta \times \eta_{c.c} \times \dot{m}_{fuel} \times LHV \quad (7)$$

Where, Θ denotes the molar Gibbs function of formation of 1.04 for natural gas [19], and $\eta_{c.c}$ is the efficiency of the combustion chamber.

The physical exergy of a closed system can be expressed as follows [17]:

$$E^{PH} = (h - h_o) - T_o \times (s - s_o) \quad (8)$$

Where, h and s represent the enthalpy and entropy respectively, while the o is a symbol of the reference condition, i.e. 15 ℃ and 1.013 bar.

In the desalination system the entropy and enthalpy of pure water were directly given from the simulation software IPSE pro, while those of salt water were adopted from [20, 21] a method calculated as follows:

$$h_{salt} = h_{salt,o} + C_{p,salt} + (T - T_o) \quad (9)$$

$$s_{salt} = s_{salt} + C_{p.salt} \ln\left(\frac{T}{T_o}\right) \quad (10)$$

Where, C_p is the salt specific heat that is equal to 0.8368 kJ/kg·K. h_o and s_o are the enthalpy and entropy of salt at reference condition.

3. Model Configuration, Result and Discussions

3.1 Micro-turbine Stand-alone

Fig. 5 shows the base model of a micro-turbine stand alone. A micro-turbine power generation cycle essentially consists of a compressor, a combustion chamber and a reciprocator. The real data of a 200 kW micro-turbine was collected from the Capstone Company. The product name is C200. This micro-turbine produces 1.3 kg/s of exhaust gas flow at a temperature of 280 ℃. The isentropic efficiencies of the turbine and compressor are 98% and 90%, respectively. On entering the compressor air is compressed to 8 bar and mixed with 0.011 kg/s of fuel in the combustion chamber. Next, the air expands in the turbine and generates 200 kW of electricity. On the bases of the second law of thermodynamics, the energy balance showed that the overall electrical efficiency of this cycle is 34%, while its carbon emission rate is 663 kg of CO_2/kW. Based on the exergy analysis, the main source of the model irreversibility was found to be the combustion chamber, causing 582 kW of exergy destruction, which represents 60% of the power plant total exergy destruction. This can be justified by both heat transfer and the chemical process that take place in the combustion chamber. In comparison with the Ref. [22], the values of the second law thermodynamic analysis showed relatively the same results. While, 54 kW of the exergy was destroyed in the micro-turbine. This is due to the exergy expansion degraded during the compression, combustion and expansion that occurred in the micro-turbine components. Next, in the compression process, 3% of exergy destruction took place in the compressor.

3.2 Micro-turbine Cascaded with Water Cooled Single-Effect Absorption Chiller

Fig. 6 illustrates the water cooled single effect absorption chiller (1A1), based on a design by the York Company, and it consists of a desorber, an evaporator, an absorber, a condenser, a heat exchanger, two pumps and throttling valves. The cycle stand alone produces a cooling capacity of 200 kW with a COP of 0.78. Validation of the single-effect absorption chiller was considered by representing cycle points on the Duhring plot, as can be seen in Fig. 7. The results based on the first law analysis showed that integrating the absorption chiller with the micro-turbine decreased the carbon emission rate by 41%, which led to a EUF of 65%. This was due to utilizing 66% of the micro-turbine's exhaust waste heat in the absorption chiller boiler. The micro-turbine is a standardised machine that is manufactured to work at a wide range of ambient temperatures [23], therefore, at a higher ambient temperature the air density is reduced, leading to less air mass flow entering the compressor, which reduces the power output of the micro-turbine. Integrating the absorption chiller in this cycle generates chilled water at 6 ℃ that cooled the inlet air to the micro-turbine compressor from ISO conditions to 7 ℃. This also stabilized the affect of ambient temperature variation on the micro-turbine performance. Based on the second law exergy analysis, the most significant exergy destruction was noticed in the absorber, due to the mixing process and heat transfer between three streams entering the absorber. These results are in agreement with the published work; for example, that of Ishida [24]. The exergy destruction of the turbine and reciprocator decreased by 28% and 54% respectively, and this was

due to the compressor air inlet cooling by the absorption chiller. In comparison to the base plant, this plant consumes only 7% more fuel, which makes the total exergy 751 kW.

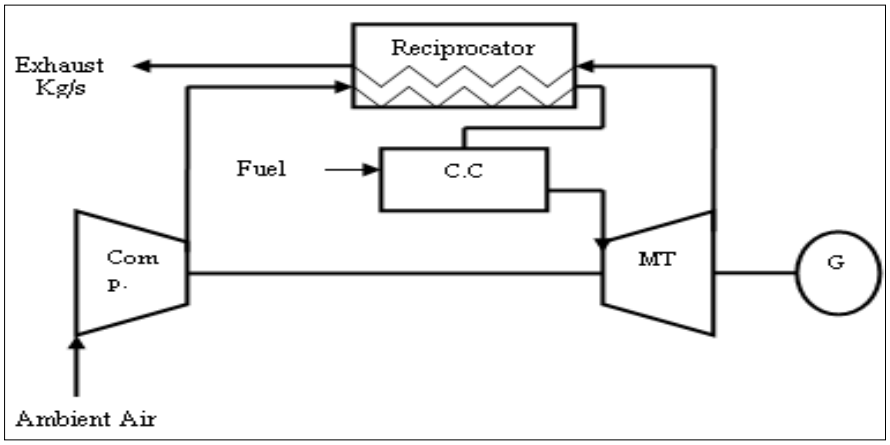

Fig. 5 The base power plant, micro-turbine 200 kW.

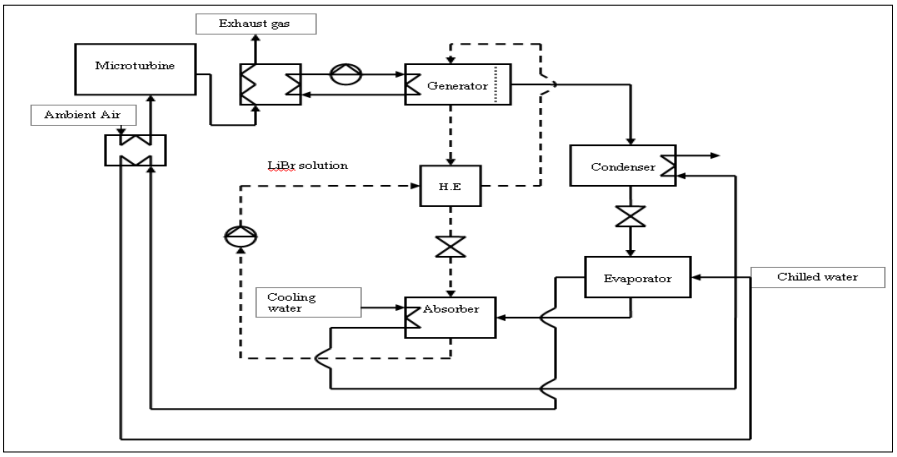

Fig. 6 Micro-turbine cascaded with water cooled single-effect absorption chiller.

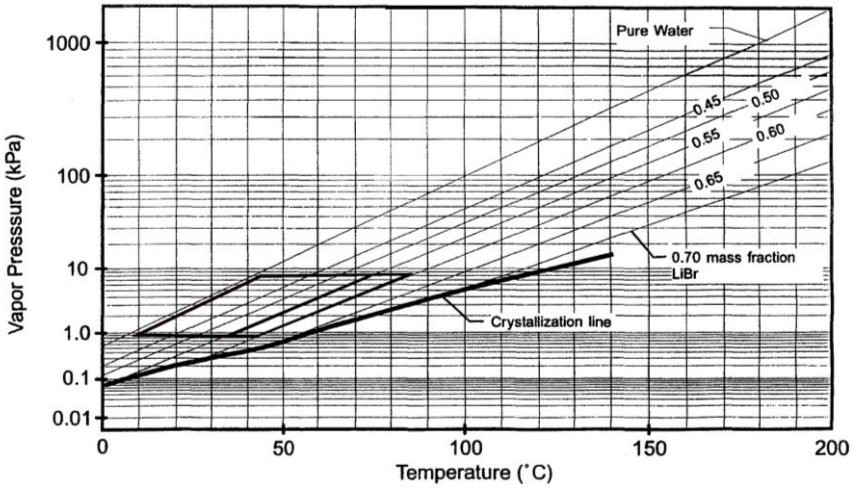

Fig. 7 Duhring plot for single-effect lithium bromide absorption chiller.

3.3 Micro-turbine Cascaded with ORC-245 fa

As seen in Fig. 8, the waste heat energy of the micro-turbine is utilized in the proposed ORC. Refrigerant 245-fa was selected to generate the cycle. The simulated results indicated the generation of an extra 20% of the total power with an ORC efficiency of 10%, and 38% of EUF. This amount of power is reasonable, as stated by Schuster [13]. A large amount of exergy destruction in the ORC was found in the evaporator due to the refrigerant changing from liquid to superheated gas. This result is in agreement with what has been mentioned in the literature by Al-Sulimani [18], while Tchanhe [11] reported that the large irreversibility occurred in the turbine due to the expansion process. This can be justified by the fact that the inlet refrigerant temperature in the turbine is higher than that in Tchanhe's study [11].

3.4 Micro-turbine Cascaded with Multi-Effect Distilled Desalination (MED)

Currently, many countries meet their fresh water requirement by investing in desalination technology. In
particular, in the Middle East, seawater desalination has become very important in providing fresh water, such as in Saudi Arabia. According to Khawji [15], Saudi Arabia is the first country to lead in desalination with 17.4% compared to the other countries. To obtain a further benefit from the waste heat energy of a micro-turbine, the simulated MED desalination model was integrated with a micro-turbine, as illustrated in Fig. 9. MED was selected because it is the only desalination method that can be operated by low grade heat energy; also, it consumes less electricity compared to RO and MSF desalination methods. Therefore, utilizing 57% of the micro-turbine's waste heat energy in MED showed a significant EUF of 72%. Also, the carbon foot print was reduced by 66%. The results also show that the Gain Output Ratio (GOR) of this cycle is 7.1 with a mass seawater intake of 1.87 kg/s and 220kW of energy. This led to a production rate of 57 m^3/d of portable water. On the basis of the second law of thermodynamics, the MED stand alone achieved an exergetic exergy of 31 %. The plant exergy destruction was mainly caused by the boiler which accounted for 6% of the total input exergy to the cycle. The complete plant is shown in Fig. 10. The Gain Output Ratio (GOR) was increased by 7% in TVC-MED desalination, while no significant difference has been found in the water production rate. The TVC-MED desalination exergetic efficiency improved by 23%; however, the highest exergy destruction was caused in the evaporators due to the extraction of the motive steam to the ejector, which takes place between the condenser and evaporator, and this led to exergy irreversibility by 22.2 kW in the ejector. As a result, TVC-MED desalination is recommended for small-scale industrial water production.

3.5 Results Summary

A comparison has been performed for all models based on the energy and exergy analysis to show a clear thermodynamic view for this study. Fig. 11 summarizes the results of the proposed simulated models. The factors considered in this comparison are the carbon emission rate, EUF, electrical and exergetic efficiency.

Fig. 11 and Fig. 12 conclude that a cascading micro-turbine with single-effect absorption chiller provided 200 kW of cooling effect that was used to stabilize the compressor inlet-air temperature. Also, the

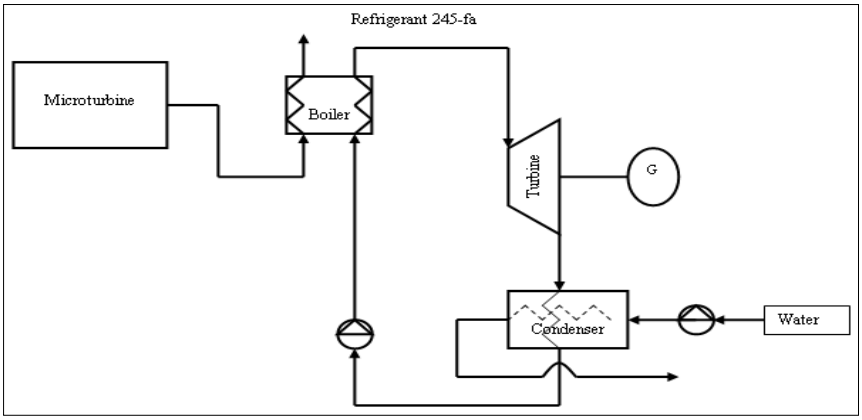

Fig. 8 Micro-turbine cascaded with ORC-245fa.

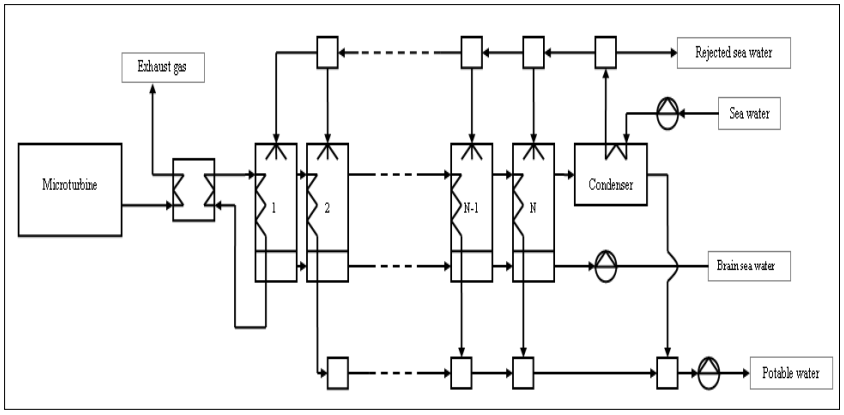

Fig. 9 Micro-turbine cascaded with multi-effect distilled desalination (MED).

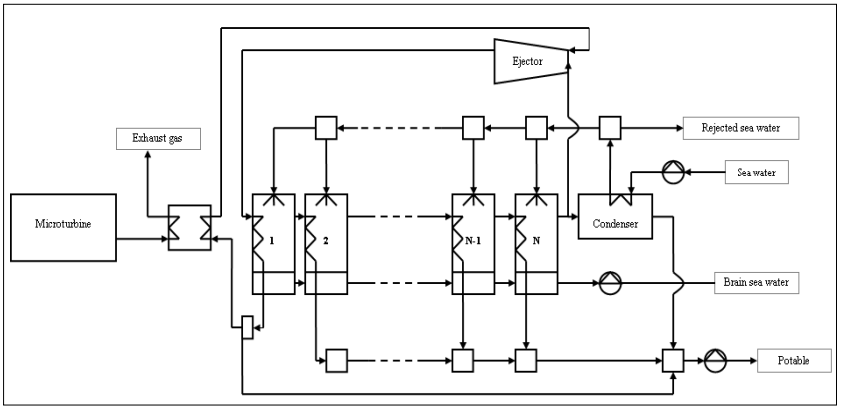

Fig. 10 Micro-turbine cascaded with TVC-MED.

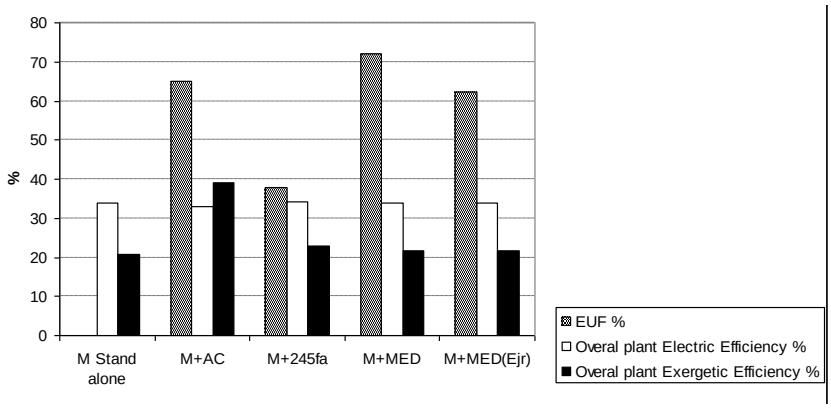

Fig. 11 Energy and exergy results for different proposed cycles.

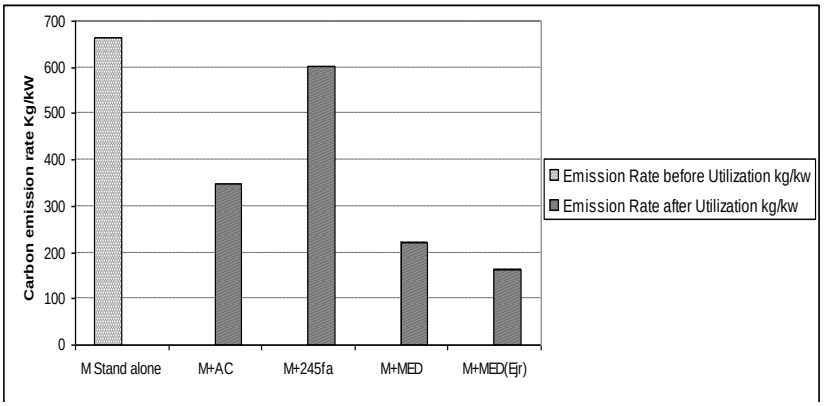

Fig. 12 Carbon emission rate for all proposed cycles.

highest exergetic efficiency was obtained. Furthermore, the highest electrical efficiency was gained by integrating the micro-turbine with ORC. This generates an additional 20% of electrical power, which improved the carbon emission rate by 10%. Moreover, 56,000 L/day of portable water can be produced by utilizing micro-turbine waste heat energy in MED desalination. This also showed the best EUF compared to other proposed cycles. In addition, a cascading micro-turbine with TVC-MED desalination showed the best reduction in carbon emission rate by 75%, and this method was thermally more efficient than traditional MED desalination, due to a 7% improvement in GOR.

4. Conclusion and Future Work

In conclusion, the micro-turbine has emerged as new generation technology to provide a reliable power that can be implemented in many commercial activities such as hospitals, schools and hotels.

Modeling and simulating micro-turbine cycles has presented the proposed cycles of this paper. A software package called IPSEpro was used to model and simulate the base and proposed plants. However, utilizing the waste heat energy of a micro-turbine in thermal processes has not been fully exploited in recent studies. The micro-turbine is known as high grade energy (work) and its low energy (heat) can be recovered for a useful purpose. The following low grade heat energy powered systems have been modeled under ISO ambient conditions (international standard organization), i.e. 15 ℃ and 1 bar, to utilize the waste heat energy of a 200 kW micro-turbine, a single-effect absorption chiller, organic ranking cycle R245 fa (ORC-R245 fa), multi-effect distillation desalination (MED) and thermal vapour compression

MED Desalination (TVC-MED). The thermal comparison was carried out based on an energy and exergy analysis in terms of electric efficiency, exergetic efficiency, carbon footprint, and Energy Utilization Factor (EUF). As a result, utilizing the exhaust waste heat energy in a single-effect absorption chiller has contributed to stabilize the ambient temperature fluctuation, and gain the best exergetic efficiency of 39%, while the EUF has reached 72% and the carbon foot print was reduced by 75% in MED and TVC-MED Desalination respectively.

The results also reveal that TVC-MED is more efficient than traditional MED as its Gain Output Ratio (GOR) is improved by 5.5%. In addition, ORC-245fa generates 20% of micro-turbine electricity generation. As it can be seen from the results, all proposed models will help to reduce the carbon emission rate, which plays a significant role in tackling the issue of global warming. Utilizing a single-effect absorption chiller will provide cooling that can be used either on site or off site, while integrating ORC will give extra electric power that can be useful for many purposes. In addition, cascading the MED and TVC-MED desalination with the micro-turbine will produce portable water that can tackle the issue of water shortages, especially in remote coastal areas. On the other hand, the obtained results also illustrate that TVC-MED desalination is more efficient than MED desalination.

This paper has only reached the halfway stage and this is an ongoing study. However, it will be supported by carrying out a number of studies, including partial load performance and parametric studies that will be performed according to the collected weather data of Jeddah city in Saudi Arabia. Moreover, a thermo economic study will be performed to show the feasibility and profitability of the proposed models in the long-term.

References

[1] J.C. Ho, K.J. Chua, S.K. Chou, Performance study of a Micro-turbine system for cogeneration application, Renewable Energy 8 (2004) 1121-1133.

[2] Appendix B: Micro-turbines and heat pumps, available online at: http://etd.rau.ac.za/theses/available/etd-05092005-124454/restricted/AppendixB.pdf.

[3] Energy Solution System, 2004, Micro-turbine CHP System, available online at: http://www.energysolutionscenter.org/distgen/AppGuide/Chapters/Chap4/4-2_Microturbines.htm#Introduction.

[4] C. Soares, Micro-turbines Application for Distributed Energy System, Oxford: Elsevier, 2007.

[5] E. Keith, R.R.A.S.A.K. Herold, Absorption Chillers and Heat Pumps, United States of America: Taylor and Francis, 1996.

[6] Z.G. Sun, Experimental investigation of integrated refrigeration system (IRS) with gas engine, compression chiller and absorption chiller, Energy 33 (2007) 413-436.

[7] Z.G. Sun, R.Z. Wang, W.Z. Sun, Energetic efficiency of a gas-engine-driven cooling and heating system, Applied Thermal Engineering 5-6 (2004) 941-947.

[8] Y. Hwang, Potential energy benefits of integrated refrigeration system with microturbine and absorption chiller, International Journal of Refrigeration 8 (2004) 816-829.

[9] H. Axelsson, S. Harvey, A. Asblad, T. Berntsson, Potential for greenhouse gas reduction in industry through increased heat recovery and/or integration of combined heat and power, Applied Thermal Engineering 1 (2003) 65-87.

[10] M.M.S. El-Din, Optimal utilization of waste heat from heat engines by use of a heat pump, Energy Conversion and Management 40 (1999) 937-949.

[11] B. Tchanche, G.R. Lambrinos, A. Frangoudakis, G. Papadakis, Exergy analysis of micro-organic Rankine power cycles for a small scale solar driven reverse osmosis desalination system, Applied Energy 87 (2010) 1295-1306.

[12] D. Wei, X. Lu, Z. Lu, J. Gu, Performance analysis and optimization of Organic Rankine Cycle (ORC) for waste heat recovery, Energy Conversion and Management 4 (2007) 1113-1119.

[13] A. Schuster, S. Karellas, E. Kakaras, H. Spliethoff, Energetic and economic investigation of Organic Rankine Cycle applications, Applied Thermal Engineering 8-9 (2009) 1809-1817.

[14] H. Shih, Evaluating the technologies of thermal desalination using low-grade heat, Desalination 1-3 (2005) 461-469.

[15] A. Khawaji, I. Kutubkhanah, W. Jong-Mihn, Advances in seawater desalination technologies, Desalination 1-3 (2008) 47-69.

[16] S.S. Technology, 2003, IPSEpro, available online at: http://www.simtechnology.com/IPSEpro/english/IPSEpro .php.

[17] A. Bejan, G. Tsatsaronis, M. Moran, Thermal Design and Optimization, New York: John Wile & Sons, 1995.

[18] F. Al-Sulaiman, I. Dincer, F. Hamdullahpur, Exergy analysis of an integrated solid oxide fuel cell and Organic Rankine Cycle for cooling, heating and power production, Journal of Power Sources 8 (2009) 2346-2354.

[19] X.J. Shi, B. Agnew, D.F. Che, Analysis of a combined cycle power plant integrated with a liquid natural gas gasification and power generation system, Proc. Inst. Mech. Eng., Part A, J. Power Energy 223 (2009).

[20] N. Kahramana, Y. Cengelb, B. Woodb, Y. Cercic, Exergy analysis of a combined RO, NF, and EDR desalination plant, Desalination 3 (2005) 217-232.

[21] Y. Cerci, Exergy analysis of a reverse osmosis desalination plant in California, Desalination 3 (2002) 257-266.

[22] M. Ameri, P. Ahmadi, S. Khanmohammadi, Exergy analysis of a 420 MW combined cycle power plant, International Journal of Energy Research 2 (2008) 175-183.

[23] H. Saravanamuttoo, P. Straznicky, C. Rogers, H. Cohen, Gas Turbine Theory, 6th ed., Parson Education Limited, ISBN: 978-0-13-222437-6, 2009.

[24] M. Ishida, J. Ji, Graphical exergy study on single stage absorption heat transformer, Applied Thermal Engineering 11 (1999) 1191-1206.